The Neuroimaging Features of Frontotemporal Dementia:

Characterising Phenotype-Associated Pathological Changes In Vivo

A dissertation submitted to the University of Dublin

for the Degree of Doctor of Philosophy

Dr. Mary Clare McKenna

Trinity College Dublin, 2023

School of Medicine

Trinity College Dublin

Supervisor:

Professor Peter Bede

Declaration, Online Access and the General Data Protection Regulation

I declare that this thesis has not been submitted as an exercise for a degree at this or any other university and it is entirely my own work. I agree to deposit this thesis in the University's open access institutional repository or allow the Library to do so on my behalf, subject to Irish Copyright Legislation and Trinity College Library conditions of use and acknowledgement. I consent to the examiner retaining a copy of the thesis beyond the examining period, should they so wish (EU GDPR May 2018).

Signed,

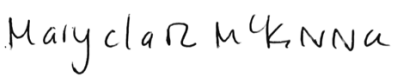

Mary Clare McKenna

9th June 2023

Declaration and Statement of Plagiarism

I declare that this work is my own, and that it is fully and explicitly acknowledged if the work of others forms any part of the thesis. Informed consent was obtained from all participants.

Signed,

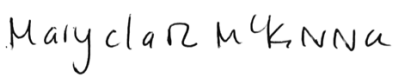

Mary Clare McKenna

9th June 2023

Acknowledgements

First and foremost I would like to thank all patients, families, caregivers, and control volunteers for their interest and participation in this project. I am in awe of their motivation and commitment to do what they can to help others.

Prof. Peter Bede – I am indebted to you for this opportunity. I have been so fortunate to work with an international leader in neurodegenerative research. You are an exemplary supervisor who has been so generous with your time, expertise, support and collaborations. I am most inspired by your exceptional infinite enthusiasm which has kept me energised throughout this project.

Prof. Siobhán Hutchinson – I am so grateful for your mentorship during these formative years of my career. I have learnt in equal measure about cognitive neurology and your kind-hearted considerate relationships with your patients.

I am also thankful for the help and support from all of the staff in the Trinity College Dublin Computational Imaging Group, St. James's Hospital Centre for Advanced Medical Imaging, and St. James's Hospital Neurology Department.

To my parents – With your love and encouragement anything is possible. You have always been a great source of inspiration, happiness and strength.

To my husband Dan – This simply would not be possible without you. You make every day and everything better. I can't wait to meet our baby girl!

Table of Contents:

List of Figures

List of Tables

Summary

Background:

Frontotemporal dementia (FTD) computational imaging studies typically investigate group-level analyses of cortical or supratentorial radiological changes. This single-centre prospective multimodal neuroimaging study of FTD phenotypes: bvFTD, nfvPPA, svPPA, and *C9orf72*+ and *C9orf72*- ALS-FTD aimed to investigate (1) group-level analyses of subcortical and infratentorial regions and (2) single-subject analyses of grey and white matter changes.

Methods:

(1) Cerebellar cortical thickness, morphometry, fractional anisotropy (FA), axial diffusivity (AxD), radial diffusivity (RD), mean diffusivity (MD).
(2) Thalamic nuclei volumetry, vertex, morphometry analyses.
(3) Standard cortical thickness and 'mosaic' *z*-score based analyses
(4) Standard diffusivity metrics and 'mosaic' *z*-score based analyses

Results:

In group-level analyses, there were FTD phenotype-specific cerebellar and thalamic signatures with selective involvement rather than global atrophy. The different imaging modalities offered complementary information. In single-subject analyses, the *z*-score based approach reliably detected FTD phenotype-specific cortical atrophy and white matter vulnerability patterns. These results were analogous to FTD-phenotype group-level analyses.

Lay Abstract

Frontotemporal dementia (FTD) is a rare type of dementia. It can affect language, behaviour and memory depending on what part of the brain is involved. It can be difficult to diagnose, especially in the early stages of the disease. The correct diagnosis is important for individual patients and from a wider research perspective. This research study used advanced magnetic resonance imaging (MRI) scans to better understand the FTD brain imaging pattern. These images are mathematically analysed by computers to calculate the size, shape, density and water diffusivity of different areas within the brain. Our study focused on (1) evaluating of the thalamus and cerebellum - which are often under investigated in FTD, and (2) using novel methods to analyse individual patient brain scans in FTD subtypes. We found that advanced MRI imaging captures thalamus and cerebellar involvement in FTD, in a pattern that is unique to each FTD subtype. We also found that novel methods can be used to reliably interpret individual patients' brain scans.

Aims and Hypothesis of the Project

Aim:

- To characterise multimodal imaging signatures of the cerebellum and thalamus in frontotemporal dementia (FTD) phenotypes

- To conduct and compare single-subject and group-level analyses of FTD phenotype-specific patterns of grey and white matter involvement

Hypothesis:

- There are FTD phenotype-specific cerebellar radiological profiles

- There are FTD phenotype-specific thalamic nuclei radiological profiles

- Single-subject analyses of grey and white matter in FTD phenotypes are analogous to well-described FTD phenotype group-level analyses.

Value of Research

This research project aims to use computational imaging to enhance our understanding of the specific imaging patterns described in frontotemporal dementia (FTD). From a patients' perspective, this research has the potential to improve early accurate diagnosis. From a clinicians' perspective, the improved characterisation of FTD-associated imaging signatures may help to differentiate FTD subtypes and to differentiate FTD from other neurodegenerative disorders. From an academic perspective, diagnostic precision enables timely accurate recruitment into clinical trials. This is particularly important as we enter the therapeutic era of targeted molecular therapies for neurodegenerative disorders. The identification of affected brain regions that are unique to FTD subtypes have the potential to be included in future machine learning classification algorithms to enhance diagnostic accuracy on a wider scale. These imaging methods could also be used as an objective measure to quantify disease burden, monitor disease progression or track response to treatment.

Outputs

Prizes:

1. **'Harold Millar' Prize for Oral Presentation**
   'Radiological features of primary progressive aphasias: a longitudinal quantitative neuroimaging study'.
   MC McKenna, S Hutchinson, P Bede.
   57th Annual Irish Neurological Association Meeting, 28th May 2021.

2. **Original Research Oral Presentation Prize**
   'The contribution of thalamic pathology to the clinical manifestations of frontotemporal dementia phenotypes'.
   MC McKenna, S Hutchinson, P Bede.
   IICN Registrar's Prize in Clinical Neuroscience, 11th Nov. 2022

3. **Original Research Oral Presentation Prize**
   'Infratentorial pathology in frontotemporal dementia subtypes'.
   MC McKenna, S Hutchinson, P Bede.
   Dementia, Delirium, Cognition Research Day, St. James's Hospital 21st Apr. 2022

4. **Original Research Oral Presentation Prize**
   'The radiological involvement of the cerebellum in frontotemporal dementia phenotypes'.
   MC McKenna, S Hutchinson, P Bede.
   2nd International Conference on Frontotemporal Dysfunction, 30th Sept. 2022

5. **Case Presentation Prize**
   'A case of parkinsonism: when to consider quantitative neuroimaging?'
   MC McKenna, J Redmond, D Bradley, P Bede.
   IICN Registrar's Prize in Clinical Neuroscience, 12th Nov. 2021.

Publications:

1. **MC McKenna,** J Lope, P Bede, EL Tan. Thalamic pathology in frontotemporal dementia: Predilection for specific nuclei, phenotype-specific signatures, clinical correlates, and practical relevance. Brain Behav. 2023;13(2):e2881. PMID: 36609810
2. **MC McKenna,** J Lope, EL Tan, P Bede. Pre-symptomatic radiological changes in frontotemporal dementia: propagation characteristics, predictive value and implications for clinical trials. Brain Imaging Behav. 2022;16(6):2755-2767. PMID: 35920960
3. **MC McKenna,** M Tahedl, J Lope, RH Chipika, S Li Hi Shing, MA Doherty, JC Hengeveld, A Vajda, RL McLaughlin, O Hardiman, S Hutchinson, P Bede. Mapping cortical disease-burden at individual-level in frontotemporal dementia: implications for clinical care and pharmacological trials. Brain Imaging Behav 2022;16(3):1196-1207. PMID: 34882275
4. **MC McKenna**, S Li Hi Shing, A Murad, J Lope, O Hardiman, S Hutchinson, P Bede. Focal thalamus pathology in frontotemporal dementia: Phenotype-associated thalamic profiles. J Neurol Sci. 2022;436:120221. PMID: 35279595.
5. **MC McKenna**, A Murad, W Huynh, J Lope, P Bede. The changing landscape of neuroimaging in frontotemporal lobar degeneration: from group-level observations to single-subject data interpretation. Expert Rev Neurother. 2022;22(3):179-207. PMID: 35227146.
6. **MC McKenna**, M Tahedl, A Murad, J Lope, O Hardiman, S Hutchinson, P Bede. White matter microstructure alterations in frontotemporal dementia: Phenotype-associated signatures and single-subject interpretation. Brain Behav. 2022;12(2):e2500. PMID: 35072974
7. **MC McKenna,** RH Chipika, S Li Hi Shing, F Christidi, J Lope, MA Doherty, JC Hengeveld, A Vajda, RL McLaughlin, O Hardiman, S Hutchinson, P Bede. Infratentorial pathology in frontotemporal dementia: cerebellar grey and white matter alterations in FTD phenotypes. J Neurol. 2021;268(12):4687-4697. PMID: 33983551
8. **MC McKenna,** P Corcia, P Couratier, WF Siah, PF Pradat, P Bede. Frontotemporal Pathology in Motor Neuron Disease Phenotypes: Insights from Neuroimaging. Front Neurol. 2021; 12:723450. PMID: 34484106
9. **MC McKenna,** J Redmond, D Bradley, P Bede. Teaching NeuroImage: Primary Familial Brain Calcification in *SLC20A2* Genotype. Neurology. 2022 Sep 20:10.1212/WNL.0000000000201343. PMID: 36127139.
10. **MC McKenna,** E McGovern, M Farrell, RP Killeen, C McGuigan, S Connolly. Neurogenic muscle hypertrophy following L5 motor radiculopathy. Pract Neurol. 2022;22(5):422-424. PMID: 35850977.
11. **MC McKenna,** J Woods, R Dolan, S Connolly. Posterior interosseous neuropathy: distinguishing from a proximal radial neuropathy. BMJ Case Rep. 2021;14(10):e245659. PMID: 34598971
12. **MC McKenna**, F Cox, S Roche, I McDonald, N Conlon, JD Edgar, et al. The management of primary immunodeficiencies in a case of classical ataxia telangiectasia. Neuroimmunology Reports. 2021;1:100011.
13. **MC McKenna,** M Marnane, BJ Sheane, S Connolly. A case of multifocal motor neuropathy after initiation of ixekizumab for psoriatic arthopathy. Rheumatology (Oxford). 2021;60(8):e282-e283. PMID: 33629111.

Poster Presentations:

1. **MC McKenna,** E Finegan, S Hutchinson, P Bede. 'The Contribution of Thalamic Pathology to the Clinical Manifestations of Frontotemporal Dementia Phenotypes'. 75th American Academy of Neurology Annual Meeting, 22nd-27th April 2023
2. **MC McKenna,** S Hutchinson, P Bede. 'Cerebellar involvement in frontotemporal dementia: the infratentorial imaging signatures of FTD phenotypes.' ABN and INA Joint Meeting, 10-12th May 2023
3. **MC McKenna**, S Hutchinson, P Bede. 'Infratentorial Pathology in Frontotemporal Dementia Phenotypes'. 74th American Academy of Neurology Annual Meeting, 24th-26th April 2022
4. **MC McKenna,** J Lope, E Ling Tan, P Bede. 'Pre-symptomatic Familial Frontotemporal Dementia Radiological Changes'. 2nd International Conference on Frontotemporal Dysfunction, 30th September 2022.
5. **MC McKenna,** S Hutchinson, P Bede. 'Thalamus Pathology in Frontotemporal Dementia Phenotypes'. 2nd International Conference on Frontotemporal Dysfunction, 30th September 2022.
6. **MC McKenna**, S Hutchinson, P Bede. 'Infratentorial Pathology in Frontotemporal Dementia Phenotypes'. Dementia, Delirium and Cognition Research and Audit Showcase, St. James's Hospital, 21st April 2022
7. **MC McKenna,** TH Mok, S Mead, S Hutchinson. 'Young Onset Dementia: A Case of Inherited Prion Disease'. Dementia, Delirium and Cognition Research and Audit Showcase, St. James's Hospital, 21st April 2022
8. **MC McKenna,** I Bruce, D Robinson, J Dunne, N Conlon, S Hutchinson. 'An Audit of the Clinical Use of Cerebrospinal Fluid Neurodegenerative Biomarkers'. Dementia, Delirium and Cognition Research and Audit Showcase, St. James's Hospital, 21st April 2022
9. **MC McKenna,** TH Mok, S Mead, S Hutchinson. 'Young Onset Dementia: A Case of Inherited Prion Disease', 58th Annual Irish Neurological Association Meeting, 12th-13th May 2022.
10. **MC McKenna,** J Kinsella, H Houlden, S Connolly. 'Dorsal Root Ganglionopathy with retained H-reflexes in CANVAS'. 58th Annual Irish Neurological Association Meeting, 12th-13th May 2022.
11. **MC McKenna**, J Kinsella, H Houlden, S Connolly. 'CANVAS-related Sensory Ganglionopathy Without Severe Ataxia: The Importance of Muscle Afferents in Proprioception'. Association of British Neurology Annual Scientific Meeting, 18th – 20st May 2022.
12. **MC McKenna**, C Kehoe, J Kinsella, C McGuigan, S Connolly. 'Evaluation of sensory neuronopathies using nerve conduction studies: don't forget the soleus H-reflex'. 32nd International Congress of Clinical Neurophysiology, 4th-8th September 2022.

1 The changing landscape of neuroimaging in frontotemporal lobar degeneration: from group-level observations to single-subject data interpretation

1.1 Introduction

The neuroimaging signature of frontotemporal lobar degeneration (FTLD) has been refined by robust computational imaging studies in recent years. This has led to the characterisation of phenotype- [1-16] and genotype-associated [17-23] patterns of preferential anatomical involvement and trajectories of longitudinal progression. These findings have contributed important academic insights to our understanding of FTLD biology. However, the practical clinical utility of group-level observations is contingent on the reliable interpretation of individual MRI scans. In recent years, a multitude of classification models have been trialled to capitalise on group-level traits and categorise single-subject MRI data into diagnostic and prognostic subgroups.

At a cohort level, grey matter (GM) analyses in FTLD readily detect cortical atrophy involving the medial-inferior orbitofrontal, anterior cingulate and anterior insular areas in the frontal lobes; the uncus, anterior, medial and lateral regions in the temporal lobes; and sometimes the lateral parietal lobes or cerebellum [1-3, 7-9, 11, 12, 24-34]. Diffusion tensor imaging (DTI) typically captures widespread white matter (WM) degeneration involving a multitude of commissural and long association tracts, such as the inferior fronto-occipital fasciculus, anterior temporal WM regions, anterior corpus callosum, bilateral anterior cingulate, uncinate, inferior and superior longitudinal fasciculus [8, 9, 11, 13, 16, 28-30, 35-42]. Subcortical GM analyses in FTLD reveal the selective

involvement of basal ganglia nuclei and limbic system structures [3, 7, 9, 30, 31, 39, 43-49]. Resting-state fMRI studies usually detect reduced salience network connectivity with the involvement of the fronto-insular, cingulate, striatal, thalamic and brainstem nodes [50-52]. These relatively consistent findings serve as the foundation for the development of single-subject MRI classification models in FTLD.

Machine-learning algorithms in neurodegenerative conditions typically use the best-performing set of MRI features rather than indiscriminately evaluating all available imaging measures that would unnecessarily add to the processing time without improving accuracy [53-57]. Different combinations of structural and functional MRI metrics are typically tested to create the most accurate classification models. Machine learning strategies are typically divided into 'supervised' and 'unsupervised' learning approaches. Unsupervised models can uncover association patterns or data clusters without human intervention or feedback. Common approaches include clustering methods such as K-means clustering, hierarchical clustering algorithms, probabilistic clustering, and dimensionality reduction strategies such as principal component analysis or singular value decomposition (SVD). The benefits of unsupervised approaches lie in their ability of discovering naturally occurring data patterns previously unknown to researchers and the reduced workload associated with the preparation and labelling of training datasets. The main drawbacks of unsupervised methods include the large training data required, considerable computational requirements, and typically slower data processing due to model complexity [58]. Supervised learning algorithms rely on meticulously labelled data to assign additional

inputs to specific categories based on regression or classification. Commonly used supervised models include linear regression, logistic regression, naïve bayes, support vector machines (SVM), decision trees, K-nearest neighbour algorithms, and random forests [59, 60]. The term semi-supervised learning is used when only part of the input data has been expertly labelled. Several models provide a group-membership probability index. Such frameworks have been successfully applied to pre-symptomatic [61-64], early [54, 65] and established [53, 66-69] cases of FTLD and have been shown to accurately differentiate FTLD from either established cases of AD or controls.

In this review, we explore the use of MRI classification models in FTLD as the neuroimaging landscape shifts from descriptive studies to the development of precision imaging biomarkers. This has potential clinical significance such as the earlier confirmation of a suspected diagnosis or classification into prognostic categories. The accuracy of proposed machine-learning approaches however has been largely tested on established FTLD cases and only more recently on pre-symptomatic or suspected cases.

1.2 Methods

A formal literature review search was conducted using the PubMed repository (last accessed on 11th February 2022). The following search strategy was used: ("Frontotemporal lobar degeneration"[Mesh] OR "Frontotemporal lobar degeneration" OR “frontotemporal dementia” [Mesh] OR “frontotemporal dementia” OR “frontotemporal degeneration” OR "Primary Progressive Aphasia” [Mesh] OR “behavioural variant frontotemporal dementia” OR “non-fluent variant primary progressive aphasia” OR “semantic-variant primary progressive aphasia” OR “FTLD” OR

“FTD” OR “bvFTD” OR “PPA” OR “nfvPPA” OR “svPPA”) AND ("Magnetic Resonance Imaging"[Mesh] OR “MRI” OR “diffusion tensor imaging” OR “functional MRI” OR “fMRI” OR “DTI”) AND ("Machine Learning"[Mesh] OR “classification” OR “accuracy” OR “deep learning” OR “support vector machine” OR “supervised machine learning” OR “unsupervised machine learning”). Pathological subgroups “tau” and “pTDP-43” were not included in the search strategy. Our search was limited to studies written in English that involved human subjects. All papers were screened by title and abstract and the full text of selected articles were then reviewed. The inclusion criteria included: (1) original research articles investigating single-subject classification of FTLD, bvFTD, PPA, nfvPPA or svPPA and (2) used classification features derived from structural or functional MRI only. We excluded studies that investigated other phenotypes such as corticobasal syndrome (CBS) and progressive supranuclear palsy (PSP). The reference lists of selected articles were also reviewed to identify additional relevant papers.

1.3 Results

This above search strategy yielded 283 papers, of which 40 articles were eligible. An additional 11 articles were identified by reviewing reference lists. A total of 51 studies were selected for systematic review **(Figure 1; Table 1**). The identified papers are discussed under five main themes of: classification of symptomatic cases; classification of pre-symptomatic FTLD; stereotyped study limitations; technological advances; and practical applications.

Figure 1: A PRISMA flowchart for systematic review of MRI classification models in FTD

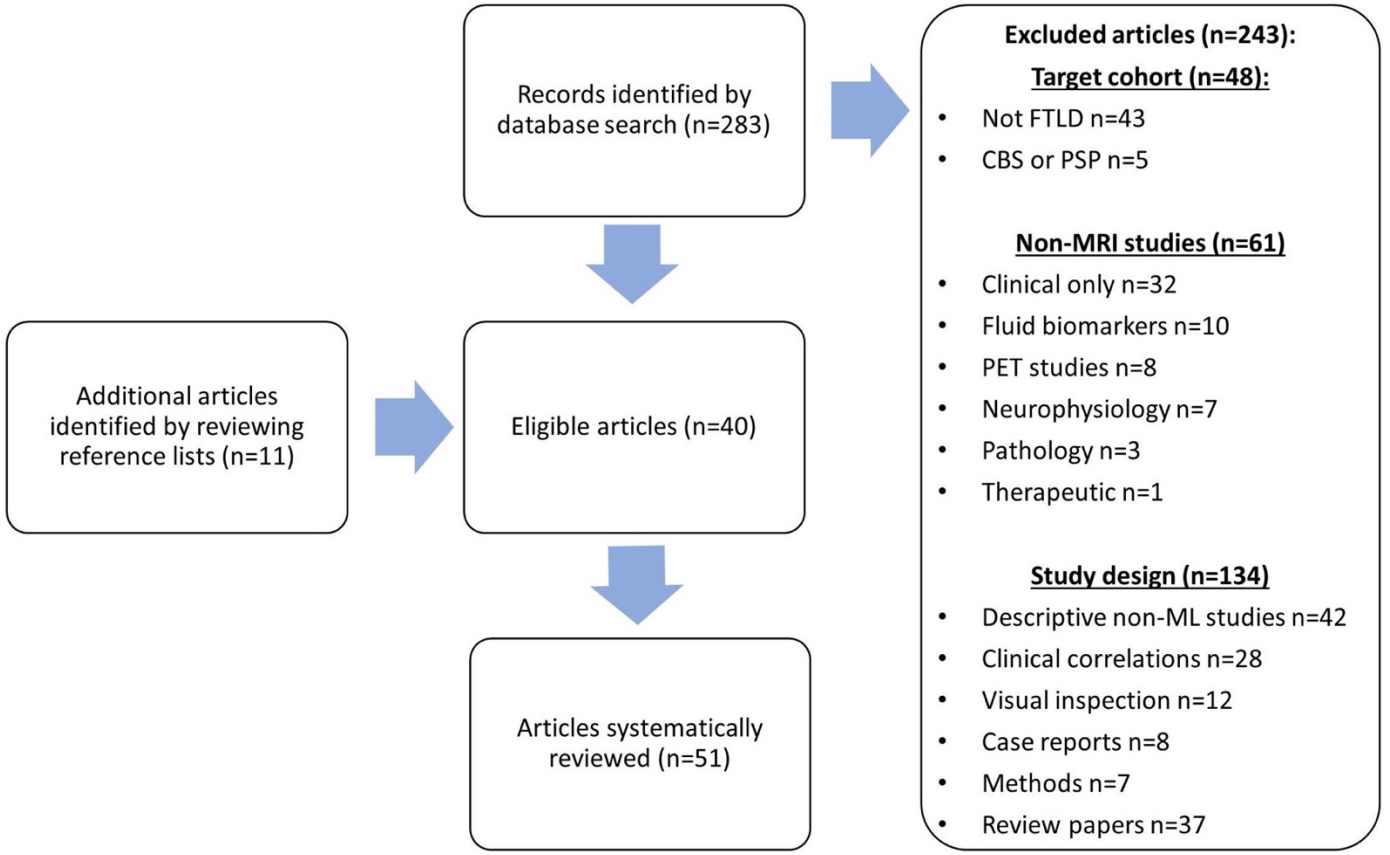

Table 1: A selection of MRI classification neuroimaging studies in cases of established, peri-diagnostic and pre-symptomatic FTD

First author, year of publication	Patient groups and cohort sizes	Clinical criteria	Symptom duration	Supporting pathological, radiological or CSF biomarkers	Study design, mathematical model, validation
Agosta et al, 2015 [70]	nfvPPA n=13 svPPA n=13 Controls n=23	PPA – Gorno Tempini 2011 [71]	nfvPPA 2 years svPPA 3 years	N/A	Binary classification Random forest
Bachli et al, 2020[72]	bvFTD n=57 AD n=29 Controls n=116	bvFTD – Rascovsky 2011 [73] AD – NIA-AA 2011 [74]	-	N/A	Binary classification Principal component analysis Logistic regression Cross validation
Bede et al, 2021[75]	FTLD n=37 ALS =214 HC =127	ALS – El Escorial [76] bvFTD – Rascovsky 2011 [73]	-	N/A	Artificial neural network framework; A multilayer perceptron model Data partitioned into: Training (68%) and testing sample (32%)
Bisenius et al, 2017[77]	nfvPPA n=16 svPPA n=17 lvPPA n=11 Controls n=20	PPA – Gorno Tempini 2011 [71]	nfvPPA 2 years svPPA 4 years lvPPA 4 years	N/A	Multi-class classification Whole-brain and ROI SVM
Bouts et al, 2018[53]	bvFTD n=23; AD n=30; Controls n=35	bvFTD – Rascovsky 2011 [73] AD – NIA-AA 2011 [74]	bvFTD 60 months AD 35 months	N/A	Binary classification Elastic net regression Cross-validation
Bron et al, 2017[65]	FTLD n=33; (bvFTD n=12; nfvPPA n=4; svPPA n=10; PPA n= 2; unclassified n=5) AD n=24 Controls n=34	bvFTD – Rascovsky 2011 [73] PPA – Gorno Tempini 2011 [71] AD – NIA-AA 2011 [74]	-	N/A	Multi-class classification Linear SVM Cross-validation
Canu et al, 2017[54]	bvFTD n=27 AD n=62 Controls n=48	bvFTD – Rascovsky 2011 [73] AD – NIA-AA 2011 [74]	bvFTD 4 years AD 4-years	[^{18}F] FDG PET-CT bvFTD (n=24); AD (n=38). CSF: bvFTD (n=9), AD (n=24).	Binary classification Random forest

First author, year of publication	Patient groups and cohort sizes	Clinical criteria	Symptom duration	Supporting pathological, radiological or CSF biomarkers	Study design, mathematical model, validation, symptom duration profile
Canu et al, 2019[78]	nfvPPA n=29 svPPA n=15 lvPPA n=15 Controls n=38	PPA – Gorno Tempini 2011 [71]	nfvPPA 3 years svPPA 4 years lvPPA 3 years	[^{18}F] FDG PET-CT: nfvPPA (n=12); svPPA (n=10); lvPPA (n=10) CSF: nfvPPA (n=12); svPPA (n=7); lvPPA (n=8)	Binary classification Random forest Logistic regression
Cajanus et al, 2018[79]	bvFTD n=50 Reference group: FTLD n=154 AD n=537 LBD n=61 SMC n= 359	bvFTD – Rascovsky 2011 [73]	bvFTD 3 years	Genetics: *C9orf72* testing in all (n=50), and confirmed in n=17	Multi-class classification Disease state index
Chagué et al, 2020[80]	bvFTD n=39 Early onset AD n=34 Late-onset AD n=49 Depression n=24	bvFTD – Rascovsky 2011 [73] AD – IWG-2 2007 [81] Depression – DSM-V 2013 [82]	bvFTD 3 years EOAD 3 years LOAD 3 years Depression 6 years	CSF in all cases (n=146)	Binary classification SVM Cross-validation
Chow et al, 2008[83]	bvFTD n=16 PPA n=14 Controls n=30	FTLD – Neary 1998 [84]	-	Pathology: bvFTD (n=6), PPA (n=4); Criteria not specified.	Binary classification Logistic regression
Davatzikos et al, 2008[85]	FTLD n=12 (bvFTD n=8, svPPA n=1; PPA n=2; CBS n=1) Controls n=49 AD n=37	FTLD - McKhann 2001[86] AD- NINCDS-ADRDA 1984 [87]	FTLD 4 years AD 4 years	N/A	Binary classification Non-linear SVM Cross-validation
Donnelly-Kehoe et al, 2019[88]	bvFTD n=44 Controls n=60	bvFTD – Rascovsky 2011 [73]	-	[^{18}F] FDG PET-CT: in some cases, details not specified	Binary classification Random forest classifier Feature selection Linear SVM Cross-validation

First author, year of publication	Patient groups and cohort sizes	Clinical criteria	Symptom duration	Supporting pathological, radiological or CSF biomarkers	Study design, mathematical model, validation, symptom duration profile
Du et al, 2006[89]	FTLD n=21 AD n=24 Controls n=25	FTLD – Neary 1998 [84] AD- NINCDS-ADRDA 1984 [87]	-	N/A	Binary classification Logistic regression
Egger et al, 2020[90]	FTLD n = 30 AD n = 30 LBD n = 30 Controls n = 30 Reference group Controls n=360	Not specified	-	[^{18}F] FDG PET-CT in all cases	Binary classification ROI and automated z-score based analysis
Feis et al, 2019[62]	Pre-symptomatic mutation carriers (n=55): *MAPT* n=8; *GRN* n=35; *C9orf72* n=12 Controls n = 48	bvFTD – Rascovsky 2011 [73] PPA – Gorno Tempini 2011 [71] ALS – Ludolph 2015 [91]	-	Genetics: FTLD pathogenic genetic mutations in all cases	Binary classification Elastic net regression Cross-validation Pre-symptomatic subjects
Feis et al, 2019[63]	Pre-symptomatic mutation carriers (n=55): *MAPT* n=8 *GRN* n=35 *C9orf72* n=12 Controls = 48	bvFTD – Rascovsky 2011 [73] PPA –Gorno Tempini 2011 [71] ALS – Ludolph 2015 [91]	-	Genetics: FTLD pathogenic genetic mutations in all cases	Binary classification Elastic net regression Cross-validation Pre-symptomatic and peri-diagnosis subjects
Feis et al, 2020[64]	Pre-symptomatic converters n=7 Pre-symptomatic non-converters n=35	bvFTD – Rascovsky 2011 [73] PPA –Gorno Tempini 2011 [71] ALS – Ludolph 2015 [91]	-	Genetics: FTLD pathogenic genetic mutations in all cases	Binary classification Elastic net regression Cross-validation Pre-symptomatic and peri-diagnosis subjects
Frings et al, 2014[92]	bvFTD n=15 AD n=14 Control n=10	bvFTD – Rascovsky 2011 [73] FTLD – Neary 1998 [84] AD – NINCDS-ADRDA 1984 [87]	-	Genetics: *C9orf72* n=3	Binary classification Logistic regression

First author, year of publication	Patient groups and cohort sizes	Clinical criteria	Symptom duration	Supporting pathological, radiological or CSF biomarkers	Study design, mathematical model, validation, symptom duration profile
Hu et al, 2021[93]	FTLD n=1250 AD n=1314 Controls n=1535	Not specified	-	N/A	Binary and multi-class classification Deep-learning based network Data augmentation model Independent validation
Kim et al, 2019[94]	FTLD n=143 AD n=50 Controls n=146	bvFTD – Rascovsky 2011 [73] PPA –Gorno Tempini 2011 [71] AD – NIA-AA 2011 [74]	FTLD 3 years svPPA 3 years nfvPPA 3 years AD 4 years	Amyloid PET scan: 18F-florbetaben 18F-flutemetamol	Binary classification Principal component analysis Linear discriminant analysis Cross-validation
Klöppel et al, 2015[67]	FTLD n=39 AD n=361 LBD n=23 Controls = 586	FTLD – Neary 1998 [84] AD – NIA-AA 2011 [74] LBD – McKeith 2005 [95]	-	[18F] FDG PET-CT: details not specified	Multi-class classification Linear SVM
Koikkalainen et al, 2016[68]	FTLD n=92 AD n=223 VD n=24 LBD n=47 Control n=118	FTLD – Rascovsky 2011 [73], Neary 1998 [84] AD – NIA-AA 2011 [74], NINCDS-ADRDA 1984 [87] VD – NINDS-AIREN [96] LBD – McKeith 1996, 2005 [95, 97]	-	CSF: details not specified	Multi-class classification Disease State Index classifier Cross-validation
Kuceyeski et al, 2013[98]	bvFTD n = 18 AD n = 18 Controls n = 19	FTLD – Neary 1998 [84] AD - NINCDS-ADRDA 1984 [87]	-	N/A	Linear discriminant analysis Loss in connectivity (LoCo) score
Ma et al, 2020[99]	FTLD n = 434 AD n=459 Controls n=1063	Not specified	-	N/A	Multi-class classification Generative adversarial neural network Cross-validation
Manera et al, 2021[100]	bvFTD n=145 Controls n= 370	bvFTD – Rascovsky 2011 [73]	Validation cohort bvFTD 5 years	Genetics: FTLD pathogenic genetic mutations in n= 75	Binary classification Random forest classifier Independent validation
McMillan et al, 2012[29]	FTLD n=50 AD n=42	bvFTD – Rascovsky 2011 [73] PPA –Gorno Tempini 2011 [71] AD – NIA-AA 2011 [74] CBS – Clinical criteria 2007 [101]	FTLD 3 years AD 3 years	CSF: n=92	Binary classification Logistic regression

First author, year of publication	Patient groups and cohort sizes	Clinical criteria	Symptom duration	Supporting pathological, radiological or CSF biomarkers	Study design, mathematical model, validation, symptom duration profile
McMillan et al, 2013	FTLD-TDP n=25 FTLD-tau n=10	N/A	FTLD-TDP 3 years FTLD-tau 3 years	Genetics: *C9orf72* n=12; *GRN* n=7; *MAPT* n=3 Pathology: FTLD TDP-43 (n=6); FTLD tau (n=7), MacKenzie 2010 [102] and 2011 [103]criteria	Binary classification Logistic regression Eigenanatomy Cross validation
McMillan et al, 2014[104]	FTLD n=72 AD n=21	bvFTD – Rascovsky 2011 [73] PPA –Gorno Tempini 2011 [71] CBS – Armstrong 2013 [105] PSP – NINDS-SPSP 1996 [106]	FTLD 4 years AD 3 years	CSF: n=93 Genetics or FTLD pathology, MacKenzie 2010 [102] (n=11)	Binary classification Linear regression Cross-validation
Meyer et al, 2017[69]	bvFTD n=52 Controls n=52	bvFTD – Rascovsky 2011 [73]	bvFTD 4 years	Genetics: FTLD pathogenic genetic mutations in n=4	Binary classification Linear SVM
Möller et al, 2015[7]	bvFTD n=24 AD n=32 Controls n=37	bvFTD – Rascovsky 2011 [73] AD – NIA-AA 2011 [74], NINCDS-ADRDA 1984 [87]	bvFTD 50 months AD 40 months	N/A	Binary classification Discriminant function analyses Cross-validation
Möller et al, 2016[107]	bvFTD n=51 AD n = 84 Controls n = 94	bvFTD – Rascovsky 2011 [73] AD – NIA-AA 2011 [74] and NINCDS-ADRDA 1984 [87]	Training set: bvFTD 45 months AD 37 months Prediction set: bvFTD 41 months AD 55 months	N/A	Binary classification SVM Discriminant functional analysis Cross-validation
Moguilner et al, 2018 [108]	bvFTD n=35 Controls n=49	Not specified	-	N/A	Binary classification SVM K-nearest neighbour Cross-validation
Moguilner et al, 2021[109]	bvFTD n=96 AD n=103 Controls n=101	Not specified	-	N/A	Binary classification Gradient boosting machine classifier (XGBoost) Independent and cross validation

First author, year of publication	Patient groups and cohort sizes	Clinical criteria	Symptom duration	Supporting pathological, radiological or CSF biomarkers	Study design, mathematical model, validation, symptom duration profile
Muñoz-Ruiz et al, 2012[49]	FTLD n = 37 AD n = 46 Progressive MCI n = 16 Stable MCI n = 48 Control n = 26	FTLD – Neary 1998 [84] AD – DSM-IV-TR 1994 [110] MCI – Clinical criteria 1997[111]	-	Pathology: FTLD TDP-43 (n=9), AD (n=4); criteria not specified. Genetics: FTLD pathogenic genetic mutations in n=3	Binary classification Regression
Raamana et al, 2014[66]	bvFTD n=30 AD n=34 Control n=14	FTLD – Neary 1998 [84] AD - NINCDS-ADRDA 1984 [87]	-	N/A	Multi-class classification Dimension reduction & Non-linear SVM Cross-validation
Staffaroni et al, 2020[112]	Pre-symptomatic mutation carriers n=127: *C9orf72* n=54 *GRN* n=37 *MAPT* n=36 Controls n=383	Not specified	-	Genetics: FTLD pathogenic genetic mutations in n=127	Binary classification Logistic regression Cross-validation
Tahmasian et al, 2016 [113]	FTLD n=20 (bvFTD n=11; nfvPPA n=5; svPPA n=4) AD n=20	N/A	bvFTD 7 years nfvPPA 4 years svPPA 6 years AD 5 years	[^{18}F] FDG PET-CT in all cases	Binary classification SVM Cross validation
Tong et al, 2017[114]	FTLD n = 92 AD n = 219 DLB n = 47 Vascular n = 24 SMC n = 118	FTLD – Rascovsky 2011 [73], Neary 1998 [84] AD – NIA-AA 2011 [74], NINCDS-ADRDA 1984 [87] DLB - McKeith 2005 [95] VD – NINDS-AIREN [96]	-	CSF: details not specified	Multi-class classification RUSBoost Feature selection SVM Random forest K-nearest neighbours Cross-validation
Torso et al, 2020[115]	FTLD n=96 (bvFTD n = 30; svPPA n = 41; nfvPPA n = 25) Controls n=84	bvFTD – Rascovsky 2011 [73] PPA –Gorno Tempini 2011 [71]	-	N/A	Binary and multi-class classification K-nearest neighbours Feature selection Principal component analysis Cross-validation

First author, year of publication	Patient groups and cohort sizes	Clinical criteria	Symptom duration	Supporting pathological, radiological or CSF biomarkers	Study design, mathematical model, validation, symptom duration profile
Torso et al, 2021 [116]	svPPA n=31 bvFTD n=37 nfvPPA n=30 PSP n=47 CBS n=39 Controls n=87	bvFTD – Rascovsky 2011 [73] PPA –Gorno Tempini 2011 [71] PSP – Höglinger 2017 [117], Litvan 1996 [106] CBS – Armstrong 2013[105]	-	Pathology: PSP n=5; CBS n=3; Criteria not specified	Binary and multi-class classification Linear discriminant analysis Feature selection Principal component analysis
Vemuri et al, 2011[118]	FTLD n = 47 AD n = 48 LBD n = 20 Control n =120	Dementia – DSM-IV [110] FTLD – Neary 1998 [84] CBS – Boeve 2003 [119] AD - NINCDS-ADRDA 1984 [87] LBD - McKeith criteria 2005 [95]	-	Pathology: in all cases - FTLD-TDP43 n=47, MacKenzie 2006 [120], 2010 [102]; AD n=48, NIA-Reagan Institute 1997 [121]; LBD n=20, McKeith 2005 [95]	Multi-class classification Differential-STAND
Vernooij et al, 2018[122]	FTLD n = 15 AD n = 21 MCI n = 6 Controls n = 4915	bvFTD – Rascovsky 2011 [73] AD – NIA-AA 2011 [74]	FTLD 2 years AD 2 years MCI 1 year	CSF: details not specified	Binary classification K nearest neighbour
Wang et al, 2016[123]	bvFTD n=55 AD n=54 Control n=57	bvFTD – Rascovsky 2011 [73] AD - NINCDS-ADRDA 2007 [81]	bvFTD 5 years AD 3 years	Pathology: bvFTD (n=13); AD (n=9); criteria not specified.	Multi-class classification Naïve Bayes classification Cross-validation
Whitwell et al, 2012[124]	FTLD n=14 Atypical AD n=14 Typical AD n=14 Controls n=20	FTLD – Neary 1998 [84] AD - NINCDS-ADRDA 1984 [87]. CBS – Boeve 2003 [119] Aphasic dementia – Caselli 1993[125], Josephs 2008[126]	Typical AD 3 years Atypical AD 3 years FTLD 4 years	Pathology: in in all cases - AD – NIA-Reagan Institute 1997 [121]; FTLD – Mackenzie 2010[102]; CBD – Dickson 2002 [127]	Binary classification Atlas based parcellation using ROI GM volumes
Wilson et al, 2009[128]	PPA n = 86 (nfvPPA n = 32; svPPA n = 38; lvPPA n = 16) Controls n = 115	nfvPPA - Neary 1998 [84] svPPA – Neary 1998 [84] lvPPA - Gorno-Tempini 2008 [129]	nfvPPA 4 years svPPA 5 years lvPPA 3 years	N/A	Binary classification Linear SVM Cross-validation

First author, year of publication	Patient groups and cohort sizes	Clinical criteria	Symptom duration	Supporting pathological, radiological or CSF biomarkers	Study design, mathematical model, validation, symptom duration profile
Young et al, 2018[130]	Pre-symptomatic FTLD n=123 *(C9orf72* n=39; *GRN* n=62; *MAPT* n=22) Symptomatic FTLD n=49 (*C9orf72* n=24; *GRN* n=14; *MAPT* n=11) Controls n=141 AD with 3T MRI n=793. (AD dementia n=117; late MCI n=164; early MCI n=243; significant memory concern n=86) AD with 1.5T MRI n=576. (AD dementia n=122; late MCI n=274) Controls n=104	Not specified	-	Genetics: FTLD pathogenic genetic mutations in n=172 CSF biomarkers: in AD cohorts	Binary and multi-class classification Subtype and stage inference (SuStaIn) Cross-validation
Yu et al, 2021[131]	Test dataset: FTLD n=47 (bvFTD n=19; svPPA n=12; nfvPPA n=2; not specified n=14); AD n=47 Controls n=47 Validation dataset: FTLD n=50 (bvFTD n=20; svPPA n=10; nfvPPA n=10; not specified n=10); AD n=50	bvFTD – McKhann 2001 [86], Rascovsky 2011 [73]. PPA - McKhann 2001 [86], Gorno-Tempini 2011 [71]. AD – NIA-AA 2011 [74], NINCDS-ADRDA 1984 [87].	-	N/A	Binary classification AD resemblance atrophy index Frontotemporal dementia index Independent validation

First author, year of publication	Patient groups and cohort sizes	Clinical criteria	Symptom duration	Supporting pathological, radiological or CSF biomarkers	Study design, mathematical model, validation, symptom duration profile
Zhang et al, 2013[132]	FTLD n=25; (bvFTD n=13; svPPA n=6; nfvPPA n=6) Controls n=19	FTLD - Neary 1998 [84]	bvFTD 6 years nfvPPA 4 years svPPA 7 years	N/A	Binary classification Logistic regression Cross-validation
Zhou et al, 2010 [50]	bvFTD n=12 AD n=12 Controls n=12	FTLD - Neary 1998 [84] AD - NINCDS-ADRDA 1984 [87]	bvFTD 4 years AD 4 years	Amyloid-β ligand PIB-PET: bvFTD n=4, AD n=5 Pathology: bvFTD n=1; Criteria not specified. Genetic: FTLD *GRN* n=1; *GRN* and *MAPT* tested in some cases	Binary and multi-class classification Linear discriminant analyses Cross validation (n=36) Independent validation (n=4)
Zhutovsky et al, 2019[133]	bvFTD n=18 Neurological diagnoses n=28 Psychiatric diagnoses n=27	bvFTD – Rascovsky 2011 [73] AD – NIA-AA 2011 [74] LBD - McKeith 2005 [95] VD – NINDS-AIREN [96] Psychiatric disorders - DSM-IV [110]	-	Genetics: *C9orf72* tested in all cases; *MAPT, GRN, PSEN1* and *APP* tested in some cases [^{18}F] FDG PET-CT details not specified CSF: details not specified.	Binary and multi-class classifications SVM Cross-validation

1.3.1 MRI classification models in symptomatic FTLD

1.3.1.1 Models using GM features alone distinguish clinical subtypes accurately in a research setting

Group-level observations consistently described phenotype- [10, 134-138] and genotype-specific [17-22, 139, 140] patterns of preferential GM cortical involvement that are relatively well preserved on longitudinal follow-up. MRI classification models are derived from these principles, using whole-brain or region of interest (ROI) analyses to examine individual scans. These machine learning algorithms are typically first trained on well-characterised cohorts and subsequently tested in two-class or multi-class settings. This whole-brain approach has been tested in differentiating FTLD from other neurodegenerative disorders or FTLD subtypes. An early MRI classification model used voxel-based analyses to categorise individual subjects based on spatial patterns of atrophy [85]. It achieved an averaged 84.3% diagnostic accuracy in distinguishing AD from FTLD. The orbitofrontal and right entorhinal cortex were identified as the best discriminating regions [85]. Whole-brain SVM classifications discriminate PPA subtypes with varying levels of accuracy: svPPA versus lvPPA (95%); svPPA versus nfvPPA (78%); and nfvPPA versus lvPPA (55%). ROI SVM classifications selected features that overlapped with regions of brain atrophy detected by group-level observations. In this study, both methods of SVM classification were comparable [77]. The selective appraisal of disease-specific regions is further evaluated in later studies. It is often used to narrow down the available input variables to the most relevant ROI and imaging metrics.

The targeted assessment of the left medial frontal region in bvFTD and the left anterior temporal region in PPA using ROI approaches can reliably distinguish these phenotypes from controls with a diagnostic accuracy of 87% and 91% respectively [83]. Similar results were achieved in a study interrogating frontal, temporal, insula and basal ganglia ROIs to differentiate bvFTD from controls achieving a diagnostic accuracy of 84.6% [69]. While these studies demonstrate methodological feasibility, it is important to recognise that it is neither clinically nor radiologically challenging to differentiate established FTLD cases from healthy controls. Accordingly, these methods have also been tested in distinguishing FTLD from other neurodegenerative disorders, mostly AD, which is more representative of the diagnostic dilemmas of clinical practice. Combined morphometric and ROI analyses of the lateral ventricle achieved a correct classification rate of 0.73 in differentiating FTLD from AD [49]. The volume of the temporoparietal cortex has also been identified as a discriminating region between FTLD and AD [124]. The involvement of the subcortical regions, specifically loss of GM volume in the caudate, resulted in an accuracy of 79% in differentiating bvFTD from AD [92]. Similar GM-based multi-class classification models were piloted using SVM [133], discriminant function analyses [107], and z-score based approaches [90]. GM data were also interpreted in step-wise hierarchal classification trees [94] first evaluating dementia versus controls, then FTLD versus AD, followed by behavioural versus language variant, and finally differentiating svPPA versus nfvPPA. The overall classification accuracy of this hierarchical classification tree was 75.8%. A number of alternative GM-based classification approaches have been

trialled including the definition of disease-specific indices such as the 'AD resemblance atrophy index' [131]. Despite the success of MRI classification models using only GM variables in discriminating FTLD from controls, subtypes and other neurodegenerative disorders, the limited pathological studies have shown that GM imaging metrics alone does not reliably determine the underlying FTLD molecular mechanism *in vivo* [141].

Many of these models achieve high diagnostic accuracy in pre-selected research samples [66, 68] but do not perform as well in a real-life clinical samples [67]. A multi-class classification study suggested that lateral ventricle displacement could discriminate bvFTD from AD or controls with an AUC 0.765 [66]. Three-way classification models were gradually developed into multi-class classification models to mirror clinical dilemmas. Structural metrics were appraised with regards to their discriminatory power between FTLD versus AD versus DLB versus vascular dementia versus healthy controls [68]. This model evaluated volumetry, morphometry, tensor-based morphometry (TBM), ROI-based grading, and vascular burden measures and relied on manifold learning. A continuous probability index was generated for each diagnostic label. An overall classification accuracy of 70.6% was achieved, and sample-size-adjusted balanced accuracy of 69.1%. It performed considerably better than visual MRI ratings. This method was most sensitive at detecting vascular dementia (96%), followed by controls (82%) and then AD (74%). It was least sensitive at detecting DLB (32%) because of the relative lack of specific imaging findings. FTLD was often misclassified as AD because of similar medial temporal lobe atrophy in 21% of cases [68]. This seems to be dependent on the

phenotype because relative sparing of the hippocampus and medial temporal lobes in atypical non-amnestic AD has been identified as a discriminating feature from FTLD [124]. In their current form, these approaches are laborious for routine clinical use, but show promise for optimisation for more viable clinical applications. For example, the combination of the two best-performing discriminatory features (vascular burden measure and ROI-based grading) yielded to a relatively high sample-size-adjusted balanced accuracy of 67.7% [68]. These approaches have been tested on 'real-world' samples, but exhibited reduced classification performance [67]. Despite achieving an AUC >0.9 in the training set, a multi-class MRI-based classification model relatively underperformed when tested in a sample from a general memory clinic (AUC = 0.76 for AD; AUC = 0.78 for FTLD; AUC = 0.97 for controls; and AUC=0. 55 for LBD) [67]. A number of innovative models have been recently trialled that offer good classification accuracy in multi-class setting [79, 93, 99, 114, 118, 130, 133].

One of the advantages of novel machine-learning frameworks is that in some models, such as artificial neural networks, categorical and continuous variables may be incorporated and many ML models can readily accommodate additional non-imaging data, such as clinical measures or other biomarker variables. The added value of clinical neuropsychological measures to structural MRI data has been consistently demonstrated [72, 123]. The diagnostic accuracy of a bvFTD vs. control classification model improved from 88% (81% sensitivity, 92% specificity) to 91% (79% sensitivity, 96% specificity) with the addition of clinical measures of semantic fluency [100]. A multimodal model incorporating GM imaging and neuropsychological measures yielded

maximal classification accuracy rates for bvFTD (0.91) [72]. Similarly, the diagnostic accuracy of a binary, nfvPPA vs. svPPA classification framework was enhanced from 90.4% to 96.2% with addition of clinical language parameters [128]. In contrast, a classification model using neuropsychological data exclusively was deemed more accurate than relying on volumetric MRI data in a two-class bvFTD vs AD model (62.4% vs. 51.4%) and three-class bvFTD vs. AD vs. control model (68.1% vs. 54.2%) [123]. In addition to clinical measures, the combination of quantitative imaging measures with visual inspection is thought to enhance diagnostic accuracy [80, 122].

1.3.1.2 The incorporation of WM variables into MRI ML models enhances classification accuracy

Similar to cortical GM patterns, group-level observations consistently describe distinctive phenotype- and genotype-specific patterns of progressive WM degeneration [7, 9, 14, 15, 36, 40, 41, 136, 142]. The computational distinction of FTLD from subtypes or other neurodegenerative disorders may be challenging based on exclusively GM variables because of overlapping patterns of atrophy [68]. The addition of WM variables or the appraisal of WM metrics alone may offers superior discriminatory power [7, 28, 29, 54, 98, 115, 132]. In FTLD there is early loss of frontal predominant WM integrity [7, 13] with significantly reduced FA in the corpus callosum [29] and uncinate fasciculus [54] perhaps preceding GM atrophy [143, 144]. The chronology of radiological changes and the hierarchy of imaging metric sensitivity are hugely important for the development of diagnostic protocols [145]. A study of MRI classification of FTLD using GM and WM imaging metrics identified novel whole-brain cortical diffusion measure

PerpPD - principal diffusion component projected onto the place perpendicular to the cortical profile – as the best-performing single feature in binary classification compared with controls and multi-class classification amongst FTLD subtypes [116]. In addition to whole-brain analyses, disease-specific regions have also been independently investigated. An MRI classification model using DTI ROI analyses of superior longitudinal fasciculi accurately distinguished pathological subtypes (96% specificity and 100% sensitivity) with significantly more WM degeneration observed in FTLD-tau compared to FTLD-pTDP43 [141]. This is considerably better than the aforementioned GM-only classification model [141].

Multimodal MRI classification models using both GM and WM indices are proving superior in the classification of FTLD subtypes [70, 78]. A multimodal nfvPPA-svPPA classification model using axial diffusivity (AxD) of the left inferior longitudinal fasciculus and uncinate fasciculus and cortical thickness of the left temporal pole and inferior frontal gyrus-pars opercularis achieved AUC 0.91 [70]. The selected features mirror the expected phenotype-specific regions of GM atrophy [1, 3-6, 10, 11, 14, 24, 27]. and WM degeneration [14, 15, 41, 142] that are described in group-level analyses. The addition of clinical language parameters adds further value and is sufficient to differentiate svPPA from nfvPPA and lvPPA. The multimodal model using clinical language parameters, left inferior parietal cortical thickness, DTI metrics of the genu of the corpus callosum, and left frontal aslant tract accurately differentiate nfvPPA versus lvPPA (AUC 0.94) [78]. It is notable that DTI imaging variables contributed higher

classification accuracies to each PPA variant compared with controls compared to cortical thickness measures [78].

This multimodal approach of combined GM and WM variables has also enhanced the classification of FTLD from other neurodegenerative disorders, particularly AD [29]. The appraisal of regional GM atrophy (precuneus, posterior cingulate and anterior temporal region) and DTI measures (corpus callosum) achieved an AUC of 0.938 in the differentiating FTLD from AD, with 87% sensitivity and 83% specificity [29]. These observations laid the foundation for data-driven volumes-of-interest (VOI) analysis of the left parietal cortex, bilateral precuneus and body of the corpus callosum achieving classification AUC = 0.874, with 89% sensitivity and 89% specificity [104]. Early WM involvement in FTLD and the cortical predominance of AD-associated radiological changes continue to be reflected in other multimodal MRI classification models. The combined interpretation of cortical thickness (right and left inferior parietal, right temporal pole, right precuneus, left isthmus cingulate) and DTI measures (FA, AxD, RD and MD of the right uncinate fasciculus and FA of the genu of the corpus callosum) yielded to accuracy values of 0.82, specificity of 76%, and 96% sensitivity [54]. Given the distinguishing subcortical grey matter signatures, subcortical grey matter metrics should also be incorporated in multi-class classification schemes. A multiparametric MRI classification model evaluating cortical GM variables, WM integrity measurements and hippocampal volume correctly classified 67-75% of bvFTD, 81-100% of AD and 97-100% controls [7]. Thus far, the evidence favours the combination of GM and WM metrics in distinguishing FTLD from

AD, but these observations need to be rigorously tested in a multi-class setting and validated in real-life, peri-diagnostic cohorts.

1.3.1.3 The addition of fMRI variables may offer additional classification benefits

Functional MRI (fMRI) probes the hypothesis of selective network failure [50, 51]. FTLD is characterised by decreased salience network and increased default mode network connectivity at a group-level [50, 51, 146, 147]. These functional abnormalities may precede clinical manifestations or structural abnormalities [23, 148]. The inclusion of fMRI variables analysing disease-specific regions may improve the accuracy of classification models [88]. A preliminary study demonstrated that a novel non-linear weighted symbolic dependence metric (wSDM) may be the optimal method of fMRI analysis rather than standard linear connectivity metrics. This method revealed reduced salience network connectivity that correctly classified bvFTD from controls [108]. Using different fMRI analysis methods, the combination of salience and executive network metrics accurately differentiate bvFTD from controls (mean accuracy = 86.43%, AUC = 0.91, sensitivity = 86.45%, specificity = 87.54%). The divergent functional connectivity patterns have also been used to differentiate FTLD from other neurodegenerative disorders, particularly AD where the inverse pattern of enhanced salience network and attenuated default mode network is described [50-52, 113, 147]. MRI classification models using combined index of salience and default mode network connectivity correctly classify bvFTD from AD and controls in binary and multi-class settings [50, 109].

This classification ability was sustained in a subset of clinically ambiguous cases [50].

Recent studies have investigated the additional diagnostic value of voxel-based arterial spin labelling (ASL). It is a non-invasive fMRI sequence that readily captures cerebral perfusion patterns [149]. Multimodal MRI classification models have tested this technique in combination with GM [89] or WM [65] metrics. The addition of ASL did not improve binary FTLD-control classification [65, 89]. It resulted in a modest improvement in differentiating FTLD from AD (AUC 0.84 vs 0.72; p=0.05) and in the three-way classification of FTLD-AD-control (AUC 0.90 vs 0.84; p=0.03)[65]. Hypoperfusion of the parietal lobe and posterior cingulate gyrus favours the diagnosis of AD. The discrimination between FTLD and AD is further improved when the anterior-to-posterior gradient of mass and perfusion are considered, with potential to achieve AUC 0.94.[89]. The performance of this classification model is comparable to previous studies in the two-class setting [66], and slightly improved in the three-class setting [66]. Despite only marginal benefits, these exploratory studies have shown that the incorporation of additional non-structural imaging data may offer classification benefits [65].

The pursuit to discover the best-performing multiparametric MRI classification model was further explored in a landmark study that tested a multitude of structural and functional imaging variables to accurately distinguish bvFTD from controls or AD [53]. This model was trained using a small number of established cases of sporadic FTLD. The combination of GM density, FA and resting state fMRI indices differentiated bvFTD from controls

with an AUC of 0.922. This model evaluated key anatomical regions including the anterior thalamic radiation, corticospinal tracts, inferior longitudinal fasciculus and hippocampal regions. The same study developed a model to differentiate bvFTD from AD by evaluating FA, MD and resting state fMRI derived independent components resulting in an AUC of 0.811. The model interrogated metrics from the following anatomical regions; uncinate fasciculus, forceps minor, cingulum bundle, corticospinal tracts and functional connectivity within the dorsal default mode network. The addition of GM metrics did not enhance the classification accuracy of the model further. Despite limited generalisability, this bvFTD-control MRI classification model has been also applied to pre-symptomatic FTLD mutation carriers to explore if early radiological alterations may also be correctly interpreted [62, 63]. The optimal combination of imaging variables continues to be defined, with the recurring theme that multimodal approach is superior at classifying single-subjects with neurodegenerative disorders according to network-based patterns of degeneration [113].

1.3.2 Classification models capture pre-symptomatic changes in FTLD

While most classification schemes were trialled on established cases with relatively long symptom duration, carefully optimised MRI classification models have the potential to support an early diagnosis. A cross-sectional study of pre-symptomatic FTLD mutation carriers found that there was no difference in structural or functional MR imaging measures in mutation carriers compared to controls [61]. Similarly, a multi-modal bvFTD MRI classification model [53] was unable to differentiate mutation carriers from

controls beyond chance with an AUC of only 0.57 [62]. Nevertheless, alternative unimodal and multimodal carrier-control models relying on structural and functional MRI measures performed modestly better than chance with an AUC of 0.68 [62]. Successful carrier-control models used exclusively white matter variables, with no additional benefit of incorporating structural grey matter or functional connectivity measures. This in line with the aforementioned chronology of early WM changes preceding frank GM atrophy in familial FTLD [21, 23, 150, 151]. In addition, individualised quantification of brain atrophy may predict conversion from pre-symptomatic or mildly symptomatic to dementia in pre-symptomatic FTLD mutation carriers [112]. While these carrier-control models are currently not sensitive enough to be used in clinical practice, these landmark studies demonstrates that subtle radiological changes may be ascertained in single-subjects before symptom onset [62]. There may have been other classification attempts of pre-symptomatic mutation carriers which were not published to due to a bias to primarily disseminate successful study outcomes.

These observations were refined by subsequent longitudinal studies that reliably differentiated pre-symptomatic FTLD mutation carriers approaching phenoconversion from controls using similar multi-modal classification models [63]. Higher classification scores were achieved in mutation carriers compared to non-carriers with no difference in the rate of progression between the two groups. However, subgroup analysis of mutation carriers revealed a significantly higher rate of progression of classification scores in those who became symptomatic compared to those

who remained asymptomatic [63]. These pre-symptomatic radiological changes emerge over a relatively short 2-year period before clinical onset, with maximal loss of WM integrity in the genu of the corpus callosum [21]. This is analogous to the accelerating evolution of pre-symptomatic cognitive and fluid biomarkers within the same timeframe [145, 152-155]. An interpretation of this is that there is a brief interval to capture pre-symptomatic radiological changes, but it is currently unknown when this window of opportunity will arise in those who are genetically susceptible [21, 63]. A preliminary study demonstrated that reduced fractional anisotropy in the forceps minor predicted phenoconversion within 4-years with AUC 0.81 [64]. This is anatomically consistent with the site of maximal pre-symptomatic WM change [21]. Additional MRI metrics did not improve classification accuracy in this cohort [64], but their potential role warrants further exploration considering that pre-symptomatic genotype-associated GM atrophy has been consistently described [22, 156].

1.3.3 Stereotyped methodological challenges drive model development

The challenges around model development and the methodological constrains of published studies are not unique to FTLD and are also shared with other neurodegenerative disorders [157-159]. In an attempt to boost sample sizes, a variety of phenotypes, genotypes and pathological subtypes may be pooled in a single training sample, which precludes the precision classification of subjects. For the generation of optimal training samples, especially when supervised models are implemented, meticulously labelled cases are required with limited within-cohort heterogeneity, so that class-specific distinctive

features can be defined. In training datasets, group membership is often only defined based on the clinical diagnosis without supporting PET imaging, wet biomarker profiles and subsequent post mortem ascertainment. The absence of neuropathological characterisation in the majority of ML studies is another significant drawback because the underlying molecular subtype is increasingly relevant for targeted therapeutic trials. Thus far, MRI classification models have primarily focused on differentiating clinical phenotypes or FTLD from AD rather than differentiating FTLD-tau from FTLD-pTDP43. Relatively distinct patterns of WM degeneration [141] and GM atrophy [27, 141, 160-162] have been proposed in the different pathological subtypes, but this needs further validation to be reliably utilised for individual data interpretation. Training datasets often encompass convenience samples with considerable clinical heterogeneity with regards to symptom duration, cognitive function and behavioural impairment. Sample heterogeneity is even more marked when pre-symptomatic cases are classified as these individuals are often scanned at different stages of their disease process with considerable variability with regards to their projected phenoconversion. If scanned too early, asymptomatic mutation carriers may elude the detection of characteristic radiological changes [62]. Moreover, in pre-symptomatic cohorts, machine-learning models are often implemented which have been developed on different cohorts [62, 63]. One classification model which has been widely utilised is derived from a relatively small number of established sporadic bvFTD cases [53] and therefore may not be optimal to detect radiological changes associated with other phenotypes and genotypes [62, 63]. The model may be too specific to

the training sample, which is another common shortcoming of classification initiatives, referred to as 'model overfitting'. The small size of the training and testing cohorts in some of the earlier machine-learning studies also contribute to the risk of model overfitting and poor generalisability.

While a multitude of ML models have been trialled in FTLD **(Table 1)**, typically only a single classification model is implemented in a given study which precludes the comparative assessment of the accuracy of various models on the same sample. This is a lost opportunity as determining the performance characteristics of several models on the same data would be hugely important for the development of real-life applications. The choice of classification models is not always justified by data characteristics; some models are contingent on stringent assumptions, the proportion of feature variables and sample size is important and models differ considerably in their ability to account for outliers and missing variables. Ideally, the choice of a specific model should depend on the characteristics of the available data, outliers, sample size, number of predictor variables etc. Another challenge of ML initiatives in neurodegeneration is model validation. Single-centre samples are typically split into training and testing samples and validation is sometime sought on external datasets. The most contentious aspect of model validation is commenting on diagnostic performance in a model which has only been tested on subjects with an established diagnosis with long symptom duration. The performance of a model should ideally be tested on either pre- or peri-symptomatic cohorts. Classifying subjects with long disease duration and marked atrophy does not mirror the clinical challenge of labelling cases with a

suspected diagnosis relatively soon after symptom onset. It seems therefore paramount to report the clinical profile of the testing dataset, particularly with regards to symptom duration and interval from diagnosis, to gauge the 'real-life' performance of a proposed diagnostic model. While validation on external datasets demonstrates model generalisability and scrutinises performance further, it introduces additional challenges. Clinical imaging data are seldom acquired with uniform pulse-sequence parameters, spatial resolution and a multitude of head-coil designs, field strengths and scanner manufacturers are used at various centres. In the academic setting, large imaging consortia recommend specific pulse sequence settings to aid data harmonisation, which help the validation of classification models. In the clinical setting, imaging protocols are often optimised for speed of data acquisition, spatial resolution may be limited, slice gaps are commonly included and diffusion tensor data are not routinely acquired preventing the quantitative interpretation of single-subject data. The binary classification schemes presented by some studies may not represent the diagnostic dilemmas faced by neurologists. Binary classification models offering AD vs. FTLD categorisation will inevitably mislabel patients with LBD or vascular dementia. Another determinant of model performance is the selection of predictor variables which often centres on common cortical grey matter metrics (thickness, volumes), white matter integrity indices (FA, RD) and subcortical structure volumes (thalamus, hippocampus). Overall subcortical volumes may not be representative of a diagnostic cohort as selective thalamic nuclear involvement, focal amygdalar pathology and preferential

hippocampal subfield degeneration characterises most neurodegenerative conditions [163, 164]. Accordingly, similar to cortical segmentation, subcortical structures should also be meticulously parcellated to ascertain group-specific disease burden patterns and aid the categorisation of individual subjects.

1.3.4 Relentless technological advances herald efficient future applications

In the past few years, considerable progress has been made in the optimisation of classification approaches **(Figure 2).** Technological developments, such as the widespread availability of high-field magnets, 'cloud' data storing and processing solutions, open-source software are just some of the factors fuelling advances in neuroimaging. Increased interest by funding agencies, well-defined regional data protection laws, large multi-site consortia and efficient international collaboration helped to overcome some of the early challenges associated with recruitment, sample sizes, scanning costs, and data processing. The larger data sets of careful harmonised protocols provide high-quality training datasets and permit more rigorous model testing and validation [79, 93, 99]. Larger datasets also allow the splitting of main diagnostic groups (AD, FTLD) into specific clinical phenotypes such as early- versus late-onset AD [80], stable- versus progressive-MCI [49], or stratification into nfvPPA versus svPPA etc. [94, 128]. The cohort sizes of recent ML studies in FTLD are much more balanced [90, 93] compared to previous studies which typically operated with a large control and AD group and a small FTLD group. Innovative pre-symptomatic studies have assessed the value of MRI measures to predict phenoconversion [64]. More recent papers offer meticulous clinical characterisation, the symptom duration profile of patients

is increasingly reported [94] and cohorts with pathologically confirmed diagnoses have now been evaluated [123]. Another strength of recently published papers is the in-depth analysis of misclassified individuals and the discussion of contributing factors [79]. The consideration of a multitude of possible diagnostic output labels in addition to AD and FTLD, such as MCI, LBD, vascular dementia, ALS, depression or psychiatric diagnoses make recent models more relevant to clinical applications [67, 68, 75, 80, 133]. Similarly, the classification of individuals with subjective memory complaints mirrors clinical scenarios better than merely testing a model with healthy subjects and those with FTLD/AD [114, 130]. The choice of mathematical models has also evolved; recent studies increasingly rely on unsupervised approaches, utilise dimensionality reduction [66] and 'deep-learning' strategies [93, 99]. Innovative approaches, such as subtype and stage inference (SuStaIn) [130], AD resemblance index, frontotemporal dementia index [131] led to excellent classification outcomes, and certain models such as generative adversarial neural networks (GAN) seem particularly robust to classify individual subjects [99]. Recent ML initiatives provide transparent feature selection descriptions and often rank the best discriminating anatomical regions and biophysical measures [75, 88, 114, 115]. The hierarchy of imaging metrics with regards to discriminatory power offer important academic insights and has practical ramifications for the development of future models.

.

Figure 2: Progress in MRI-based machine-learning in FTD: methodological and conceptual developments

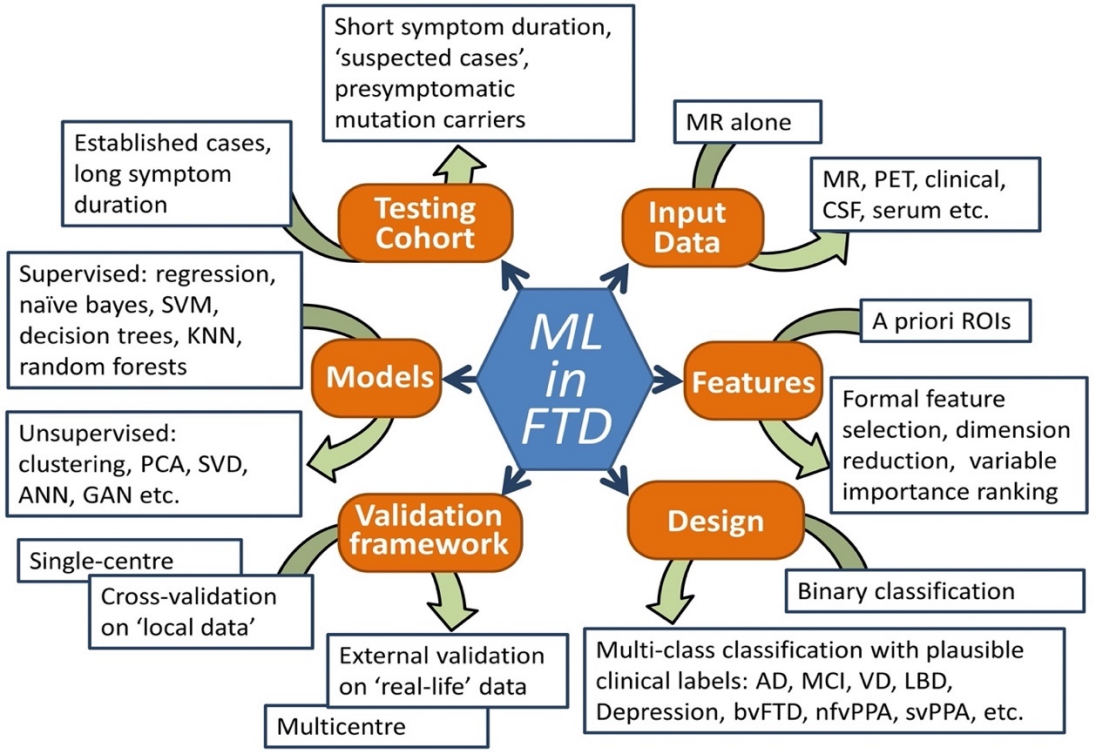

AD – Alzheimer's disease; ANN – artificial neural networks; bvFTD – behavioural variant FTD; DLB – dementia with Lewy bodies; FTD – frontotemporal dementia; GAN - generative adversarial neural network; KNN - K-nearest neighbour; MCI – mild cognitive impairment; ML – machine learning; nfvPPA – non-fluent variant primary progressive aphasia; PCA - principal component analysis; PPA – primary progressive aphasia; ROI – region of interest analysis; SVD - singular value decomposition; SVM – support vector machine; svPPA – semantic variant primary progressive aphasia; VD – vascular dementia

1.3.5 Practical clinical applications of MRI classification models

While diagnostic classification algorithms have originally been developed in the academic setting, they have the potential to be optimised for viable clinical applications. From a clinical perspective, there is a pressing need to develop panels of diagnostic, prognostic and monitoring biomarkers to track longitudinal changes and gauge response to therapy in clinical trials [145]. Prolonged diagnostic uncertainty is associated with considerable anxiety in both suspected patients and their caregivers. Late recruitment into pharmacological trials, when considerable degenerative changes have already taken place, is likely to limit the therapeutic or neuroprotective potential of putative disease-modifying drugs. On clinical grounds alone, it can be challenging to differentiate early neurodegenerative disorders, such as early FTLD from AD [165-167], and validated imaging (amyloid PET, tau PET, MRI) or biofluid (CSF or serum) markers offer diagnostic clarification in these circumstances [168-170]. The inclusion of MRI classification models presents the opportunity to enhance the diagnostic pathway in tandem with other biomarkers [171]. This is with the stipulation that MRI scans should only be interpreted with reference to the clinical context. In neurodegenerative conditions, quantitative MRI offers the advantage of determining the extent of cerebral disease-burden and the trajectory of longitudinal progression non-invasively with limited cost implications [172]. There is the potential for widespread use of these machine learning algorithms that may be readily exchanged between centres [173] without being significantly affected by differences in MRI parameters [72]. Diagnostic accuracy is crucial to recruit

suspected patients into clinical trials at an earlier stage, and the accurate distinction of FTLD-tau from FTLD-pTDP43 has gained unprecedented relevance in upcoming clinical trials. Preliminary studies indicate that ML methods may also have a prognostic role such as predicting likely symptom onset in pre-symptomatic FTLD mutation carriers [174]. This would allow the clinical team to facilitate timely organisation of care, resource allocation and set expectations for the patient and their caregivers about the timing of symptom onset.

1.4 Discussion

The potential role of MRI-based classification in aiding an early diagnosis in FTLD has been compellingly demonstrated by pioneering studies. Existing frameworks need further optimisation and validation in large pre-symptomatic or early-symptomatic FTLD cohorts stratified by phenotype and genotype. The key limitations of early machine learning studies in FTLD stem from small sample sizes, reliance on binary classification models, and limited clinical profiling which resulted in modest diagnostic performance, poor generalisability and model overfitting. A stereotyped weakness of existing studies is model testing with established, advanced FTLD cases with long symptom duration which does not mirror real-life clinical dilemmas, where suspected patients with short symptom duration need to be accurately labelled. Rigorous model testing and validation on peri-diagnostic cohorts is indispensable to demonstrate the purported diagnostic utility of such models. Despite their considerable academic and clinical importance, pre-symptomatic studies in FTLD are relatively scarce, owing to the limited number of suitable

participants who undergo predictive genetic testing for familial FTLD. The methodological constraints of early machine-learning studies in FTLD have been gradually overcome by robust multi-centre studies. A series of clinically relevant multi-class classification studies have been recently published categorising individual patients into a multitude of clinically plausible diagnostic labels such as AD, VD, LBD, MCI etc. Recent studies increasingly rely on large, uniformly acquired imaging datasets offering ample opportunities for robust cross-validation. Pre-symptomatic imaging data have been interrogated with regards to predicting phenoconversion and symptomatic patients were classified into the prognostic categories. Classification models have their respective advantages and drawbacks, therefore the choice of a specific model needs to be carefully justified based on the characteristics of the available data and the classification performance of several models should ideally be evaluated on the same dataset. Classification models differ considerably in their ability to accommodate missing data, interpret both continuous and categorical input variables, manage outliers, provide feature importance ranking, tolerate non-normally distributed input variables, homoscedasticity and multicollinearity. Flexible unsupervised models, such as deep neural networks and GAN are increasingly utilised which don't rely on stringent mathematical assumptions compared to more conventional models. Dimension reduction strategies and feature importance ranking are increasingly reported which help the streamlining and development of future models. Small, single-centre studies have been gradually superseded by collaborative, multi-centre initiatives which generate adequate sample sizes

for well-powered analyses. Owing to technological and conceptual advances, the development of radiological classification models in FTLD has gained unprecedented momentum in recent years. Once only explored in the academic setting, classification models are now close to become practical clinical tools. While radiological ML algorithms are mathematically complex and computationally intense, clinician-friendly user interfaces can be readily developed to provide speedy, automated diagnostic probability scores based on large normative datasets. With further optimisation, classification frameworks may soon be developed into viable clinical applications to expedite the diagnostic process and categorise individual patients into fine-grained diagnostic, phenotypic and prognostic categories. Recent advances in the field indicate a paradigm shift in the clinical role of neuroimaging in FTLD which has evolved from merely out ruling alternative diagnoses to the precision computational interpretation of single-subject data.

Machine-learning algorithms are likely to become an integral part of the diagnostic process in FTLD, patient stratification in pharmaceutical trials, and assigning patients into prognostic categories. Existing models will no doubt be optimised further and the sample size limitations of current studies will be overcome through international collaboration. While model development will continue to be spearheaded by academic experts, and large training datasets will be compiled by international consortia, user-friendly interfaces are likely to be developed for clinicians to interpret their patients' imaging data on cloud-based solutions. Instead of providing a definite diagnostic label for clinicians, future ML applications will provide diagnostic

probability values. Pioneering ML applications currently only trialled in the academic setting are likely to filter down to routine clinical care. In neurodegenerative conditions, we are likely to witness a paradigm shift from the visual inspection of medical images to the quantitative interpretation of spatially-coded data using automated computational methods. The continued refinement and optimisation of ML applications will undoubtedly curtail the diagnostic journey of patients with neurodegenerative conditions and facilitate an earlier entry into clinical trials.

1.5 Conclusions

Single-subject imaging data interpretation is an emerging field of neuroimaging which is a rapidly developing interface of clinical neurology, academic radiology and applied mathematics. Emerging frameworks have demonstrated the potential of observer-independent subject classification, but considerable improvements are needed before these methods can be integrated into routine clinical practice. Optimised machine-learning methods show the promise of accurately classifying single subjects into diagnostic groups, prognostic categories and detecting pre-manifest neurodegenerative change in mutation carriers. The landmark studies reviewed in this paper herald a paradigm shift from group-level radiological descriptions to pragmatic clinical applications.

2 Pre-symptomatic radiological changes in frontotemporal dementia: implications for clinical trials

2.1 Introduction

Frontotemporal dementia (FTD) incorporates a wide range of neurodegenerative disorders that present with diverse clinical phenotypes, radiological signatures, and underlying molecular pathology. A genetic cause is determined in approximately 30% of cases [175]. The most common genotypes include autosomal dominant mutations in chromosome 9 open reading frame 72 (*C9orf72*), progranulin (*GRN*), or microtubule-associated protein tau (*MAPT*) genes. In recent years, there have been concerted efforts to characterise the sequential cascade of clinical, imaging and biofluid alterations in the pre-symptomatic phase of familial FTD [176]. These initiatives help to capture accruing disease-burden before it is clinically evident and imaging data provide additional insights on anatomical patterns of disease propagation. The practical aspiration of presymptomatic studies is to ascertain potential prognostic indicators, predict the clinical phenotype, forecast phenoconversion and suggest a window for viable therapeutic intervention. Given the increasing recognition of the clinical relevance of presymptomatic changes in familial FTD, the radiology literature of pre-symptomatic FTD is systematically reviewed.

2.2 Methods

A systematic literature review was conducted using the MEDLINE database in accordance with the Preferred Reporting Items for Systematic Reviews and Meta-Analyses (PRISMA) recommendations. The core search

terms ‘frontotemporal dementia’, ‘FTD’, ‘frontotemporal lobar degeneration’ or ‘FTLD’ were individually combined with the keywords ‘pre-symptomatic’, ‘presymptomatic’, ‘asymptomatic’, ‘pre-clinical’, ‘prodromal’ or ‘pre-manifest’. This was followed by searching these pairings in combination with ‘magnetic resonance imaging’, ‘MRI’, ‘positron emission tomography’, ‘PET’, ‘MR spectroscopy’, ‘MRS’, ‘brain imaging’ or ‘neuroimaging’. The database search was limited to human studies written in English. It was last accessed in April 2022. Duplicate records were removed. A single reviewer individually screened and assessed the 116 records for eligibility. The inclusion criteria consisted of original research papers that investigated pre-symptomatic radiological changes in the most common FTD genotypes: *C9orf72*, *GRN* and *MAPT*. Additional relevant records were identified from reference lists. Based on the above criteria a total of 68 eligible records were reviewed, grouped according to genotype and stratified according to imaging modality **(Figure 3).**

Figure 3: A PRISMA flowchart for systematic review of pre-symptomatic radiological changes in FTD

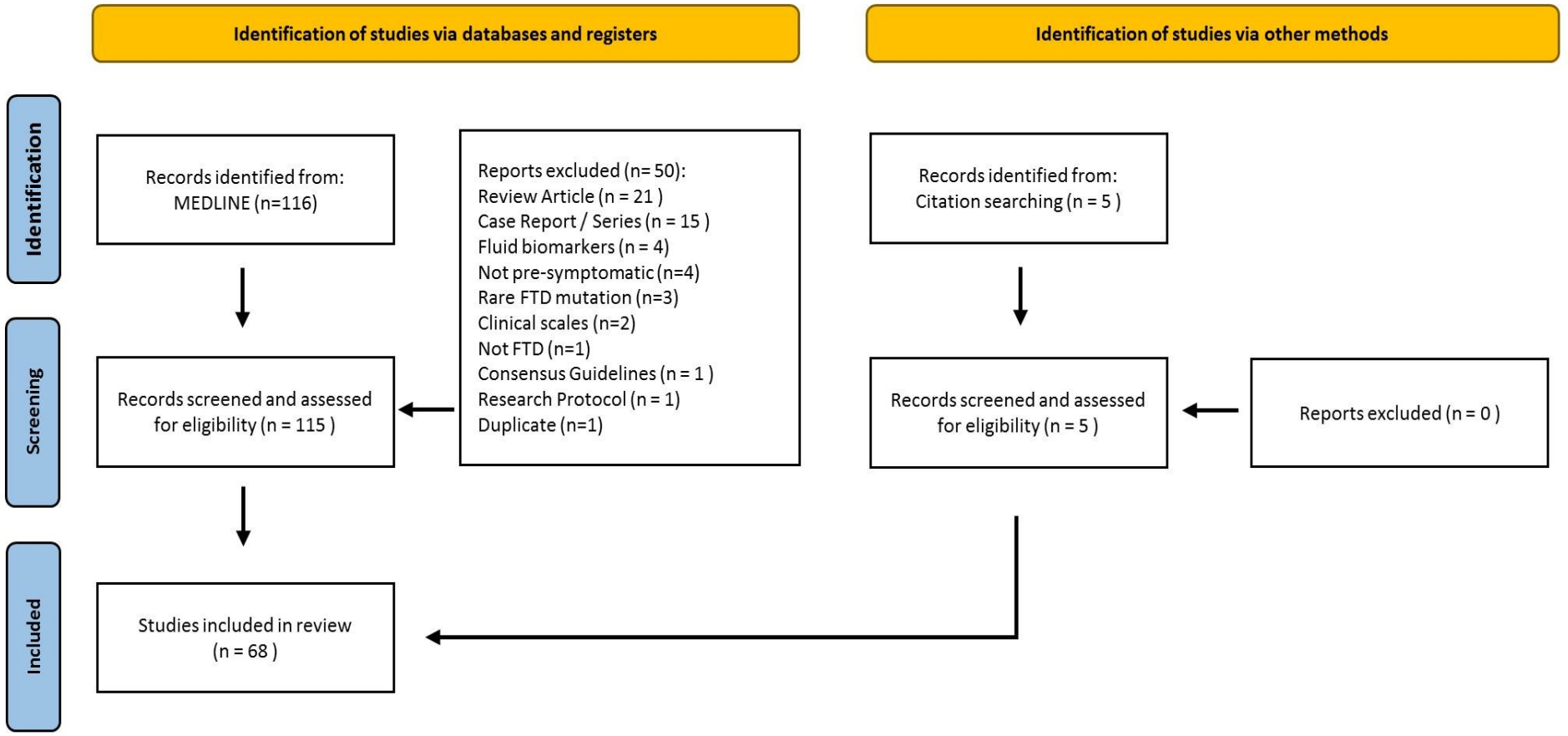

2.3 Results

Based on the above search criteria, 68 original research studies were identified that investigated pre-symptomatic radiological changes in *C9orf72*, *GRN* and *MAPT* mutation carriers **(Figure 3; Table 2)**. There were 26 studies that included more than one genotype; 15 studies investigated only *C9orf72* mutation carriers; 18 studies enrolled only *GRN* mutation carriers; and 9 studies evaluated only *MAPT* mutation carriers. The median (range) sample size for all genotypes was 15 (3-141); for *C9orf72* mutation carriers it was 28 (3-108); for *GRN* mutation carriers it was 32 (5-142); and for *MAPT* mutation carriers it was 13 (3-54). Only a minority of studies (28%) had a longitudinal design with a median (range) follow-up interval of 2 (1-8) years. Most of the studies relied on a single imaging modality (66%). The most common data acquisition technique was MRI (97%) that was interpreted in grey matter analyses (75%), white matter analyses (34%), functional analyses (29%) and spectroscopy (4%). There was a paucity of PET imaging studies (12%). Identified studies are first stratified according to the underlying genotype and then discussed from a methodological, academic and clinical viewpoint.

Table 2: Study characteristics of pre-symptomatic neuroimaging initiatives in the most common FTD genotypes

	All genotypes	***MAPT***	***C9orf72***	***GRN***
Reviewed Studies	68	34	37	43
% of studies from database	100% (68/68)	50% (34/68)	54% (37/68)	63% (43/68)
Sample size per genotype - Average	23	18	36	47
Sample size per genotype - Median	15	13	28	32
Sample size per genotype - Range	(3-141)	(3-54)	(3-108)	(5-142)
Longitudinal	28% (19/68)	30% (10/34)	30% (11/37)	28% (12/43)
Follow-up – Average (years)	2.6	3.5	2	2.7
Follow-Up – Median (years)	2	3	1.5	2
Follow up – Range (years)	(1-8)	(1-8)	(1-6)	(1-6)
Multimodal % (n)	44% (30/68)	29% (10/34)	35% (13/37)	42% (18/43)
MRI % (n)	97% (66/68)	97% (33/34)	97% (36/37)	100% (43/43)
Grey Matter Analyses % (n)	75% (51/68)	68% (23/34)	81% (29/36)	81% (35/43)
White Matter Analyses % (n)	34% (23/68)	26% (9/34)	33% (12/36)	30% (13/43)
Functional MRI % (n)	29% (20/68)	29% (10/34)	25% (9/36)	37% (16/43)
MR Spectroscopy % (n)	4% (3/68)	9% (3/34)	0% (0/36)	0% (0/43)
PET % (n)	12% (8/68)	9% (3/34)	8% (3/37)	5% (2/43)

2.3.1 *C9orf72*

The majority of radiological studies of pre-symptomatic *C9orf72* GGGGCC repeat expansion carriers describe widespread structural and functional changes. It remains debated whether such findings represent neurodevelopmental or neurodegenerative change given the early onset and relatively slow progression [177]. It has been proposed that radiological changes may begin in the thalamus and posterior cortical regions, later involving the frontotemporal regions, and may be identified up to 25 years before symptom onset [22]. Preliminary multimodal MRI classification models have shown that individual radiological changes may not be evident until a few years before symptom onset in pre-symptomatic FTD mutation carriers [63]. We next discuss the evidence of pre-symptomatic radiological changes in *C9orf72* repeat expansion mutation carriers **(Table 3)**.

Widespread cortical and subcortical grey matter (GM) pathology is often detected but may be too subtle for visual detection [178]. Cortical thinning is observed in the frontal [179-181], temporal [179, 180, 182], parietal [179-182], and occipital cortices [182]. Volume loss is relatively symmetrical [183], involving the frontal [22, 156, 181, 183-187], temporal [22, 156, 181, 183, 184, 186-188], parietal [156, 181, 183, 184, 188], insular [22, 181, 183, 185-187], cerebellar [22, 156, 181, 183, 188, 189] regions. Relatively selective cerebellar involvement has been suggested by some [189] with the preferential degeneration of lobules VIIa, VIIb, Crus I and II [156, 183]. In an admixed group of pre-symptomatic FTD mutation carriers, there is also early change in ventricular volume compared to controls [190]. Subcortical [191] degeneration has been recently further characterised by reports of preferential degenerative change in specific subcortical sub-regions. Focal

thalamic changes [22, 156, 179, 181, 183-186, 188, 192, 193] have been described in the anterior [192, 193], laterodorsal [183], lateral geniculate nuclei [183] as well as in pulvinar regions [183]. Preferential caudate [179, 182, 187], putamen [182, 183, 187], amygdala [183, 187, 194] and hypothalamus [183] pathology has also been described. In some studies degenerative changes were only detected in older cohorts aged >40 years [188]. This trend of progressive changes in older subgroups was shown in a study that described widespread changes in pre-symptomatic cohorts aged >40years compared with those aged <40 years [184]. The rate of cortical thinning has been calculated as either faster [180] or no different [195] compared to controls. Patterns of atrophy have been evaluated [186] to predict phenoconversion [112]. The level of educational attainment [196, 197] and *TMEM106B* genotype [197] are considered to be modifying factors. Some pre-symptomatic structural changes are thought to be associated with early behavioural changes; apathy has been linked to frontal and cingulate pathology [198]; and impaired social cognition to insula, basal ganglia, amygdala, and frontotemporal involvement [187]. In addition to standard morphometric and volumetric GM methods, a number of novel analysis pipelines have also been implemented. Early abnormal gyrification index has been described in the left anterior cingulate cortex, left precentral gyrus, right inferior parietal, and right superior occipital regions decades before expected symptom onset [199]. This anatomical pattern is similar to the focal regions of atrophy described in both pre-symptomatic and symptomatic cases, despite no corresponding cortical thickness abnormalities detected in this study [199]. Neurite orientation dispersion and density imaging (NODDI) also detected more widespread GM abnormalities in frontal, temporal parietal, occipital and insular regions

compared to conventional volumetric measures [200]. Reduced cortical surface area has been described in a similar but more restricted anatomical distribution to symptomatic cohorts, particularly in the ventrofrontal regions [180]. It is noteworthy that a minority of published studies do not detect any pre-symptomatic GM pathology [195, 201-203].

Widespread WM degeneration has been repeatedly described in pre-symptomatic *C9orf72* repeat expansion carriers typically involving the corpus callosum [184, 204], thalamic radiation [181, 184, 188], uncinate fasciculus [185], superior longitudinal fasciculus [181], inferior longitudinal fasciculus [185], corticospinal tracts [181, 185, 205], orbitofrontal regions [204] and other frontal WM tracts [181, 185, 188]. These structural changes may be associated with incipient executive dysfunction, specifically reduced verbal fluency [204]. It is proposed that WM pathology may precede or occur in tandem with GM degeneration [184, 188, 204, 205]. Recent MRI classification models in pre-symptomatic FTD mutation carriers indicate that the earliest radiological changes occur in the WM because WM features offer the best discriminating value from controls [62]. Longitudinal studies have shown strikingly inconsistent results depending on cohort and region of interest (ROI) characteristics. In pre-symptomatic *C9orf72* carriers aged >40 years, significant baseline cervical spinal cord WM atrophy was described, with ensuing corticospinal tract (CST) FA reductions on interval imaging over an 18-month period [205]. In contrast, no significant progression of brain imaging changes were identified over a 12-month follow-up period [204]. Similar to GM analyses, novel WM methods have also been increasingly implemented. Neurite orientation dispersion and density imaging (NODDI) readily detects corticospinal and frontotemporal WM tracts

abnormalities with greater sensitivity than standard diffusivity metrics in pre-symptomatic *C9orf72* cohorts [200]. A minority of studies do not detect any pre-symptomatic diffusivity abnormalities [195]. However, subtle internal capsule (IC) and the corpus callosum (CC) changes may be detected on longitudinal follow-up in some of these studies [195]. The pre-symptomatic phase of *C9orf72* is not thought to be associated with increased WM hyperintensity burden [206].

Functional imaging changes are also evident several years before symptom onset [185, 202, 207, 208], sometimes preceding the detection of structural imaging abnormalities [195, 202]. [^{18}F] FDG-PET studies demonstrate significant frontotemporal hypometabolism in the insular cortex, central opercular cortex, basal ganglia and thalami [202, 209], with the additional involvement of the inferior parietal lobes and adjacent regions [202]. A [^{11} C]UCB-J PET study has shown pre-symptomatic synaptic density reduction in the thalamus that was most marked in pulvinar and ventral-posterior regions with progressive cortical and subcortical loss of synaptic density [210]. Preliminary studies using arterial spin labelling (ASL) have described cerebral hypoperfusion in the insula, orbitofrontal, anterior cingulate, temporal and inferior parietal cortices up to 12.5 years before expected symptom onset [211]. Functional connectivity alterations have also been described [185, 195] that may [195] or may not [185] occur with associated structural changes. A longitudinal study described increased sensorimotor network connectivity adjacent to regions which later become affected in symptomatic cohorts [195]. In contrast, reduced functional connectivity has been described in thalamic, frontotemporal and motor networks in a less extensive but similar anatomical distribution to symptomatic cohorts [212]. It is hypothesised that the maintenance of functional

network topography facilitates cognitive resilience in face of relentless structural changes [208, 213]. The integrity of these functional networks then rapidly declines as patients become symptomatic [208].

Table 3: Imaging studies of pre-symptomatic *C9orf72* mutation carriers

First author, year of publication	Study groups and cohort sizes	Study design	Follow-up	Imaging methods
Structural MRI				
Bertrand et al, 2018 [184]	Pre-symptomatic *C9orf72* n= 41 Controls n=39	Cross-sectional Case control	N/A	MRI – TIV, DTI
Bocchetta et al, 2021[183]	Pre-symptomatic: *C9orf72* n=107; *MAPT* n=47; *GRN* n=125 Symptomatic: *C9orf72* n=63; *MAPT* n=20; *GRN* n=43 Controls n=298	Cross-sectional Case control	N/A	MRI – Cortical and subcortical volumes
Cash et al, 2018[156]	Pre-symptomatic: *C9orf72* n=40; *MAPT* n=23; *GRN* n=65 Symptomatic: *C9orf72* n=25; *MAPT* n=10; *GRN* n=12 Controls n=144	Cross-sectional Case control	N/A	MRI - VBM
Caverzasi et al, 2019 [199]	Pre-symptomatic *C9orf72* n=15 Controls n=67	Cross-sectional Case control	N/A	MRI – Cortical thickness, local gyrification index
Convery et al, 2020[203]	Pre-symptomatic: *C9orf72* n=73; *MAPT* n=39; *GRN* n=104 Symptomatic: *C9orf72* n=31; *MAPT* n=10; *GRN* n=24 Controls n=181	Cross-sectional Case control	N/A	MRI - VBM
Cury et al, 2019[192]	Pre-symptomatic: *C9orf72* n=72; *MAPT* n=8; *GRN* n=53 Controls n= 98	Cross-sectional Case control	N/A	MRI – Large diffeomorphic deformation metric mapping
Floeter et al, 2016 [201]	Pre-symptomatic: *C9orf72* n= 7 Symptomatic *C9orf72* n=20 Sporadic ALS n=22 Controls n=28	Longitudinal Case-control	6-18 months	MRI – Cortical thickness and volumetry
Fumagalli et al, 2018[178]	Pre-symptomatic: *C9orf72* n=42; *MAPT* n=24; *GRN* n=66 Symptomatic: *C9orf72* n=31; *MAPT* n=15; *GRN* n=17 Controls n=148	Cross-sectional Case control	N/A	MRI- VBM
Gazzina et al, 2019[196]	Pre-symptomatic: *C9orf72* n=31; *MAPT* n=20; *GRN* n=65 Controls n=113	Longitudinal Case-control	4 years	MRI – GM volume
Le Blanc et al, 2020 [180]	Pre-symptomatic *C9orf72* n=83 Symptomatic *C9orf72* n= 54 Control n=249	Cross-sectional Case control	N/A	MRI – Cortical thickness, cortical surface area

First author, year of publication	Study groups and cohort sizes	Study design	Follow-up	Imaging methods
Structural MRI				
Lulé et al, 2020[204]	Pre-symptomatic *C9orf72* n=21; *SOD1* n=15 Controls n=91	Longitudinal Case-control	12-months	MRI - DTI
Malpetti et al, 2021[198]	Pre-symptomatic *C9orf72* n=108, *MAPT* n=54, *GRN* n=142 Controls n=296	Longitudinal Case-control	2-years	MRI – GM volume
Olney et al, 2020[186]	Pre-symptomatic mutation carriers n=103 Mild symptomatic carriers n=43 Dementia n=72 Controls n=102	Cross-sectional Case control	N/A	MRI – Cortical volumes
Panman et al, 2019[181]	Pre-symptomatic *C9orf72* n=12, *MAPT* n=15, *GRN* n=33 Controls n=53	Longitudinal Case-control	2-years	MRI – VBM, Cortical thickness, DTI
Papma et al, 2017 [188]	Pre-symptomatic *C9orf72* n=18 Control n=15	Cross-sectional Case control	N/A	MRI – VBM, DTI
Popuri et al, 2018[179]	Pre-symptomatic *C9orf72* n=15, *GRN* n=9 Controls n=38	Cross-sectional Case control	N/A	MRI – Cortical thickness, subcortical volumes
Premi et al, 2017[197]	Pre-symptomatic *C9orf72* n=33, *MAPT* n=14, *GRN* n=61 Controls n=123	Cross-sectional Case control	N/A	MRI – Cortical, subcortical and cerebellar volumes
Querin et al, 2019 [205]	Pre-symptomatic *C9orf72* n= 40 Controls n=32	Longitudinal Case-control	18-months	MRI – Total, GM and WM cervical spinal cord CSA, DTI
Rohrer et al, 2015[22]	Pre-symptomatic *C9orf72* n=18, *MAPT* n=15, *GRN* n=45 Symptomatic *C9orf72* n=16, *MAPT* n=11, *GRN* n=13 Controls n=102	Cross-sectional Case control	N/A	MRI – Cortical and subcortical volumes
Russell et al, 2020[187]	Pre-symptomatic *C9orf72* n=106, *MAPT* n=49, *GRN* n=123 Symptomatic *C9orf72* n=53, *MAPT* n=18, *GRN* n=32	Cross-sectional	N/A	MRI - VBM
Staffaroni et al 2021[112]	Pre-symptomatic mutation carriers n=46 Symptomatic mutation carriers n=81 Controls n=101 Reference n=383	Longitudinal	2-years	MRI – GM volume

First author, year of publication	Study groups and cohort sizes	Study design	Follow-up	Imaging methods
Structural MRI				
Sudre et al, 2017[206]	Pre-symptomatic *C9orf72* n=28, *MAPT* n=8, *GRN* n=25 Symptomatic *C9orf72* n=23, *MAPT* n=13, *GRN* n=7 Controls n= 76	Cross-sectional Case control	N/A	MRI – WMH
Tavares et al, 2019[190]	Pre-symptomatic *C9orf72* n=13, *MAPT* n=4, *GRN* n=29 Controls n= 56	Longitudinal Case-control	1-year	MRI – Ventricular volumes
Walhout et al, 2015 [182]	Pre-symptomatic *C9orf72* n=16 Symptomatic *C9orf72* n=14 Control n=51	Cross-sectional Case control	N/A	MRI – Cortical thickness, subcortical volumes, DTI
Wen et al, 2019[200]	Pre-symptomatic *C9orf72* n=38 Control n=29	Cross-sectional Case control	N/A	MRI – Volumetry, DTI, NODDI
Functional MRI				
Feis et al, 2018[62]	Pre-symptomatic: *C9orf72* n=72; *MAPT* n=8; *GRN* n=35 Controls n = 48	Cross-sectional Case control	N/A	MRI – GMD, WMD, DTI, rs-fMRI
Feis et al, 2019[63]	Pre-symptomatic *C9orf72* n=12, *MAPT* n=8, *GRN* n=35 Controls = 48	Longitudinal Case-control	6-years	MRI- GMD, DTI, rs-fMRI
Lee et al, 2017[185]	Pre-symptomatic *C9orf72* n=15 Control n=15	Cross-sectional Case control	N/A	MRI – VBM, DTI, rs-fMRI
Mutsaerts et al, 2019[211]	Pre-symptomatic *C9orf72* n=34, *MAPT* n=18, *GRN* n=55 Controls n= 113	Cross-sectional Case control	N/A	MRI – ASL
Premi et al, 2019 [207]	Pre-symptomatic *C9orf72* n=82, *MAPT* n=45, *GRN* n=122 Controls n= 223	Cross-sectional Case control	N/A	MRI - rs-fMRI
Rittman et al, 2019[208]	Pre-symptomatic *C9orf72* n=17, *MAPT* n=13, *GRN* n=40 Symptomatic *C9orf72* n=12, *MAPT* n=11, *GRN* n=6 Controls n= 86	Cross-sectional Case control	N/A	MRI - Task-free fMRI
Shoukry et al, 2020 [212]	Pre-symptomatic *C9orf72* n=15 Symptomatic *C9orf72* n=27 Controls n=48	Longitudinal Case-control	6-months 18-months	MRI – rs-fMRI
Tsvetanov et al, 2021[213]	Pre-symptomatic *C9orf72* n= 39, *MAPT* n=19, *GRN* n= 63 Controls n=134	Cross-sectional Case control	N/A	MRI – GM volume, rs-fMRI

First author, year of publication	Study groups and cohort sizes	Study design	Follow-up	Imaging methods
Functional MRI				
Waugh et al, 2021 [195]	Pre-symptomatic *C9orf72* n = 15 Symptomatic *C9orf72* n=27 Controls n=34	Longitudinal Case-control	18-months	MRI – Cortical thickness, volumetry, DTI, rs-fMRI
Positron Emission Tomography				
De Vocht et al, 2020 [209]	Pre-symptomatic *C9orf72* n = 17 Controls n=25	Cross-sectional Case-Control	N/A	[^{18}F] FDG PET-CT
Malpetti et al, 2021[210]	Pre-symptomatic *C9orf72* n = 3 Symptomatic *C9orf72* n=1 Controls n= 19	Cross-sectional Case-Control	N/A	MRI and [^{11} C]UCB-J PET
Popuri et al, 2021 [202]	Pre-symptomatic *C9orf72* n= 15 Controls n=20	Cross-sectional Case-Control	N/A	MRI and [^{18}F] FDG PET-CT

2.3.2 *GRN*

In pre-symptomatic *GRN* mutation carriers, there is ample radiological evidence of structural and functional alterations, typically involving frontal, parietal and subcortical regions in a similar but more restricted pattern to symptomatic cases [20]. These findings may be evident several years before symptom onset but may be very subtle or elude detection for a variety of reasons that are later discussed. They are best detected in mutation carriers who are approaching the expected age of phenoconversion [21]. Herein we summarise the observed pre-symptomatic radiological findings **(Table 4).**

In pre-symptomatic *GRN* mutation carriers, several studies report no difference in cortical or subcortical volumes compared to controls [61, 151, 179, 181, 183, 214-217]. The ability to detect GM pathology may depend on the interval to projected phenoconversion [156, 178] and subtle changes may require longitudinal follow-up for detection [218]. GM degeneration is typically not appreciated on visual rating scales [178]. GM volume loss is thought to first occur in insular regions [22, 156, 176, 219, 220] up to 15-years before symptom onset [22]; followed by frontal [20, 156, 220, 221], parietal [22, 156, 186, 219], temporal [22, 156, 176, 186, 218, 220], occipital [221] and subcortical atrophy [22, 156]. Frontal lobe changes typically involve orbitofrontal [20, 220] and posterior [156] regions; these early alterations may be associated with progressive apathy [198]. The temporal lobe alterations may be predominantly anterior [156, 220], posterior [186], and lateral [218]. Longitudinal studies have detected the greatest rate of atrophy in the pre-symptomatic phase in the frontal [220, 221], parietal [221] and occipital [220] lobes. Characteristic asymmetry [22] and differences in ventricular volumes [190] may be detected a few years before symptom onset. Pre-symptomatic subcortical

changes are also readily detected in *GRN* mutation carriers. Anterior thalamic shape deformation was described at least 5-years before symptom onset [192]. The thalamus and basal ganglia have both been implicated in an admixed group of pre-symptomatic and symptomatic *GRN* mutation carriers [187]. The characterisation of atrophy patterns may be used to discriminate pre-symptomatic and symptomatic FTD mutation carriers [112]. The degree of GM volume loss may be influenced by level of educational attainment [196, 197], which is further modulated by the *TMEM106B* genotype [197]. Other modifiers include high leukocyte mRNA levels of inflammation-related *TMEM40* and *LY6G6F* that are associated with greater parietal and superior frontal lobe atrophy respectively [222].

Pre-symptomatic *GRN* mutation carriers also exhibit extensive WM degeneration [21] which may be evident several years before symptom onset [20] and rapidly progresses prior to phenoconversion [21]. The loss of WM integrity detected by diffusivity metrics typically involves the corpus callosum [21, 220], superior longitudinal fasciculus [20, 176, 220], corticospinal tracts [20, 220], the cingulum [20], uncinate [151, 176] and inferior occipitofrontal fasciculi [151]. There is progressive WM degeneration that is maximal in the genu of the corpus callosum [21, 220] and the right-sided superior longitudinal fasciculus [220] in the 2-years prior to symptom onset [21]. Patterns of preferential WM vulnerability depend on the subsequent clinical phenotype, with early involvement of the uncinate fasciculus in non-fluent primary progressive aphasia (nfvPPA) and of the superior longitudinal fasciculus in behavioural variant FTD (bvFTD) [176]. There thought to be an increased burden of WM hyperintensities [223] that accumulate over time, particularly in the periventricular frontal, parietal and

occipital regions [206, 223]. These WM hyperintensities have been linked to executive dysfunction, *TMEM106B* risk genotype, low GM volume, and elevated neurofilament light chains [223]. The sequential order of radiological changes is yet to be determined. Some studies suggest that WM degeneration precedes GM degeneration [62, 176]; while other studies suggest that it occurs simultaneously [21]. The best-performing multimodal MRI classification models use exclusively WM features to categorise individual pre-symptomatic mutation carriers [224], highlighting the superior specificity of WM signatures [62]. This is further supported by data-driven disease progression modelling initiatives that relied on cross-sectional data to estimate the cascade of biomarkers and suggest that WM diffusivity abnormalities preceded GM loss, and that the left hemisphere is involved before the right hemisphere [176]. These diffusivity abnormalities however are typically only detected 2-4 years prior to symptom onset [21]. This may explain why some studies do not detect any WM diffusivity alterations [61, 181], WM volume loss [151] or WM hyperintensities [206] in pre-symptomatic *GRN* mutation carriers. As a consequence, MRI-based classification scores often remain similar to controls until approaching phenoconversion [63].

Pre-symptomatic functional imaging changes have also been described [207]. In [^{18}F] FDG-PET studies, asymmetric cerebral hypometabolism is typically reported involving either the left [218] or right [225] hemisphere – primarily localised to the frontal [218, 225], insular [225] or temporal [218] lobes. Regional cerebral hypometabolism is thought to precede structural imaging changes and may be detected up to 20-years before expected symptom onset [218]. Studies using arterial spin labelling (ASL), a non-invasive method of

quantifying cerebral perfusion, have demonstrated reduced cerebral blood flow in frontal, temporal, parietal and subcortical regions in pre-symptomatic FTD mutation carriers up to 12.5 years before expected symptom onset [211, 226]. In pre-symptomatic *GRN* mutation carriers, asymmetric frontoparietal hypoperfusion involving the bilateral anterior cingulate/paracingulate, right anterior insula/orbitofrontal, and right supramarginal/angular gyri has been reported [211, 226]. Functional connectivity deficits have also been repeatedly described involving the frontal [216, 227], parietal [216, 227], and thalamic [217] regions which may also precede structural deficits [216, 217]. Both decreased and increased functional connectivity have been reported depending on the age profile, education and definition of seed regions. Cognitive reserve is also an important modifying factor [228, 229] which should be considered in the interpretation of clinico-radiological correlations. Altered dynamic functional connectivity with increased activation of the insula and parietal regions has been recently reported [230]. Initial hyperconnectivity involving the salience [214, 217], default mode [217], perirolandic [217] and language networks [217] has been described. The latter was asymmetric with progressively reducing connectivity with age [217]. Other studies identified reduced salience network connectivity [228]. It remains unclear whether increased connectivity represents a compensatory mechanism [217] reduced inhibition or stems from methodological factors [231]. Some studies suggest that the maintenance of functional network organisation contributes to cognitive resilience in face of evolving structural degeneration [208, 213, 232]. The subsequent loss of functional network organisation is associated with emergent cognitive symptoms [208, 213].

While some studies detect complex functional reorganisation, others do not detect functional connectivity alterations [20, 61, 207, 230].

Table 4: Imaging studies of pre-symptomatic *GRN* mutation carriers

First author, year of publication	Study groups and cohort sizes	Study design	Follow-up	Imaging methods
Structural MRI				
Bocchetta et al, 2021[183]	Pre-symptomatic: *C9orf72* n=107; *MAPT* n=47; *GRN* n=125 Symptomatic: *C9orf72* n=63; *MAPT* n=20; *GRN* n=43 Controls n=298	Cross-sectional Case control	N/A	MRI – Cortical and subcortical volumes
Borrego-Écija et al, 2021[215]	Pre-symptomatic *GRN* n=100 Controls n=94	Cross-sectional Case control	N/A	MRI – Cortical thickness
Borroni et al, 2008 [151]	Pre-symptomatic *GRN* n=7 Controls n=15	Cross-sectional Case control	N/A	MRI – VBM, DTI
Cash et al, 2018[156]	Pre-symptomatic: *C9orf72* n=40; *MAPT* n=23; *GRN* n=65 Symptomatic: *C9orf72* n=25; *MAPT* n=10; *GRN* n=12 Controls n=144	Cross-sectional Case control	N/A	MRI - VBM
Chen et al, 2020[221]	Pre-symptomatic *GRN* n=8 Symptomatic *GRN* n=5 Controls n=10	Longitudinal Case-control	3 years	MRI – TBM-SyN
Convery et al, 2020[203]	Pre-symptomatic: *C9orf72* n=73; *MAPT* n=39; *GRN* n=104 Symptomatic: *C9orf72* n=31; *MAPT* n=10; *GRN* n=24 Controls n=181	Cross-sectional Case control	N/A	MRI - VBM
Cury et al, 2019[192]	Pre-symptomatic: *C9orf72* n=72; *MAPT* n=8; *GRN* n=53 Controls n= 98	Cross-sectional Case control	N/A	MRI – Large diffeomorphic deformation metric mapping
Fumagalli et al, 2018[178]	Pre-symptomatic: *C9orf72* n=42; *MAPT* n=24; *GRN* n=66 Symptomatic: *C9orf72* n=31; *MAPT* n=15; *GRN* n=17 Controls n=148	Cross-sectional Case control	N/A	MRI- VBM
Gazzina et al, 2018[219]	Pre-symptomatic *GRN* n=19 Controls n=17	Cross-sectional Case control	N/A	MRI – Cortical volume, thickness and surface area
Gazzina et al, 2019[196]	Pre-symptomatic: *C9orf72* n=31; *MAPT* n=20; *GRN* n=65 Controls n=113	Longitudinal Case-control	4 years	MRI – GM volume
Jiskoot et al, 2019[21]	Pre-symptomatic *GRN* n=30; *MAPT* n=13 Controls n=30	Longitudinal Case-control	4 years	MRI – VBM, DTI
Malpetti et al, 2021[198]	Pre-symptomatic *C9orf72* n=108, *MAPT* n=54, *GRN* n=142 Controls n=296	Longitudinal Case-control	2-years	MRI – GM volume

First author, year of publication	Study groups and cohort sizes	Study design	Follow-up	Imaging methods
Structural MRI				
Milanesi et al, 2013 [222]	Pre-symptomatic *GRN* n=14 Symptomatic *GRN* n=15 FTD *GRN* negative n=16 Controls n=11	Cross-sectional Case control	N/A	MRI - VBM
Olm et al, 2018 [220]	Pre-symptomatic *GRN* n=11 Controls n=11	Longitudinal Case-control	2-years	MRI – GM density, DWI
Olney et al, 2020[186]	Pre-symptomatic mutation carriers n=103 Mild symptomatic carriers n=43 Dementia n=72 Controls n=102	Cross-sectional Case control	N/A	MRI – Cortical volumes
Panman et al, 2019[181]	Pre-symptomatic *C9orf72* n=12, *MAPT* n=15, *GRN* n=33 Controls n=53	Longitudinal Case-control	2-years	MRI – VBM, Cortical thickness, DTI
Panman et al, 2021 [176]	Pre-symptomatic *GRN* n=56 Symptomatic *GRN* n=35 Controls n=35	Cross-sectional	N/A	MRI – Volumetry, DTI
Paternicò et al, 2016[233]	Pre-symptomatic *GRN* n=11 Controls n=11 Symptomatic *GRN* n=14 FTD *GRN* negative n=28 Controls n=15	Cross-sectional Case control	N/A	MRI - WMH
Popuri et al, 2018[179]	Pre-symptomatic *C9orf72* n=15, *GRN* n=9 Controls n=38	Cross-sectional Case control	N/A	MRI – Cortical thickness, subcortical volumes
Premi et al, 2017[197]	Pre-symptomatic *C9orf72* n=33, *MAPT* n=14, *GRN* n=61 Controls n=123	Cross-sectional Case control	N/A	MRI – Cortical, subcortical and cerebellar volumes
Rohrer et al, 2015[22]	Pre-symptomatic *C9orf72* n=18, *MAPT* n=15, *GRN* n=45 Symptomatic *C9orf72* n=16, *MAPT* n=11, *GRN* n=13 Controls n=102	Cross-sectional Case control	N/A	MRI – Cortical and subcortical volumes
Russell et al, 2020[187]	Pre-symptomatic *C9orf72* n=106, *MAPT* n=49, *GRN* n=123 Symptomatic *C9orf72* n=53, *MAPT* n=18, *GRN* n=32	Cross-sectional	N/A	MRI - VBM

First author, year of publication	Study groups and cohort sizes	Study design	Follow-up	Imaging methods
Structural MRI				
Staffaroni et al 2021[112]	Pre-symptomatic mutation carriers n=46 Symptomatic mutation carriers n=81 Controls n=101 Reference n=383	Longitudinal	2-years	MRI – GM volume
Sudre et al, 2017[206]	Pre-symptomatic *C9orf72* n=28, *MAPT* n=8, *GRN* n=25 Symptomatic *C9orf72* n=23, *MAPT* n=13, *GRN* n=7 Controls n= 76	Cross-sectional Case control	N/A	MRI – WMH
Sudre et al, 2019[223]	Pre-symptomatic *GRN* n=101; (Longitudinal n=39) Symptomatic *GRN* n=32; (Longitudinal n=12) Controls n=203; (Longitudinal n=73)	Longitudinal Case-control	Not specified Annual MRI	MRI – GMD, WMH
Tavares et al, 2019[190]	Pre-symptomatic *C9orf72* n=13, *MAPT* n=4, *GRN* n=29 Controls n= 56	Longitudinal Case-control	1-year	MRI – Ventricular volumes
Functional MRI				
Borroni et al, 2012 [214]	Pre-symptomatic *GRN* n=9 Symptomatic *GRN* n=7 FTD *GRN* negative n=16 Controls n=24	Cross-sectional Case control	N/A	MRI – VBM, rs-fMRI
Dopper et al, 2014 [23]	Pre-symptomatic *GRN* n=28; *MAPT* n=9 Controls n=38	Cross-sectional Case control	N/A	MRI – VBM, DTI, rs-fMRI
Dopper et al, 2016 [226]	Pre-symptomatic *GRN* n=23; *MAPT* n=11 Controls n=31	Longitudinal Case-control	2-years	MRI – ASL
Feis et al, 2018[62]	Pre-symptomatic: *C9orf72* n=72; *MAPT* n=8; *GRN* n=35 Controls n = 48	Cross-sectional Case control	N/A	MRI – GMD, WMD, DTI, rs-fMRI
Feis et al, 2019[61]	Pre-symptomatic *GRN* n=28; *MAPT* n=11 Controls = 36	Cross-sectional Case control	N/A	MRI – VBM, DTI, rs-fMRI
Feis et al, 2019[63]	Pre-symptomatic *C9orf72* n=12, *MAPT* n=8, *GRN* n=35 Controls = 48	Longitudinal Case-control	6-years	MRI- GMD, DTI, rs-fMRI
Lee et al, 2019[217]	Pre-symptomatic *GRN* n=14 Pre-clinical *GRN* n=3 Controls n=30	Cross-sectional Case control	N/A	MRI – VBM, Task-free fMRI

First author, year of publication	Study groups and cohort sizes	Study design	Follow-up	Imaging methods
Functional MRI				
Mutsaerts et al, 2019[211]	Pre-symptomatic *C9orf72* n=34, *MAPT* n=18, *GRN* n=55 Controls n= 113	Cross-sectional Case control	N/A	MRI – ASL
Pievani et al, 2014[20]	Pre-symptomatic *GRN* n=5 Controls n=5	Cross-sectional Case control	N/A	MRI – Cortical thickness, DTI, rs-fMRI
Premi et al, 2013 [228]	Pre-symptomatic *GRN* n= 17 Symptomatic *GRN* n= 12 FTD *GRN* negative n=20	Cross-sectional Case control	N/A	MRI - rs-fMRI
Premi et al, 2014 [227]	Pre-symptomatic *GRN* n= 17 Symptomatic *GRN* n= 14 FTD *GRN* negative n=38	Cross-sectional Case control	N/A	MRI – GM volume, rs-fMRI
Premi et al, 2016 [216]	Pre-symptomatic *GRN* n= 17 Symptomatic *GRN* n= 14 Controls n=33	Cross-sectional Case control	N/A	MRI – VBM, rs-fMRI
Premi et al, 2019 [207]	Pre-symptomatic *C9orf72* n=82, *MAPT* n=45, *GRN* n=122 Controls n= 223	Cross-sectional Case control	N/A	MRI - rs-fMRI
Premi et al, 2021 [230]	Pre-symptomatic *GRN* n=141 Controls n=282	Cross-sectional Case-control	N/A	MRI – TIV, rs-fMRI
Rittman et al, 2019[208]	Pre-symptomatic *C9orf72* n=17, *MAPT* n=13, *GRN* n=40 Symptomatic *C9orf72* n=12, *MAPT* n=11, *GRN* n=6 Controls n= 86	Cross-sectional Case control	N/A	MRI - Task-free fMRI
Tsvetanov et al, 2021[213]	Pre-symptomatic *C9orf72* n= 39, *MAPT* n=19, *GRN* n= 63 Controls n=134	Cross-sectional Case control	N/A	MRI – GM volume, rs-fMRI
Positron Emission Tomography				
Caroppo et al, 2015 [218]	Pre-symptomatic *GRN* n = 16 Controls n=17	Longitudinal Case-control	20-months	MRI – Cortical thickness [^{18}F] FDG PET-CT
Jacova et al, 2013 [225]	Pre-symptomatic *GRN* n = 9 Controls n=11	Cross-sectional Case control	N/A	MRI [^{18}F] FDG PET-CT

2.3.3 *MAPT*

Pre-symptomatic *MAPT* mutation carriers exhibit evidence of insidious radiological involvement, typically beginning in the medial temporal lobes, extending to the insula and accelerating 2-years before symptom onset [21, 22, 181, 226, 234]. Multimodal MRI based classification models suggest that individual radiological changes may not detectable until a few years before phenoconversion [63, 224]. Evidence for pre-symptomatic radiological changes in *MAPT* mutation carriers is summarised in **Table 5.**

Pre-symptomatic cortical [22, 181] and subcortical [22, 192] GM pathology may be detected up to 15-years before symptom onset. In the pre-symptomatic phase, cortical changes may be detected in the insula, anterior cingulate, orbitofrontal and medial temporal regions [22, 156, 181, 186, 235]. Medial temporal lobe atrophy may even be detected by visual inspection using visual rating scales [178]. In pre-symptomatic FTD mutation carriers, there is also a difference in ventricular volume [190]. In the minimal and mild symptomatic phase, GM degeneration extends to involve the dorsolateral temporal cortex [183], cingulate cortex and lingual gyrus in the occipital lobe [236]. This peri-symptomatic involvement of the cingulate cortices has been linked to progressive apathy [198]. Subcortical involvement has been described in the anterior thalamus in an admixed group of pre-symptomatic FTD mutation carriers [192]. Amygdalar [22, 183] and hippocampal pathology [22, 181, 183, 237] have been detected in a subgroup of pre-symptomatic *MAPT* carriers, but this is not a universal finding [238]. However, significant differences may only be detected if the volumes of specific subregions are estimated rather than considering the overall volume of the entire structure. For instance, the

selective involvement of the accessory basal and superficial nuclei subregions of the amygdala may be detected before the total volume of the amygdala changes [183]. In pre-symptomatic FTD mutation carriers, the quantification of individual GM patterns may be used to predict disease progression [112, 224]. Level of educational attainment [196, 197] and *TMEM106B* genotype [197] are considered individual modifying factors. In some studies, GM pathology is not detected for a variety of reasons that are later discussed [23, 61, 183].

There is also evidence for genotype-specific patterns of WM degeneration involving the frontotemporal tracts [23]. A longitudinal study of pre-symptomatic *MAPT* mutation carriers demonstrated entorhinal WM pathology that extended into the limbic and frontotemporal projections after phenoconversion [239]. Loss of WM integrity has also been described in the bilateral uncinate fasciculus, left anterior thalamic radiation, left inferior fronto-occipital fasciculus [23, 181] evolving 2-years before phenoconversion, but not earlier than this [21]. While the involvement of the uncinate fasciculus is not unique to this genotype, it was more markedly involved in pre-symptomatic *MAPT* mutation carriers compared to *GRN* mutation carriers [21]. In contrast, another study only found uncinate involvement in symptomatic cases [239]. The chronology of sequential GM and WM pathology is not well defined. Multimodal MRI classification studies indicate that the earliest pre-symptomatic changes are WM alterations in FTD mutation carriers [62]; whereas other studies suggest simultaneous GM and WM pathology, with predominant loss of WM integrity [21]. Conversely, frank diffusivity abnormalities may not be readily identified in pre-symptomatic *MAPT*

mutation carriers [21, 61, 236] and no marked WM hyperintensity burden has been detected [206].

MR spectroscopy studies have suggested a relatively stereotyped sequence of events, beginning with increased m-Ins/Cr ratio (indicators of glial activity), followed by decreased NAA/m-Ins ratio (markers of loss of neuronal integrity) and subsequent atrophy [240]. MRS studies of presymptomatic *MAPT* mutation carriers are predominantly single voxel studies focusing on different regions of interests (ROIs) such as the posterior cingulate gyrus inferior precuneus [234, 238] or medial frontal lobe [241]. Similar to structural findings, these radiological changes accelerate in the 2-years preceding symptom onset [234]. Cross-sectional studies have reported divergent results of NAA/Cr ratios: some studies have demonstrated decreased NAA/Cr ratios in the medial frontal lobe [241]; and other studies have shown no difference in the posterior cingulate gyrus inferior precuneus [238]. Given that decreased NAA/Cr ratio is a relatively consistent finding in symptomatic *MAPT* mutation carriers, these findings may signal impending phenoconversion [238].

Pre-symptomatic PET studies have used different radiotracers. An [^{18}F] flortaucipir PET study showed slightly elevated binding in the insula, frontal, parietal and medial temporal lobe indicating tau pathology [242], A multi-modal PET study showed dopaminergic dysfunction in the putamen using l-[β-^{11}C]dopa PET, and variable levels of glial activation using [^{11}C]DAA1106 PET in the frontal, occipital and posterior cingulate cortices [237]. An [^{18}F] FDG-PET study demonstrated anterior cingulate hypometabolism [235]. Studies using arterial spin labelling have detected a trend of relatively symmetrical perfusion reduction in the frontal and subcortical areas in *MAPT* mutation

carriers [226] up to 12.5 years before expected symptom onset [211]. fMRI studies have supported the notion of accruing radiological findings prior to phenoconversion [207, 226]. Altered functional connectivity has been reported in the default mode network preceding structural atrophy [148]. It has been repeatedly proposed that preserved functional network integrity enables cognitive resilience in the setting of pre-symptomatic functional and structural radiological abnormalities [208, 213]. It is noteworthy however that pre-symptomatic functional connectivity alterations may not readily detected in *MAPT* mutation carriers [23, 61].

Table 5: Imaging studies of pre-symptomatic *MAPT* mutation carriers

First author, year of publication	Study groups and cohort sizes	Study design	Follow-up	Imaging methods
Structural MRI				
Bocchetta et al, 2021[183]	Pre-symptomatic: *C9orf72* n=107; *MAPT* n=47; *GRN* n=125 Symptomatic: *C9orf72* n=63; *MAPT* n=20; *GRN* n=43 Controls n=298	Cross-sectional Case control	N/A	MRI – Cortical and subcortical volumes
Cash et al, 2018[156]	Pre-symptomatic: *C9orf72* n=40; *MAPT* n=23; *GRN* n=65 Symptomatic: *C9orf72* n=25; *MAPT* n=10; *GRN* n=12 Controls n=144	Cross-sectional Case control	N/A	MRI - VBM
Chen et al, 2019[239]	Pre-symptomatic *MAPT* n=12 Symptomatic *MAPT* n=10 Controls n=20	Longitudinal Case-control	4-years	MRI - DTI
Convery et al, 2020[203]	Pre-symptomatic: *C9orf72* n=73; *MAPT* n=39; *GRN* n=104 Symptomatic: *C9orf72* n=31; *MAPT* n=10; *GRN* n=24 Controls n=181	Cross-sectional Case control	N/A	MRI - VBM
Cury et al, 2019[192]	Pre-symptomatic: *C9orf72* n=72; *MAPT* n=8; *GRN* n=53 Controls n= 98	Cross-sectional Case control	N/A	MRI – Large diffeomorphic deformation metric mapping
Domínguez-Vivero et al, 2020[236]	Pre-clinical *MAPT* n=12; (Pre-symptomatic n=6/12) Controls n=44	Cross-sectional Case-Control	N/A	MRI – VBM, WMH, DTI
Fumagalli et al, 2018[178]	Pre-symptomatic: *C9orf72* n=42; *MAPT* n=24; *GRN* n=66 Symptomatic: *C9orf72* n=31; *MAPT* n=15; *GRN* n=17 Controls n=148	Cross-sectional Case control	N/A	MRI- VBM
Gazzina et al, 2019[196]	Pre-symptomatic: *C9orf72* n=31; *MAPT* n=20; *GRN* n=65 Controls n=113	Longitudinal Case-control	4 years	MRI – GM volume
Jiskoot et al, 2019[21]	Pre-symptomatic *GRN* n=30, *MAPT* n=13 Controls n=30	Longitudinal Case-control	4-years	MRI – VBM, DTI
Malpetti et al, 2021[198]	Pre-symptomatic *C9orf72* n=108, *MAPT* n=54, *GRN* n=142 Controls n=296	Longitudinal Case-control	2-years	MRI – GM volume
Olney et al, 2020[186]	Pre-symptomatic mutation carriers n=103 Mild symptomatic carriers n=43 Dementia n=72 Controls n=102	Cross-sectional Case control	N/A	MRI – Cortical volumes

First author, year of publication	Study groups and cohort sizes	Study design	Follow-up	Imaging methods
Structural MRI				
Panman et al, 2019[181]	Pre-symptomatic *C9orf72* n=12, *MAPT* n=15, *GRN* n=33 Controls n=53	Longitudinal Case-control	2-years	MRI – VBM, Cortical thickness, DTI
Premi et al, 2017[197]	Pre-symptomatic *C9orf72* n=33, *MAPT* n=14, *GRN* n=61 Controls n=123	Cross-sectional Case control	N/A	MRI – Cortical, subcortical and cerebellar volumes
Rohrer et al, 2015[22]	Pre-symptomatic *C9orf72* n=18, *MAPT* n=15, *GRN* n=45 Symptomatic *C9orf72* n=16, *MAPT* n=11, *GRN* n=13 Controls n=102	Cross-sectional Case control	N/A	MRI – Cortical and subcortical volumes
Russell et al, 2020[187]	Pre-symptomatic *C9orf72* n=106, *MAPT* n=49, *GRN* n=123 Symptomatic *C9orf72* n=53, *MAPT* n=18, *GRN* n=32	Cross-sectional	N/A	MRI - VBM
Staffaroni et al 2021[112]	Pre-symptomatic mutation carriers n=46 Symptomatic mutation carriers n=81 Controls n=101 Reference n=383	Longitudinal	2-years	MRI – GM volume
Sudre et al, 2017[206]	Pre-symptomatic *C9orf72* n=28, *MAPT* n=8, *GRN* n=25 Symptomatic *C9orf72* n=23, *MAPT* n=13, *GRN* n=7 Controls n= 76	Cross-sectional Case control	N/A	MRI – WMH
Tavares et al, 2019[190]	Pre-symptomatic *C9orf72* n=13, *MAPT* n=4, *GRN* n=29 Controls n= 56	Longitudinal Case-control	1-year	MRI – Ventricular volumes
Functional MRI				
Dopper et al, 2014[23]	Pre-symptomatic *GRN* n=28, *MAPT* n=9 Controls n=38	Cross-sectional Case control	N/A	MRI – VBM, DTI rs-fMRI
Dopper et al, 2016 [226]	Pre-symptomatic *GRN* n = 23, *MAPT* n = 11 Controls n=31	Longitudinal Case-control	2-years	MRI – ASL
Feis et al, 2018[62]	Pre-symptomatic: *C9orf72* n=72; *MAPT* n=8; *GRN* n=35 Controls n = 48	Cross-sectional Case control	N/A	MRI – GMD, WMD, DTI rs-fMRI
Feis et al, 2019[61]	Pre-symptomatic *GRN* n=28, *MAPT* n=11 Controls = 36	Cross-sectional Case control	N/A	MRI – VBM, DTI rs-fMRI
Feis et al, 2019[63]	Pre-symptomatic *C9orf72* n=12, *MAPT* n=8, *GRN* n=35 Controls = 48	Longitudinal Case-control	6-years	MRI- GMD, DTI, rs-fMRI

First author, year of publication	Study groups and cohort sizes	Study design	Follow-up	Imaging methods
Functional MRI				
Mutsaerts et al, 2019[211]	Pre-symptomatic *C9orf72* n=34, *MAPT* n=18, *GRN* n=55 Controls n= 113	Cross-sectional Case control	N/A	MRI – Arterial spin labelling
Premi et al, 2019 [207]	Pre-symptomatic *C9orf72* n=82, *MAPT* n=45, *GRN* n=122 Controls n= 223	Cross-sectional Case control	N/A	MRI - rs-fMRI
Rittman et al, 2019[208]	Pre-symptomatic *C9orf72* n=17, *MAPT* n=13, *GRN* n=40 Symptomatic *C9orf72* n=12, *MAPT* n=11, *GRN* n=6 Controls n= 86	Cross-sectional Case control	N/A	MRI - Task-free fMRI
Tsvetanov et al, 2021[213]	Pre-symptomatic *C9orf72* n= 39, *MAPT* n=19, *GRN* n= 63 Controls n=134	Cross-sectional Case control	N/A	MRI – GM volume, rs-fMRI
Whitwell et al, 2011[148]	Pre-symptomatic *MAPT* n=8 bvFTD n=21 Controls n=8; Controls n=21	Cross-sectional Case-Control	N/A	fMRI
Magnetic Resonance Spectroscopy				
Chen et al, 2019[234]	Pre-symptomatic *MAPT* n=8	Longitudinal	8-years	Single voxel ^{1}H MRS; posterior cingulate
Chen et al, 2019[241]	Pre-symptomatic *MAPT* n=9 Symptomatic *MAPT* n=10 Controls n=25	Cross-sectional Case-Control	N/A	Single voxel ^{1}H MRS; medial frontal lobe
Kantarci et al, 2010[238]	Pre-symptomatic *MAPT* n=14 Symptomatic *MAPT* n=10 Controls n=24	Cross-sectional Case-Control	N/A	Single voxel ^{1}H MRS; posterior cingulate, inferior precuneus
Positron Emission Tomography				
Clarke et al, 2021[235]	Pre-symptomatic *MAPT* n=6 Controls n=12	Cross-sectional Case-Control	N/A	[^{18}F] FDG-PET-CT: Regional standard uptake value ratios
Miyoshi et al, 2010 [237]	Pre-symptomatic *MAPT* n=3 Controls n=9	Cross-sectional Case-Control	N/A	[^{11}C] DAA1106 PET l-[β-^{11}C] dopa PET [^{11}C] N-methylpiperidin-4-yl acetate PET
Wolters et al, 2021[242]	Pre-symptomatic *MAPT* n= 6 Symptomatic *MAPT* n=3 AD n=52 Controls n=30	Cross-sectional Case-Control	N/A	[^{18}F] flortaucipir PET scan

2.4 Discussion

There is a consensus in the literature that pre-symptomatic structural and functional imaging changes may be detected in *C9orf72*, *GRN*, and *MAPT* mutation carriers several years before expected symptom onset, which become particularly marked in the period leading up to phenoconversion. A multitude of imaging methods has been successfully implemented in presymptomatic gene carriers and the various modalities not only offer complementary information but are relatively consistent with regards to anatomical patterns of preferential vulnerability. Despite considerable methodological differences, focus on diverse ROIs, and divergent cohort characteristics, consensus study findings can be identified. In pre-symptomatic *C9orf72* mutation carriers, there is widespread cortical and subcortical GM involvement beginning in the thalamus and posterior cortical regions, gradually involving the frontotemporal regions. This is coupled with extensive WM degeneration, frontotemporal hypometabolism and altered functional connectivity involving thalamic, frontotemporal and motor networks. In pre-symptomatic *GRN* mutation carriers, there is relatively asymmetric cortical and subcortical GM pathology often spreading from insular regions, gradually involving frontal, parietal, temporal and thalamic brain regions. There is also extensive WM degeneration in particular at the genu of the corpus callosum, increased WM hyperintensity burden, asymmetric frontotemporal hypometabolism and altered functional connectivity in thalamic, frontal and parietal circuits. In pre-symptomatic *MAPT* mutation carriers, there is more focal GM involvement centred on the medial temporal lobe, later involving the insula and frontal regions. WM

degeneration in pre-symptomatic *MAPT* is particularly marked in the uncinate fasciculus. There is also ample evidence of frontal and subcortical hypometabolism and altered functional connectivity involving frontal networks. Multi-parametric imaging studies also offer insights regarding the likely chronology of radiological changes and biological cascades preceding phenoconversion **(Figure 4).** While there is no definite consensus on a specific timeline, there are indications of early metabolic and functional changes followed by structural degeneration before symptom onset. Classification studies have consistently highlighted that WM features best discriminate pre-symptomatic mutation carriers from controls suggesting that WM alterations are relatively specific and early radiological features.

It is increasingly debated whether pre-symptomatic radiological changes, particularly in *C9orf72* mutation carriers, may represent early neurodegeneration or neurodevelopmental abnormalities [177, 243]. In favour of neurodegeneration, *C9orf72* mutation carriers exhibit a slowly evolving progressive radiological profile that is considered to represent the insidious pathological process several decades before symptom onset [183, 184]. Moreover, there are well described patterns and stages of pTDP-43 pathology in *C9orf72* mutation carriers [244]. In favour of a neurodevelopmental process, the trajectory of structural and functional imaging deficits in *C9orf72* mutation carriers is deemed to be relatively similar to expected age-related changes observed in controls [185, 199]. Some longitudinal studies do not detect progression, albeit short follow-up intervals may be ill-suited to detect subtle progressive changes [181]. In addition, animal studies suggest that *C9orf72* protein plays a fundamental role in central nervous system development [245]

and have observed altered synaptic structure in *C9orf72* mutation carriers [246]. The reality may lie somewhere in-between with pre-symptomatic radiological changes capturing both early phases of neurodegeneration superimposed on pre-existing neurodevelopmental abnormalities [177].

Figure 4: A schematic diagram of the likelihood of detecting radiological change in pre-symptomatic FTD genotypes

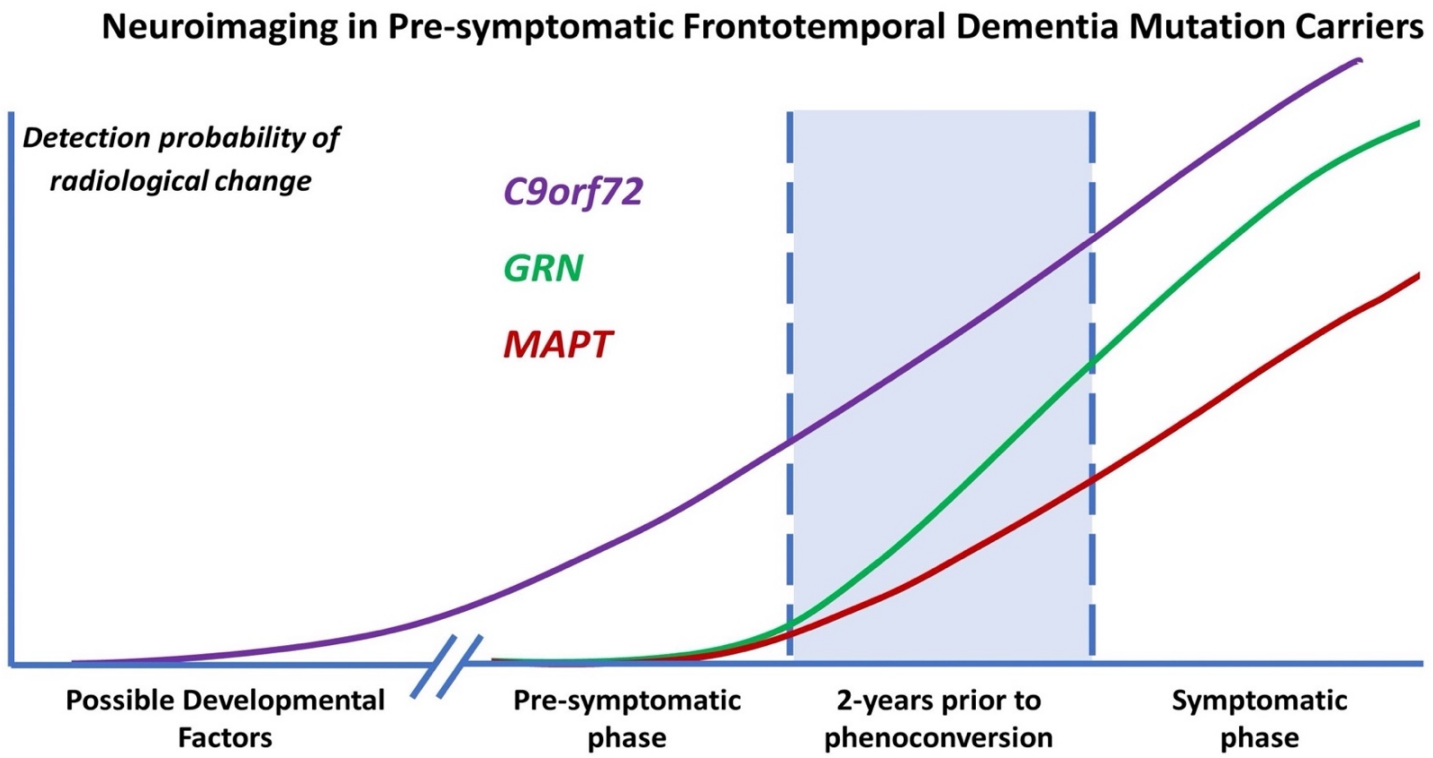

A schematic representation of the detection likelihood of presymptomatic radiological change in the most common FTD-associated genetic variants. In *C9orf72* mutation carriers, it is hypothesised that neurodevelopmental factors may be at play in conjunction with slowly progressive neurodegeneration. In *GRN* mutation carriers, the disease process is thought to accelerate 2-years before phenoconversion. In *MAPT* mutation carriers, disease burden accrues 2-years before phenoconversion, but at a relatively slower rate than in *GRN*.

Presymptomatic radiological observations may have important practical implications: predicting phenotype, heralding phenoconversion, tracking disease progression, and optimising the timing of clinical trial enrolment. The prospect of predicting subsequent clinical phenotype is seldom addressed in the current literature. This is important to explore in longitudinal studies traversing phenoconversion as some genotypes, such as *C9orf72*, may evolve into distinctly different clinical phenotypes along the ALS-FTD spectrum [142, 247, 248]. Presymptomatic spinal cord pathology in hexanucleotide expansion carriers is likely to predict ALS-FTD rather than FTD [205] highlighting the role of quantitative cord imaging techniques [249, 250]. While machine-learning (ML) frameworks have been successfully applied to imaging data of symptomatic patient cohorts [75, 159, 224], their potential has not been systematically examined in presymptomatic mutation carriers. The role of imaging in clinical trials is of particular interest given the advances in gene-specific therapeutic strategies, such as antisense oligonucleotides [155, 251]. The exact timing of early intervention is yet to be defined. Lessons from other neurodegenerative disorders suggest that therapeutic efficacy should be first demonstrated in early symptomatic cohorts, and later across the spectrum of disease [252]. Potential benefits may not be appreciated if tested in exclusively pre-symptomatic cohorts [252]. In genetic FTD, very early symptomatic disease may be captured by combining the accelerating peri-diagnostic radiological changes in tandem with fluid biomarkers [169]; thus facilitating optimal timing for clinical trial enrolment. Imaging could also be used to track disease burden objectively in individual subjects [33, 253]. Similarly to other neurodegenerative conditions, longitudinal imaging studies in FTD should be complemented by

wet biomarkers and comprehensive clinical profiling [158, 254-256]. Future clinical trials would need to adhere to standardised terminology because the terms 'asymptomatic', 'pre-symptomatic', 'pre-symptomatic', 'pre-clinical', 'pre-manifest' and 'prodromal' are used inconsistently and often interchangeably. Recently proposed nomenclature divides the overarching 'pre-symptomatic' phase into: 'pre-manifest' whereby there is only biomarker evidence of disease; and 'prodromal' whereby there may be detectable clinical signs without fulfilling the diagnostic criteria [257].

While there is a likely reporting bias for significant radiological changes, pre-symptomatic changes are often not detected. The study population sometimes comprises an admixed cohort of pathogenic mutation carries, ages, subsequent clinical phenotypes, and individual modifying factors [145]. Familial FTD is a relatively low-incidence condition that sometimes leads to admixed studies of pre-symptomatic *C9orf72*, *GRN* and *MAPT* mutation carriers to boost sample sizes despite each genetic condition exhibiting relatively specific imaging signatures. However, if the participants are stratified according to the underlying genotype, studies may be underpowered to ascertain pathological changes [61]. Clinical phenotypes are also associated with distinct patterns of lobar atrophy, particularly *GRN* which may evolve to bvFTD or nfvPPA phenotypes [216, 217]. Recent studies have shown that the pre-symptomatic cascade may be relatively uniform in nfvPPA and more diverse in bvFTD [176]. The interval to phenoconversion is likely to be a key determinant of the success in detecting presymptomatic changes. Concomitant GM and WM degeneration can be often detected a few years before symptom onset [61, 181, 215]. The characteristic asymmetric cortical atrophy

associated with *GRN* is only typically appreciated within this time window [178]. The inclusion of participants with considerable differences in their estimated interval to symptom onset, especially younger participants, may preclude detection of subtle pre-symptomatic radiological changes that evolve closer to the time of symptom onset [61, 215]. For example, GM degeneration may be detected in *MAPT* and *GRN* mutation carriers 2-years before symptom onset, but not in those who did not convert to during follow-up [21]. Differences in terminology, methodological strategies, ROI priorities, demographic profiles, choice of controls, statistical thresholds all add the apparent inconsistency of findings in the literature. Longitudinal studies are needed to capture progressive changes which are not appreciated in cross-sectional analyses [226], but the follow-up interval may be too short to detect insidious changes and map propagation patterns [181]. While imaging changes in mutation carriers offer invaluable insights into the relatively arcane presymptomatic phase of the disease, these observations may not be transferable to sporadic FTD.

2.5 Conclusions

Genotype-specific imaging changes may be detected several years before symptom onset in pre-symptomatic familial FTD mutation carriers, but robust multimodal, multi-timepoint longitudinal studies are required for the nuanced characterisation of the evolution of structural and functional changes.

3 Frontotemporal pathology in motor neuron disease phenotypes: insights from neuroimaging

3.1 Introduction

This review explores the role of neuroimaging in characterising frontotemporal pathology in motor neuron diseases (MNDs). While frontotemporal involvement has been extensively investigated in amyotrophic lateral sclerosis (ALS) **(Table 6)**, it is relatively under evaluated in other MND phenotypes, such as primary lateral sclerosis (PLS) **(Table 7)**, progressive muscular atrophy (PMA), spinal bulbar muscular atrophy (SBMA), spinal muscular atrophy (SMA), hereditary spastic paraplegia (HSP), poliomyelitis and post poliomyelitis syndrome (PPS) **(Table 8)**. PMA, SBMA, SMA and poliomyelitis were once regarded as pure anterior horn cell disorders, but emerging data shows that the central nervous system is more widely involved than previously thought [258, 259]. PLS was traditionally considered a pure UMN condition, but extra-motor manifestations are now gradually recognised [260] **(Figure 5).** The ALS-FTD continuum of neurodegenerative disorders share common clinical, radiological, genetic and pathological features [261, 262]. Similar cognitive and behavioural manifestations, however, have also been described in the non-ALS MND phenotypes [263, 264]. The low incidence of these slowly progressive UMN or LMN predominant disorders coupled with heterogeneous frontotemporal manifestations are all factors that may contribute to delayed or mistaken diagnoses [265-268]. Caregiver burden is not only heightened by diagnostic delay, but may be exacerbated by considerable behavioural challenges [269, 270]. Frontotemporal involvement may impact on entry into

clinical trials and decision to participate in research studies, potentially leading to participation bias. From an academic viewpoint, there are synergistic efforts to evaluate frontotemporal disease burden using computational imaging in combination with clinical instruments. In parallel, these advances help to advance our understanding of disease pathology, propagation patterns and the dynamics of anatomical spread. The objective of this review is to collate evidence from robust neuroimaging studies, distil emerging research trends, identify pertinent gaps in the literature, highlight clinical implications and postulate research priorities in the evaluation of frontotemporal pathology across the spectrum of MND phenotypes.

Table 6: Selection of original neuroimaging research articles in ALS since 2015 with more than 30 patients.

First author, Year of publication	Sample Size Study participants	Study Design	Follow-up interval (months)	Raw imaging data/imaging technique
Agosta et al, 2016	ALS n=56 UMN phenotype n=31 LMN phenotype n=14	Cross-sectional case-control Multi-centre	N/A	MRI - Cortical thickness, DTI
Alshikho et al, 2018	ALS n=53 PLS n=11	Longitudinal case-control Single-centre	6-months	MRI - Cortical thickness, DTI [^{11}C]-PBR28 PET
Alruwaili et al, 2018	ALS n=30	Cross-sectional case-control Single-centre	N/A	MRI – VBM, DTI
Basaia et al, 2020	ALS n = 173 PLS n = 38 PMA n = 28	Cross-sectional case-control Multi-centre	N/A	MRI – DTI, rs-fMRI Global brain network analysis Functional connectivity analysis
Bede et al, 2015	ALS = 36	Cross-sectional case-control Single-centre	N/A	MRI - DTI
Bede et al, 2016	ALS = 70	Cross-sectional case-control Single-centre	N/A	MRI - Cortical and subcortical morphometry, DTI
Bede et al, 2018	ALS n=32	Longitudinal case-control Single-centre	4-months 8-months	MRI – VBM, cortical thickness, DTI
Bede et al, 2019	ALS n=100 PLS n=33 FTD n=30	Longitudinal case-control Single-centre	4-months	MRI - Volumetry, vertex, morphometry
Bede et al, 2020	ALS n=100 PLS n=33 FTD n=30	Longitudinal case-control Single-centre	4-months	MRI - Volumetry
Chipika et al, 2020	ALS n=100 PLS n=33	Cross-sectional case-control Single-centre	N/A	MRI – Volumetry, morphometry
Christidi et al, 2017	ALS n=42	Cross-sectional case-control Single-centre	N/A	MRI - DTI
Christidi et al, 2018	ALS n=50	Cross-sectional case-control Single-centre	N/A	MRI – VBM, DTI

First author, Year of publication	Sample Size Study participants	Study Design	Follow-up interval (months)	Raw imaging data/imaging technique
Christidi et al. 2019	ALS=50 AD =18	Cross-sectional case-control Single-centre	N/A	MRI - Hippocampal volumetry, DTI
Consonni et al, 2018	ALS n=48	Cross-sectional case-control Single-centre	N/A	MRI - Cortical thickness
Illán-Gala et al, 2020	ALS n=31 bvFTD n=20	Cross-sectional case-control Single-centre	N/A	MRI - Cortical thickness, DTI
Machts et al, 2015	ALS n=67	Cross-sectional case-control Multi-centre	N/A	MRI - Subcortical volumetry, shape, density
Masuda et al, 2016	ALS n=51	Cross-sectional case-control Single-centre	N/A	MRI – VBM, DTI
Rosskopf et al, 2015	ALS n = 140 PLS n = 30	Cross-sectional case-control Single-centre	N/A	MRI – DTI
Srivastava et al, 2019	ALS = 65	Cross-sectional case-control Multi-centre	N/A	MRI - MRS
Shen et al, 2016	ALS = 638	Cross-sectional case-control Multi-centre	N/A	MRI - VBM
Westeneng et al, 2015	ALS n=112	Longitudinal case-control Single-centre	5.5 months	MRI - Subcortical volumetry and shape

Table 7: Selection of original neuroimaging research articles in PLS

First author, Year of publication	Sample Size Study participants	Study Design	Follow-up interval (months)	Raw imaging data/imaging technique
Agosta et al, 2016	ALS n=56 UMN phenotype n=31 LMN phenotype n=14	Cross-sectional case-control Multi-centre	N/A	MRI - Cortical thickness, DTI
Alshikho et al, 2018	PLS n=11 ALS n=53	Longitudinal case-control Single-centre	6-months	MRI, Cortical thickness, DTI [^{11}C]-PBR28 PET
Basaia et al, 2020	ALS n = 173 PLS n = 38 PMA n = 28	Cross-sectional case-control Multi-centre	N/A	MRI – DTI, rs fMRI Global brain network analysis Functional connectivity analysis
Bede et al, 2019	PLS n=33 ALS n=100 FTD n=30	Longitudinal case-control Single-centre	4-months	MRI - Volumetry, vertex and morphometry
Bede et al, 2020	PLS n=33 ALS n=100 FTD n=30	Longitudinal case-control Single-centre	4-months	MRI - Volumetry
Canu et al, 2013	PLS n=21	Cross-sectional case-control Single-centre	N/A	MRI – DTI
Chan et al, 1999	PLS n=18 ALS n=15	Cross-sectional case-control Single-centre	N/A	MRI - MRS
Charil et al, 2009	PLS n=9 ALS n=38	Cross-sectional case-control Single-centre	N/A	MRI – MTI, DWI, MRS
Chipika et al, 2020	PLS n=33 ALS n=100	Cross-sectional case-control Single-centre	N/A	MRI- Volumetry, morphometry
Clark et al, 2018	PLS n=18 Pre-PLS n=13	Longitudinal case-control Single-centre	1-2 years	MRI – Volumetry, cortical thickness, DTI, rs-fMRI, task-based fMRI
Fabes et al, 2017	PLS n=6 ALS n=43	Longitudinal case-control Single-centre	Not specified	MRI -FLAIR signal intensity
Finegan et al, 2019	PLS n=49 ALS n=100	Cross-sectional case-control Single-centre	N/A	MRI – VBM, DTI
Finegan et al, 2019	PLS n=33 ALS n=100	Cross-sectional case-control Single-centre	N/A	MRI – Volumetry, morphometry, vertex

First author, Year of publication	Sample Size Study participants	Study Design	Follow-up interval (months)	Raw imaging data/imaging technique
Finegan et al, 2020	PLS n=33 ALS n=100	Cross-sectional case-control Single-centre	N/A	MRI - Subcortical volumetry
Finegan et al, 2021	PLS n = 40	Cross-sectional case-control Single-centre	N/A	MRI – VBM, DTI, subcortical volumetry
Kolind et al, 2013	PLS n = 7 ALS n=23	Longitudinal case-control Single-centre	7-months	MRI - mcDESPOT
Kwan et al, 2013	PLS n=22 ALS n=21	Longitudinal case-control Single-centre	2-years	MRI - Cortical thickness, volumetry, DTI
Menke et al, 2012	PLS n=3 ALS n=21	Longitudinal case-control Single-centre	6-months	MRI – DTI
Meoded et al, 2013	PLS n=17 ALS n=13	Cross-sectional case-control Single-centre	N/A	MRI – VBM, DTI
Meoded et al, 2014	PLS n=16	Cross-sectional case-control Single-centre	N/A	MRI – rs-fMRI
Mitsumoto et al, 2007	PLS n= 6 ALS n= 49 PMA n= 9	Longitudinal case-control Single-centre	Every 3-months for 15-months	MRI – DTI, MRS
Paganoni et al, 2018	PLS n=10	Cross-sectional case-control Single-centre	N/A	MRI - Cortical thickness, DTI [^{11}C] PBR28 PET
Tartaglia et al, 2009	PLS n=11	Cross-sectional case-control Single-centre	N/A	MRI - Volumetry
Tu et al, 2019	PLS n=10 ALS n=9	Cross-sectional case-control Single-centre	N/A	MRI - DTI
Turner et al, 2007	PLS n=4 ALS n=34	Cross-sectional case-control Single-centre	N/A	[^{11}C]-flumazenil PET
Unrath et al, 2010	SBMA n=20 HSP n=24 PLS n=25	Cross-sectional case-control Single-centre	N/A	MRI - DTI

First author, Year of publication	Sample Size Study participants	Study Design	Follow-up interval (months)	Raw imaging data/imaging technique
Van der Graaff et al, 2010	PLS n=12 ALS n=24 PMA n=12	Longitudinal case-control Single-centre	6-months	MRI - MRS
Van der Graff et al, 2011	ALS n=12 PLS n=12 PMA n-12	Longitudinal case-control Multi-centre	6-months	MRI - DTI
Van Weehaeghe et al, 2016	PLS n=10 ALS n=105	Cross-sectional case-control Single-centre	N/A	[^{18}F]-FDG PET
Zhai et al, 2003	PLS n=10	Cross-sectional case-control Single-centre	N/A	MRI - MRS

Table 8: Selection of original neuroimaging research articles in PMA, SMA, SBMA, PPS and HSP

First author, Year of publication	Sample Size Study participants	Study Design	Follow-up interval (months)	Raw imaging data/imaging technique
Progressive muscular atrophy				
Agosta et al, 2016	ALS n=56 UMN phenotype n=31 LMN phenotype n=14	Cross-sectional case-control Multi-centre	N/A	MRI - Cortical thickness, DTI
Basaia et al, 2020	ALS n = 173 PLS n = 38 PMA n = 28	Cross-sectional case-control Multi-centre	N/A	MRI – DTI, rs- fMRI Global brain network analysis Functional connectivity analysis
Kew et al, 1994	ALS n = 6 LMN phenotype n = 5	Cross-sectional case-control Single-centre	N/A	Rs-PET, Task-based PET
Mitsumoto et al, 2007	PMA n= 9 PLS n= 6 ALS n= 49	Longitudinal case-control Single-centre	Every 3-months for 15-months	MRI – DTI, MRS
Quinn et al, 2012	ALS = 20 PMA = 5	Cross-sectional case-control Single-centre	N/A	MRI - MRS
Raaphorst et al, 2014	ALS = 21 PMA = 18	Cross-sectional case-control Multi-centre	N/A	MRI - Task-based fMRI
Van der Graaff et al, 2010	PMA n=12 PLS n=12 ALS n=24	Longitudinal case-control Multi-centre	6-months	MRS
Van der Graaff et al, 2011	PMA n-12 ALS n=12 PLS n=12	Longitudinal case-control Multi-centre	6-months	MRI - DTI
Spinal muscular atrophy				
De Borba et al, 2020	SMA type III (n=19) SMA type IV (n=6)	Cross-sectional case-control Single-centre	N/A	MRI - Cortical thickness, volumetry
Mendonça et al, 2019	SMA type 0 (n=3)	Longitudinal case-control Single-centre	1-3 years	MRI
Querin et al, 2019	SMA type III (n=19) SMA type IV (n=6)	Cross-sectional case-control Single-centre	N/A	MRI - Cortical thickness, DTI

First author, Year of publication	Sample Size Study participants	Study Design	Follow-up interval (months)	Raw imaging data/imaging technique
Spinal-bulbar muscular atrophy				
Garaci et al, 2015	SBMA n=8	Cross-sectional case-control Single-centre	N/A	MRI - DTI
Karitzky et al, 1999	SBMA n=9	Cross-sectional case-control Single-centre	N/A	MRI - MRS
Kassubek et al, 2007	SBMA n=18	Cross-sectional case-control Single-centre	N/A	MRI- VBM
Lai et al, 2013	SBMA n=10	Cross-sectional case-control Single-centre	N/A	[^{18}F]-FDG PET
Mader et al, 2002	SBMA n=10	Cross-sectional case-control Single-centre	N/A	MRI - MRS
Pieper et al, 2013	SBMA n = 8	Cross-sectional case-control Single-centre	N/A	MRI – VBM, DTI
Unrath et al, 2010	SBMA n=20 HSP n=24 PLS n=25	Cross-sectional case-control Single-centre	N/A	MRI - DTI
Post-polio syndrome				
Bruno et al, 1994	PPS n=22	Cross-sectional case-control Single-centre	N/A	MRI
Demir et al, 2012	PPS n=11	Cross-sectional case-control Single-centre	N/A	MRI
Li Hi Shing et al, 2021	PPS n=36	Cross-sectional case-control Single-centre	N/A	MRI - Cortical thickness, subcortical GM, DTI
Li Hi Shing et al, 2021	PPS n=36 ALS n=88	Cross-sectional case-control Single-centre	N/A	MRI – Morphometry, DTI
Trojan et al, 2014	PPS n=42 MS n=49	Cross-sectional case-control Single-centre	N/A	MRI – Volumetry

First author, Year of publication	Sample Size Study participants	Study Design	Follow-up interval (months)	Raw imaging data/imaging technique
Hereditary spastic paraplegia				
Aghakhanyan et al, 2014	HSP n=12	Cross-sectional case-control Single-centre	N/A	MRI – DTI
Agosta et al, 2015	HSP n=44	Cross-sectional case-control Single-centre	N/A	MRI – VBM, DTI
Duning et al, 2010	HSP n=6	Cross-sectional case-control Single-centre	N/A	MRI – Volumetry, DTI
Erichsen et al, 2009	HSP n=8	Cross-sectional case-control Single-centre	N/A	MRS – Volumetry
Faber et al, 2018	HSP n=25	Cross-sectional case-control Single-centre	N/A	MRI- Cortical thickness, subcortical volumes, DTI
França et al, 2012	HSP n=5	Cross-sectional case-control Single-centre	N/A	MRI – VBM, DTI
Kassubek et al, 2006	HSP n=33	Cross-sectional case-control Single-centre	N/A	MRI - Brain parenchymal fractions
Koritnik et al, 2009	HSP n=12	Cross-sectional case-control Single-centre	N/A	MRI - Task-based fMRI
Liao et al, 2018	HSP n=12	Cross-sectional case-control Single-centre	N/A	MRI – rs-fMRI
Lindig et al, 2015	HSP n=15	Cross-sectional case-control Single-centre	N/A	MRI - VBM, DTI
Montanaro et al 2020	HSP n=31	Longitudinal case-control Single-centre	30-months	MRI – VBM, DTI, MRS
Oğuz et al, 2013	HSP n=4	Cross-sectional case-control Single-centre	N/A	MRI - DTI
Pan et al, 2013	HSP n=5	Cross-sectional case-control Single-centre	N/A	MRI -DSI
Rezende et al, 2015	HSP n=11	Cross-sectional case-control Single-centre	N/A	MRI – Volumetry, DTI
Scheuer et al, 2005	HSP n=18	Cross-sectional case-control Single-centre	N/A	MRI [^{18}F]-FDG PET

First author, Year of publication	Sample Size Study participants	Study Design	Follow-up interval (months)	Raw imaging data/imaging technique
Hereditary spastic paraplegia				
Stromillo et al, 2011	HSP n=10	Cross-sectional case-control Single-centre	N/A	MRI – Volumetry, MRS
Tomberg et al, 2012	HSP n=9	Cross-sectional case-control Single-centre	N/A	MRI - Task-based fMRI
Unrath et al, 2010	SBMA n=20 HSP n=24 PLS n=25	Cross-sectional case-control Single-centre	N/A	MRI - DTI
Warnecke et al, 2007	HSP n=6	Cross-sectional case-control Single-centre	N/A	MRI - DTI

Figure 5: The motor and cognitive spectrum in MND phenotypes

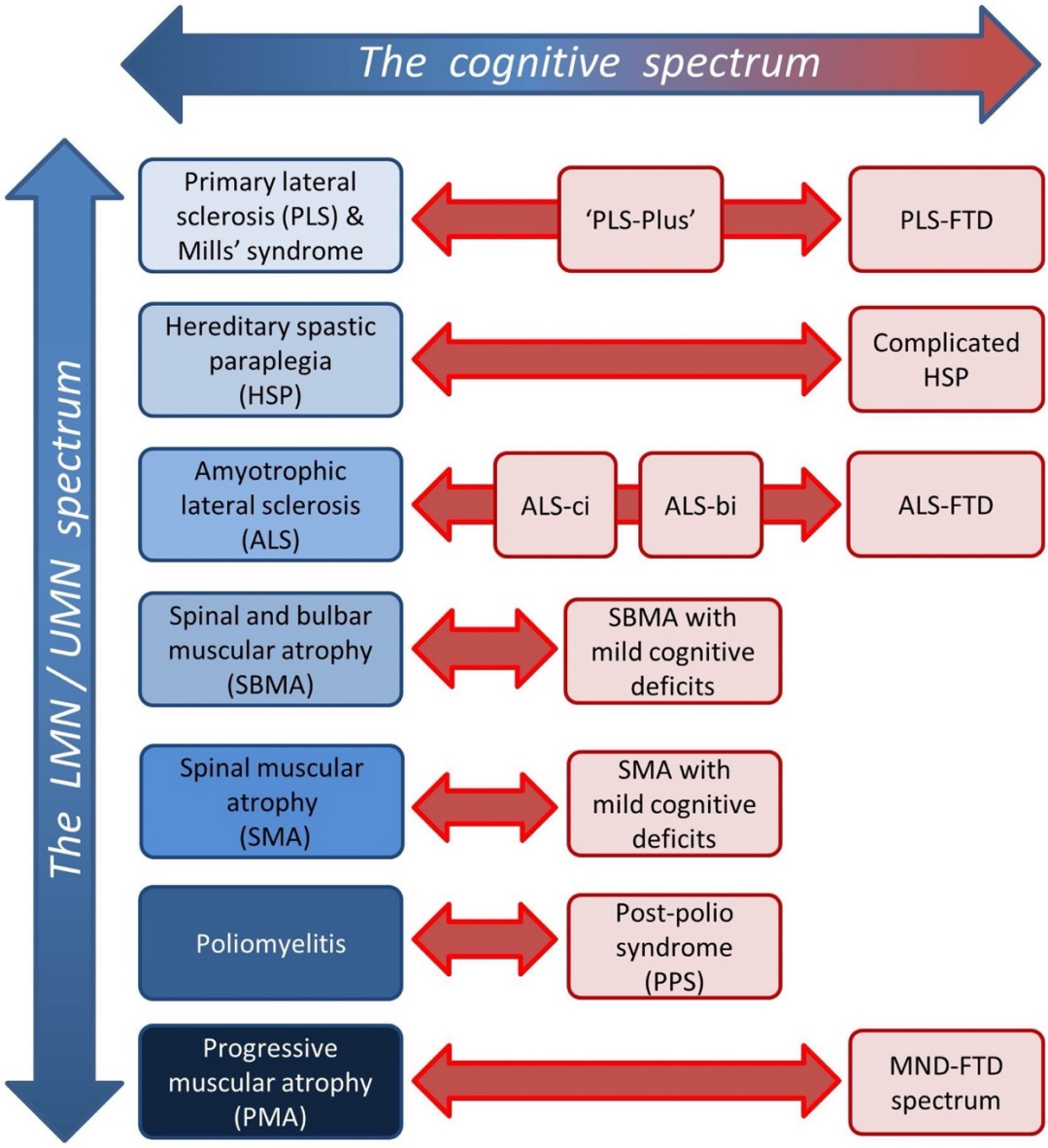

Dimensions of disease heterogeneity in MND; the spectrum of relative upper/lower motor neuron involvement and the spectrum of extra-motor manifestations.

3.2 Methods

This is a focused review of original neuroimaging studies that investigated frontotemporal pathology in the following MND phenotypes; PLS, PMA, SBMA, SMA, PPS, HSP and ALS. The search engines PubMed and Google Scholar were used to identify key papers. Individual MND phenotypes were searched paired with keywords 'MRI', 'PET', 'brain imaging', 'neuroimaging' or 'frontotemporal'. Only articles in English were reviewed. Editorials, opinion pieces and review articles were not selected. Additional papers were considered based on the reference list of reviewed publications. One hundred forty-two original research neuroimaging studies were identified. Given the paucity of prospective neuroimaging studies in non-ALS MNDs, case series, neuropsychology and post mortem studies were also reviewed in these conditions. The selected articles were systematically evaluated for cohort numbers, study design, clinical assessment, imaging methods, and anatomical focus.

3.3 Results

3.3.1 Primary lateral sclerosis

PLS is an upper motor neuron disorder that typically presents with insidious spino-bulbar spasticity in adulthood [271, 272]. It is often associated with pseudobulbar affect that may trigger self-imposed social isolation. Extra-motor manifestations are increasingly recognised in PLS [264, 273], occurring in a similar behavioural and cognitive profile to ALS [264] and rarely fulfilling the diagnostic criteria for FTD [264, 273]. Such deficits include impaired social cognition, executive function, verbal fluency, language or apathy [260, 263, 264, 273]. The reported cases of frank FTD evolved several years after the insidious

onset of UMN signs and were associated with progressive radiological frontotemporal atrophy [273]. This is in line with the mounting body of neuroimaging evidence that supports widespread frontotemporal involvement in PLS [260, 274, 275].

The radiological profile of PLS varies from limited extra-motor involvement to widespread pathology [272]. Structural and diffusion data revealed degenerative changes in the fornix, body of the corpus callosum, anterior cingulate, dorsolateral prefrontal, insular, opercular, orbitofrontal and temporal regions [260, 272, 274-277]. Some studies have explored associations with underlying structural abnormalities focusing on apathy, impaired executive function, language and verbal fluency deficits [260, 275, 278]. Longitudinal studies have yielded inconsistent findings with regards to progressive pathology [279-284]. A case report described progressive cortical atrophy over an 8.5-year timeframe [285]. These observations would suggest that contrary to ALS, longer follow-up intervals may be required in PLS to characterise radiological trajectories. Extra-motor findings in PLS are also supported by metabolic and functional imaging studies. PET imaging studies have detected prefrontal and premotor areas of hypometabolism in PLS that are almost indistinguishable from the patterns seen in ALS [286-288]. Whilst primarily used in a research setting, novel PET radioligand binding studies have also demonstrated alterations beyond the motor system, in the bilateral anterior cingulate gyri and in left superior temporal lobe [271, 286, 289-291]. MR Spectroscopy in PLS has mostly focused on the evaluation of the motor rather than extra-motor regions [280, 292]. Similar to ALS, it shows reduced N-acetyl aspartate/creatinine ratios [280, 292-295] and increased myo-inositol/creatinine

ratios [293] in the motor cortex suggestive of neuronal dysfunction and gliosis respectively. Resting-state fMRI studies report increased functional connectivity in frontotemporal networks [278, 296] which has been associated with executive dysfunction [278, 297]. Similar to ALS, increased functional connectivity is typically considered a 'compensatory response' to structural degeneration [278].

The few post-mortem studies are concordant with the extra-motor radiological profile of PLS [298-305]. Frontotemporal lobar degeneration has been detected with some cases revealing ubiquitin- and TDP-43-immunoreactive neuronal cytoplasmic inclusion bodies in frontotemporal and hippocampal areas . Post-mortem studies seldom have accompanying comprehensive clinical information, but when available, features of nfvPPA or bvFTD have been described [298, 304].

3.3.2 Progressive muscular atrophy

PMA is a clinical diagnosis that is defined by a gradually progressive isolated lower motor neuron disorder, evolving over many years [306]. Reports of extra-motor involvement are inconsistent which is further complicated by the debate on whether PMA is a distinct entity or embedded within the spectrum of ALS [307-310]. There are undeniably shared clinical, radiological and pathological features, albeit less severe compared to ALS. While the initial exclusive LMN clinical presentation distinguishes PMA from ALS, patients with PMA often later develop UMN signs [309]. The cognitive profile is also strikingly similar to ALS, with varying levels of executive function, language, fluency and memory affected [264, 311]. In contrast, minimal behavioural impairment is

observed, and very few patients with PMA fulfil the diagnostic criteria for FTD [264, 311].

Some imaging studies have identified radiological abnormalities in a distribution that may explain these cognitive deficits [311, 312]. Structural analyses have reported loss of white matter integrity in inferior frontal, dorsolateral pre-frontal and hippocampal regions [276]. A task-based fMRI study utilising a letter fluency task as a test of executive function showed impaired letter fluency and abnormal pre-frontal activation [313]. As a counter-argument, a recent study in PMA reported preserved structural integrity with no functional connectivity alterations [297]. Neither MRI spectroscopy nor PET imaging studies have identified radiological abnormalities in extra-motor regions [314, 315]. It is noteworthy that a dedicated neuropsychological study failed to find a difference between patients with PMA compared to controls [316]. Potential shortcomings of the study designs must be considered, including small numbers of patients and the lack of sensitivity of either the chosen task or the imaging modality [315].

The shared neuropathological hallmarks also lend support to the opinion that PMA is part of the ALS clinicopathological continuum [307-309]. The pathological substrates of TDP-43 positive inclusions and occasional fused-in-sarcoma (FUS)-positive basophilic inclusions are observed in both conditions, but at a lesser burden and more limited distribution in PMA [310, 317]. Post-mortem studies in PMA typically describe LMN degeneration, occasional pyramidal tract degeneration, and additional TDP-43 positive inclusions in the primary motor cortex and hippocampus even in the absence of UMN degeneration [310, 317]. These findings raise the question, if in fact the results of

PMA studies should be streamlined, interpreted and analysed under the umbrella of ALS.

3.3.3 Spinal muscular atrophy

SMA is an autosomal recessive disorder that is caused by either homozygous deletions or loss of function mutations in the survival motor neuron 1 (*SMN1*) gene resulting in a deficiency of survival motor neuron (SMN) protein [318]. It typically manifests as a proximal, predominantly symmetrical motor weakness. The phenotype is stratified in levels of decreasing severity from type 0 to type IV, depending on age of symptom onset and achievement of developmental milestones [318]. There are preliminary signals of cerebral involvement in the more severe phenotypes, but it is not yet clear if there is preferential involvement of frontotemporal regions.

The only two cross-sectional quantitative multimodal MRI brain studies evaluated the same 25 treatment naïve adults with type III or type IV SMA initially focusing on the cerebrum and then the cerebellum [258, 259]. No supratentorial cortical atrophy was detected [258], but focal cerebellar changes were noted. In the more severe clinical phenotypes, qualitative MRI brain scans have captured more dramatic findings [319-322]. In type 0 SMA, widespread supratentorial, and sometimes infratentorial, brain atrophy has been reported. A longitudinal case series of patients with type 0 SMA showed interval radiological abnormalities involving the thalamus and basal ganglia [320, 322]. Similar radiological findings have been described in type I SMA [321]. For the most part, neuropsychological studies demonstrate preserved cognition [323-326]. This is with the caveat that these studies are mostly limited to children

and omit the more severe clinical phenotypes [327]. Some aspects of childhood development are even deemed superior compared to healthy controls [328-332]. The only neuropsychological study of adults with type II or type III SMA described normal rather than superior cognitive abilities. This study reported a possible adaptive mechanism of an inverse correlation between executive function and physical ability, but the level of executive function did not exceed healthy controls [323]. In contrast, there are indications of attention and executive function deficits in children with type I SMA [327, 333].

The post mortem examination of the brain is often confounded by coexistent anoxic changes [334, 335]. The more severe clinical phenotypes display more widespread features of degeneration involving the cerebral cortex, thalamus, brainstem and some cranial nerve nuclei that are congruent with ante mortem radiological abnormalities [322, 336]. Most of these regions seem spared in the milder phenotypes [334, 335, 337]. This has been interpreted as selective neuronal network degeneration occurring below a threshold of SMN protein, although the true clinical significance of this is unknown [336]. Overall, the radiological characterisation of the more severe clinical phenotypes has proven challenging because of the rarity of the condition, significant disability and limited life expectancy. In the advent of gene therapy, there may be opportunities for future research in this cohort.

3.3.4 Spinal and bulbar muscular atrophy (Kennedy's disease)

SBMA, also known as Kennedy's disease, is an X-linked trinucleotide repeat disorder due to expansion of cytosine-adenine-guanine (CAG) repeat in the androgen receptor gene [338]. It is a multisystem disorder that typically presents in men in their fourth decade of life with slowly progressive

weakness, bulbar involvement and muscle atrophy due to insidious lower motor neuron degeneration [339, 340]. Relatively mild cognitive deficits have been consistently described [341-343]. While it is a multi-system disorder, the involvement of the central nervous system has been relatively under-evaluated from a radiological viewpoint[338].

The few brain imaging studies indicate various degree of frontotemporal involvement [344-346]. Quantitative MRI analyses demonstrate a spectrum of frontal grey and white matter abnormalities ranging from entirely unaffected to subtle grey matter atrophy and extensive white matter degeneration [344, 345]. Widespread loss of white matter integrity has been reported in the brainstem, corticospinal tracts and limbic system [344, 347, 348]. A single PET imaging study showed hypometabolism in frontal areas [346]. The results of conflicting MR spectroscopy studies highlight that subclinical neuronal dysfunction may not be detected by certain imaging protocols [349, 350]. A long echo-time MR spectroscopy study demonstrated altered metabolite ratios in the brainstem and motor regions [349]; however, a short echo-time MR spectroscopy study failed to reproduce these findings [350]. The discrepancy in these results may be explained by the potential pitfall of artificial metabolite elevation because of either metabolite signal overlap or incorrect baseline determination in short echo-time MR spectroscopy [351]. These radiological findings are complemented by consistent reports of neuropsychological dysfunction in this cohort albeit mostly at a subclinical level [341-343]. Deficits may be so subtle that performance on standard tests of executive function can be normal [341, 342]. Mild deficits in social cognition have

also been recorded [342]. In contrast, single cases of more severe frontal dysfunction have been repeatedly described [352, 353].

Most post-mortem studies in SBMA focus on cardinal spinal cord, peripheral nerve and proximal muscle changes [340, 353, 354]. The pathological examination of cerebral hemispheres is seldom reported. A post-mortem report of an SBMA patient with significant cognitive impairment demonstrated marked diffuse subcortical gliosis in the pre-frontal region, hippocampus and the degeneration of fronto-bulbar fibres in the midbrain without accompanying cortical pathology [353]. Immunohistochemical studies have shown that the pathogenic nuclear mutant *AR* protein is present in abundance in the central nervous system; supporting the rationale to systematically evaluate cerebral changes in future SBMA studies [355].

3.3.5 Poliomyelitis and post-polio syndrome

Post-polio syndrome is characterised by progressive muscular weakness with or without pain, fatigue and muscle atrophy in patients who have recovered from a distant polio infection [356]. Patients often report diverse cognitive symptoms, mostly deficits in attention or memory; however objective evidence is strongly confounded by comorbid factors such as fatigue [357-360]. The reportedly high prevalence of extra-motor symptoms is contrasted by the relative lack of cerebral radiological abnormalities in post-polio syndrome [361].

A quantitative MRI study detected minimal cortical and subcortical atrophy, involving the cingulate gyrus, temporal pole and left nucleus accumbens [361]. These subtle changes were not appreciated in other studies [356, 362]. Qualitative MRI studies either identified no abnormalities or discrete

subcortical hyperintensities that were hypothesised to contribute to the disabling comorbid fatigue [357, 363, 364]. Patients with post-polio syndrome frequently exhibit high levels of self-reported fatigue, apathy and verbal fluency deficits. In the absence of widespread frontotemporal imaging abnormalities, these extra-motor symptoms are postulated to be multifactorial in origin with factors such as low mood, poor sleep and polypharmacy all playing an additive role [361].

These observations are corroborated by historical pathological studies that demonstrate preferential involvement of the brainstem rather than the cerebrum [357, 365, 366]. This is further complicated by reports of patients with a history of polio, who later develop sporadic ALS and demonstrate mixed neuropathological features including the hallmarks of both diseases [367, 368].

3.3.6 Hereditary spastic paraplegia

Hereditary spastic paraplegias (HSPs) are a clinically and genetically heterogenous group of neurodegenerative disorders that present as progressive limb weakness and spasticity. They were traditionally divided into 'pure' or 'complicated' phenotypes based on the absence or presence of extra-motor involvement respectively [369]. In recent times, there has been a shift to stratify these cohorts in accordance with their genetic diagnoses [370]. Interestingly, there are radiological indicators of frontotemporal dysfunction irrespective of the subgroup.

Brain imaging studies have shown a reduction in whole brain volume in both clinical phenotypes [371]. In pure HSP the volume of grey matter volume is thought to be mostly preserved, whereas in complicated HSP the volume of cortical and deep grey matter may be reduced. The only longitudinal study

detected no change in cerebral volume over a 2-year follow-up period [372]. This is with the caveat that longer time intervals may be required to detect a significant change. Loss of white matter integrity has been identified in the corpus callosum, in the frontotemporal and parietal regions in both groups [347, 369, 372-375]. The severity of these findings correlate with the degree of cognitive impairment [369]. Given the relative cortical sparing, cognitive deficits in these cohorts were postulated to be primarily subcortical in origin [374, 376, 377]. This was supported by MR spectroscopy reports of abnormal metabolic ratios in the subcortical white matter [372, 378-384]. PET imaging studies detected cortical hypometabolism, sometimes implicating the frontotemporal regions [385-391]. This was accompanied by clinical measures of frontal dysfunction [390, 391]. Resting-state fMRI studies have shown altered functional connectivity involving the primary motor cortex, insula and superior frontal gyrus [392]. Task-based fMRI studies typically report abnormal activation patterns in sensorimotor areas whilst performing motor tasks [393, 394].

In the advent of genotyping, there has been a focused effort to define the radiological signatures of specific genotypes. Spastic paraplegia 4 (SPG4) is the most common autosomal dominant HSP subtype that is characterised by widespread white matter degeneration with relatively preserved grey matter [374, 395, 396]. Subclinical cognitive deficits have been described that later follow a more rapid trajectory of decline escalating in the eights decade of life [397-400]. Spastic paraplegia 11 (SPG11) and spastic paraplegia 7 (SPG7) are rare autosomal recessive HSP subtypes that reveal white matter degeneration involving the frontotemporal regions amongst other features [370, 376, 380, 401-405]. Varying degrees of cognitive deficits including attention, memory, and

executive dysfunction have been described in these genotypes and others [377, 405, 406].

The few post-mortem studies corroborate the radiological descriptions of frontotemporal pathology. Autopsy reports of those with a clinical rather than genetic diagnosis must be interpreted with caution. In clinically defined cases, marked cerebral atrophy and severe gliosis of the cerebral white matter has been described sometimes preferentially involving prefrontal and frontal areas [407-409]. In SPG11, widespread frontotemporal cortical degeneration has been described [266]. Similar pathological observations have been reported in SPG4, in addition to widespread ubiquitin positivity [399].

3.3.7 Amyotrophic lateral sclerosis

ALS is the most common form of MND that is characterised by progressive upper and lower motor neuron degeneration in the motor cortex, brainstem nuclei and anterior horn of the spinal cord. It begins with progressive limb-onset or bulbar-onset muscle weakness that clinically manifests as cramps, fasciculations, muscle wasting, difficulty swallowing or speaking before ultimately advancing to respiratory failure [410]. Additional cognitive and/or behavioural impairment is universally recognised and a minority of patients with ALS also fulfil the diagnostic criteria for FTD [411].

Clinical observations are widely supported by extra-motor neuroimaging findings. Structural imaging consistently reveals frontotemporal grey and white matter degeneration [201, 412-427]. Grey matter atrophy has been described in the anterior cingulate, insula, operculum, inferior frontal gyrus, superior temporal gyrus, cerebellum, parietal and occipital cortex [201, 312, 417, 423, 425-433]. White matter degeneration has been detected in the body of the corpus

callosum, inferior longitudinal fasciculus, uncinate fasciculus, cerebellum, inferior frontal, middle temporal, superior temporal, orbitofrontal, occipital and parietal regions [312, 412-424, 431, 433-435]. These anatomical findings are often linked to structure-specific behavioural or cognitive deficits [201, 312, 424, 425, 427, 434, 436-441], but similar patterns have been described in the absence of overt cognitive impairment [312, 429, 431, 442, 443]. Extra-motor changes were initially considered to be more prominent in those with *C9orf72* genotype compared to those with sporadic ALS [201, 442], but widespread frontotemporal involvement is not unique to *C9orf72* [444]. Subcortical grey matter involvement can also be readily detected in the hippocampus, amygdala, thalamus, caudate nucleus, putamen, nucleus accumbens and globus pallidus [247, 423, 429, 433, 434, 441, 442, 445-448]. Progressive brainstem pathology has also been reported preferentially involving the pons and the medulla oblongata [449, 450]. Structural and diffusion studies are complemented by robust metabolic and functional imaging studies. PET imaging studies have shown frontotemporal hypometabolism involving the dorsolateral prefrontal, orbitofrontal, anterior frontal and anterior temporal areas [288, 451-453] and regional hypometabolism has been linked to cognitive deficits in ALS [452, 454, 455]. PET imaging abnormalities may precede the detection of cortical atrophy [456]. While in their infancy, novel PET radioligand studies highlight microglial activation in frontotemporal regions, suggestive of localised inflammatory processes [291, 457-461]. MR spectroscopy detects extra-motor abnormalities, potentially before the emergence of clinical symptoms [462]. It shows reduced N-acetyl-aspartate indicative of neuronal dysfunction in the mid-cingulate gyrus [463], dorsolateral [315, 464], ventrolateral [465] and mesial prefrontal cortices [462, 466]. Sometimes these

frontal lobe abnormalities are subtle [467] and may be associated with measures of executive dysfunction [315, 464, 467]. Resting-state fMRI studies captured both increased and decreased functional connectivity within networks that mediate specific behavioural and cognitive functions [468-474]. Task-based fMRI studies have linked these abnormal activation patterns with different facets of cognition, specifically executive function [475-477], social cognition [476, 478-482], memory [479, 483, 484] and language [485]. Executive dysfunction is associated with increased activation of the right superior and inferior frontal areas [476], left superior and mid temporal gyrus and left anterior cingulate gyrus [475] and decreased activation in the left precentral gyrus [475], and dorsolateral pre-frontal cortex [475, 477, 485]; impaired social cognition is associated with increased activation in the prefrontal cortex [476, 478, 480, 481], right supramarginal area [482], right posterior temporal sulcus and decreased activation in the bilateral hippocampus [481]; memory deficits are associated with increased activation in the hippocampus [483] and superior frontal gyrus [484], and decreased activation in the right pre-frontal cortex [484]; and finally impaired language is associated with decreased activation patterns in the pre-frontal cortex, right cingulate gyrus and left temporal lobes [485]. For the most part there are increased [476, 478, 480, 483] or co-existing [475, 477, 479, 481, 482, 484] activation patterns which suggests either loss of inhibitory dysfunction or partial compensation to overcome early functional impairment [232, 486, 487]. Overall there does not seem to be a consistent compensatory or inhibitory effect which suggests that these patients may have been captured at different stages of disease. Functional studies have also been widely utilised to evaluate extra-pyramidal dysfunction in ALS [488, 489]. Emerging functional modalities, such as

magnetoencephalography or spectral EEG have also confirmed widespread extra-motor dysfunction and as these technologies develop they are likely to contribute important additional insights [490-494]. The majority of imaging studies in ALS explored the underpinnings of the most commonly affected neuropsychological domains [485, 495], such as the substrate of verbal fluency deficits, executive dysfunction and behavioural impairment, but with the recognition of the relatively high prevalence of impairments in social cognition, memory deficits and of apathy, the focus of imaging studies is likely to gradually shift [496-501]. Imaging changes in ALS are typically solely interpreted based on genetic and clinical profiles, and seldom correlated with other markers such biofluid markers [158, 502, 503]. The radiological patterns identified by various imaging studies are largely congruent with the distribution of pathological TDP-43 (pTDP-43) aggregates in extra-motor brain regions [504-508]. Patients with ALS-FTD are thought to carry increased extra-motor pTDP-43 burden compared to patients without cognitive impairment [507]. A study of patients with cognitive impairment revealed correlations between regional pTDP-43 load and executive, language and fluency deficits [504].

3.4 Discussion

This review collates evidence of radiological frontotemporal involvement in common MND phenotypes. Existing neuroimaging studies suggest that frontotemporal degeneration may be readily detected in ALS and PLS; a varying degree of frontotemporal pathology may be captured in PMA, SBMA and HSP. Cerebral involvement without regional predilection may be exhibited in the more severe clinical phenotypes of SMA; and there is limited evidence for cerebral changes in PPS **(Figure 6, Table 9).** These radiological

features may precede clinical symptoms, and longitudinal studies often capture gradual progression. Imaging studies in MND suffer from considerable inclusion bias because of disease-specific factors. Patients with significant apathy, motor disability, respiratory compromise or sialorrhea are less likely to participate or return for follow-up imaging. This inherent bias in exclusively imaging-based studies precludes estimating the prevalence of frontotemporal pathology in these conditions. Herein we will discuss the potential clinical and academic implications of these findings mostly referring to the widely published ALS neuroimaging studies because of the surprising paucity of non-ALS MND literature.

Figure 6: Cognitive and anatomical vulnerability in MND phenotypes

	PLS	HSP	ALS	SBMA	SMA	PPS	PMA
Clinical	UMN Gradual Adulthood	UMN Gradual Adulthood	LMN or UMN Variable onset Adulthood	LMN Gradual Adulthood	LMN Gradual Childhood	LMN Gradual Adulthood	LMN Gradual Adulthood
Cognitive	Executive Function Verbal Fluency Language Social Cognition Apathy - - FTD	Executive Function - - - - Memory Attention FTD	Executive Function Verbal Fluency Language Social Cognition Apathy Memory - FTD	Executive Function - - Social Cognition - - - -	- - - - - - - -	- Verbal Fluency - - Apathy - - -	Executive Function Letter Fluency Language - - Memory - FTD
Imaging	Frontal Temporal - Subcortical Cerebellum Brainstem	Frontal - Parietal Subcortical Cerebellum Brainstem	Frontal Temporal - Subcortical Cerebellum Brainstem	Frontal - - - Cerebellum Brainstem	- - - -Cerebellum	- - - - - -	Frontal - - - - -

Table 9: An overview of preferential anatomical involvement in MND phenotypes

PLS	**Grey Matter**	Primary motor cortex and precentral gyrus Prefrontal cortex and inferior frontal gyrus - insular, opercular and orbitofrontal regions Mesial temporal lobe Anterior cingulate cortex Cerebellum
	White Matter	Corticospinal tracts Corpus callosum Fornix Superior longitudinal fasciculus Brainstem – pons, medulla Cerebellum
	Subcortical	Nucleus accumbens Thalamus Hippocampus
PMA	**Grey Matter**	Primary motor cortex and precentral gyrus Prefrontal cortex and inferior frontal gyrus – insular regions
	White Matter	Corticospinal tracts Corpus callosum Fornix Superior longitudinal fasciculus Uncinate fasciculus
	Subcortical	Hippocampus
SMA	**Grey Matter**	Global without regional predilection in severe cases Cerebellum
SBMA	**Grey Matter**	Frontal lobes (subtle)
	White Matter	Corticospinal tracts Inferior frontal Brainstem – midbrain Cerebellum
PPS	**Grey Matter**	Cingulate gyrus (subtle) Temporal pole (subtle)
	Subcortical	Nucleus accumbens

HSP	**Grey Matter**	Primary motor cortex Limbic Parietal Cerebellum
	White Matter	Corticospinal tracts Corpus callosum Frontal Parietal-occipital Brainstem Cerebellum
	Subcortical	Thalamus Basal ganglia
ALS	**Grey Matter**	Primary motor cortex and precentral gyrus Prefrontal cortex and inferior frontal gyrus - insular, opercular and orbitofrontal regions Mesial temporal lobe Anterior cingulate cortex Parietal Occipital Cerebellum
	White Matter	Corticospinal tracts Corpus callosum Arcuate fasciculus Inferior longitudinal fasciculus Uncinate fasciculus Fornix Brainstem Cerebellum
	Subcortical	Thalamus Hippocampus Amygdala Caudate nucleus Putamen Nucleus accumbens Globus pallidus

In clinical practice, the wide spectrum of frontotemporal manifestations in ALS are already incorporated in the clinical diagnostic criteria [411]. It is anticipated that these features will be a fundamental part of future revisions, in conjunction with supportive neuroimaging data [509]. Despite implications for survival [510], clinical staging systems of ALS have omitted to include a cognitive facet thus far [511, 512]. These observations have also not yet translated into the diagnostic criteria of other MND phenotypes. While such deficits are increasingly recognised in PLS, they are deemed too infrequent to be included in the core clinical features [513]. The link between FTD and other rare MND phenotypes may have important implications for everyday clinical practice, particularly given that many non-ALS MND phenotypes are associated with longer survival than ALS [514]. The awareness of possible frontotemporal dysfunction may prompt the use of neuropsychological screening tests in the routine evaluation of these patients. Validated, disease-specific screening tools are preferred to generic instruments, and these are available in ALS [515, 516]. Several of these are adapted to motor disability and dysarthria, and interrogate domains commonly affected in ALS. It is worth noting that patients with predominant frontotemporal cognitive deficits should be screened for incipient motor deficits [517]. The early recognition of neuropsychological deficits is crucial for individualised patient care including: the appraisal of decision-making capacity, caregiver support, resource allocation and the anticipation of management challenges [270]. It may also allow clinicians to consider pharmacological and non-pharmacological interventions such as cognitive or behavioural rehabilitation. In the context of FTD, this is primarily focused on

developing compensatory skills for adapting to functional impairments with the lowest level of assistance required. For example, an electronic device calendar is a daily planning tool that can be used to establish routines and set reminders to initiate activities such as taking medications [518]. There is also an evolving interest in early language therapy interventions [519, 520]. The education of caregivers is crucial to identify unmet needs of the patient that may trigger behavioural problems. These measures have proven to be beneficial to both the patient and their caregivers [518].

In tandem, technological innovations have enriched the supportive radiological data. High-field MRI generates better quality images and acceleration techniques enable shorter data acquisition that may be better tolerated by patients. Quantitative MRI analyses using validated computational pipelines and reliance on robust comparative, correlative and classifier models enhance the clinical interpretation of vast imaging datasets [157]. The advent of structural and functional connectivity studies have ignited interest in the concept of disease-specific selective network degeneration rather than the emphasis on focal pathology [521]. These methods have proven particularly useful to differentiate clinical phenotypes and map longitudinal changes in neurodegenerative disorders [432, 521]. Novel MRI pulse sequences, non-Gaussian diffusion models such as DKI or NODDI, quantitative susceptibility mapping, and multi-voxel spectroscopy are just some of the promising new tools enriching our armamentarium of imaging tools [522-524]. While these methods continue to be tested in the research community they have not been implemented in routine clinical radiology protocols [62].

Frontotemporal involvement across the spectrum of MND phenotypes has important implications for clinical trials. It invites the opportunity for the development of radiological biomarkers that quantify and track frontotemporal involvement. This has the potential to enrich the clinical dataset by detecting subtle imaging abnormalities that prompt the use of targeted neuropsychological tests which may have been overlooked by general screening tools. These metrics can be applied to enhance study designs, prognostic modelling and outcome analyses. This matter has been brought to the forefront as we enter the therapeutic era after decades of minimal treatment prospects [525]. The pioneering gene therapy trials have primarily focused on clinical outcome measures such as motor milestones, requiring artificial ventilation and survival [526-528]. This is also relevant because there has been interest in developing adjunctive interventions such as transcranial or neuromuscular magnetic stimulation [529, 530]. These methods are not only applicable to symptomatic patients but also to those in the pre-symptomatic stages of their disease . In ALS, genotype-specific radiological alterations have been detected in pre-symptomatic carriers of pathogenic mutations decades before the onset of clinical symptoms [22, 184, 185]. Awareness of associated behavioural and cognitive impairment allows for due preparation and adaption of study designs if required. To date, there has been hesitancy in utilising radiological biomarkers as outcome measures in MND clinical trials because of the perceived low sensitivity and presumed need for increased sample size. However, it is increasingly recognised that the accuracy improves with targeted appraisal of disease-specific regions rather than routine whole-brain analyses [69]; and the application of machine-learning

algorithms may facilitate the interpretation of single-subject scans [69]. Nevertheless, despite optimal planning, these deficits could pose a unique challenge that hinders patients' enrolment and participation in future clinical trials.

As we begin to incorporate these developments into clinical practice and clinical trial designs, there are pressing academic questions to be elucidated. First and foremost, it is uncertain if the motor or extra-motor changes evolve in sequence or in parallel across all phenotypes. This topic is probably best explored in ALS where there is a unique opportunity to study the pre-symptomatic phase in carriers of pathogenic *C9orf72* repeat expansions. In this cohort, radiological co-existence of motor and extra-motor involvement has been consistently described [22, 184, 185, 188]. Overall, the topography of radiological alterations is largely similar but less marked than what is described in symptomatic cases. It is unclear if the initial pattern dictates the ultimate clinical phenotype given that both FTD and ALS may have co-existent subclinical motor and extra-motor manifestations [185, 531, 532]. It is also unclear whether these findings solely represent early neurodegenerative changes; some postulate that they capture a developmental abnormality [185]. From a clinical perspective, early cognitive deficits have been described in pre-symptomatic carriers of *C9orf72* expansion before the phenotype is defined [22, 184, 185, 188]. The notion of cognitive reserve has been increasingly evaluated in ALS which may impact on the sequence of symptom manifestation. It suggests that those with a high level of cognitive reserve, often proxied with educational attainment, require a greater degree of brain pathology to meet the threshold for clinical

symptoms [533]. This concept has been investigated in greater detail in FTD, but similar themes are also emerging in ALS. The level of cognitive reserve appears to predict cognitive performance and the degree of brain imaging abnormalities [534-536]. These observations suggest that patient-specific factors influence the chronology of clinically evident symptoms. Some argue that the debate of whether extra-motor or motor symptoms emerge first in ALS is antiquated and that cognition and motor function are inseparably intertwined [537]. It is hypothesised that the selective deficit in action words and verb processing detected in patients with ALS is in fact a cognitive manifestation of motor dysfunction [537]. Although some disagree and consider it to be a feature of executive dysfunction [538]. Task-based fMRI studies in healthy controls have consistently shown that reading action words activates areas along the motor strip that were responsible for conducting these movements [539]. In ALS, action observation and motor imagery are routinely utilised in fMRI studies to compensate for motor disability [540].

Cognitive deficits in specific domains have been linked to the degeneration of single structures in MND [275, 312, 424, 425, 427, 448, 495]. Often there is frank dissociation between cognitive and radiological findings [361, 369], but a reporting bias for confirmed associations prevents the gauging of this occurrence. Correlation analyses in ALS linked apathy to anterior cingulate and accumbens nucleus degeneration [438-440], and memory impairment to hippocampal degeneration [441]. Linking cognitive deficits to single structures however may be a reductionist approach, which overlooks the role of complex cortico-subcortical networks in mediating cognitive functions [541]. Accordingly, the underpinnings of neuropsychological deficits are probably best evaluated

at a circuitry-integrity level instead of seeking associations with focal structures [521]. Traditional structural measures are increasingly complemented by connectivity metrics to appraise the integrity of functional circuits [491, 493]. The selective vulnerability of functional networks is thought to drive cardinal manifestations of neurodegenerative conditions [521]. It may or may not be associated with focal atrophy of crucial nodes within these networks [542].

There are stereotyped shortcomings in the current literature that remain to be addressed. First, the low incidence of these conditions leads to small sample size despite multi-centre collaborations. Second, while case-control study designs are often used to evaluate these rare disorders, this cross-sectional approach is suboptimal to characterise dynamically evolving processes. Furthermore, the indolent progression of the non-ALS MND phenotypes may require relatively long follow-up intervals to detect progressive radiological changes [372]. Third, co-existing neurodegenerative disorders are potential confounders, such as behavioural variant Alzheimer's dementia. To account for this, the use of serum or cerebrospinal fluid biomarkers should be considered in future study methods to enhance diagnostic certainty. Fourth, there is a scarcity of pre-symptomatic studies and often these cohorts are not followed longitudinally until phenoconversion . Fifth, the diagnostic criteria are not well-defined in some MNDs [306]. The diagnosis of 'definite PLS' requires a symptom duration of at least 4 years which may further limit the number of patients available for recruitment [543]. Sixth, imaging studies often concentrate on supratentorial cortical regions, overlooking the contribution of subcortical and cerebellar pathology to cognitive and behavioural manifestations . The sensitivity limitations of single

imaging modalities are seldom acknowledged. Subtle abnormalities may not be detected, considerable neuronal loss may ensue before it becomes radiologically evident. Seventh, the practical implications of cognitive deficits need to be specifically investigated. The presence of cognitive impairment in ALS is considered a negative prognostic indicator that is associated with increased caregiver burden, reduced quality of life and reduced survival; whereas the implications of cognitive impairment in other MND phenotypes is woefully under-evaluated despite their markedly longer survival [510]. Finally, there is a disappointing lack of post-mortem validation of radiological findings. This is further complicated by the inherent bias of the pathological literature to favour atypical cases that are unlikely to represent the true hallmarks of these conditions .

This paper offers an overview of imaging efforts across the spectrum of MNDs to investigate frontotemporal disease expansion. It highlights the disproportionate emphasis on ALS, which offers valuable lessons to conduct similar studies in other MND phenotypes. This discrepancy is in part driven by the rarity of other MND phenotypes relative to ALS. Radiological observations have meaningful impact on the direction of future clinical practice and research. It highlights the rationale for routine screening for frontotemporal dysfunction to inform individualised patient care. Future research projects should specifically focus on addressing existing gaps in our current knowledge. The quality of the data may be enhanced by using multiparametric imaging protocols, longitudinal study designs and the inclusion of pre-symptomatic cohorts where possible. The opportunity for international collaborations

through carefully harmonised protocols should be explored to maximise the number of study participants in low incidence phenotypes.

3.5 Conclusions

In contrast to ALS, the quantitative characterisation of frontotemporal disease burden in non-ALS MND phenotypes remains relatively under investigated. The nuanced evaluation of frontotemporal dysfunction across the entire spectrum of MNDs has important pragmatic implications for individualised clinical care, caregiver support, clinical trial designs and more broadly, for our understanding of disease biology which was once considered to be limited to the pyramidal and anterior horn cells.

4 A systematic review of quantitative spinal cord imaging in neurodegenerative and acquired spinal cord disorders.

4.1 Introduction

Recent methodological advancements in quantitative spinal cord imaging have facilitated the objective appraisal of spinal cord pathology across a spectrum of genetic and acquired conditions. These imaging methods may be divided into structural, microstructural or metabolic. Structural imaging methods includes spinal cord cross-sectional area (CSA) which is a surrogate marker for whole spinal cord atrophy. It is estimated over a representative number of T1- or T2-weighted slice images at specific vertebral levels. Spinal cord segmentation methods have permitted selective appraisal of cervical cord grey matter (GM) and white matter (WM). Microstructural imaging methods include diffusion tensor imaging (DTI), magnetization transfer (MT) and inhomogeneous magnetization transfer (ihMT) imaging. DTI-derived metrics - fractional anisotropy (FA), radial diffusivity (RD), axial diffusivity (AxD) and mean diffusivity (MD) - evaluate WM tract-specific degeneration. Novel MT and ihMT imaging both assess myelination integrity. Metabolic imaging methods includes spectroscopy which measures a selection of neurometabolites including: N-acetyl aspartate (NAA) which is a marker of neuronal integrity; creatine (Cr), tissue energy metabolism; choline (Cho), membrane integrity; and myo-Inositol (m-Ins), glial function. Together these imaging methods generate complimentary information that inform the topography and extent of spinal cord involvement. This systematic review

summarises the existing literature on quantitative spinal cord imaging in select neurodegenerative and acquired conditions. The potential clinical applications, academic contributions, study limitations and future directions are also discussed.

4.2 Methods

A literature review was conducted using the PubMed repository (last accessed on 6th April 2023) in accordance with the “preferred reporting items for systematic reviews and meta-analyses” (PRISMA) guidelines. The following search strategy was used: (“Spinal Cord” OR “Cervical Cord”) AND (“Magnetic resonance imaging” OR “MRI” OR “DTI” OR “diffusion tensor imaging” OR “MRS” OR “magnetic resonance spectroscopy”) AND ("Neurodegenerative” OR "Neuromuscular” OR "Motor neuron disease" OR "primary lateral sclerosis" OR "PLS" OR "ALS" OR "amyotrophic lateral sclerosis" OR “MND” OR "SBMA" OR "spinobulbar muscular atrophy" OR "Kennedy’s disease” OR "spinal muscular atrophy" OR "SMA" OR "hereditary spastic paraparesis" OR "hereditary spastic paraplegia" OR "HSP" OR "Parkinson’s disease" OR “Parkinson disease” OR "Huntington’s disease" OR “Huntington disease” OR "Spinocerebellar ataxia" OR "SCA" OR "Friedreich’s Ataxia" OR “Friedreich ataxia” OR "Subacute combined degeneration" OR "Spinal cord ischemia" OR "Spinal cord infarct*" OR "tropical spastic paraparesis" OR "poliomyelitis" OR "HIV myelitis" OR "HIV myelopathy" OR "HIV vacuolar myelopathy" OR "ganglionopathy" OR "sensory neuronopathy"). The database search was limited to studies written in English and only involving human participants. A single reviewer (MCMcK) individually screened the 1,555 abstracts for eligibility. All original research articles that investigated quantitative spinal

cord imaging in neurodegenerative, neuromuscular, vascular or infectious disorders were included. Review and methodology papers were excluded. Structural, inflammatory, neoplastic and traumatic spinal cord disorders were also excluded. The reference lists of selected articles were reviewed to identify additional related papers. Identified original research articles were reviewed for diagnosis, sample sizes, genetic information, study design, imaging methods, and the main quantitative spinal cord imaging results. A total of 77 studies were included **(Figure 7)**. The results of these studies are next discussed stratified by clinical diagnosis.

Figure 7: A PRISMA flowchart for systematic review of quantitative spinal cord imaging in neurodegenerative and acquired spinal cord disorders.

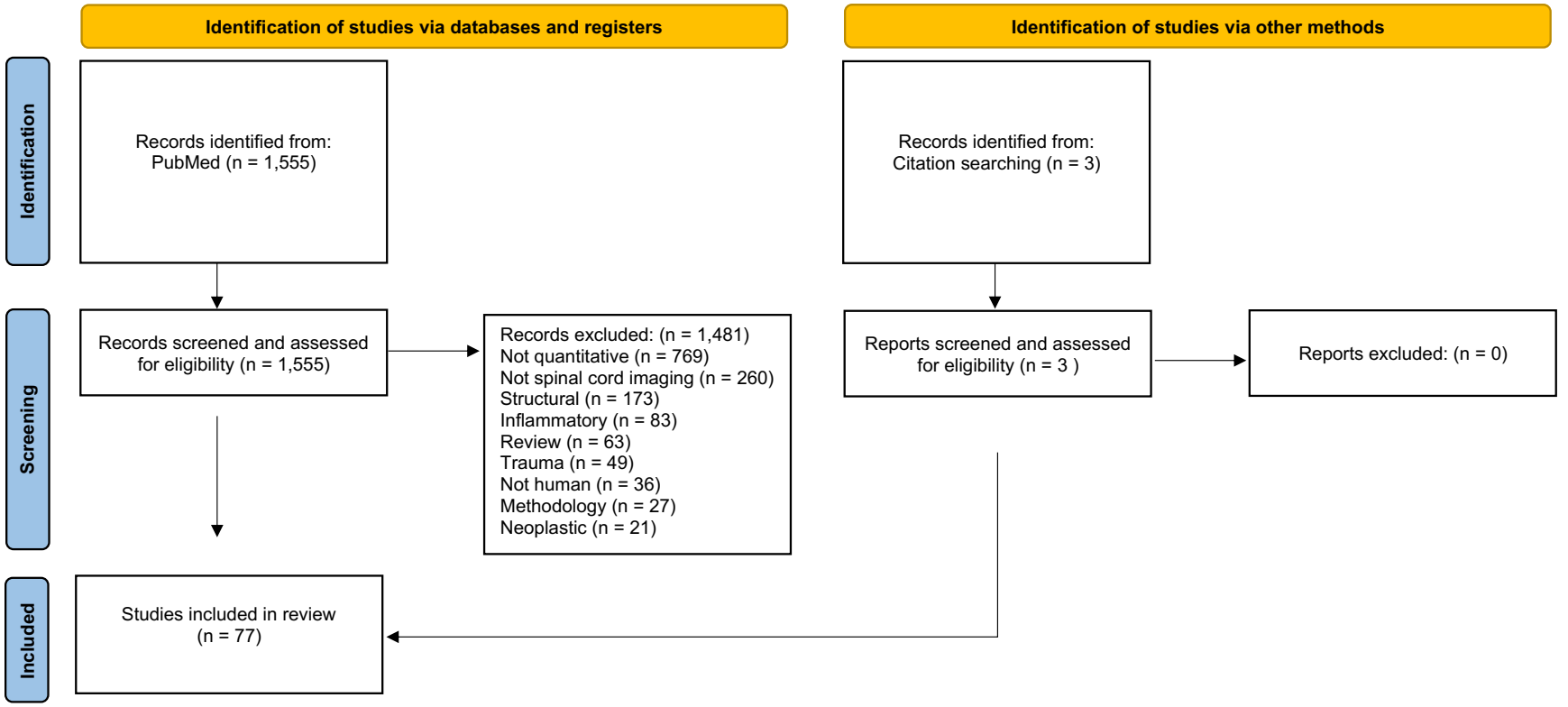

4.3 Results

4.3.1 Motor neuron disease

4.3.1.1 Amyotrophic lateral sclerosis

Amyotrophic lateral sclerosis (ALS) is a progressive neurodegenerative disorder affecting the upper and lower motor neurons in the motor cortex, brainstem and anterior horn of the spinal cord. It is the most common type of motor neuron disease (MND). Clinical phenotypes are defined by the initial affected region with subsequent overlap as the disease progresses; for example, limb-onset ALS begins with muscle weakness, wasting and cramps in the arms and/or legs and later develops bulbar or respiratory involvement. It may be sporadic or familial. There has been an increased interest in quantifying spinal cord atrophy and T2 hyperintensities in ALS. The most common quantitative imaging modalities used include cervical cord area or volume (66%; 21/32) [60, 205, 544-562]; followed by diffusivity (47%; 15/32) [60, 205, 554-560, 563-568]; magnetization transfer ratio (MTR) (19%; 6/32) [60, 555-558, 561]; T2 hyperintensities (13%; 4/32) [559, 560, 569, 570]; spectroscopy (9%; 3/32) [571-573]; and a single study used novel inhomogeneous magnetization transfer ratio (ihMTR) (3%; 1/32) [558]. Several of these studies are multimodal (31%; 10/32) [60, 205, 554-561]. Most studies used 3.0T MRI (75%; 24/32). All studies specifically appraised the cervical spinal cord; and a single study evaluated the whole spinal cord [551]. The mean number of participants was 33 (1-158); and mean disease duration was 27 (7-77) months. Some studies had additional genetic data (38%; 12/32) that varied from tested on a case-by-case basis to systematically testing all cases for common familial ALS genetic mutations. There were some longitudinal studies (25%; 8/32) [205, 547, 548, 553, 554, 556, 559, 562

with a mean follow-up duration of 9 (3-18) months. There were a few pre-symptomatic studies [205, 544, 572]. No studies had post-mortem data. We next summarise the existing literature of quantitative spinal cord imaging data in ALS **(Table 10)**.

In ALS, there is progressive [547, 548, 553, 556, 559, 562] cervical cord atrophy [545-549, 551-557, 559, 560, 562] without flattening [552, 553] in a caudal direction [547-550] compared to controls. This pattern of atrophy indicates preferential motor neuron vulnerability of the lateral corticospinal tracts (CST) in the cervical cord [551, 552]. This is reiterated a high resolution 7.0T MRI study that identified T2 hyperintensities along the lateral CSTs in the cervical cord in ALS [570]. Spinal cord GM and WM segmentation has consistently identified GM and WM atrophy in the cervical cord in ALS [545, 546, 549, 558]. This has recently been facilitated by phase sensitive inversion recovery (PSIR) MR sequence that minimises motion sensitivity and susceptibility [545, 549]. A cross-sectional study that stratified patients according to a clinical staging system reported initial GM atrophy in King's stage 1, followed by progressive GM and WM atrophy in all cervical cord segments increasing in a caudal direction in King's stage >/= 2 [549]. This study predicted that the earliest detectable changes occur in the GM at C3-C4 level, and may even be detected several months before symptom onset [549]. The only whole spine imaging study in ALS reported selective degeneration of C4-C7 at the cervical cord enlargement with no evidence of thoracolumbar atrophy; hence suggesting that future ALS studies should focus on dedicated cervical cord imaging [551]. Whole cervical cord atrophy may be used to map longitudinal changes in ALS [553]; whereas GM cervical cord atrophy may be used to differentiate ALS from controls [546]. In contrast, no

significant difference in the anterior-posterior diameter [569] or mean cross-sectional area (CSA) [550] of the cervical cord has occasionally been reported in ALS literature; but this has been attributed to several factors including small cohorts [550] and low resolution imaging [569]. Regarding ALS phenotypes, there was no significant difference in cervical cord involvement [549]; however there was a trend towards more marked cervical cord involvement in those with upper-limb onset [548, 554] or upper-limb involvement [549, 551] ALS compared to other ALS phenotypes. Bulbar-onset ALS seemed to be the least affected [545, 554]. Regarding ALS genotypes, cervical cord atrophy is readily demonstrated in *SOD1* [561], *VAPB* [544] and *C9orf72* [205, 547] ALS. No longitudinal changes were noted in a cohort of *C9orf72* ALS at short interval follow-up [547]. These radiological changes may even be detected in pre-symptomatic cohorts [205, 544]. There was whole cervical cord atrophy in pre-symptomatic *VAPB* that was more marked in symptomatic *VAPB* [544]; and WM cervical cord atrophy in pre-symptomatic *C9orf72* aged >40 years without progressive GM or WM cervical cord atrophy at 18-months follow-up [205].

Regarding diffusivity, there is reduced FA of the whole cervical cord in ALS [554, 557, 560, 564, 565, 567] in a caudal direction [555, 565, 568] that may be segmented into the central cord [568], anterior [554, 564, 568], lateral [554, 555, 558, 563, 564, 566, 568] or posterior [554, 555, 568] columns. This may be accompanied by increased RD [554, 555, 565, 566], increased MD [554, 566] or reduced AxD [558] in the lateral CSTs and the posterior columns; however, significant changes in MD [565, 567] or AxD [554, 565] are not always detected. The results of longitudinal cervical cord DTI studies differ depending on follow-up interval: no significant changes are detected at 6-months [554]; reduced FA at 9-months [559]; increased MD at 9-months [559] – 1-

year [554]; and increased RD at 1-year [554]. Regarding ALS phenotypes, there was a trend towards reduced FA in upper-limb onset ALS [554], with bulbar-onset ALS once again being the least affected [554, 567]. Regarding ALS genotypes, reduced FA is captured in pre-symptomatic *C9orf72* [205] and symptomatic *SOD1* [555] ALS. In pre-symptomatic *C9orf72* carriers, there were no changes in baseline DTI metrics, and progressively reduced FA in the CSTs at 18-month follow-up [205]. In a subset of pre-symptomatic *C9orf72* mutation carriers aged >40 years with a family history of ALS, reduced FA in the CSTs was also detected at baseline [205]. It is hypothesised that this radiological observation may help identify those *C9orf72* mutation carriers who are more likely to convert to ALS rather than frontotemporal dementia (FTD) phenotype [205].

Regarding spectroscopy, reduced NAA/Cr [571-573], NAA/m-Ins [571-573], NAA/Cho [572], Cho/Cr [573] ratios and increased m-Ins/Cr [571] ratio are detected in the cervical cord in ALS compared with controls – with some subtle differences between studies [571, 573]. Reduced NAA indicates neuronal loss; increased Cho levels suggests inflammation [571]; and increased m-Ins represents gliosis [571]. A similar profile of metabolic changes were captured in the cervical cord of presymptomatic *SOD1* carriers (reduced NAA/Cr, NAA/m-Ins and m-Ins/Cr ratios) [572]; thus suggesting early radiological metabolic changes precede clinical or neurophysiological changes [572].

The few studies that evaluate MTR in cervical cord in ALS capture progressively [556] reduced MTR ratios [60, 555-558], particularly in the lateral corticospinal tracts [555, 556, 558] in a caudal direction [555]. In a single study of *SOD1* ALS, no significant difference in MTR ratio was detected [561]. The only study investigating ihMTR in the cervical cord in ALS revealed reduced ihMT in all

regions of interest (ROI) including total WM, anterior GM, CSTs and posterior columns in the cervical cord [558]. This study suggested that this novel technique may be more sensitive at detecting microstructural changes than conventional MTR or DTI metrics, but this needs to be clarified in future studies [558].

Together these complementary structural spinal cord imaging methods may be combined to improve differentiating patient with ALS from healthy controls [60, 554]. A multi-modal classification model using cervical cord CSA, DTI and MTR variables accurately differentiated ALS from controls with a sensitivity of 88% and specificity of 85% (AUC 0.96). The best-performing individual variables were RD, followed by FA, and then CSA at C5 spinal level [60]. Multi-modal cervical cord imaging data may also be used to develop prognostic models [546, 557].

In terms of clinical correlations, whole cervical cord atrophy correlates with muscle strength [555, 556], respiratory involvement [562], disease duration [549, 552, 561], and disease severity as measured by revised ALS functional rating scale (ALSFRS-R) [546, 548, 552-554, 556, 558, 561]. Disease progression as measured by longitudinal ALSFRS-R scores correlates with whole cervical cord atrophy in sporadic ALS but not *C9orf72* ALS [547]. The specific location of cervical cord atrophy corresponds with associated muscle weakness [555]. WM and GM cervical cord atrophy also independently correlate with disease severity [549, 554]. WM cervical cord atrophy has a greater association with disease severity [549, 554] and additional association with disease duration compared with GM cervical cord atrophy [549]. Diffusivity metrics correlate with motor tasks [565], muscle strength [558], respiratory involvement [565], disease duration [558] and disease severity [554-556, 560, 565]. In particular, reduced FA of whole cervical cord

[554, 558, 560, 565] or lateral CST [555, 556] correlated with muscle strength [558, 565], disease severity [554-556, 560] and rate of disease progression [567]. Magnetic resonance spectroscopy (MRS) studies of the cervical cord in ALS reveal that altered metabolic ratios are associated with respiratory involvement (reduced NAA/m-Ins [571, 573], NAA/Cho [573] and NAA/Cr [571]) or disease severity (reduced NAA/Cr [571] and NAA/m-Ins [571]). MTR and ihMT metrics also correlated with muscle strength and disease duration [558]. Sometimes there is a lack of clinical correlation with structural [544, 545, 547, 559, 560], diffusivity [559, 563, 564, 566] or metabolic [572, 573] data which is later discussed.

4.3.1.2 Primary lateral sclerosis

Primary lateral sclerosis (PLS) is an MND subtype that is characterised by exclusively upper motor neuron degeneration. It typically presents as gradual-onset of lower limb stiffness and spasticity. The 3.0T MRI quantitative imaging studies that evaluate spinal cord involvement in PLS include one cross-sectional [574] and two longitudinal studies [547, 548]. The mean follow-up was 6-months. Spinal cord area [547, 548], diffusivity [574] and myelin water imaging (MWI) using gradient and spin echo sequence (GRASE) [574] were measured. The mean number of participants was 9 (2-18). The participants were sometimes considered in a larger group of ALS [548] **(Table 10).**

In a clinically heterogenous group of MNDs that mostly included ALS and a few participants with PLS, there was cervical spinal cord atrophy with a trend towards longitudinal progression at 6-months follow-up [548]. The presence of cervical cord atrophy was confirmed in a cohort of PLS, but no longitudinal changes were noted at 6-months follow-up [547]. A single DTI study revealed increased RD in the cervical spinal cord GM and reduced FA in the

cervical spinal whole cord, GM and lateral funiculi compared to controls [574]. Novel GRASE MWI identified low myelin water fraction in the lateral funiculi, suggesting that there is demyelination in the CSTs [574]. Baseline cervical cord CSA correlated with disease severity as measured by ALSFRS-R in a cohort of PLS [547] and in a clinically heterogenous group of ALS and PLS [548]. Disease progression measured by longitudinal ALSFRS-R scores correlated with cervical cord atrophy in PLS [547].

4.3.1.3 Progressive muscular atrophy

Progressive muscular atrophy (PMA) is an MND subtype that is characterised by exclusively lower motor neuron degeneration. It clinically presents with progressive muscle wasting and weakness. It typically has a better prognosis than ALS. There are two quantitative spinal cord imaging studies that specifically evaluate this cohort **(Table 10).** There is varied nomenclature, with one study referring to this cohort as 'sporadic adult onset lower MND' [569]. The mean number of participants was 38 (19-56). The initial 1.5 T MRI cross-sectional study did not detect any changes in cervical spinal cord thickness of signal alterations in PMA compared with controls [569]. In contrast, a recent 3.0 T MRI longitudinal study detected progressive upper cervical cord atrophy in PMA over a median follow-up of 5.5 (3-59) months [547]. Cervical cord atrophy in PMA correlated with disease progression (longitudinal ALSFRS-R score) but not disease severity (ALSFRS-R score) [547].

4.3.1.4 Spinal and bulbar muscular atrophy (Kennedy's disease)

Spinal and bulbar muscular atrophy (SBMA), also known as Kennedy's disease, is an X-linked autosomal recessive MND caused by a trinucleotide repeat in the *AR* gene. It clinically presents with insidiously progressive bulbar

dysarthria and dysphagia with weakness and wasting of the proximal extremities. It may be associated with features of androgen insensitivity. The radiological involvement of the spinal cord in SBMA has been explored in two cross-sectional studies that primarily investigated ALS but also included small cohorts of SBMA **(Table 10).** The mean number of genetically confirmed participants was 12.5 (6-19). The mean disease duration was 20.25 (16.5-24) years. In SBMA, there is cervical and thoracic spinal cord atrophy compared to controls and significant cervical cord atrophy when compared with ALS and purely lower MND [569]. This may have been because of statistically longer disease duration in the SBMA cohort when compared to the ALS cohort [569]. This spinal cord atrophy is postulated to be because of marked dorsal column involvement of the fasciculus gracilis and cuneatus [569]. There was no significant difference in diffusivity metrics in the cervical spinal cord in SBMA compared to controls [567].

4.3.1.5 Post-polio syndrome

Post-polio syndrome (PPS) is a condition that may develop several years after polio infection. It presents as generalised fatigue, progressive muscle weakness and atrophy. A single cross-sectional case-control imaging study investigates spinal cord involvement in PPS [575] **(Table 10).** It revealed that there was reduced cervical and thoracic spinal cord area in PPS compared with controls. The degree of spinal cord atrophy was more marked in those with progressive disease. This significantly correlated with muscle strength in the corresponding myotomes and was associated with PPS-related functional decline. These findings suggest that these findings of spinal cord atrophy may be related to a post-infectious secondary neurodegenerative process [575].

4.3.1.6 Spinal muscular atrophy

Spinal Muscular Atrophy (SMA) is an autosomal recessive neuromuscular disease that is caused by mutations in the *SMN1* gene. It typically presents with gradually progressive muscle weakness involving the arms, legs and respiratory muscles. The clinical phenotype is stratified according to disease severity (in decreasing order from type 0-type IV). There have been a few cross-sectional [576-578] and one longitudinal [579] imaging studies investigating cervical cord involvement in SMA **(Table 10).** All studies were conducted on 3.0T MRI scanners. All studies investigated spinal cord cross-sectional area [576-579]; and two studies also investigated DTI metrics [577, 578]. All participants had a genetically confirmed diagnosis. The summarised results pertain to type III or IV clinical phenotype [576-579]; only a single participant had the more severe type II clinical phenotype [578]. The mean number of participants was 17 (10-25). The mean disease duration was 28 years.

In SMA, there is cervical cord atrophy [576, 577], with selective GM degeneration [577]. A significant cervical cord atrophy gradient is described, that is most prominent in regions that innervate proximal muscles (mainly C3-C6 vertebral levels) [576]. It is hypothesised that this pattern of anteroposterior cervical cord atrophy indicates anterior horn cell atrophy [576]. In addition, there was increased AxD in the cervical cord GM [578]. No other DTI abnormalities were noted [577, 578]. However, these structural (GM CSA [578]) and microstructural (DTI AxD [577]) cervical cord changes are not always captured. The only longitudinal study showed that there was no significant difference in cervical cord GM or WM cross-sectional area over 2-years [579]. This may be because of very slow disease progression or early degenerative changes

without subsequent progression [579]. This observation could preclude the use of structural cervical cord as an objective biomarker in SMA clinical trials [579]. This needs to be further investigated in multi-modal longitudinal studies including microstructural and metabolic modalities. In addition, there is variable clinical correlation of these imaging findings. A single study suggested that cervical cord GM cross-sectional area at C3-C4 significantly correlated with deltoid muscle strength [577]. The remainder did not find any correlation between clinical measures and imaging findings [576, 578].

Table 10: Quantitative spinal cord imaging studies in MND phenotypes

Year	Author	Participants	Symptom duration	Study design	Follow-up	MRI technique	Post-mortem	Genetics
ALS								
2009	Agosta	ALS n=17 Controls n=20	27 months	Longitudinal Case control	9 months	Spinal cord area DTI T2 hyperintensities	No	N/A
2018	Agosta	*SOD1* ALS n=20; Sporadic ALS n=11	*SOD1* ALS 70 months Sporadic ALS 30 months	Cross-sectional Case control	N/A	Spinal cord area MTR	No	*SOD1* ALS n=20
2022	Barry	ALS n=15 Controls n=17	13 months	Cross-sectional Case control	N/A	Spinal cord area	No	*C9orf72* n=1; *SOD1* n=1; *TBK1* n=1; Unknown n=12
2014	Branco	ALS n=43 Controls n=43	34 months	Cross-sectional Case control	N/A	Spinal cord area	No	N/A
2016	Budrewicz	ALS n=15 Controls n=15	7 months	Cross-sectional Case control	N/A	DTI	No	N/A
2011	Carew	ALS n=14 Controls n=16	27 months	Cross-sectional Case control	N/A	MRS	No	N/A
2011	Carew	Presymptomatic *SOD1* n=24 *SOD1* ALS n=23 Controls n=29	*SOD1* ALS 567 days	Cross-sectional Case control	N/A	MRS	No	Presymptomatic *SOD1* n=24 ALS *SOD1* n=23
2013	Cohen-Adad	ALS n=29 Controls n=21	1 year	Cross-sectional Case control	N/A	Spinal cord area DTI MTR	No	*SOD1* n=2 Sporadic n=27
2013	Cohen-Adad	ALS n=1 Controls n=1	23 months	Cross-sectional Case control	N/A	T2 hyperintensities	No	N/A
2017	deAlbuquerque	ALS n=27 Controls n=27	30 months	Longitudinal Case control	8 months	Spinal cord area	No	*C9orf72* negative ALS n=27
2014	El Mendili	ALS n=29, baseline ALS n=14, follow-up	27 months	Longitudinal Case series	11 months	Spinal cord area DTI MTR	No	N/A

Year	Author	Participants	Symptom duration	Study design	Follow-up	MRI technique	Post-mortem	Genetics
ALS								
2018	Fukui	ALS n=38; HSP n=7; SBMA n=6 Controls n=8	ALS - 1 year HSP - 15 years SBMA - 17 years	Cross-sectional Case control	N/A	DTI	No	SBMA n=6
2018	Grolez	ALS n=40 Controls n=21	N/A	Longitudinal Case control	3 months	Volumetry	No	N/A
2015	Iglesias	ALS n=21 Controls n=21	27 months	Cross-sectional Case control	N/A	DTI	No	N/A
2013	Ikeda	ALS n=19 Controls n=20	20 months	Cross-sectional Case control	N/A	MRS	No	N/A
2022	Leoni	Pre-symptomatic *VAPB* n=10; *VAPB* ALS n=20; Sporadic ALS n=20; Controls n=30	6 years	Cross-sectional Case control	N/A	Spinal cord area	No	Pre-symptomatic and symptomatic *VAPB* ALS n=30; Sporadic ALS (*SOD1, VAPB, C9orf72, ATXN2* negative) n=20
2010	Nair	ALS n=14 Controls n=15	2 years	Cross-sectional Case control	N/A	DTI	No	N/A
2023	Nigri	ALS n=48 Controls n=17	14 months	Cross-sectional Case control	N/A	Spinal cord area	No	Sporadic ALS *C9orf72, SOD1, FUS, OPTN, TARDBP negative*
2018	Olney	ALS n=10 Controls n=10	44 months	Cross-sectional Case control	N/A	Spinal cord area	No	N/A
2018	Paquin	ALS n=29 Controls n=22	N/A	Cross-sectional Case control	N/A	Spinal cord area	No	*SOD1* n=2
2019	Patzig	ALS n=14 Controls n=15	20 months	Cross-sectional Case control	N/A	DTI	No	N/A
2020	Pisharady	ALS n=20 Controls n=20	39 months	Longitudinal Case control	6-months (n=10) 12-months (n=11)	Spinal cord area DTI	No	N/A
2018	Querin	ALS n=60 Controls n=45	30 months	Cross-sectional Case control	N/A	Spinal cord area DTI MTR	No	N/A

Year	Author	Participants	Symptom duration	Study design	Follow-up	MRI technique	Post-mortem	Genetics
ALS								
2017	Querin	ALS n=49	28 months	Cross-sectional Case series	N/A	Spinal cord area DTI MTR	No	N/A
2019	Querin	Presymptomatic *C9orf72* n=40 Controls n=32	N/A	Longitudinal Case control	18 months	Spinal cord area DTI	No	*C9orf72* n=40
2017	Rasoanandrianina	ALS n=10 Controls n=20	16 months	Cross-sectional Case control	N/A	Spinal cord area DTI MTR ihMTR	No	N/A
2005	Sperfeld	ALS n=39 LMND n=19 SBMA n=19 Controls n=96	ALS 3 years LMND 21 years SBMA 24 years	Cross-sectional Case control	N/A	T2 hyperintensities AP diameter	No	SBMA n=19
2023	Toh	ALS n=75 Controls n=13	17 months	Cross-sectional Case control	N/A	Spinal cord area	No	Case-by-case basis, and not systematically in all patients. *C9orf72* n=1; and *SOD1* n=1
2007	Valsasina	ALS n=28 Controls n=20	26 months	Cross-sectional Case control	N/A	Spinal cord area DTI T2 hyperintensities	No	N/A
2019	Van der Burgh	*C9orf72*-ALS n=108, 64 *C9orf72+*ALS n=26; 18 PLS n=28; 18 PMA n=56; 41 Controls n=114, 54 (n=baseline, follow-up)	*C9orf72*-ALS 14 months *C9orf72+*ALS 12 months PLS 91 months PMA 20 months	Longitudinal Case control	*C9orf72*-ALS 5 months *C9orf72+*ALS 5 months PLS 7 months PMA 5 months	Spinal cord area	No	*C9orf72+*ALS n=26
2014	Wang	ALS n=24 Controls n=16	Range: 6-42 months	Cross-sectional Case control	N/A	DTI	No	N/A
2020	Wimmer	ALS n=158 (incl. PLS n=9) Controls n=86	16 months	Longitudinal Case control	6-months	Spinal cord area	No	ALS n=63; *SOD1* and *C9orf72* (*SOD1+* n=7, *C9orf72+* n=7)

Year	Author	Participants	Symptom duration	Study design	Follow-up	MRI technique	Post-mortem	Genetics
PLS								
2019	Dvorak	PLS n=2 RRMS n=1 PPMS n=1 NMO n=2	N/A	Cross-sectional Case control	N/A	DTI MWI	No	N/A
2019	Van der Burgh	*C9orf72*-ALS n=108, 64 *C9orf72+*ALS n=26; 18 PLS n=28; 18 PMA n=56; 41 Controls n=114, 54 (n=baseline, follow-up)	*C9orf72*-ALS 14 months *C9orf72+*ALS 12 months PLS 91 months PMA 20 months	Longitudinal Case control	*C9orf72*-ALS 5 months *C9orf72+*ALS 5 months PLS 7 months PMA 5 months	Spinal cord area	No	*C9orf72+*ALS n=26
2020	Wimmer	ALS n=158 (incl. PLS n=9) Controls n=86	16 months	Longitudinal Case control	6-months	Spinal cord area	No	ALS n=63; *SOD1* and *C9orf72* (*SOD1+* n=7, *C9orf72+* n=7)
PMA								
2005	Sperfeld	ALS n=39 LMND n=19 SBMA n=19 Controls n=96	ALS 3 years LMND 21 years SBMA 24 years	Cross-sectional Case control	N/A	T2 hyperintensities AP diameter	No	SBMA n=19
2019	Van der Burgh	*C9orf72*-ALS n=108, 64 *C9orf72+*ALS n=26; 18 PLS n=28; 18 PMA n=56; 41 Controls n=114, 54 (n=baseline, follow-up)	*C9orf72*-ALS 14 months *C9orf72+*ALS 12 months PLS 91 months PMA 20 months	Longitudinal Case control	*C9orf72*-ALS 5 months *C9orf72+*ALS 5 months PLS 7 months PMA 5 months	Spinal cord area	No	*C9orf72+*ALS n=26
SBMA								
2018	Fukui	ALS n=38; HSP n=7; SBMA n=6 Controls n=8	ALS - 1 year HSP - 15 years SBMA - 17 years	Cross-sectional Case control	N/A	DTI	No	SBMA n=6

Year	Author	Participants	Symptom duration	Study design	Follow-up	MRI technique	Post-mortem	Genetics
SBMA								
2005	Sperfeld	ALS n=39 LMND n=19 SBMA n=19 Controls n=96	ALS 3 years LMND 21 years SBMA 24 years	Cross-sectional Case control	N/A	T2 hyperintensities AP diameter	No	SBMA n=19
PPS								
2022	Wendebourg	PPS n=20 Controls n=20	44 months	Cross-sectional Case control	N/A	Spinal cord area	No	N/A
SMA								
2016	El Mendili	SMA n=18 (IIIa n=5; IIIb n=10; IV n=3) Controls n=18	26 years	Cross-sectional Case control	N/A	Spinal cord area	No	*SMN1* SMA Type III or IV n=18
2021	Querin	SMA Type III or IV n=14	N/A	Longitudinal Case series	24 months	Spinal cord area	No	*SMN2* 4 copies n=11 *SMN2* 3 copies n=3
2019	Querin	SMA n=25 (III n=19; IV n=6) Controls n=25	30 years	Cross-sectional Case control	N/A	Spinal cord area DTI	No	*SMN1* SMA Type III or IV n=25
2019	Stam	SMA n=10 (II n=1; IIIa n=4; IIIb n=5) Controls n=30	N/A	Cross-sectional Case control	N/A	Spinal cord area DTI	No	SMA Type II or III n=10

4.3.2 Hereditary ataxias

4.3.2.1 Autosomal dominant hereditary ataxias

4.3.2.1.1 Spinocerebellar ataxia

Spinocerebellar ataxia (SCA) refers to a heterogenous group of autosomal dominant nucleotide repeat expansion neurodegenerative disorders that are primarily characterised by cerebellar degeneration. It may be associated with other clinical features such as parkinsonism, pyramidal signs, peripheral neuropathy or urinary dysfunction. The degree of radiological spinal cord involvement is informed by cross-sectional case-control studies, and two longitudinal studies spanning over 1-5 years [580, 581] **(Table 11)**. All studies only evaluate the cervical cord focusing on spinal cord area [580-587] and eccentricity [582-584, 586]. The majority of studies used 3.0T MRI [580, 582-584, 586], with older studies using 1.5T [585] or 0.5T [581] MRI. There was a mean of 42 (7-210) participants in each subgroup, most of whom had a genetic diagnosis. No post-mortem data was available. The mean disease duration was 9-years. Two of the studies included pre-symptomatic cohorts [583, 587].

Quantitative imaging studies have captured cervical cord atrophy and flattening in SCA1 [581, 584], SCA3 [581-583] and SCA7 [586]. It is hypothesised that this indicates preferential involvement of the posterior columns [582, 583] and spinocerebellar tracts [587]. In SCA3, cervical cord atrophy may be detected in pre-symptomatic [583, 587], early [585], or established cohorts [587]. A cross-sectional study of SCA3 described a relatively linear pattern of progressive cervical cord atrophy in pre-symptomatic and symptomatic cohorts that were further stratified by disease duration (<5years, 5-10 years, 10-15 years and >15 years)

[583]. However, these findings failed to be replicated in longitudinal studies [580, 581]. This may be because participants had long-standing disease and already had maximal spinal cord atrophy [580]. In SCA6, which is often considered a pure cerebellar degeneration phenotype, no cervical cord atrophy was detected [585]. However, there was a suggestion of subtle spinal cord changes because lower mean CSA of cervical cord correlated with more severely impaired patients [585].

These radiological measures may [582, 584, 586] or may not [585] correlate with clinical parameters. The degree of cervical cord atrophy correlates with disease severity and is associated with disease duration in SCA1 [584], SCA3 [582], and SCA7 [586]. In some instances, the clinical-radiological correlation between disease severity and cervical cord atrophy may be greater than other imaging biomarkers - such as cerebellum or brainstem imaging metrics [584].

4.3.2.2 Autosomal recessive hereditary ataxias

4.3.2.2.1 Friedreich's ataxia

Friedreich's ataxia (FDRA) is an autosomal recessive trinucleotide repeat expansion disorder that clinically manifests as progressive dysarthria, limb- and gait-ataxia, and loss of lower limb reflexes. It is a multi-system disorder that is associated with cardiac involvement. It is radiologically characterised by cerebral, cerebellar and cervical cord atrophy. The degree of spinal cord involvement has been quantified in cross-sectional [588-592] and longitudinal [593] imaging studies that primarily focus on spinal cord area and eccentricity [588-593], followed by two DTI studies [590, 593] and a single MRS study [593] **(Table 11).** All studies were conducted using 3.0T MR scanners. All participants had a genetically confirmed diagnosis of FRDA. No post-mortem

data was available. The mean number of participants was 68 (21-256). The mean disease duration was 12.5 years.

Quantitative imaging studies have consistently demonstrated cervical and thoracic spinal cord atrophy and increased eccentricity in FDRA compared to controls [588-593]. There is greater atrophy in the cervical cord; and greater anteroposterior flattening in the distal thoracic cord [589]. These findings may be captured in early disease [592]. It is suggested that this pattern indicates preferential degeneration of the dorsal columns, lateral CSTs and spinocerebellar tracts [588, 589, 592]. DTI studies have shown reduced FA, increased RD, increased MD and sometimes increased AxD [590, 593] in total WM, dorsal columns, fasciculus gracilis, fasciculus cuneatus, and corticospinal tracts in the cervical spinal cord WM [590]. A single MRS study revealed decreased total N-acetyl-aspartate (tNAA), increased m-Ins, and a decreased ratio tNAA/m-Ins in the cervical cord compared to controls [593]. A single centre longitudinal study in FDRA demonstrated a significant decline in spinal cord CSA, followed by tNAA/m-Ins ratio, and then a trend towards decreased FA at 1-year and 2-year follow-up intervals [593]. Longitudinal atrophy was only observed in the cervical spinal cord WM and not GM [593]. There are future plans to establish a longitudinal multi-modal multi-site imaging study to better evaluate these radiological changes in FDRA that will include spinal cord area, diffusivity and spectroscopy metrics [594].

These radiological findings consistently correlate with clinical measures [588-590, 592, 593]. The cervical cord CSA correlates with disease duration [589, 590] and disease severity as measured by Friedreich's Ataxia Rating Scales (FARS) [588, 590, 592, 593], Scale for Assessment and Rating of Ataxia (SARA) [589, 593],

Inventory of Non-Ataxia Signs [589] or Spinocerebellar Ataxia Functional Index (SCAFI) [589]. DTI [590, 593] and MRS [593] metrics also correlated with disease severity [590, 593]; the former specifically involving the total WM, dorsal columns, fasciculus cuneatus, fasciculus gracilis and corticospinal tracts. DTI metrics of the CST also correlated with disease duration [590].

It is often questioned whether these spinal cord imaging findings represent developmental or neurodegenerative changes [588, 589]. Recent studies suggest developmental with superimposed neurodegenerative changes [591-593]. Cross-sectional studies have shown progressive cervical cord atrophy after 10-years old with stable preserved eccentricity [591, 592]. This suggests degenerative CST and developmental dorsal column abnormalities [592]. The only longitudinal study has demonstrated progressive cervical spinal cord structural and metabolic imaging changes [593]. This highlights that spinal cord CSA may be a potential imaging biomarker to monitor disease progression, but this would need to be confirmed on further longitudinal studies [592].

4.3.2.2.2 Autosomal recessive cerebellar ataxia type 1

Autosomal recessive cerebellar ataxia type 1 (ARCA1) is a progressive cerebellar syndrome that is caused by a mutation in the *SYNE1* gene. It may be associated with cognitive impairment and pyramidal signs. A single cross-sectional case-control study did not identify any cervical cord atrophy in a small cohort of ARCA1 compared with controls **(Table 11).** It was suggested that the presence or absence of cervical cord atrophy may helpful to differentiate autosomal recessive ataxias e.g. FDRA. This is with the caveat that the small sample size may have affected the power of this study [595].

Table 11: Quantitative spinal cord imaging studies in hereditary ataxias

Year	Author	Participants	Symptom duration	Study design	Follow-up	MRI technique	Post-mortem	Genetics
SCA								
2021	Faber	SCA3 ataxic n=210 SCA3 Pre-ataxic n=48 Controls n=63	SCA3 ataxic 13 years	Cross-sectional Case control	N/A	Spinal cord area	No	SCA3 Ataxic n=210 SCA3 Pre-ataxic n=48
2015	Fahl	SCA3 n=48 Controls n=48	9 years	Cross-sectional Case control	N/A	Spinal cord area	No	SCA3 n=48
2021	Hernandez-Castillo	SCA7 n=48 Controls n=48	10 years	Cross-sectional Case control	N/A	Spinal cord area	No	SCA7 n=48
1996	Higgins	Autosomal dominant SCA n=34 Controls = not specified	N/A	Longitudinal Case control	1-year	Spinal cord area	No	SCA1n=7 SCA3n=17 Not SCA1 or SCA3 n=10
2008	Lukas	SCA3 n=14 SCA6 n=10 Controls n=24	SCA3 7 years SCA6 9 years	Cross-sectional Case control	N/A	Spinal cord area	No	SCA3 n=14; SCA6 n=10
2017	Martins Jr	SCA1 n=31 Controls n=31	8 years	Cross-sectional Case control	N/A	Spinal cord area	No	SCA1 n=31
2020	Piccinin	SCA3 n=23 Controls n=22	9 years	Longitudinal Case control	5 years	Spinal cord area	No	SCA3 n=23
2018	Rezende	SCA3 n=79 Pre-symptomatic SCA3 n=12 Controls n=91	10 years	Cross-sectional Case control	N/A	Spinal cord area	No	SCA3 n=79 Pre-symptomatic SCA3 n=12

Year	Author	Participants	Symptom duration	Study design	Follow-up	MRI technique	Post-mortem	Genetics
FDRA								
2013	Chevis	FRDA n=33 Controls n=30	11 years	Cross-sectional Case control	N/A	Spinal cord area	No	FRDA n=33
2019	Dogan	FDRA n=21 Controls n=22	19 years	Cross-sectional Case control	N/A	Spinal cord area Volumetry	No	FRDA n=21
2022	Hernandez	FDRA n=30 Controls n=30	11 years	Cross-sectional Case control	N/A	Spinal cord area DTI	No	FDRA n=30
2022	Joers	FDRA n=28 Controls n=20	6 years	Longitudinal Cross-sectional Case control	1-year n=21 2-year n=19	Spinal cord area DTI MRS	No	FDRA n=28
2018	Rezende	FDRA n=38 (Adult FDRA n=25; Young-onset FDRA n=12) Controls n=37	Adult FDRA 15 years Young FDRA 6 years	Cross-sectional Case control	N/A	Spinal cord area	No	FDRA n=38
2023	Rezende	FDRA n=256 Controls n=223	14 years	Cross-sectional Case control	N/A	Spinal cord area	No	FDRA n=256
ACRA								
2018	Gama	*SYNE1* n=6 Controls n=6	10 years	Cross-sectional Case control	N/A	Spinal cord area	No	*SYNE1* n=6

4.3.3 Hereditary spastic paraplegia

Hereditary spastic paraplegia (HSP) refers to a heterogenous group of neurodegenerative disorders. It may be classified according to phenotype or genotype. 'Pure-HSP' (pHSP) phenotype refers to clinical presentation limited to progressive lower limb weakness and spasticity; and 'complicated-HSP' (cHSP) phenotype extends beyond this involving other additional systems. The radiological evidence for spinal cord involvement in HSP is informed by cross-sectional case-control studies **(Table 12).** The mean number of study participants was 18 (5-40). The mean disease duration was 18 years. Most participants had a genetic diagnosis [369, 377, 396, 596-603]. For the purpose of analyses, participants were either stratified by clinical phenotype [369, 602, 604] or genetic diagnoses [377, 396, 597-601]. There was no post-mortem data. The majority of studies evaluate spinal cord area and eccentricity [369, 377, 396, 596-598, 600-602, 604]. Four studies also investigated diffusivity metrics [567, 599, 600, 603]. All studies evaluated the cervical cord, with some also appraising the thoracic cord [596-600, 602, 604]**.** Most studies used a 3.0T MRI scanner [377, 396, 597-599, 601, 603], followed by 1.5T [369, 596, 600, 602] and a single study used 1T MRI [604].

In clinically-defined cohorts, marked cervical and thoracic cord atrophy is described in pHSP and cHSP compared with controls [369, 596, 602]. In a cohort of pHSP, only reduced anteroposterior diameter of thoracic cord was detected compared with controls [604]. Despite the distinctly different phenotypes, there was no difference in the degree of spinal cord atrophy in pHSP compared with cHSP [369, 602]. There was also no difference in DTI metrics in a clinically heterogenous group of HSP as part of an ALS study [567].

In genetically-defined cohorts, varying degrees of spinal cord atrophy are described in SPG4 [396, 600, 601], SPG5 [598, 599], SPG6 [596], SPG8 [596], SPG11 [377, 601]; sometimes in SPG3A [596, 597, 601]; but not in SPG7 [601]. The mild spinal cord atrophy captured in SPG3A [596] may elude detection [601]. The pattern of spinal cord atrophy is characterised by the lack of changes in spinal cord eccentricity [377, 396] and greater involvement of the thoracic cord [596, 598]. This suggests preferential degeneration of the CSTs and other descending motor tracts. DTI studies have also revealed tract-specific degeneration with reduced FA, MA and increased RD in the pyramidal tracts and reduced FA in the dorsal columns in the cervical cord in a genetically heterogenous group of HSP [603]. In SPG4, there was reduced FA in the dorsal columns, lateral and ventral funiculi in the cervical and thoracic spinal cord; and increased RD at the lower cervical and upper thoracic levels [600]. In SPG5, there was reduced FA, elevated RD and elevated MD in the WM, dorsal columns, and bilateral lateral corticospinal tracts in the cervical and upper thoracic cord [599].

These radiological observations may [377, 600, 601, 603] or may not [369, 596, 599, 601-603] correlate with clinical measures. Disease duration and severity was associated with reduced cervical cord GM area in SPG4 [601] and reduced cervical cord CSA in SPG11 [377]. Disease severity was also associated with FA in the lateral funiculi [600], and RD in the dorsal columns [603] of the cervical cord in SPG4. However, spinal cord atrophy does not always correlate with clinical metrics in clinically- [369, 602] or genetically-defined HSP [596, 601]. This may be in part because of a 'ceiling effect' whereby participants are captured in late disease, with accrued disability and established spinal cord atrophy [369, 601].

Table 12: Quantitative spinal cord imaging studies in HSP

Year	Author	Participants	Symptom duration	Study design	Follow-up	MRI technique	Post-mortem	Genetics
2015	Agosta	pHSP n=20; cHSP n=24 Controls n=19	pHSP 26 years cHSP 18 years	Cross-sectional Case control	N/A	Spinal cord area	No	SPG4 n=11; SPG11 n=3; SPG15 n=2; SPG3A n=1; SPG5 n=1; SPG7 n=1; SPG10 n=1
2018	Faber	SPG11 n=25 Controls n=25	13 years	Cross-sectional Case control	N/A	Spinal cord area	No	SPG11 n=25
2018	Fukui	HSP n=7 SBMA n=6, ALS n=38 Controls n=8	HSP: 15 years SBMA: 17 years ALS 1 year	Cross-sectional Case control	N/A	DTI	No	SBMA n=6
2005	Hedera	HSP n=13 (SPG4 n=5; SPG3A n=3; SPG8 n=3; SPG6 n=2) Controls n=38	22 years	Cross-sectional Case control	N/A	Spinal cord area	No	SPG4 n=5; SPG3A n=3; SPG8 n=3; SPG6 n=2
2022	Hocquel	SPG3A n=5 Controls n=8	26 years	Cross-sectional Case control	N/A	Spinal cord area Volumetry	No	SPG3A n=5
1997	Krabbe	Autosomal dominant pHSP n=16 Controls n=8	Range: 4-31 years	Cross-sectional Case control	N/A	Spinal cord area	No	N/A
2022	Lindig	HSP n=40 (SPG7 n=15; SPG4 n=12; SPG5 n=4; SPG11 n=1) Controls n=125	17 years	Cross-sectional Case control	N/A	DTI	No	SPG7 n=15; SPG4 n=12; SPG5 n=4; SPG11 n=1
2022	Liu	SPG5 n=17 Controls n=17	18 years	Cross-sectional Case control	N/A	DTI	No	SPG5 n=17
2022	Navas-Sanchez	SPG4 n=12 Controls n=14	22 years	Cross-sectional Case control	N/A	Spinal cord area DTI	No	SPG4 n=12
2021	Qianqian	SPG5 n=17 Controls = not specified	14 years	Cross-sectional Case control	N/A	Spinal cord area	No	SPG5 n=17
2014	Rezende	SPG4 n=11 Controls n=23	14 years	Cross-sectional Case control	N/A	Spinal cord area	No	SPG4 n=11
2021	Servelhere	HSP n=37 (SPG3A n=7; SPG4 n=12; SPG7 n=10; SPG11 n=8) Controls n=21	22 years (SPG3A 33; SPG4 21; SPG7 27; SPG11 10 years)	Cross-sectional Case control	N/A	Spinal cord area	No	SPG3A n=7; SPG4 n=12; SPG7 n=10; SPG11 n=8
2005	Sperfeld	pHSP n=20; cHSP n=10 Controls n=54	pHSP: 20 years cHSP 15 years	Cross-sectional Case control	N/A	Spinal cord area	No	SPG4 n=6 in pHSP group

4.3.4 Other genetic neurodegenerative disorders

4.3.4.1 Huntington's disease

Huntington's disease (HD) is an autosomal dominant trinucleotide repeat expansion neurodegenerative disorder. It clinically manifests as a triad of motor, psychiatric and cognitive impairment. There are two quantitative imaging studies that specifically investigate cervical spinal cord involvement in HD **(Table 13).** These studies demonstrate progressive reduced upper cervical cord area in early [605] and established [606] disease. Cervical cord atrophy may [606] or may not [605] be detected in pre-symptomatic cases. There are also mixed reports of clinical-radiological correlations of cervical cord atrophy with motor deficits in HD [605, 606]. These discrepancies may be for a variety of reasons that are later discussed [606]. Similar to other neurodegenerative conditions, it is often questioned whether these radiological changes capture developmental or disease-related changes. The trajectory of progressive cervical cord atrophy correlating with motor deficits indicates that these changes occur during the clinical stages of HD rather than developmental process [605, 606].

4.3.4.2 Adrenoleukodystrophy

X-linked adrenoleukodystrophy (ALD) is a rare inborn error of metabolism that is caused by mutations in the *ABCD1* gene. It results in defective peroxisomal beta-oxidation causing very long-chain fatty acids accumulation in plasma and tissues. It is sometimes referred to as 'metabolic hereditary spastic paraplegia' or 'adrenomyeloneuropathy' because it clinically presents as a spectrum of adult-onset adrenocortical insufficiency, progressive myelopathy and peripheral neuropathy. Spinal cord imaging studies in ALD appraise the spinal cord area [607-609] and diffusivity metrics [607,

[608] **(Table 13).** The mean number of participants was 20 (6-42), with mean disease duration of 12.5 years. The two longitudinal studies have a mean follow-up of 1.5 years [609]. One study also included pre-symptomatic participants [609]. We next summarise the existing spinal cord imaging data in ALD.

Spinal cord imaging studies in ALD reveal reduced total CSA of the cervical and thoracic cord [607-609], that was more marked in the thoracic region [607, 608]. There was flattening of the cervical cord which suggests selective dorsal column degeneration [609]. Longitudinal studies capture a trend toward reduced CSA of the upper cervical cord at 1-year [609]; and progressive upper thoracic cord atrophy with a trend towards reduced CSA of the lower cervical cord at 2-years [608]. There was no difference in cervical cord CSA in asymptomatic patients compared with controls [609]. DTI studies reveal reduced FA [607, 608], reduced AxD [607], increased RD [607] in the WM of the upper cervical cord, and a trend towards reduced FA in the GM of the lower cervical cord [607]. There is significantly reduced FA, increased MD and increased RD in the WM of the upper cervical cord on 2-year follow-up [608]. Cervical cord atrophy may correlate with disease severity [609]; however sometimes no clinical correlations with spinal cord area or DTI metrics are observed [607].

Table 13:Quantitative spinal cord imaging studies in other genetic neurodegenerative disorders

Year	Author	Participants	Symptom duration	Study design	Follow-up	MRI technique	Post-mortem	Genetics
HD								
2014	Muhlau	HD n=51 Alzheimer's disease n=35 Controls n=227	N/A	Cross-sectional Case control	N/A	Spinal cord area	No	HD n=51
2017	Wilhelms	HD n=17 Presymptomatic HD n=27	N/A	Cross-sectional Longitudinal Case control	Presymptomatic HD 23 months	Spinal cord area	No	HD n=44
ALD								
2016	Castellano	ALD n=13 Controls n=13	11 years	Cross-sectional Case control	N/A	Spinal cord area DTI	No	ALD n=13
2019	Politi	ALD n=6 Controls n=6	N/A	Longitudinal Case control	23 months	Spinal cord area DTI	No	ALD n=6
2020	vandeStadt	ALD n=42 Controls n=32	15 years	Cross-sectional Longitudinal Case control	1-year, n=26	Spinal cord area	No	ALD n=42

4.3.5 Acquired spinal cord disorders

4.3.5.1 Sensory neuronopathy

Sensory neuronopathy is characterised by selective dorsal root ganglia degeneration. It clinically presents with ataxia and sensory symptoms. It may be idiopathic or secondary to autoimmune, paraneoplastic, infectious, metabolic, toxic or genetic causes. Spinal cord imaging may show non-enhancing T2 hyperintensities of the posterior columns. Two quantitative 3.0T MRI studies further evaluate this: a cross-sectional study using DTI metrics [610]; and a longitudinal study measuring spinal cord area and diameter and signal intensity of the dorsal root ganglion, posterior columns and C7 nerve root [611] **(Table 14)**. The mean number of participants was 18 (9-28) [610, 611], encompassing a wide range of acquired aetiologies. The mean disease duration was 8 (4-11) years.

Spinal cord imaging studies reveal decreased area and increased signal intensity in the dorsal root ganglion and posterior columns, and decreased area of the C7 nerve root in sensory neuronopathy compared to disease- and healthy-control groups detected using multiple-echo data image combination (MEDIC) and coronal turbo inversion recovery magnitude (TIRM) sequences [611]. A single DTI study demonstrated reduced FA in the cervical spinal cord at C3-C4 that accurately differentiated a heterogenous group of sensory neuronopathies from disease- and healthy-controls [610]. Both the MEDIC posterior column hyperintensities [611] and reduced cervical cord FA [610] are observed in patients without the characteristic T2-weighted posterior column abnormalities, even in those with short disease duration <1-year [610]. This suggests that these imaging methods may be more sensitive at detecting

spinal cord involvement in sensory neuronopathy. Longitudinal observations in a single case suggest that these radiological changes begin in the nerve root (initial increased signal intensity of C7 nerve root) and progress towards the posterior columns (subsequent reduced signal intensity of C7 nerve root and increased signal intensity of posterior columns) [611].

These radiological findings did not correlate with measures of disease severity [610, 611]. Reduced cervical cord FA only correlated with pain scores (Leeds Assessment of Neuropathic Symptoms and Signs), indicating that sensory neuronopathy is associated with neuropathic pain [610]. The lack of clinical correlations may be due to a combination of factors that are later discussed.

4.3.5.2 HTLV-1 associated myelopathy and tropical spastic paraparesis

HTLV-1 associated myelopathy/tropical spastic paraparesis (HAM/TSP) is a post-infectious myelopathy that presents as a gradually progressive spastic paraparesis that may be associated with sphincter involvement and sensory disturbance. The typical spinal imaging features include spinal cord atrophy and increased signal in the lateral columns. This has been further evaluated in cross-sectional case-control quantitative imaging studies [612-615] **(Table 14)**. Most studies used 3.0 T MRI [613-615]; and a single study used 1.5 T MRI [612]. These studies investigated spinal cord area [613-615], volumetry [612, 615], T2 hyperintensities [615] and diffusivity metrics [615]. All studies appraised the cervical and thoracic spinal cord [612-615] and a single study included the lumbar spinal cord [613]. A single study included post-mortem data [614]. The mean number of symptomatic definite or possible HAM/TSP participants was 12.5 (7-18); and the mean number of asymptomatic HTLV-1 carriers was 6 (2-11).

The mean symptom duration was 8.75 years. The results are summarised below:

In definite HAM/TSP, there was reduced cervical [612-615], thoracic [612-615], and lumbar [613] spinal cord atrophy compared to controls. This was demonstrated by both reduced spinal cord area [612-615] and volume [612, 615]. The degree of volume loss was greater in the thoracic cord [612, 615]. These observations were more pronounced in those with longer disease duration [615]. Spinal cord atrophy was confirmed pathologically; it was more prominent in the WM, especially in the lateral columns [614]. In those with possible HAM/TSP, there were reduced thoracic cord volumes that were close to or within the cord volume range of definite HAM/TSP [612]. In asymptomatic HTLV-1 carriers, the spectrum of spinal cord atrophy ranged from normal [612, 613, 615]; to intermediate between normal and definite HAM/TSP [613]; and similar pattern of spinal cord atrophy to definite HAM/TSP [613]. In definite HAM/TSP, focal T2 hyperintensities were demonstrated in the bilateral anterolateral and dorsal columns extending over several spinal segments [615]. DTI captured reduced FA in the ventral and dorsal spinal tracts compared to controls. No focal lesions or DTI abnormalities were detected in asymptomatic HTLV-1 carriers [615].

The imaging findings variably correlated with clinical metrics [613, 615]. Reduced cervical cord area [613, 615] and volume [615] correlated with disease duration; reduced cervical and thoracic cord area correlated with the Ambulation Index (an ordinal scale based on the 25-foot timed walk test) [613]; and reduced FA in the dorsal tracts correlated with American spinal cord injury association (ASIA) score [615]. In contrast, the imaging metrics did not correlate with clinical measures of disease severity in other studies [612, 614].

4.3.5.3 Vascular

Spinal cord infarction is rare type of ischemic stroke. It may involve the anterior or posterior spinal cord arteries that both present with distinct clinical syndromes. Anterior spinal cord infarction presents with acute onset of back pain, bilateral lower limb weakness and numbness, sphincter disturbance and relative sparing of proprioception and vibration. Posterior spinal cord infarction presents with unilateral sensory loss including impaired proprioception and vibration. It may be idiopathic or secondary to atherosclerosis, trauma or other rarer causes such as fibrocartilaginous embolism. It is radiologically characterised by abnormal T2 signal in the affected vascular territory. There is a single longitudinal case series that quantified dynamic FA variations in spinal cord infarction [616] **(Table 14).** It revealed initial reduced FA in the spinal cord in both cases [616]. This was followed by decreasing FA in the case with worsening symptoms and increasing FA in the case with improving symptoms [616]. It was hypothesised that the younger age and possibly smaller volume infarct may account for the clinical and radiological improvement in the latter case [616].

Table 14: Quantitative spinal cord imaging studies in acquired spinal cord disorders

Year	Author	Participants	Symptom duration	Study design	Follow-up	MRI technique	Post-mortem	Genetics
HAM/TSP								
2014	Evangelou	Definite HAM/TSP n=5 Possible HAM/TSP n=2 Asymptomatic HTLV1 n=2 Controls n=5	8 years	Cross-sectional Case control	N/A	Volumetry	No	N/A
2014	Liu	HAM/TSP n=18 Asymptomatic HTLV1 n=4 MS n=18 Controls n=10	11 years	Cross-sectional Case control	N/A	Spinal cord area	No	N/A
2017	Taniguchi	HAM/TSP n=15 Controls n=20	4 years	Cross-sectional Case control	N/A	Spinal cord area	Yes	N/A
2014	Vilchez	HAM/TSP n=10 Asymptomatic HTLV1 n=11 Controls n=18	12 years	Cross-sectional Case control	N/A	Spinal cord area Volumetry DTI T2 hyperintensities	No	N/A
Spinal Cord Infarct								
2013	Theaudin	Spinal cord infarct n=2	2-3 days	Longitudinal Case series	Day 3-4; 9-10; 15-22	DTI	No	N/A
Sensory Neuronopathy								
2012	Bao	Sensory neuronopathy n=9 Disease controls n=16 (ALS n=14, SACD n=2) Controls n=20	4 years	Cross-sectional Longitudinal Case control	4, 8 and 14 months (n=3)	Spinal cord area MEDIC TRIM DRG, posterior column, C7 nerve diameter and signal intensity.	No	N/A
2016	Casseb	Sensory Neuronopathy n=28 (Idiopathic n=18; Sjogren's n=4; Other: autoimmune hepatitis, paraneoplastic, HTLV, MGUS, VB12 n=6) Disease controls n=14 (Diabetes n=14) Controls n=20	11 years	Cross-sectional Case control	N/A	DTI T2 hyperintensities	No	N/A

4.4 Discussion

These observations have potential clinical applications and academic contributions. From a clinical perspective, the distinct patterns of spinal cord involvement with tract-specific degeneration may be used as an adjunctive diagnostic tool. For example, structural imaging studies revealing spinal cord atrophy with increased eccentricity suggest preferential dorsal column degeneration, as seen in FDRA, SCA and ALD; whereas spinal cord atrophy without increased eccentricity suggests preferential corticospinal tract degeneration, as seen in ALS and HSP. MRI classification models may use these distinct patterns to differentiate diseases from controls or from other differential diagnoses. Thus far this has only been explored in ALS whereby a multi-modal MR classification model using cervical cord cross-sectional area, DTI and MTR variables accurately differentiated ALS from controls [60]. There is scope to explore the use of best-performing spinal cord imaging variables for MRI classification models in other conditions. Quantitative spinal cord imaging data may also be used as an imaging biomarker in clinical trials. The currently used clinical scales are subjective, subject to inter-rater variability, and may not capture changes in slowly progressive neurodegenerative disorders; whereas quantitative imaging metrics offer objective data that may precede these clinical changes. It also may be used to quantify baseline disease burden, track disease progression, and assess treatment efficacy in clinical trials of disease modifying therapies. This concept was demonstrated in a preliminary study of *SPG5* that identified T9 spinal cord area as a potential clinical trial primary endpoint; however the proposed study duration of 14-years was too long to be applicable to real-world clinical trials [598].

Interestingly, it is often a criticism that the time-interval in longitudinal imaging studies is too short to capture significant radiological changes, however this timing would be more representative of the real-world applications in clinical trials that are usually conducted over relatively short intervals. From an academic perspective, these studies have enhanced our understanding of disease pathogenesis by detailing the extent and location of spinal cord involvement across a wide-spectrum of disorders. In some genetic conditions, it may even be detected in the pre-symptomatic phase. There is also an ongoing debate whether these spinal cord imaging changes represents developmental, neurodegenerative or neurodegenerative superimposed on developmental changes in certain conditions. For example: progressive cervical cord atrophy with stable increased eccentricity in FDRA suggests degenerative corticospinal tract and developmental dorsal column abnormalities [591, 592].

Despite ongoing improvements in spinal cord imaging study designs and imaging methods, several limitations must be highlighted. First, study sample sizes are often small owning to the rarity of these conditions, and certain cases may be excluded because they are already on disease-modifying therapies [579]. Second, there are heterogenous study samples whereby different disease stages [614], phenotypes and genotypes are considered together in an effort to boost sample sizes. Third, the utilised clinical scoring scales are seldom disease-specific or disability-specific for cervical cord involvement [559, 610, 611]; for example, ALSFRS-R is not validated in MND subtypes PMA and PLS [545]. Fourth, there is scope to improve MR imaging acquisition and resolution via higher MRI field strength, cardiac- and

respiratory-gating [579]. Fifth, MRI localization is important to ensure that the affected region is evaluated; some condition preferentially involve the cervical or thoracic cord. Sixth, different imaging methods capture different stages and aspects of neurodegeneration that may not be reflected in the chosen clinical measures [572, 573, 596, 607]. Finally, there are limitations that are specific to longitudinal studies: selection bias - patients with more severe disease may not be able to participate in follow-up assessments; 'ceiling effect' - patients with long-standing disease may already have maximal spinal cord atrophy at initial assessment [580]; and the interval may be too short to capture significant radiological changes in slowly progressive neurodegenerative disorders [579]. However, as previously mentioned short-interval studies may be better representative of real-world applications in clinical trials that are usually conducted over a relatively short duration. Overall some of these limitations may explain the lack of clinical correlation with these imaging findings.

Quantitative spinal cord imaging is likely to be utilised as an adjunctive diagnostic tool and objective radiological biomarker for clinical trials. Future studies should focus on using multi-parametric MRI data to improve disease-specific spinal cord imaging signatures. This could help to develop MRI classification models to differentiate disease from controls or other differential diagnoses. In addition, key methodological advancements are required before these academic observations translate into the real-world clinical setting, for example: multi-site collaborations to enhance homogenous sample sizes; new higher field strength MRI scanners utilizing cardiac- and respiratory-gating to improve data acquisition and resolution; imaging focused on affected spinal cord regions – such as the cervical spinal cord in

ALS [551] - to minimise scanning time and patient discomfort; and complementary post-mortem data to validate these radiological findings.

4.5 Conclusions

This review has outlined the structural, microstructural and metabolic spinal cord involvement across a wide spectrum of neurodegenerative and acquired disorders. The most commonly studied conditions include ALS, followed by HSP and then SCA. There is increasing evidence that there is radiological involvement of the spinal cord in several other conditions.

5 Infratentorial pathology in frontotemporal dementia: cerebellar grey and white matter alterations in frontotemporal dementia phenotypes

5.1 Introduction

The function of the cerebellum continues to be defined, particularly with respect to its physiological role in cognition and behaviour. Clinical observations from acquired cerebellar pathologies have consistently highlighted the posterior predominance of cognitive functioning in the cerebellum [617, 618] and imaging studies have confirmed the specific role of lobules VI, VIIA, VIIB, IX and crus I/II in mediating cognitive processes [619-621]. Posterior cerebellar injuries may manifest in multi-domain cognitive deficits including verbal memory, language, visuospatial, executive function and sequencing abilities; while cognition may be relatively preserved in those with anterior cerebellar insults [622]. Cerebellar pathology may contribute to impairments in social cognition [623], language deficits [624] and pathological crying and laughing [625, 626]. Lesions of the vermis have been linked to emotional dysregulation such as irritability, impulsivity and disinhibition [627]. While the neuropsychological sequelae of acute vascular, neoplastic and inflammatory cerebellar pathologies are widely recognised, cognitive deficits associated with slowly progressive neurodegenerative conditions are less well characterised. There is a striking paucity of imaging data on cerebellar involvement in FTD [628-630] despite ample post mortem evidence of cerebellar pathology [631]. A recent meta-analysis noted lobule VI, VIIb, VIIIb atrophy in bvFTD, crus I and lobule VI volume loss in svPPA [632]. Genetic FTD subtypes

appear to exhibit specific grey matter cerebellar abnormalities [628-630, 633, 634]. The *C9orf72* genotype has been linked to focal crus I and lobule VIIa degeneration, *MAPT* mutation associated with vermis pathology, and *GRN* mutation with relatively preserved cerebellar integrity [629]. Interestingly, regional cerebellar atrophy was detected in asymptomatic *C9orf72* mutation carriers [156]. ALS-FTD has been linked to superior (lobules I-VI), crus and vermis degeneration [635]. Other cerebellar regions, such as the cerebellar crura and lobule VI may be involved in all FTD subtypes [632]. This region is often labelled 'the cognitive cerebellum' because of its central role in cognitive processing; the extent of atrophy in this area is thought to correlate with cognitive performance across a multitude of domains [630, 632]. Existing studies suggest that cerebellar abnormalities are most widespread in those with ALS-FTD and bvFTD, and may be relatively focal in those with svPPA or nfvPPA [630, 633, 635]. Selective cerebellar atrophy seems to mirror patterns of cerebral cortical pathology [636, 637] and are likely to be defined by cerebello-cerebral connectivity. These observations further support the 'dysmetria of thought theory' whereby cerebellar lesions result in individual patterns of cognitive dysfunction dependent on the cortico-cerebellar tracts involved [638]. The majority of cerebellar imaging studies in FTD solely appraise grey matter alterations, white matter degeneration is less well characterised in vivo, and there is a lack of cerebellar functional and metabolic studies. Cerebellar hypometabolism have been reported [632, 639, 640] but the majority of PET studies focus on supratentorial regions.

Post-mortem studies in FTD also disproportionately focus on supratentorial regions. Much of the limited post-mortem data of cerebellar

pathology in FTD pertains to a select cohort of those carrying the *C9orf72* mutation. In such cases, TDP-43 negative, ubiquitin and p62-positive neuronal cytoplasmic inclusions were noted in the granular layer of the cerebellar cortex, but these findings are not exclusive to this genotype [631, 641, 642]. Cerebellar atrophy has been described in those carrying the *C9orf72* gene mutation, but not in those carrying the *MAPT* mutation [641, 643]. A case series of two sisters with a clinical diagnosis of bvFTD and no established genetic mutation, demonstrated abundant abnormal tau deposition in the cerebellum, with a distinctly different morphology from the more common tauopathies [644].

Emerging imaging and post mortem data lends credence to the body of evidence that cerebellar involvement may contribute to the clinical manifestations of FTD. These observations provide the rationale to characterise cerebellar signatures in FTD phenotypes using a multiparametric grey and white matter imaging protocol. The main objective of this FTD study is to ascertain if focal cerebellar degeneration may be identified in vivo and establish phenotype-specific and overlapping radiological features.

5.2 Methods

5.2.1 Participants

A total of 156 participants were included in a prospective imaging study of frontotemporal dementia; 7 patients with behavioural-variant FTD ('bvFTD', mean age 60.71±3.3), 12 patients with non-fluent-variant primary progressive aphasia ('nfvPPA', mean age 61.5±2.96), 3 patients with semantic-variant primary progressive aphasia ('svPPA', mean age 61.66±6.42), 12 ALS-FTD patients carrying *C9orf72* GGGGCC hexanucleotide repeat expansions

('C9+ALSFTD', mean age 58.65±11.22), 12 *C9orf72* negative ALS-FTD patients repeats ('C9-ALSFTD', mean age 59.95±7.67), and 110 healthy controls ('HC', mean age 59.21±10.5). All participants provided informed consent in accordance with the Medical Ethics Approval of the research project (Beaumont Hospital, Dublin, Ireland). Exclusion criteria included prior traumatic brain injury, cerebrovascular events, comorbid neoplastic, paraneoplastic or neuroinflammatory diagnoses. FTD and ALS-FTD was diagnosed based on the Rascovsky criteria [645] and participating ALS patients had 'probable' or 'definite' ALS according to the revised El Escorial research criteria. Healthy controls were unrelated to patients and had no known family history of neurodegenerative conditions.

5.2.2 Magnetic resonance imaging

Imaging data were acquired on a 3 Tesla Philips Achieva Magnetic resonance (MR) platform with an 8-channel receive-only head coil. The standardised imaging protocol included a high-resolution T_1-weighted (T1w) and a 32-direasction diffusion tensor imaging (DTI). T1w was acquired with a 3D Inversion Recovery prepared Spoiled Gradient Recalled echo (IR-SPGR) sequence with the following parameters; field-of-view (FOV) of 256 x 256 x 160 mm, flip angle = 8°, spatial resolution of 1 mm^3, SENSE factor = 1.5, TR/TE = 8.5/3.9 ms, TI =1060 ms. DTI data were acquired with a spin-echo echo planar imaging (SE-EPI) pulse sequence using a 32-direction Stejskal-Tanner diffusion encoding scheme, FOV = 245 x 245 x 150 mm, 60 slices with no interslice gap, spatial resolution = 2.5 mm^3, TR/TE = 7639 / 59 ms, SENSE factor = 2.5, b-values = 0, 1100 s/mm^2, dynamic stabilisation and spectral presaturation with inversion recovery (SPIR) fat suppression.

5.2.3 Cerebellar morphometry

First, total intracranial volumes (TIV) were estimated for each subject to be used as a covariate in subsequent region-of interest (ROI) morphometric analyses. As described previously[441, 449] TIV estimation was performed by linearly aligning each participant's skull-stripped brain image to the MNI152 standard, and the inverse of the determinant of the affine registration matrix was calculated and multiplied by the size of the template. FMRIB's FSL-FLIRT was used for spatial registration and FSL-FAST for tissue type segmentation. Partial grey matter, white matter and CSF volumes were added for TIV estimation. Grey matter pathology in the FTD groups was evaluated by ROI morphometry using FMRIB's FSL suite. Pre-processing steps included skull-removal (BET), motion-corrections and tissue-type segmentation[194]. Grey-matter partial volume images were aligned to the MNI152 standard space using affine registration. A study-specific grey matter template was created representing each study group to which the grey matter images of each participant were subsequently non-linearly co-registered. Permutation based non-parametric inference was utilised to contrast each patient group with healthy control implementing the threshold-free cluster enhancement (TFCE) method. Design matrices included group membership, age, sex and TIV [646]. Statistics were restricted to a cerebellar ROI mask defined by label 1 of the MNI structural atlas. Resulting statistical maps were thresholded at $p < 0.05$ and visualised in FSLeyes. The aid the localisation of statistically significant clusters the Diedrichsen probabilistic atlas was used as undelay[647].

5.2.4 Cerebellar cortical thickness analyses

To evaluate cerebellar cortical thickness alterations, the cerebellum was segmented using a validated parcellation algorithm [648-650]. A patch-based segmentation algorithm was then applied to obtain cerebellar GM metrics for each lobule, separately for the right and left cerebellar hemispheres [648]. As a quality-control step, anatomical parcellation and tissue-type segmentation was individually verified for each subject. The following labels were used to retrieve regional cortical thickness values: lobules I-V, lobule VI, lobule VIIb, lobules VIII-X, Crus I, and Crus II. To test the effect of group membership on cerebellar cortical thickness in each lobule, Multivariate analyses of covariance (MANCOVAs) were conducted for the right and left cerebellar hemispheres separately, designating lobular cortical thickness as dependent variable, group membership as independent factor and age and gender as covariates. In case of a significant multivariate omnibus test, post-hoc comparisons were considered significant at $p<0.05$, following false-discovery rate (FDR) corrections for multiple comparisons to reduce Type I error.

5.2.5 Cerebellar white matter analyses

Raw DTI data underwent eddy current corrections and skull removal before a tensor model was fitted to generate maps of fractional anisotropy (FA), axial diffusivity (AxD), and radial diffusivity (RD). The tract-based statistics (TBSS) module of FMRIB's software library was utilised for non-linear registration and skeletonisation of individual DTI images. A mean FA mask was created, and each subject's individual AD, FA and RD images were merged into 4-dimensional (4D) AD, FA and RD image files. The input file order matched the group membership variables in the design matrix. Permutation-

based non-parametric inference was used for the two-way, voxelwise comparison of diffusivity parameters between each FTD group and controls using design matrix-defined contrasts which included age and gender as covariates. The study specific white matter skeleton was masked by atlas-defined labels for the entire cerebellum (left and right hemispheres) to restrict analyses to the cerebellum. The threshold-free cluster enhancement (TFCE) method was applied and results considered significant at a $p < 0.01$ TFCE family-wise error (FWE).

5.2.6 Genetic testing

Pathogenic GGGGCC hexanucleotide repeat expansions in *C9orf72* were screened for with repeat-primed PCR as described previously [247, 272]. Amplified DNA fragments were evaluated with the Applied Biosystems 3130xl Genetic Analyser (Foster City, CA, USA) and visualised using GeneMapper version 4.0. GGGGCC hexanucleotide repeat expansions longer than 30 were considered positive. Participating patients were also screened and tested negative for other mutations associated with ALS and FTD: *SOD1, ALS2, SETX, SPG11, FUS, VAPB, ANG, TARDBP, FIG4, OPTN, ATXN2, VCP, UBQLN2, SIGMAR1, CHMP2B, PFN1, ERBB4, HNRNPA1, MATR3, CHCHD10, UNC13A, DAO, DCTN1, NEFH, PRPH, SQSTM1, TAF15, SPAST, ELP3, LMNB1, SARM1, C21orf2, NEK1, FUS, CHMP2B, GRN, MAPT, PSEN1, PSEN2, TBK1.*

5.3 Results

5.3.1 Cerebellar morphometry

Region-of-interest morphometry in a study-specific, atlas-defined cerebellar grey matter mask revealed phenotype-specific patterns of atrophy at $p < 0.05$ TFCE (corrected for age, sex and TIV). GGGGCC hexanucleotide

repeat carrying ALS-FTD patients exhibited symmetric lobule VIII and lobule V atrophy. *C9orf72* negative ALS-FTD patients displayed lobule V, VI, VIII and vermis atrophy. Behavioural variant FTD patients showed vermis, lobule V, lobule VII and symmetric posterior-inferior volume reductions. Non-fluent variant primary progressive aphasia patients exhibited widespread atrophy including lobules V, VI, VIII, and the vermis. Semantic variant FTD patients displayed volume loss in crus I, Crus II, and lobule V on the left **(Figure 8)**.

Figure 8: Cerebellar morphometry

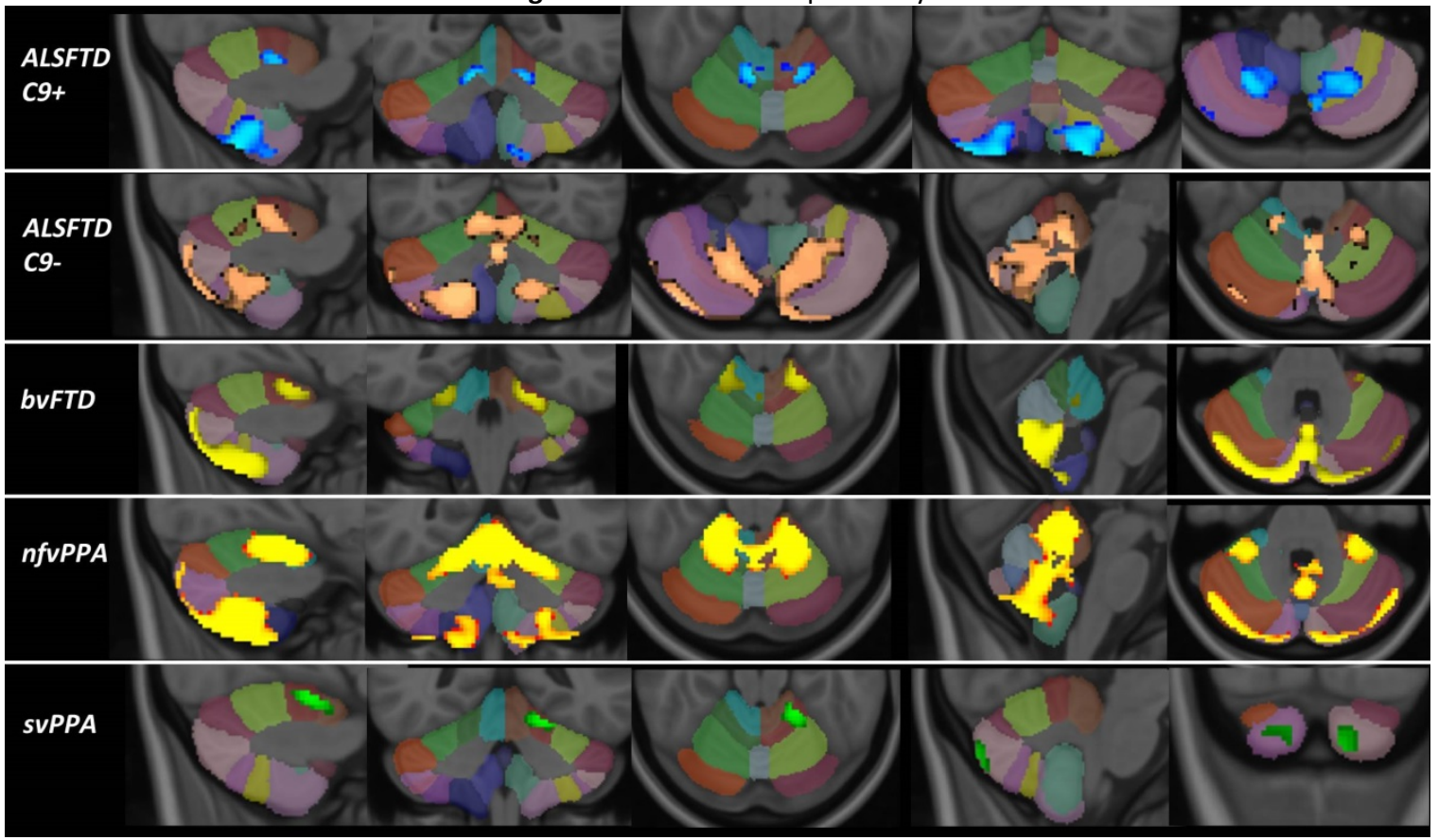

Cerebellar grey-matter changes in FTD phenotypes at $p < 0.05$ TFCE corrected for age, gender and TIV. Focal changes in C9+ALSFTD are indicated in blue, C9-ALSFTD in copper colour, bvFTD in yellow, nfvPPA red-yellow, svPPA in green. The Diedrichsen probabilistic cerebellar atlas is presented as underlay to aid localisation.

5.3.2 Cerebellar cortical thickness analyses

The evaluation of cortical thickness profiles revealed the preferential involvement of specific cerebellar lobules in FTD phenotypes with the apparent sparing of other cerebellar regions. Following FDR corrections and statistical adjustments for demographic factors, *C9orf72* positive ALS-FTD patients exhibited reduced cortical thickness in Lobule IV, VI,VIIb, Crus I & II. Crus II and lobule VI was affected in both cerebellar hemispheres **(Table 15)**. Cortical thinning did not reach statistical significance in *C9orf72* negative ALS-FTD patients in any of the evaluated cerebellar regions. Patients with behavioural variant FTD showed cortical thinning in crus I and a trend of thinning post FDR in lobule VII of the right cerebellar hemisphere. Patients with non-fluent variant primary progressive aphasia (nfvPPA) exhibited lobule VI, VIIb, crus I & II. Lobule VI and crus II atrophy was observed in each hemisphere. Patients with semantic variant FTD (svPPA) showed lobule VIIb, crus I & II degeneration in the right cerebellar hemisphere.

Table 15: Cerebellar cortical thickness profile of the ALS-FTD spectrum

Cerebellar Lobule		Cortical thickness: Estimated Marginal Mean ± Standard Error (mm)						Statistics						
		HC	ALS-FTD-C9-	ALS-FTD-C9+	bvFTD	nfvPPA	svPPA	F, p-value	Univariate effect size	HC vs ALSFTDC9-	HC vs ALSFTDC9+	HC vs bvFTD	HC vs nfvPPA	HC vs svPPA
Left [a]	**I-II**	1.416 ±0.031	1.678 ±0.074	1.437 ±0.074	1.432 ±0.124	1.604 ±0.095	1.749 ±0.190	F = 3.045, p = 0.012	η^2p = 0.085	**0.015**	0.9	0.94	0.21	0.23
	III	3.213 ±0.035	3.355 ±0.083	3.269 ±0.083	3.058 ±0.140	3.182 ±0.107	3.501 ±0.214	F = 1.198, p = 0.312	η^2p = 0.035	0.26	0.73	0.47	0.9	0.36
	IV	4.913 ±0.014	4.930 ±0.033	4.817 ±0.033	4.788 ±0.055	4.891 ±0.042	4.919 ±0.084	F = 2.462, p = 0.035	η^2p = 0.070	0.82	**0.06**[t]	0.133	0.82	0.95
	V	4.898 ±0.015	4.875 ±0.035	4.803 ±0.034	4.796 ±0.058	4.816 ±0.045	4.873 ±0.089	F = 2.095, p = 0.069	η^2p = 0.060	0.73	0.072	0.23	0.23	0.9
	VI	4.978 ±0.011	4.917 ±0.026	4.898 ±0.026	4.907 ±0.044	4.880 ±0.034	4.975 ±0.067	F = 3.431, p = 0.006	η^2p = 0.095	0.15	**0.05**	0.26	**0.06**[t]	0.97
	VIIB	4.608 ±0.021	4.566 ±0.049	4.476 ±0.049	4.470 ±0.082	4.408 ±0.063	4.467 ±0.125	F = 3.164, p = 0.009	η^2p = 0.088	0.61	0.076	0.26	**0.036**	0.46
	VIIIA	4.649 ±0.018	4.662 ±0.041	4.643 ±0.041	4.502 ±0.070	4.598 ±0.053	4.637 ±0.107	F = 1.023, p = 0.406	η^2p = 0.030	0.9	0.94	0.168	0.54	0.94
	VIIIB	4.514 ±0.032	4.671 ±0.076	4.430 ±0.076	4.322 ±0.129	4.711 ±0.098	4.582 ±0.196	F = 2.290, p = 0.048	η^2p =0.065	0.21	0.49	0.3	0.21	0.9
	IX	3.570 ±0.043	3.621 ±0.101	3.398 ±0.101	3.298 ±0.170	3.715 ±0.130	3.504 ±0.260	F = 1.363, p = 0.241	η^2p = 0.040	0.82	0.26	0.26	0.47	0.9
	X	2.491 ±0.042	2.299 ±0.099	2.468 ±0.098	2.273 ±0.0166	2.609 ±0.127	2.710 ±0.254	F = 1.400, p = 0.227	η^2p = 0.041	0.23	0.9	0.38	0.55	0.51
	Crus I	4.575 ±0.021	4.516 ±0.049	4.377 ±0.049	4.445 ±0.083	4.405 ±0.063	4.353 ±0.126	F = 4.241, p = 0.001	η^2p = 0.114	0.46	**0.003**	0.27	0.072	0.23
	Crus II	4.365 ±0.026	4.290 ±0.062	4.097 ±0.062	4.390 ±0.104	4.090 ±0.080	3.983 ±0.159	F = 5.695, p < 0.001	η^2p = 0.148	0.46	**0.003**	0.9	**0.015**	0.095

Right[b]	**I-II**	1.354 ±0.029	1.636 ±0.068	1.386 ±0.068	1.462 ±0.114	1.569 ±0.087	1.587 ±0.174	F = 3.878, p = 0.002	η^2p = 0.106	**0.001**	0.85	0.56	0.09	0.4
	III	3.092 ±0.032	3.167 ±0.076	3.118 ±0.076	3.163 ±0.128	3.142 ±0.098	3.139 ±0.196	F = 0.234, p = 0.947	η^2p = 0.007	0.56	0.85	0.8	0.83	0.86
	IV	4.772 ±0.019	4.755 ±0.045	4.714 ±0.045	4.758 ±0.076	4.819 ±0.058	4.794 ±0.116	F = 0.475, p = 0.795	η^2p = 0.014	0.85	0.45	0.86	0.65	0.86
	V	4.752 ±0.018	4.679 ±0.043	4.648 ±0.043	4.686 ±.072	4.735 ±0.055	4.703 ±0.110	F = 1.399, p = 0.227	η^2p = 0.041	0.26	0.11	0.56	0.85	0.85
	VI	4.928 ±0.011	4.880 ±0.026	4.855 ±0.026	4.883 ±0.043	4.835 ±0.033	4.901 ±0.066	F = 2.768, p = 0.020	η^2p = 0.078	0.23	**0.054**[t]	0.52	**0.054**[t]	0.85
	VIIB	4.788 ±0.017	4.695 ±0.041	4.608 ±0.041	4.610 ±0.069	4.665 ±0.053	4.399 ±0.106	F = 6.938, p < 0.001	η^2p = 0.175	0.14	**0.001**	**0.07**[t]	0.11	**0.001**
	VIIIA	4.642 ±0.017	4.600 ±0.039	4.571 ±0.039	4.522 ±0.066	4.576 ±0.050	4.448 ±0.101	F = 1.849, p = 0.106	η^2p = 0.053	0.52	0.24	0.23	0.44	0.18
	VIIIB	4.573 ±0.026	4.593 ±0.061	4.497 ±0.061	4.454 ±0.103	4.519 ±0.079	4.673 ±0.157	F = 0.695, p = 0.628	η^2p = 0.021	0.85	0.45	0.45	0.73	0.74
	IX	3.763 ±0.037	3.70 ±0.088	3.609 ±0.088	3.485 ±0.148	3.720 ±0.113	3.720 ±0.226	F = 1.148, p = 0.337	η^2p = 0.034	0.86	0.26	0.21	0.85	0.86
	X	2.251 ±0.036	2.105 ±0.085	2.146 ±0.085	1.996 ±0.143	2.228 ±0.110	2.170 ±0.219	F = 1.127, p = 0.348	η^2p = 0.033	0.26	0.45	0.23	0.86	0.85
	Crus I	4.636 ±0.022	4.572 ±0.051	4.524 ±0.051	4.393 ±0.086	4.429 ±0.066	4.157 ±0.131	F = 5.628, p < 0.001	η^2p = 0.146	0.45	0.15	**0.047**	**0.03**	**0.001**
	Crus II	4.576 ±0.024	4.499 ±0.055	4.412 ±0.055	4.381 ±0.093	4.364 ±0.071	4.035 ±0.142	F = 5.637, p < 0.001	η^2p = 0.147	0.41	**0.047**	0.15	**0.043**	**0.001**

Note. HC = healthy controls; Estimated marginal means ± S.E. for cortical thickness are adjusted for age and gender.
Post-hoc univariate comparisons across groups were performed only in case of a significant multivariate omnibus test:
[a] Pillai's Trace = 0.623; F (12,60) = 1.864; p < 0.001; η^2p = 0.125; [b] Pillai's Trace = 0.575; F (12,60) = 1.701; p = 0.001; η^2p = 0.115;
Bold p-values are significant at p < 0.05, after false-discovery rate correction for multiple comparisons.
Partial η^2 effect size is interpreted as small (η^2p = 0.01), medium (η^2p = 0.06) or large (η^2p = 0.14). [t] statistical trend at p ≤ 0. 07

5.3.3 Cerebellar white matter alterations

Permutation-based nonparametric statistics confirmed focal diffusivity alterations at $p < 0.01$ TFCE (corrected for age & sex) in a study-specific cerebellar white matter skeleton. Reduced fractional anisotropy, reduced axial diffusivity and increased radial diffusivity were detected in each FTD phenotype with reference to healthy controls. Patterns of white matter vulnerability varied along the ALS-FTD spectrum **(Figure 9).** *C9orf72* positive ALS-FTD patients exhibited reduced FA in the superior cerebellar peduncle, reduced AxD in Crus I & II, and increased RD in lobules I-IV as well as in the superior peduncle. *C9orf72* negative ALS-FTD patients displayed widespread, symmetric, multi-lobular FA reductions, focal AxD reduction in the right lobule V, and increased RD in crus I & II in the right cerebellar hemisphere. Patients with behavioural variant FTD showed FA reductions in nearly the entire cerebellar white matter skeleton, reduced AxD in crus I & II, and widespread areas of increased RD in particular in lobule VI. Patients with non-fluent variant primary progressive aphasia (nfvPPA) exhibited multi-lobular FA and AxD reductions and similarly widespread RD increases. Patients with semantic variant FTD (svPPA) showed superior-predominant symmetric FA reductions centred on lobule V, reduced AxD in Crus I, and no RD alterations at $p < 0.01$.

Figure 9: Cerebellar white matter analyses

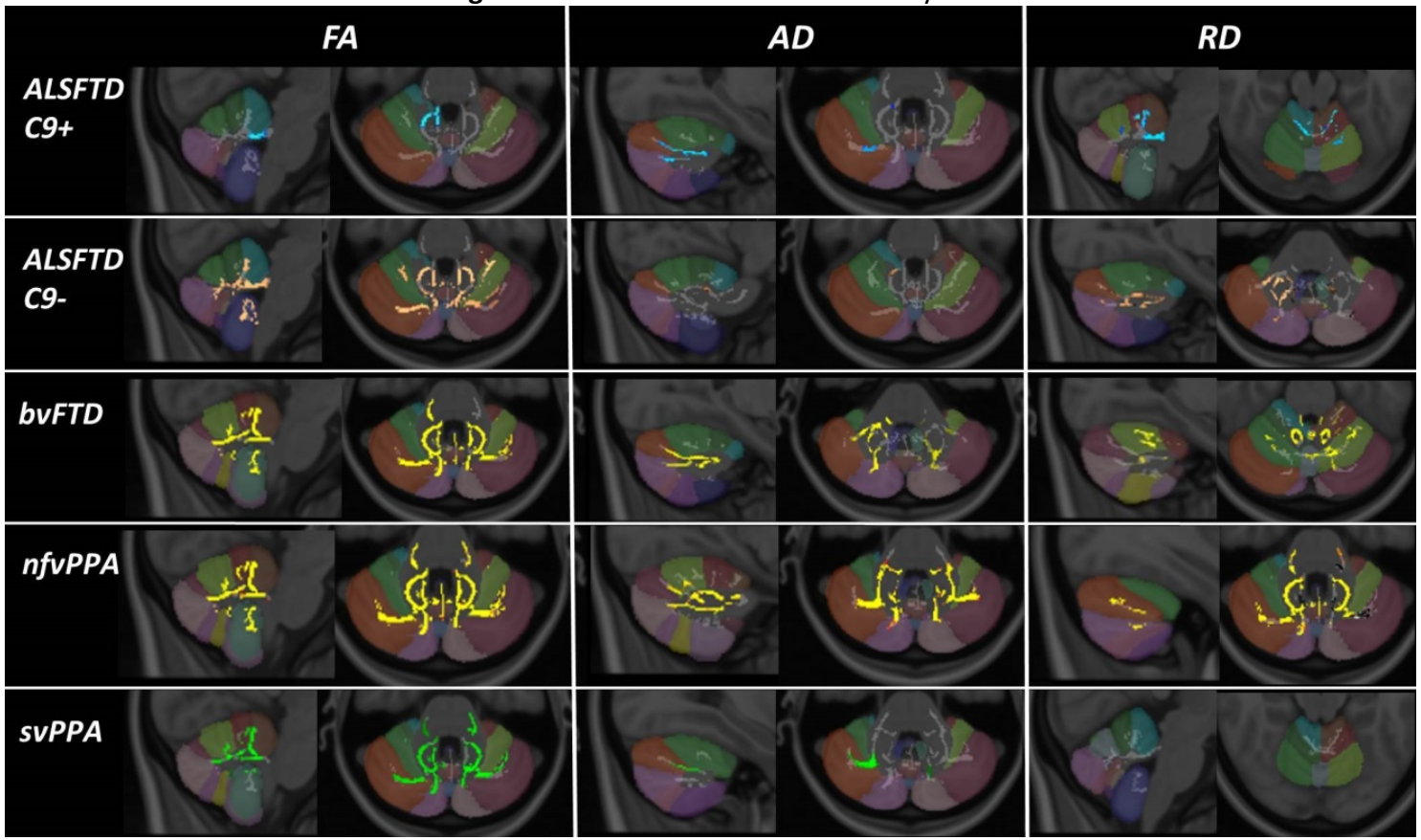

Tract-based white matter cerebellar changes in FTD phenotype as identified by FA, AxD and RD alterations at $p < 0.01$ TFCE adjusted for age and gender. Changes in C9+ALSFTD are indicated in blue, C9-ALSFTD in copper colour, bvFTD in yellow, nfvPPA red-yellow, svPPA in green. The Diedrichsen probabilistic cerebellar atlas is presented as underlay to aid localisation.

5.3.4 Summary of findings

The integration of findings across multiple imaging modalities revealed the selective involvement of cerebellar regions with relatively distinctive imaging signatures along the ALS-FTD spectrum **(Table 16).**

Table 16: Summary of focal cerebellar findings in ALS-FTD spectrum across the five imaging modalities

Study Group	Morphometry	FA	AxD	RD	Cortical Thickness
C9+ALSFTD	Lobule V, VIII	Superior peduncle	Crus I & II	Lobules I-IV Superior peduncle	Lobule IV, VI, VII Crus I & II
C9-ALSFTD	Lobule V, VI, VIII Vermis	Widespread multi-lobular	Lobule V	Crus I & II	Nil at $p < 0.05$ post FDR
bvFTD	Lobule V, VII Vermis	Widespread multi-lobular	Crus I & II	Widespread multi-lobular	Lobule VII Crus I
nfvPPA	Lobule V, VI, VIII Vermis	Widespread multi-lobular	Widespread multi-lobular	Widespread multi-lobular	Lobule VI, VII Crus I & II
svPPA	Lobule V, crus I & II	Lobule V Superior cerebellum	Crus I	Nil at $p<0.01$	Lobule VII, crus I & II

5.4 Discussion

Our study indicates that clinical subtypes of FTD exhibit individual patterns of cerebellar degeneration; these changes are widespread in nfvPPA and bvFTD, but relatively focal in svPPA. Marked cerebellar differences were detected between C9+ALSFTD and C9-ALSFTD. Our data suggest that certain cerebellar regions, such as lobule V, VI, VIII, vermis, Crus I and II, are more susceptible to degeneration in FTD than other areas. While our findings are in line with previous reports[630, 632] one of the novelty of our study is the detection of lobule V degeneration across the clinical spectrum of FTD. This lobule is part of the anterior cerebellar lobe that primarily mediates sensorimotor functions [620, 651, 652]. However, dichotomising motor and cognitive functions to the anterior and posterior cerebellum may be simplistic; lobule V is also involved in verbal working memory, emotion and rhythm processing [619, 620]. This region has previously been implicated in bvFTD cohorts including those with ALSFTD[628]. We have also demonstrated that the cerebellar vermis is involved in nfvPPA, C9-ALSFTD-, and to a greater extent in bvFTD. Vermis degeneration has been previously linked to bvFTD and described in ALSFTD [628, 630, 632, 635]. This region is often referred to as the 'limbic cerebellum' because of its role in emotion processing and its connectivity with the limbic and paralimbic regions[619]. Structural abnormalities in this region may manifest in a myriad of irregular social or emotional behaviours, including aggression, irritability and disinhibition [627, 653, 654]. A similar constellation of symptoms may occur in opsoclonus myoclonus syndrome, a post-infectious or paraneoplastic disorder that preferentially involves the cerebellar vermis [655]. These observations are further supported

by altered cerebello-cerebral connectivity in bipolar affective disorder [650, 656]. The functional topography of the cerebellum has been gradually elucidated [657] and careful meta-analyses have ascribed specific higher-level cognitive functions to distinct cerebellar areas[619, 620]. The affected regions identified in our study within the 'cognitive cerebellum' are involved in emotional processing, attention, executive function, working memory, language including expressive language, and social cognition [619, 620, 658]. Functional MRI studies have confirmed the co-activation of posterior cerebellar and prefrontal cortices during cognitive tasks, patterns which are distinctly different from the activation of the anterior cerebellum and sensorimotor cortices during motor tasks [621, 659, 660]. This pattern of connectivity has been replicated in greater detail in post-mortem studies [661, 662].

We predominantly observed symmetric cerebellar degeneration, with the exception right hemisphere dominant cortical thinning in bvFTD and svPPA. The asymmetric cerebellar findings in svPPA may be linked to the similarly lateralised pathology at a supratentorial level and potentially mediated by crossed cerebellar network [142, 619, 620, 630, 663]. It is noteworthy however that, exclusively left-sided lobule V, crus I-II volume reductions were noted in svPPA on morphometric analyses. These observations highlight that different imaging modalities capture different aspects of cerebellar degeneration[493].

We detected markedly divergent grey and white matter changes in *C9orf72* positive and *C9orf72* negative ALSFTD patients. In contrast to the widespread atrophy observed in C9+ALSFTD, cortical thinning did not reach statistical significance in C9-ALSFTD. This is consistent with the more extensive

cerebellar involvement associated with the *C9orf72* mutation [156, 629, 642, 643]. Cerebellar, cerebral and spinal changes have also been detected in presymptomatic GGGGCC hexanucleotide repeats expansion carriers [155, 249, 664, 665]. It is noteworthy however that, p62-immunoreactive TDP-43 negative neuronal cytoplasmic inclusions were noted in cerebellar granule cells irrespective of *C9orf72* status [631, 643]. Widespread cerebellar and cerebral degeneration have also been consistently noted in ALS and PLS cohorts without FTD [491, 666, 667]. Dysarthria, pseudobulbar affect, and cognitive deficits are commonly observed in ALS, and cerebellar pathology may contribute to these symptoms [496, 500, 668-670]. Interestingly, we detected higher cortical thickness in lobules I-II in *C9orf72* negative ALSFTD compared to controls, which may be in line with the proposed compensatory role of the cerebellum in ALS [231, 488, 671].

Our findings may have clinical implications. Patients with clinical and genetic FTD subtypes attend a broad range of specialist including neurologist, psychiatrists and medicine for the elderly physicians. Clinical assessments may be heavily weighted towards cognitive and behavioural testing. If a cerebellar exam is performed at all, there is likely to be a greater emphasis on eliciting physical clinical signs. Post-mortem studies that confirmed cerebellar involvement in *C9orf72* highlighted the absence of overt ante mortem cerebellar signs such as ataxia without considering cognitive manifestations [642, 643]. It is conceivable that a formal cerebellar examination was not performed in some of these cases, and subtle cerebellar deficits may remain unrecognised. Since in our study lobule V degeneration was a consistent finding in all FTD subtypes, and this structure is a principal hub of cerebro-

cerebellar sensorimotor networks, we suggest that formal cerebellar examination should be performed in all patients with suspected FTD. In addition, sequencing tasks (visual, verbal, behavioural and spatial) could be considered as a screening tool for cerebellum-associated cognitive dysfunction [622]. In those with apparent autosomal dominant inheritance who test negative for common FTD genes, it is important to consider SCA17; as it may initially resemble bvFTD [672]. The establishment of phenotype-specific imaging signatures and biomarker profiles may also aid the accurate categorisation of single subject datasets into relevant diagnostic, phenotypic or prognostic groups [55, 60, 158, 503, 673].

In addition to the lack of molecular profiling, a key limitation of our study is the sample size of our cohorts, particularly in those with PPA. Accordingly, our data need to be replicated in larger cohorts and validated by the dedicated assessment of the cerebellum post mortem. Longitudinal radiological data acquisition may help to further elucidate the dynamic biological processes underpinning the progressive symptoms observed clinically [172]. Future cerebellar studies in FTD may benefit from complementing quantitative MRI analyses with [^{18}F] FDG-PET to establish the comparative detection sensitivity of the two modalities. While previous PET studies captured cerebellar hypometabolism no convergent patterns have been identified [632, 639, 640].

Our own findings, and the limited literature available, suggest that cerebellar degeneration is an important, albeit under investigated facet of FTD research, which merits dedicated clinical, imaging and post mortem studies. The characterisation of cerebellar pathology in FTD is not merely an

academic pursuit. The concomitant degeneration of interconnected infra- and supra-tentorial regions indicates connectivity-mediated propagation mechanisms, which may aid the identification of novel therapeutic targets. The demonstration of markedly divergent cerebellar signatures across the spectrum of FTDs serves as a reminder that FTD is a pathologically heterogeneous condition and the quest for 'one drug for all' is a naïve notion. In line with the principles of precision medicine, phenotype- and genotype-specific disease-modifying strategies are likely offer therapeutic benefits. Pioneering antisense oligonucleotide (ASO) studies in *C9orf72* give cause for optimism to target specific genotypes and coordinated research efforts targeting tau may also pave the way to breakthrough individualised therapies[155, 674]. The refinement of clinical screening tools and the development of disease-specific imaging protocols may not only assist the accurate categorisation of suspected FTD patients but serve as biomarkers in future clinical trials.

5.5 Conclusions

Our data indicate unique cerebellar imaging signatures in FTD phenotypes with the selective involvement of specific lobules. It is conceivable that facets of behavioural and cognitive impairment previously exclusively attributed to supratentorial regions, may in part stem from cerebellar degeneration. Our findings highlight the involvement of infratentorial regions in FTD and support the evolving role of the cerebellum in cognitive and behavioural manifestations.

6 Thalamic pathology in frontotemporal dementia: predilection for specific nuclei, phenotype-specific signatures, clinical correlates and practical relevance

6.1 Introduction

Frontotemporal dementia (FTD) encompasses a clinically and genetically diverse spectrum of neurodegenerative disorders. While phenotype-specific cortical signatures and anatomical patterns of hypometabolism are well-defined, the in-depth characterisation of subcortical pathology is a relatively recent aspiration of quantitative neuroradiology. The contribution of multi-synaptic cortico-thalamic circuits to physiological behavioural, executive and language functions are relatively well established [541, 675]. Accordingly, in this review, we first introduce the structural and functional anatomy of the thalamus followed by a systematic review of thalamic involvement across the FTD spectrum stratified according to phenotype, genotype and pathological subtype.

The thalami are deep paramedian grey matter structures, located superior to the midbrain, joined by the interthalamic adhesion. They are enclosed in a white matter external medullary lamina and separated by a Y-shaped white matter internal medullary lamina that divides the thalamus into anterior, medial and lateral anatomical regions. The lateral region is further subdivided into lateral, ventral and posterior divisions. Each anatomical region contains a subset of thalamic nuclei: anterior thalamic nucleus in the anterior region; medial dorsal and midline nuclei in the medial region; lateral posterior and lateral dorsal nuclei in the lateral division of the lateral region; ventral

anterior, ventral lateral, ventral posterolateral and ventral medial nuclei in the ventral division of the lateral region; and pulvinar, lateral and medial geniculate nucleus nuclei in the posterior division of the lateral region. The thalamic nuclei also include intralaminar nuclei within the internal medullary lamina; and reticular nucleus on the lateral surface of the thalamus [676].

Functionally, the thalamus mediates a multitude of both sensory and non-sensory processes that extend well beyond these structural boundaries **(Figure 10).** The sensory functions are classically mapped onto the ventral posterolateral, ventral medial, lateral and medial geniculate nuclei; specifically peripheral sensory information (e.g. temperature, pain, vibration, touch, proprioception) is relayed via the ventral posterolateral nuclei, taste and facial sensation via the ventral medial nuclei, visual sensory information via the lateral geniculate nuclei and auditory sensory information via the medial geniculate nuclei [677]. Motor and language functions are relayed by the ventral anterior, ventral lateral, ventral posterolateral and ventral medial nuclei [677]. Limbic processes are conveyed by anterior, ventral anterior, medial dorsal, lateral dorsal and pulvinar nuclei [677, 678]. The anterior nuclei give rise to the thalamocingulate tract, an integral part of the Papez circuit that plays a central role in episodic memory [679, 680]. Associative functions are mediated by midline nuclei; medial dorsal, lateral posterior and pulvinar nuclei [677, 678]. This area plays a complex role in cognition and the integration of somatosensory and visuospatial information [677]. The intralaminar and reticular nuclei contribute to arousal and alertness [677].

The thalamus is part of a wider network of cortico-subcortical circuits including the basal ganglia that mediate cognitive and behavioural functions

[541, 675]. Each thalamic sub-region is linked with specific cortical areas via thalamocortical and corticothalamic projections forming closed-loop networks [681, 682]. Macroscopically, the anterior thalamic radiation primarily connects the anterior and medial thalamic regions with the limbic and frontal cortices; the superior thalamic radiation links ventral thalamic regions to the precentral and postcentral gyri; and the posterior thalamic region project to parietal and occipital regions via the posterior thalamic radiation [683]. Within these large anatomical labels, there are several specific thalamocortical tracts, such as the thalamocingulate tract connecting the anterior thalamus with the cingulate cortex in Papez circuit [679, 680]. Functional MR imaging studies confirm cortico-thalamic-cortical connections between the prefrontal cortex and mediodorsal, ventral anterior nuclei and anterior thalamic region; the temporal cortex and medial pulvinar and medial geniculate nuclei; the parietal and occipital cortices and lateral pulvinar and lateral geniculate nuclei; the somatosensory cortex with anterior pulvinar and ventral posterolateral nuclei; the motor and premotor cortex with ventral anterior, ventral lateral, and mediodorsal nuclei [684, 685]. The disruption of specific thalamocortical circuits has been linked to fairly specific neuropsychological manifestations, such as executive dysfunction, apathy, disinhibition or depression [675, 686, 687].

From an imaging perspective, the thalamus is often simplistically considered as a single structure but recent advances in computational imaging have permitted the nuanced appraisal of specific nuclei. With increasing interest in subcortical structures in FTD, we review the existing evidence of thalamic involvement across the FTD spectrum stratified by phenotype, genotype and pathological subtype. The main objectives of this review is the

description of phenotype- and genotype-associated intra-thalamic signatures based on consensus research findings, highlighting inconsistencies among published papers, identifying innovative research strategies as well as methodological shortcomings to propose desirable study designs for future initiatives, a synthesis of academic contributions and reflecting on the potential clinical relevance of thalamic pathology in FTD.

Figure 10: A schematic diagram of thalamo-cortical circuits

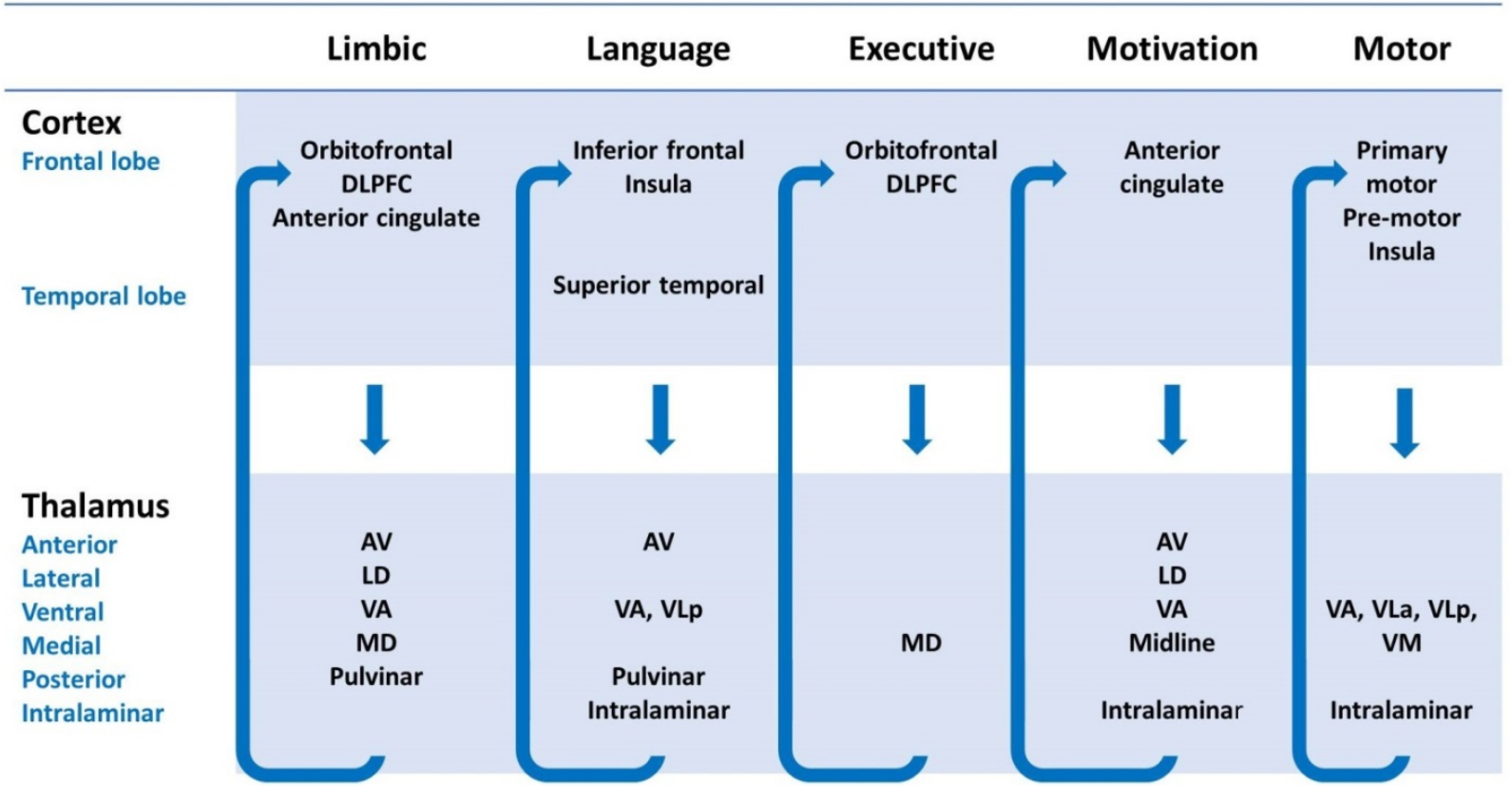

A schematic diagram of distinct thalamo-cortical circuits, their main thalamic components, cortical projections and associated physiological role;
AV: anterior ventral; DLPFC: dorsolateral prefrontal cortex; LD: lateral dorsal; MD: medial dorsal; VA: ventral anterior; VLa: ventral lateral anterior; VLp: ventral lateral posterior; VM: ventral medial.

6.2 Methods

A formal literature review was conducted using the PubMed repository (last accessed on 16th May 2022) in accordance with the 'preferred reporting items for systematic reviews and meta-analyses' (PRISMA) guidelines. The following search strategy was used: ("frontotemporal dementia" [Mesh] OR "frontotemporal dementia" [tw] OR "FTD" [tw] OR "frontotemporal lobar degeneration" [tw] OR "FTLD" [tw] OR "*C9orf72*" [tw] OR "*MAPT*" [tw] OR "*GRN*" [tw]) AND ("thalamus"[Mesh] OR "thalam*" [tw] OR "subcortical") AND ("neuroimaging" [Mesh] OR "MRI" [tw] OR "magnetic resonance imaging" [tw] OR "brain imaging" [tw] OR "neuroimaging" [tw] OR "PET" [tw] OR "positron emission tomography" [tw] OR "pathology" [Mesh] OR "autopsy" [Mesh] OR "neuropathology" [Mesh] OR "post-mortem" [tw]). The database search was limited to studies written in English that involved human subjects. A single reviewer (MCMcK) individually screened and assessed the 266 records for eligibility. All original research articles that investigated radiological or pathological involvement of the thalamus in FTD were included. Reviews, editorials and case reports were excluded. Studies limited to corticobasal syndrome (CBS) and progressive supranuclear palsy (PSP) phenotypes were also excluded. The reference lists of selected articles were reviewed to identify additional, potentially relevant papers **(Figure 11).** Identified original research articles were individually reviewed for cohort sizes, demographic profile, clinical categorisation, genetic information, imaging methods, study design, cross-sectional versus longitudinal data collection, main findings, anatomical predilection, the battery of

accompanying clinical tests, and the presence of presymptomatic or post-mortem data.

Figure 11: A PRISMA flowchart for systematic review of thalamic involvement in FTD

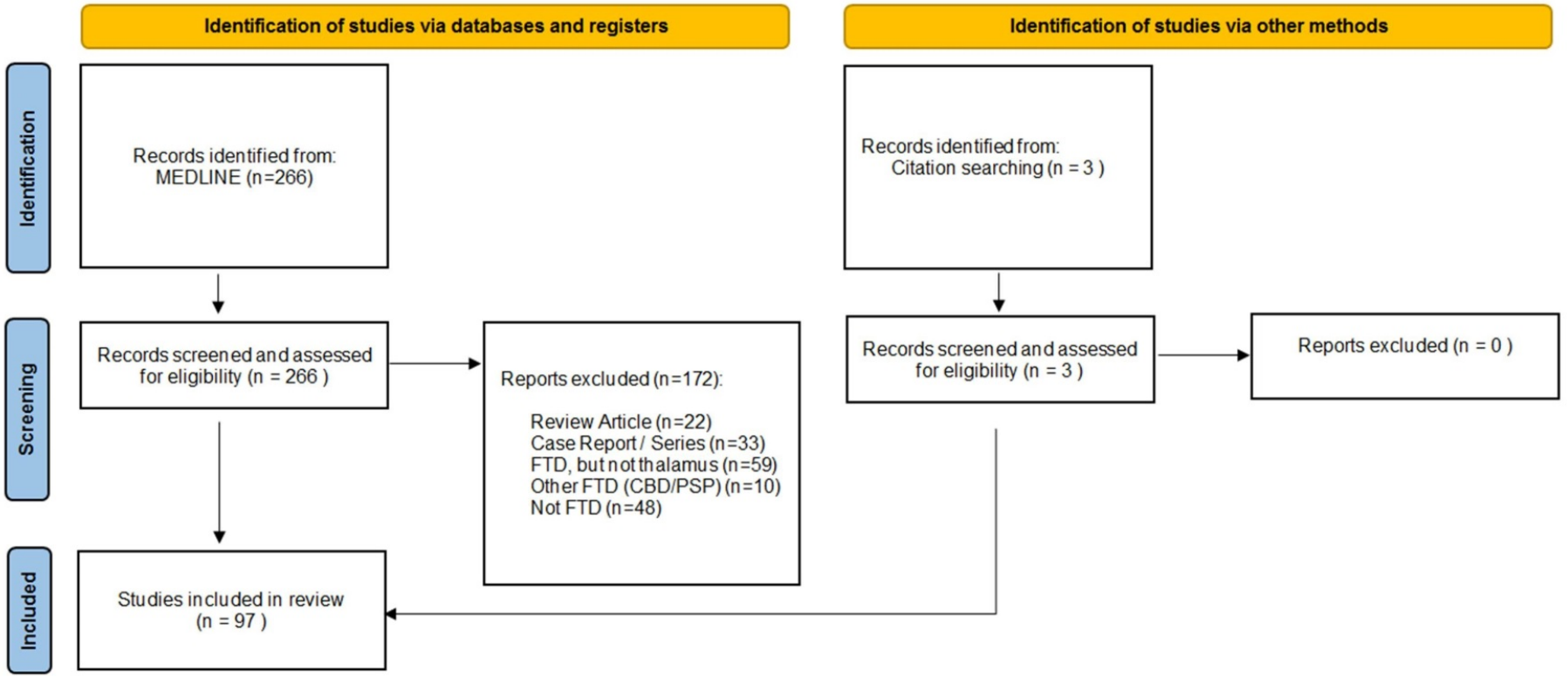

6.3 Results

A total of 97 original research articles met the inclusion criteria. The majority of these studies were exclusively imaging-based (79%; n=77/97); some had both imaging and pathology data (18%; n=18/97); and very few reported pathological data only (3%; n=3/97) **(Table 17).** The studies were typically unimodal (73%; n=71/97). The most commonly used imaging modality was MRI (88%; n=85/97) including grey matter (77%; n=75/97) **(Table 18),** white matter (20%; n=19/97) **(Table 19)** and functional (13%; n=13/97) **(Table 20)** analyses. A minority of studies used PET imaging (16%; n=16/97) **(Table 21).** The thalamus was most often considered as a single structure, and seldom segmented into specific nuclei (4%; n=4/97) [183, 193, 247, 688] . Only a minority of studies were longitudinal (13%; n=13/97) with a mean interval follow-up of 1.3±0.5 years. The participants were stratified according to phenotype (78%; n=76/97); genotype (46%; n=45/97); or pathology (21%; n=20/97). Pre-symptomatic familial FTD mutation carriers were occasionally included (19%; n=18/97) **(Table 22).** The results of these studies are summarised according to phenotype, genotype and pathological diagnoses.

Table 17: Neuropathological studies of thalamic involvement in FTD

Neuropathology					
First author, year of publication	**Patient groups and cohort sizes**	**Study design**	**Neuropathology**	**Follow-up duration**	**Imaging modality**
Brettschneider et al, 2014 [244]	FTLD-TDP n=39 (bvFTD n=39) (*C9orf72* n=12; *GRN* n=6)	Cross-sectional Case-series	All cases	N/A	N/A
Kawles et al, 2022 [689]	FTLD-TDP type C n=10 (svPPA n=7; bvFTD n=3)	Cross-sectional Case-series	All cases	N/A	N/A
Yang et al, 2017 [690]	*C9orf72* positive bvFTD n=13 Sporadic bvFTD n=8 Sporadic ALS n=7 Controls n=7	Cross-sectional Case-control	All cases	N/A	N/A

Table 18: Grey matter imaging studies of thalamic involvement in FTD

Structural (Segmentation and Volumetry)					
First author, year of publication	**Patient groups and cohort sizes**	**Study design**	**Neuropathology**	**Follow-up**	**Imaging modality**
Ahmed et al, 2016 [691]	bvFTD n=19 svPPA n=15 AD n=15 Controls n=25	Cross-sectional Case control	N/A	N/A	VBM
Ahmed et al, 2019 [692]	bvFTD n=28 AD n=16 Controls n=19	Cross-sectional Case control	N/A	N/A	VBM
Ahmed et al, 2021[693]	bvFTD n=58 (*C9orf72+* n=17) ALS-FTD n=41 (*C9orf72+* n=12) Controls n=58	Cross-sectional Case control	N/A	N/A	Cortical, subcortical, WM volumes
Bede et al, 2018 [663]	bvFTD n=10 nfvPPA n=11 svPPA n=5 ALS-FTD *C9orf72+* n=14; *C9orf72-* n=12 ALS without cognitive impairment n=36 Controls n=50	Cross-sectional Case control	N/A	N/A	Cortical thickness Subcortical volume and density Connectivity-based segmentation
Bocchetta et al, 2018 [694]	FTD n=341 Phenotypes: bvFTD n=141; svPPA n=76; nfvPPA n=103; FTD-ALS n=7; PPA unspecified n=14) Genotypes: *MAPT* n=24; *C9orf72* n=24; *GRN* n=15 Pathology: Tau n=40; TDP-43 n=61; FUS n=3 Controls n=99	Cross-sectional Case control	TDP43 n=61 Tau n=40 FUS n=3	N/A	Volumetry
Bocchetta et al, 2019 [695]	svPPA n=24 Controls n=72	Cross-sectional Case control	N/A	N/A	Cortical and subcortical volumes
Bocchetta et al, 2020 [696]	FTLD TDP-43 Type C n=19 Controls n=81	Longitudinal n=14 Case control	All cases	Not specified	Volumetry

Structural (Segmentation and Volumetry)					
First author, year of publication	**Patient groups and cohort sizes**	**Study design**	**Neuropathology**	**Follow-up**	**Imaging modality**
Bocchetta et al, 2020 [688]	FTD n=402 Phenotypes: bvFTD n=180; svPPA n=85; nfvPPA n=114; FTD-ALS n=8; PPA unspecified n=15 Genotypes: *MAPT* n=27; *C9orf72* n=28; *GRN* n=18 Pathology: Tau n=37; TDP-43 n=38; FUS n=4 Controls n=104	N/A	TDP43 n=38 Tau n=37 FUS n=4	N/A	Volumetry Thalamic nuclei segmentation
Bocchetta et al, 2021[183]	Pre-symptomatic *MAPT* n=47; *GRN* n=125; *C9orf72* n=107 Mild symptomatic *MAPT* n=13; *GRN* n=30; *C9orf72* n=32 Symptomatic *MAPT* n=20; *GRN* n=43; *C9orf72* n=63 Controls n=298	Cross-sectional Case control	N/A	N/A	Cortical and subcortical volumes
Branco et al, 2018 [697]	ALS n=50 (Cognitively impaired ALS n=12) Controls n=38	Cross-sectional Case control	N/A	N/A	Cortical thickness Subcortical volume DTI
Cajanus et al, 2020 [698]	FTLD *C9orf72*+ n=26 (bvFTD n=19, PPA n=5; FTD-ALS n=2) FTLD *C9orf72*- n=52 (bvFTD n=35; PPA n=14; FTD-ALS n=3)	Longitudinal n=11	N/A	23 months	Cortical thickness Subcortical volume
Cardenas et al, 2007 [699]	FTD n=22 (ALS-FTD n=5) Controls n=22	Cross-sectional Case control	Pick's disease n=2 FTD-ubiquitin n=2 ALS-FTD n=1	N/A	Morphometry
Cash et al, 2018 [156]	Pre-symptomatic *MAPT* n=23; *GRN* n=65; *C9orf72* n=40 Symptomatic *MAPT* n=10; *GRN* n=; *C9orf72* n=25 Controls n=144	Cross-sectional Case control	N/A	N/A	VBM
Chang et al, 2005 [430]	ALS n=10 FTD-ALS n=10 Controls n=22	Cross-sectional Case control	N/A	N/A	VBM

Structural (Segmentation and Volumetry)					
First author, year of publication	**Patient groups and cohort sizes**	**Study design**	**Neuropathology**	**Follow-up**	**Imaging modality**
Chipika et al, 2020 [247]	*C9orf72* + ALS n=12 (ALS-FTD n=8/12) *C9orf72* - ALS n=88 (ALS-FTD n=7/88) PLS n=33 Controls n=117	Cross-sectional Case control	N/A	N/A	TIV Thalamus segmentation Thalamus vertex analyses Thalamus morphometry
Convery et al, 2020 [203]	Pre-symptomatic *MAPT* n=39; *GRN* n=104; *C9orf72* n=73 Symptomatic *MAPT* n=10; *GRN* n=24; *C9orf72* n=31 Controls n=181	Cross-sectional Case-control	N/A	N/A	VBM
Cury et al, 2019 [192]	Pre-symptomatic *MAPT* n=26; *GRN* n=53; *C9orf72* n=34 Controls n= 98	Cross-sectional Case control	N/A	N/A	Large diffeomorphic deformation metric mapping
De Reuck et al, 2014 [700]	FTLD n=37 AD n=46 ALS n=11 LBD n=13 PSP n=14 VD n=16 Controls n=15	Cross-sectional Case control	All cases	N/A	Quantification MRI GRE iron
De Reuck et al, 2017 [701]	ALS n=12 FTLD n=38 (FUS n=6; Tau n=13; TDP43 n=19) Controls n=28	Cross-sectional Case control	All cases	N/A	Quantification of MRI GRE iron
Devenney et al, 2017 [702]	bvFTD n=36; (*C9orf72+* n=9/36) FTD-ALS n=20 (*C9orf72+* n=5/20) Controls n=23	Cross-sectional Case control	N/A	N/A	VBM
Devenney et al, 2021 [703]	ALS n=28 ALS-Plus n=9 ALS-FTD n=11 bvFTD n=27 Controls n=25	Cross-sectional Case-control	N/A	N/A	VBM

Structural (Segmentation and Volumetry)					
First author, year of publication	**Patient groups and cohort sizes**	**Study design**	**Neuropathology**	**Follow-up**	**Imaging modality**
Fletcher et al, 2015 [704]	FTLD n=31 (sporadic n=24/31) Phenotype: bvFTD n=15; svPPA n=11; nfvPPA n=5 Genotype: *C9orf72* n=6; *MAPT* n=2 AD n=20	Cross-sectional Case-control	N/A	N/A	VBM
Garibotto et al, 2011 [705]	bvFTD n=38 svPPA n=9 nfvPPA n=6 Controls n=25	Cross-sectional Case-control	N/A	N/A	Subcortical volume
Harper et al, 2017 [706]	Dementia n=186 (AD n= 107; DLB n=25; FTLD n=54 [3R-tau n=11; 4R-tau n=17; TDP43A n=12; TDP43C n=14]) Controls n=73	Cross-sectional Case-control	All cases	N/A	VBM
Hornberger et al, 2012 [680]	In vivo: bvFTD n=15; AD n=19; controls n=18 Post-mortem: bvFTD n=19; AD n=18; controls n=20	Cross-sectional Case-control	Post-mortem cohort: bvFTD n=19 [TDP type A n=6; TDP type B n=3; Tau n=10 – Picks disease n=7; CBD n=3]; AD n=18; Controls n=20	N/A	VBM DTI
Irwin et al, 2013 [707]	*C9orf72+* n=64 (ALS n=31; FTD n=22 [bvFTD n=17; svPPA n=1; nfvPPA n=4]; ALS-FTD n=9; AD n=2) *C9orf72-* n=79 (ALS n=36; FTD n=43 [bvFTD n=23; svPPA n=7; CBS n=2]; ALS-FTD n=10; AD n=1)	Cross-sectional Case-control	*C9orf72+* n=13 *C9orf72-* n=12	N/A	VBM
Irwin et al, 2016 [708]	Pick's disease n=21 (bvFTD n=16; nfvPPA+bvFTD n=1; ALS-FTD n=1; CBS n=2; AD n=1) Imaging controls n=60	Cross-sectional Case series	All cases	N/A	GMD DTI
Kumfor et al, 2015 [709]	svPPA n=11 bvFTD n=13 Controls n=11	Cross-sectional Case-control	N/A	N/A	VBM

Structural (Segmentation and Volumetry)					
First author, year of publication	**Patient groups and cohort sizes**	**Study design**	**Neuropathology**	**Follow-up**	**Imaging modality**
Landin-Romero et al, 2017 [710]	bvFTD n=37 AD n=41 Controls n=33	Longitudinal Case-control	N/A	1-, 2-, 3, 4-years	Cortical thickness Subcortical volumes
Links et al, 2009 [711]	FTD n=21 Controls n=21	Cross-sectional Case-series	N/A	N/A	Subcortical volumes
Machts et al, 2015 [448]	*C9orf72+* ALS n=67 (ALS-FTD n=7; ALS ci/bi n=18; ALS-cn n=42) Controls n=39	Cross-sectional Case-control	N/A	N/A	Subcortical volume, density, shape
Mahoney et al, 2011 [712]	svPPA n=43	Cross-sectional Case-control	N/A	N/A	VBM
Manera et al, 2019 [713]	bvFTD n=70 Controls n=133	Longitudinal Case-control	N/A	1-year	Deformation-based morphometry
Mann et al, 1993 [714]	FTD n=10 FTD-ALS n=6	Cross-sectional Case series	All cases	N/A	Cortical thickness Cortical, subcortical CSA Cortical ribbon length
McKenna et al, 2021 [193]	bvFTD n=10 nfvPPA n=15 svPPA n=5 ALS-FTD *C9orf7+* n=20; *C9orf72-* n=20 Controls n=100	Cross-sectional Case control	N/A	N/A	Thalamus segmentation Thalamus vertex analyses Thalamus morphometry
McMillan et al, 2015 [715]	*C9orf72+* n=55 (In vivo n=20; Post-mortem n=35)	Longitudinal n=11	*C9orf72+* n=35	1-year	GM density
Meysami et al, 2022 [716]	bvFTD n=20 EOAD n=45	Cross-sectional	N/A	N/A	Volumetry
Mioshi et al, 2013 [717]	FTD n=52 AD n=20 Controls n=18	Cross-sectional Case control	N/A	N/A	VBM
Möller et al, 2015 [718]	FTD n=24 AD n=72 Controls n=72	Cross-sectional Case control	N/A	N/A	Subcortical volume

Structural (Segmentation and Volumetry)					
First author, year of publication	**Patient groups and cohort sizes**	**Study design**	**Neuropathology**	**Follow-up**	**Imaging modality**
Pasquini et al, 2020 [719]	FTD n=16 bvFTD n=5; bvFTD-ALS n=9; ALS n=2 FTLD-TDP-B n=10; FTLD-TDP-U n=3; ALS-TDP n=3 *C9orf72+* n=7; *C9orf72*- n=9	Cross-sectional Case series	All cases	N/A	VBM
Popuri et al, 2018 [179]	Pre-symptomatic *C9orf72* n=15; *GRN* n= 9 Controls n=38	Cross-sectional Case control	N/A	N/A	Cortical thickness Subcortical volume
Possin et al, 2012 [720]	MCI n=53 Dementia n=110 (bvFTD n=32; AD n=32; svPPA n=25; nfvPPA n=6; PSP n=10; CBS n=5) Controls n=37	Cross-sectional Case control	N/A	N/A	Volumetry
Rohrer et al, 2010 [160]	FTLD-TDP43 n=28 Type1 n=9; Type2 n=5; Type3 n=10; Unspecified n=4) Controls n=50	Cross-sectional Case control	All cases	N/A	VBM
Rohrer et al, 2015 [22]	Pre-symptomatic *MAPT* n=15; *GRN* n=45; *C9orf72* n=18 Symptomatic *MAPT* n=11; *GRN* n=13; *C9orf72* n=16 Controls n=102	Cross-sectional Case control	N/A	N/A	Cortical, subcortical volumes
San Lee et al, 2020 [721]	nfvPPA n=38 Controls n=76	Cross-sectional Case control	N/A	N/A	Cortical thickness Subcortical shape and volume
Seeley et al, 2008 [146]	bvFTD n=45 Controls n=45	Cross-sectional Case control	N/A	N/A	VBM
Sellami et al, 2018 [722]	Familial FTD mutation carriers n=167 (*GRN* n=75; *C9orf72* n=60; *MAPT* n=32)	Cross-sectional Case control	N/A	N/A	VBM
Sha et al, 2012 [723]	*C9orf72+* n=31 (bvFTD n=15; FTD-ALS n=11; ALS n=5) Disease controls n=73 (bvFTD n=48, FTD-ALS n=19; ALS n=6)	Cross-sectional Disease control	N/A	N/A	VBM

Structural (Segmentation and Volumetry)					
First author, year of publication	**Patient groups and cohort sizes**	**Study design**	**Neuropathology**	**Follow-up**	**Imaging modality**
Spinelli et al, 2021[724]	Genetic FTLD n=66 Phenotype: bvFTD n=12; bvFTD-ALS n=5; nfvPPA n=3; svPPA n=2; ALS n=35; PMA n=6; PLS n=3 Genotype: *C9orf72* n=33; *TARDBP* n=10; *GRN* n=8; *C9orf72*+*GRN* n=1; *C9orf72*+*TARDBP* n=1 *SOD1* n=7; *FUS* n=2; *TBK2* n=2; *MAPT* n=1; *TREM2* n=1 Sporadic FTLD n=61 Phenotype: bvFTD n=12; nfvPPA n=2; svPPA n=2; ALS n=37; PMA n=5; PLS n=3	Cross-sectional Case control	N/A	N/A	VBM
Sturm et al, 2017 [725]	bvFTD n=20 AD n=15 Controls n=39	Cross-sectional Case control	N/A	N/A	VBM
Sturm et al, [726] 2018	bvFTD n=30 AD n=25 Controls n=25	Cross-sectional Case control	N/A	N/A	VBM
Toller et al, 2020 [727]	Sporadic bvFTD n=154 Pre-symptomatic genetic FTD n=71 Behavioural MCI n=12 (*C9orf72* n=5; *MAPT* n=3; *GRN* n=4) Genetic bvFTD n=71 (*C9orf72* n=36, *MAPT* n=26, *GRN* n=9) Controls n=140	Longitudinal n=62: behavioural MCI n=7; sporadic bvFTD n=35; genetic bvFTD n=20; controls n=53)	N/A	Not specified	VBM
van der Burgh et al, 2020 [728]	ALS n=292 (*C9orf72+* n=24) Controls n=156	Longitudinal (ALS n=150; *C9orf72*-n=133; *C9orf72+* n=17; Controls n=72)	N/A	5 months	Cortical thickness Subcortical volumes DTI

Table 19: Grey and white matter imaging studies of thalamic involvement in FTD

Diffusion imaging and white matter analyses					
First author, Year of publication	**Patient groups and cohort sizes**	**Study design**	**Neuropathology**	**Follow-up**	**Imaging modality**
Bede et al, 2013 [442]	*C9orf72*+ ALS n=9 (ALS-FTD n=6; ALS executive dysfunction n=2) *C9orf72*+ ALS n=30 (ALS-FTD n=3; ALS executive dysfunction n=2) Controls n=40	Cross-sectional Case-control	N/A	N/A	VBM Cortical thickness DTI
Bertrand et al, 2019 [184]	Pre-symptomatic *C9orf72* n= 41 Control n=39	Cross-sectional Case control	N/A	N/A	Cortical, subcortical volumes DTI
Daianu et al, 2016 [40]	bvFTD n=20 EOAD n=23 Controls n=33	Cross-sectional Case control	N/A	N/A	DTI
Downey et al, 2015 [729]	bvFTD n=29 svPPA n=15 Controls n=37	Cross-sectional Case control	N/A	N/A	VBM DTI
Floeter et al, 2016 [201]	*C9orf72*+ n =28 (Asymptomatic n=7) (ALS n=11; ALS-FTD n=7; bvFTD n=3) Controls n=28	Longitudinal n=20 Case control	N/A	6-months (n=19); 18-months (n=12)	DTI
Jakabek et 2018 [39]	bvFTD n=24 Controls n=24	Cross-sectional Case control	N/A	N/A	Cortical, subcortical volumes DTI
Mahoney et al, 2012 [642]	*C9orf72*+ n=19 (bvFTD n=12; FTD-ALS n=3; nfvPPA n=1; not specified n=3)	Cross-sectional Case series	n=6	N/A	VBM Volumetry Cortical thickness DTI
Masuda et al, 2016 [443]	ALS-nc n=19 ALS-ci n=25 ALS-FTD n=7	Cross-sectional Case control	N/A	N/A	VBM DTI

Diffusion imaging and white matter analyses					
First author, Year of publication	**Patient groups and cohort sizes**	**Study design**	**Neuropathology**	**Follow-up**	**Imaging modality**
Möller et al, 2015 [7]	AD n=39 bvFTD n=30 Controls n=41	Cross-sectional Case control	N/A	N/A	VBM Subcortical segmentation DTI
Panman et al, 2019 [181]	Pre-symptomatic *GRN* n=33; *MAPT* n=15; *C9orf72* n=12 Controls n=53	Longitudinal Case-control	N/A	2-years	VBM Cortical thickness DTI
Pampa et al, 2017 [188]	Pre-symptomatic *C9orf72* n=18 Control n=15	Cross-sectional Case control	N/A	N/A	VBM DTI
Spotorno et al, 2020 [730]	bvFTD n=20 Controls n=22	Cross-sectional Case control	N/A	N/A	VBM DTI

Table 20: Functional MRI imaging studies of thalamic involvement in FTD

fMRI					
First author, year of publication	**Patient groups and cohort sizes**	**Study design**	**Neuropathology**	**Follow-up**	**Imaging modality**
Agosta et al, 2017 [731]	*C9orf72*+ ALS n=19 Sporadic n=29; early onset n=14; ALS-ci n=24 Controls n=22	Cross-sectional Case-control	N/A	N/A	Cortical thickness Subcortical volume DTI fMRI
Dopper et al, 2016 [226]	Pre-symptomatic *MAPT* n = 11; *GRN* n = 23 Controls n=31	Longitudinal Case-control	N/A	2 years	fMRI - ASL
Farb et al, 2013 [732]	bvFTD n=8 svPPA n=8 Controls n=16	Cross-sectional Case-control	N/A	N/A	fMRI – Independent component analysis
Feis et al, 2019 [61]	Pre-symptomatic *MAPT* n=11; *GRN* n=28 Controls = 36	Cross-sectional Case control	N/A	N/A	VBM DTI rs-fMRI
Lee et al, 2014 [733]	*C9orf72*+ n=14 (bvFTD n=9; FTD-ALS n=5) *C9orf72*- n=14 (bvFTD n=9; FTD-ALS n=5) Controls n=14	Cross-sectional Case-control	N/A	N/A	VBM fMRI – Intrinsic connectivity network
Lee et al, 2017 [185]	Pre-symptomatic *C9orf72* n=15 Control n=15	Cross-sectional Case control	N/A	N/A	VBM DTI fMRI - Intrinsic connectivity network
Lee et al, 2019 [217]	Pre-symptomatic *GRN* n=14 Pre-clinical *GRN* n=3 Controls n=30	Cross-sectional Case control	N/A	N/A	VBM fMRI - Intrinsic connectivity network
Ng et al, 2021 [734]	bvFTD n=14 AD n=50 Controls n=47	Cross-sectional Case control	N/A	N/A	rs-fMRI
Rijpma et al, 2022 [735]	bvFTD n=44 Controls n=44	Cross-sectional Case control	N/A	N/A	fMRI - Intrinsic connectivity network
Rombouts et al, 2003 [736]	FTD n=7 AD n=7	Cross-sectional Case control	N/A	N/A	rs-fMRI

fMRI					
First author, year of publication	**Patient groups and cohort sizes**	**Study design**	**Neuropathology**	**Follow-up**	**Imaging modality**
Shoukry et al, 2020 [212]	Pre-symptomatic *C9orf72* n=15 Symptomatic *C9orf72* n=27 Controls n=48	Longitudinal Case-control	N/A	6-months 18-months	MRI – rs-fMRI
Toller et al, 2018 [737]	Neurodegenerative disorder n=103 (bvFTD n=14; AD n=29; PSP n=20; svPPA n=21; nfvPPA n=19) Controls n=65	Cross-sectional Case control	N/A	N/A	fMRI - Intrinsic connectivity network
Zhou et al, 2010 [50]	bvFTD n=12 AD n=12 Controls n=12	Cross-sectional Case control	N/A	N/A	fMRI - Intrinsic connectivity network

Table 21: PET imaging studies of thalamic involvement of FTD

PET					
First author, year of publication	**Patient groups and cohort sizes**	**Study design**	**Neuropathology**	**Follow-up duration**	**Imaging modality**
Cistaro et al, 2014 [738]	*C9orf72+* ALS n=15 Sporadic ALS-FTD n=12 Sporadic ALS-cn n=30 \	Cross-sectional Case-Control	N/A	N/A	[^{18}F] FDG PET-CT
De Vocht et al, 2020 [209]	Pre-symptomatic *C9orf72* n = 17 Controls n=25	Cross-sectional Case-Control	N/A	N/A	[^{18}F] FDG PET-CT
Diehl-Schmid et al, 2007 [739]	bvFTD n=22 Controls n=15	Longitudinal Case-Control	N/A	19.5 months	[^{18}F] FDG PET-CT
Diehl-Schmid et al, 2019 [740]	FTLD *C9orf72+* n=22 FTLD *C9orf72-* n=22 Controls n=23	Cross-sectional Case-Control	N/A	N/A	[^{18}F] FDG PET-CT
Frisch et al, 2013 [741]	FTLD n=11 (svPPA n=5; bvFTD N=4; mixed n=2) AD n=19 Controls n=13	Cross-sectional Case-Control	N/A	N/A	VBM [^{18}F] FDG PET-CT
Grimmer et al, 2004 [742]	FTD n=10 Controls = not specified	Longitudinal Case-Control	N/A	17 months	[^{18}F] FDG PET-CT
Ishii et al, 1998 [639]	FTD n=21 AD n=21 Controls n=21	Cross-sectional Case-Control	N/A	N/A	[^{18}F] FDG PET-CT
Jang et al, 2018 [743]	FTD n=4 (bvFTD n=2; nfvPPA n=1; svPPA n=1) AD n=2 Controls n=2	Cross-sectional Case-Control	N/A	N/A	MRI [^{18}F]-Florbetaben amyloid PET THK5351 and AV-1451 tau PET
Jeong et al, 2005 [744]	FTD n=29 Controls n=11	Cross-sectional Case-Control	N/A	N/A	[^{18}F] FDG PET-CT
Leuzy et al, 2015 [745]	bvFTD n=5 Controls n=10	Cross-sectional Case-Control	N/A	N/A	VBM [^{18}F] FDG PET-CT [^{11}C] ABP688 PET

PET					
First author, year of publication	**Patient groups and cohort sizes**	**Study design**	**Neuropathology**	**Follow-up**	**Imaging modality**
Malpetti et al, 2021[210]	Pre-symptomatic *C9orf72* n = 3 Symptomatic *C9orf72* n=1 Controls n= 19	Cross-sectional Case-Control	N/A	N/A	MRI [^{11} C] UCB-J PET
Matias-Guiu et al, 2015 [746]	FTD n=33 AD n=33 Other diagnoses n=33	Cross-sectional Case-Control	N/A	N/A	[^{18}F] FDG PET-CT
Poljansky et al, 2011 [747]	FTLD n=16 (bvFTD n=9; nfvPPA n=4; svPPA n=3) AD n=16 MCI n=11	Cross-sectional Case-Control	N/A	N/A	[^{18}F] FDG PET-CT
Popuri et al, 2021 [202]	Pre-symptomatic *C9orf72* n=15 Controls n=20	Cross-sectional	N/A	N/A	Volumetry [^{18}F] FDG PET-CT
Schaeverbeke et al, 2018 [748]	PPA n=20 (nfvPPA n=12; svPPA n=5; lvPPA n=3) Controls n=64	Cross-sectional Case-Control	N/A	N/A	MRI – VBM [^{18}F]-THK5351 PET [^{11}C]-Pittsburgh Compound B PET
Soleimani-Meigooni et al, 2020 [749]	AD n=8 FTLD tau n=9 (PSP n=4; CBD n=2; *MAPT* n=2; AGD n=1) FTLD Non-tau n=3 (*GRN* n=1; *C9orf72* n=1; *FUS* n=1)	Cross-sectional	All cases	N/A	MRI 18F-flortaucipir PET

Table 22: A summary of studies evaluating thalamic pathology in FTD

Reviewed Studies	**n=97**
Phenotype	78% (76/97)
bvFTD	63% (48/76)
FTD-ALS	36% (27/76)
svPPA	28% (21/76)
FTLD unspecified	22% (17/76)
nfvPPA	21% (16/76)
PPA unspecified	4% (3/76)
Genotype	46% (45/97)
C9orf72	93% (42/45)
GRN	38% (17/45)
MAPT	33% (15/45)
Other	4% (2/45)
Pathology	21% (20/97)
TDP-43	70% (14/20)
Tau	40% (8/20)
FUS	25% (5/20)
FTLD unspecified	25% (5/20)
Longitudinal	13% (13/97)
Follow-up – Average (years)	1.3±0.5 years.
Follow-Up – Median (years)	1±0.5 years.
Follow up – Range (months)	5 – 26 months
Pre-symptomatic	19% (18/97)
Multimodal % (n)	27% (26/97)
MRI % (n)	88% (88/97)
Grey Matter Analyses % (n)	77% (75/97)
White Matter Analyses % (n)	20% (19/97)
Functional MRI % (n)	13% (13/97)
PET % (n)	16% (16/97)

A summary of studies evaluating thalamic pathology in FTLD: patient cohorts, study designs and imaging modalities. bvFTD – behavioural variant frontotemporal dementia; *C9orf72* - chromosome 9 open reading frame 72; FTLD – frontotemporal lobar degeneration; FTD-ALS – FTD- amyotrophic lateral sclerosis; FUS – fused in sarcoma; *GRN* – progranulin; *MAPT* - microtubule-associated protein tau; nfvPPA – non-fluent variant primary progressive aphasia; PET – positron emission tomography; PPA – primary progressive aphasia; svPPA – semantic variant primary progressive aphasia; TDP-43 - TAR DNA-binding protein 43

6.3.1 Phenotypes

The most commonly evaluated clinical phenotypes included bvFTD (63%; n=48/76); followed by FTD-ALS (36%; n=27/76); svPPA (28%; n=21/76); and nfvPPA (21%; n=16/76). Participants were sometimes grouped together under the umbrella of "unspecified FTD" or "PPA" [699, 736, 750] (**Table 22**). Thalamic atrophy is thought to be most marked in FTD-ALS [751], followed by bvFTD, nfvPPA and svPPA [688, 694]. The degree of thalamic volume loss is sometimes more severe in bvFTD than FTD-ALS [714] but differences in symptom duration are seldom accounted for [155]. Post-mortem studies have confirmed thalamic atrophy in all FTD phenotypes, sometimes commenting on the affected region [752], but seldom mentioning specific nuclei [160, 162, 714, 752, 753].

6.3.1.1 Behavioural variant FTD (bvFTD)

In bvFTD, diffuse thalamic atrophy [691-693, 699, 705, 745] involving all thalamic nuclei [193] is often detected. There is particular predisposition to medial dorsal [146, 688], lateral dorsal [688] and midline [688] pathology which is consistent with post mortem observations [244]. The pulvinar nuclei [193, 726] may or may not [688] be involved. Subtle changes may be captured relatively early, before becoming increasing widespread as the disease progresses [146, 710, 713]. The degree of thalamic atrophy is more prominent in *C9orf72* mutation carriers [693, 707, 723], which is discussed in more detail below. Morphometric findings are complemented by insights from other imaging modalities such as the reduced integrity of the anterior thalamic radiation [7, 39, 40, 730]; decreased salience [50, 734, 735, 737] and limbic [732] network connectivity traversing the thalamic nodes; bilateral thalamic hypometabolism [639, 742, 744, 745, 754]; decreased [^{11}C]-ABP688 [745] and increased [^{18}F]-THK5351 [748] radiotracer uptake

in the bilateral thalami – the latter indicating non-specific neurodegeneration [743]. Paradoxical thalamic hypertrophy, as a potential compensatory mechanism, has also been described in regions projecting to the medial pre-frontal cortex [39].

Thalamic atrophy in bvFTD has been linked to a multitude of cognitive, perceptual, functional, and behavioural impairments. Cognitive impairment is readily associated with anterior thalamic atrophy [680] that may be preceded by functional working memory network impairment [736]. Detailed neuropsychological testing often reveals impaired object memory [709], visual memory [741], and design fluency [720]. Perceptual impairment and psychosis-like symptoms were also associated with anterior thalamic involvement [703]. Functional impairment has been linked to medial dorsal nuclei atrophy [717]. Social cognition and behavioural impairment [725-727, 735] may be associated with pulvinar nuclei atrophy. Reduced limbic connectivity of the anterior thalamus has been linked to apathy [732]. Additionally, there is a trend towards greater posterior thalamic atrophy in those with apathy compared to those without apathy [711]. Thalamic atrophy has also been linked to altered eating behaviour [691] and body composition [692]. Thalamic hypometabolism has been associated with the re-emergence of primitive reflexes in an admixed group of FTD phenotypes [746].

6.3.1.2 Amyotrophic Lateral Sclerosis – Frontotemporal Dementia (ALS-FTD)

Thalamic atrophy [193, 443, 448, 663, 693] is thought to be particularly striking [751] in ALS-FTD with relatively symmetrical [694] involvement of the anterior (anterior ventral), medial (midline, medial dorsal), lateral (lateral dorsal, lateral posterior), ventral (ventral anterior, ventral lateral) and intralaminar

nuclei [193, 448, 688]. There is a particular predilection for the lateral dorsal nuclei [193, 448, 688]. The posterior (pulvinar, lateral and medial geniculate) [193, 430] and additional ventral (ventral medial, ventral posterolateral) [193] aspects are sometimes also implicated. There may be early signs of thalamic atrophy in sporadic ALS with cognitive [697] or behavioural [728] impairment that does not meet criteria for FTD, but this may not always be the case [443, 728]. Post-mortem studies readily confirm widespread thalamic degeneration in ALS-FTD [714]. Thalamic atrophy may be particularly marked in *C9orf72* hexanucleotide expansion carriers [663, 693, 707, 723, 731], which is expanded below in detail. The above findings are complemented by white matter analyses that capture reduced superior thalamic radiation integrity [443]. Preferentially affected thalamic regions project to motor [448, 663], sensory [448, 663] and limbic [448] areas underpinning cognitive correlates [448, 697] and perceptual impairment [702, 703].

6.3.1.3 Semantic variant primary progressive aphasia (svPPA)

Thalamic atrophy tends to be relatively subtle in svPPA and may only be a feature of late-stage disease [695]. This may explain the strikingly conflicting accounts on the presence [691] or absence [663, 696, 705] of thalamic involvement in svPPA. If detected, there is thought to be a predilection for anterior (anterior ventral), medial (medial dorsal, midline), lateral (lateral dorsal, lateral posterior), or posterior (lateral geniculate) nuclei [193, 688]. Post-mortem studies suggest anterior predominant thalamic atrophy [679] which occasionally extends to involve the intralaminar [688] and more posterior (pulvinar, medial geniculate) nuclei [193, 712]. It tends to be left-lateralised [193, 691, 694, 695], yielding the highest asymmetry indexes among FTD phenotypes [694]. In contrast, morphometric changes may be more pronounced in the right thalamic

hemisphere [193]. WM analyses reveal anterior thalamic radiation degeneration [729]. In a small FTD cohort which included svPPA, bilateral thalamic hypometabolism was described [747]. Functional analyses show reduced limbic connectivity via the anterior thalamus [732]. Nuclear imaging studies demonstrate elevated tau-tracer [^{18}F]-THK5351 binding in the thalamus [748] indicative of a neurodegenerative process [743]. Radiological changes in the thalamus have been linked to apathy [732], impaired social cognition [729], altered eating behaviour [691], as well as auditory symptoms which were specifically associated with medial geniculate nucleus atrophy [712].

6.3.1.4 Non-fluent variant primary progressive aphasia (nfvPPA)

Bilateral, [193, 663, 705] but left hemisphere predominant thalamic atrophy is typically described in nfvPPA [193, 721]. Relatively selective anterior (anterior ventral), medial (medial dorsal, midline), lateral (lateral dorsal, lateral posterior), ventral (ventral anterior, ventral lateral, ventral posterolateral, ventral medial) and posterior (medial geniculate) nuclear involvement has been reported [688]. The pulvinar [193] and sometimes lateral geniculate nuclei [193, 688] in the posterior region are typically spared. Extensive intra-thalamic density reductions are reported [193], particularly in areas projecting to motor regions [663]. In a small cohort of FTD patients that included nfvPPA, bilateral thalamic hypometabolism was readily captured [747]. Nuclear imaging studies revealed increased tau-tracer [^{18}F]-THK5351 binding in the thalamus [748], suggestive of focal neurodegeneration [743].

6.3.2 Genotypes

The most common genotypes included in FTD thalamus studies are *C9orf72* (93%; n=42/45); followed by *GRN* (38%; n=17/45); and *MAPT* (33%;

n=15/45) mutation carriers as well as less common genotypes such as *TARDBP, SOD1, FUS, TBK1* or *TREM2* (4%; 2/45). These are low incidence disorders, leading to small sample sizes, and often pooled analyses of genetically admixed cohorts are performed. The degree of thalamic atrophy is more marked in familial FTD compared with sporadic FTD [724], particularly *C9orf72* mutation carriers [181, 183, 688, 694]. Pre-symptomatic studies in familial FTD indicate that some of the earliest changes may occur in the thalamus [192]. Next, we discuss genotype-specific patterns of thalamic involvement in familial FTD [688, 694].

6.3.2.1 C9orf72

Thalamic atrophy [156, 179, 193, 642, 663, 698, 723, 724, 728, 733] is well-established in *C9orf72* hexanucleotide expansion carriers, and widely corroborated by pathological studies [690, 707, 755-757]. It may be symmetrical [694], or lateralised. The inconsistency with regards to laterality may stem from small sample sizes, but right-sided predominance is often observed in *C9orf72*-associated ALS-FTD [723, 731], and relative left-predominance was noted in *C9orf72*-associated bvFTD [723, 733]. The spectrum of thalamic involvement also ranges from relatively focal medial dorsal pathology [247]; to more widespread anterior (anterior ventral), lateral (lateral dorsal, lateral posterior), ventral (ventral anterior, ventral lateral) and posterior (pulvinar) thalamic disease-burden [193]; to encompassing all thalamic nuclei [183, 688]. Pulvinar atrophy was previously proposed as a *C9orf72*-specific trait [203, 688, 733], but not confirmed by others [183, 193, 247, 758]. Thalamic atrophy may be too subtle for detection on visual inspection [723]. In *C9orf72*-associated ALS-FTD, there may be a preferential involvement of thalamic subregions with motor and sensory thalamo-cortical projections [663].

Grey matter findings are complemented by WM analyses that consistently capture anterior thalamic radiation changes in both ALS and ALS-FTD phenotypes [201, 442, 642]. Functional studies invariably detect reduced connectivity in thalamus-seeded circuits [212] and the salience network [733]. [^{18}F] FDG PET-CT studies are consistent in identifying bilateral thalamic hypometabolism [738, 740, 749]. The radiological involvement of the thalamus may be associated with elevated serum neurofilament light chains [698], cognitive [201, 759], behavioural [201, 724, 733] and perceptual impairment [203, 702, 704] in symptomatic disease. In pre-symptomatic GGGGCC hexanucleotide carriers, similar grey matter [22, 156, 179, 181, 183-185, 188, 192], white matter [181, 184, 188, 201], functional [185]; and [^{18}F] FDG PET-CT [202, 209] thalamus signatures are described as in symptomatic cohorts. Nuclear imaging studies capture pre-symptomatic synaptic density reduction with a predilection to pulvinar and ventral-posterior thalamic subregions [210]. Pre-symptomatic metabolic changes in the thalamus may precede structural alterations [202] or changes in CSF markers such as neurofilament light chain [209]. Longitudinal studies suggest that thalamic atrophy remains relatively stable during the pre-symptomatic phase [181], accelerates around phenoconversion [183], and either plateaus [728] or progresses [760] thereafter.

6.3.2.2 GRN

The *GRN* genotype typically involves most thalamic nuclei, particularly the anterior [724] (anterior ventral [183]), medial (medial dorsal and midline [183]) and lateral (lateral dorsal [183]) regions. There are conflicting reports of posterior (pulvinar [688], medial [183] and lateral [183] geniculate nucleus) and lateral (ventral medial [688]) thalamic involvement. This genotype has the highest

degree of asymmetric [694] thalamic involvement amongst all genotypes, which may be related to the most commonly associated clinical phenotype, nfvPPA [694, 761]. Thalamic atrophy is typically first detected as symptoms emerge [183] and seldom evident before this [61, 179]. Pre-symptomatic studies reveal thalamic hypoperfusion [226] and symmetrical thalamo-cortical hyper-connectivity involving the salience, language and default mode networks [217]. Thalamic involvement in *GRN* has been linked to psychotic symptoms, such as delusions and hallucinations [722].

6.3.2.3 MAPT

In *MAPT* mutation carriers, widespread thalamic atrophy is typically detected [183, 688], with marked involvement of medial (medial dorsal and midline [183]) and lateral (lateral dorsal [183]) regions. Reports of posterior thalamic nuclei involvement (pulvinar [688] and lateral geniculate [183] nuclei) are inconsistent [183, 688]. WM analyses reveals loss of the left anterior thalamic radiation integrity compared to controls [181].

6.3.3 Histopathology

The most common molecular finding is pTDP-43 (70%; n=14/20); followed by Tau (40%; n=8/20); and FUS (25%; n=5/20). Pathological diagnoses are sometimes grouped together under the umbrella of FTD/FTLD (25%; n=5/20) **(Table 22).** Only a minority of FTD studies provide dedicated thalamic histopathology data, either exclusively (3%; n=3/97) or accompanying imaging data (18%; n=17/97). The most marked thalamic involvement is reported in pTDP43-opathies, followed by tau-opathies and then minimal involvement in FUS-opathies [694]. Pathology-specific pattern of thalamic degeneration may be used to differentiate subtypes [694]. The medial

dorsal nucleus is the only nucleus affected in all pathological subgroups [688]. In addition, there is a significant burden of iron deposition in the thalamus across the FTLD spectrum compared to other neurodegenerative disorders [700, 701]. Herein, we summarise the thalamic involvement in the pathological subtypes of FTD/FTLD spectrum.

6.3.3.1 pTDP-43

The propagation of pTDP-43 pathology is divided into four sequential stages, with thalamic pathology defining the second pathological stage [244]. Thalamic atrophy [690, 699, 719] is well described in pTDP-43-opathies, with preferential anterior [680] and medial [719] involvement. Thalamic iron deposition is also reported [701]. pTDP-43 pathology is divided into A, B or C subtypes that are associated with distinct phenotypes and pathological patterns of thalamic involvement [688]. Volumetric analyses of pathologically confirmed cases of harmonised classified [103] type A pTDP-43 pathology revealed thalamic atrophy within a group of admixed clinical phenotypes including bvFTD, FTD-ALS and nfvPPA [160]. This pathological subtype is associated with widespread thalamic atrophy [160, 706] implicating thalamic nuclei in the anterior (anterior ventral), medial (medial dorsal, midline, intralaminar), lateral (ventral anterior, ventral lateral, lateral posterior, lateral dorsal) and the posterior (lateral geniculate nucleus) region [688]. This contrasts the relatively focal thalamic atrophy observed in type B pTDP-43 [688] which is associated with bvFTD, FTD-ALS and nfvPPA phenotype [103]; and the rather limited thalamic involvement noted in type C pTDP-43 pathology [688] which is associated with svPPA or bvFTD phenotype [103]. In the latter, there may [688, 689, 706] or may not [689, 696] be thalamic involvement at all; if affected it is limited to the medial dorsal nuclei [688]. These

post mortem observations [160] have clinical implications as subtle thalamic involvement in type B and C pTDP-43 pathology may evade radiological detection.

6.3.3.2 Tau

Thalamic atrophy is commonly observed in Tau-opathies [680, 699], further divided into tau-Pick's, tau-PSP, tau-CBD and FTDP-17 [688]. The propagation of tau pathology in Pick's disease is divided into four sequential stages, implicating the thalamus in the second pathological stage [708]. The thalamic involvement in Pick's disease [706] involves the anterior (anterior ventral), medial (medial dorsal, midline); lateral (lateral posterior, ventral anterior, ventral lateral, ventral posterolateral) and posterior region (medial geniculate nucleus) [688]. There is also thalamic involvement in tau-PSP [706] affecting the medial (medial dorsal, intralaminar) and lateral (ventral anterior and ventral lateral) nuclei; in tau-CBD [706] affecting the anterior (anterior ventral), medial (medial dorsal, midline and intralaminar), and lateral (ventral anterior, ventral lateral, lateral posterior, and particularly lateral dorsal) nuclei; and in FTDP-17 affecting the medial (medial dorsal, ventral medial, midline), lateral (lateral posterior, ventral lateral, ventral posterolateral) and posterior (medial and lateral geniculate) nuclei [688]. The different patterns of involvement may be influenced by the associated clinical phenotype [680].

6.3.3.3 FUS

The few studies that include FUS-opathies indicate that there is only minimal thalamic involvement without significant asymmetry [694]. The medial dorsal nuclei are the only affected thalamic nuclei [688]. Similar to pTDP-43-opathies, iron deposition may also be observed in the thalamus [701].

6.4 Discussion

There is compelling evidence for thalamic involvement across the clinical, genetic and molecular spectrum of FTD **(Table 23).** This is demonstrated by thalamic volume loss involving the anterior nuclei, medial nuclei and lateral division nuclei within the lateral region in all clinical phenotypes, genotypes and most pathological subtypes **(Table 23).** The consistent involvement of these regions within the cortico-subcortical circuits is likely to contribute to some of the cardinal manifestations of FTD such as limbic dysfunction, behavioural and emotional regulation impairment [688]. There is pan-thalamic degeneration of most thalamic nuclei in bvFTD and nfvPPA; more selective thalamic involvement in ALS-FTD; and focal thalamic atrophy in svPPA. Thalamic atrophy is more marked in familial FTD. There is diffuse thalamic nuclei atrophy in all genotypes with varying degrees of posterior thalamus involvement. PPA phenotypes and *GRN* genotypes exhibit particularly asymmetric thalamic atrophy. The few available pathology studies demonstrate a variable degree of posterior and ventral thalamic involvement across the pathological subtypes. It is most widespread in the type A subtype of the pTDP-43-opathies; tau-CBD subtype of tau-opathies; and minimal involvement in FUS-opathies. Thalamic atrophy, amongst other areas of grey matter degeneration observed in the FTD, may be accompanied by elevated serum [698, 730] neurofilament light chain which is a non-specific marker of neurodegeneration.

Table 23: A synthesis of focal thalamic volume alterations from published research papers with respect to anatomical predilection

FTLD Spectrum	Phenotype				Genotype			Pathological		
Thalamic regions and sub-regions	**bvFTD**	**FTD-ALS**	**nfvPPA**	**svPPA**	***C9orf72***	***MAPT***	***GRN***	**pTDP-43**	**Tau**	**FUS**
Anterior										
Anterior	+	+	+	+	+	+	+	+/-	+/-	-
Medial										
Medial dorsal	+	+	+	+	+	+	+	+	+	+
Midline	+	+	+	+	+/-	+	+	+/-	+/-	-
Lateral										
Lateral										
Lateral posterior	+	+	+	+	+	+	+	+/-	+/-	-
Lateral dorsal	+	+	+	+	+	+	+	+/-	+/-	-
Ventral										
Ventral anterior	+	+	+	-	+	+	+	+/-	+/-	-
Ventral lateral	+	+	+	-	+	+	+	+	+	-
Ventral posterolateral	+	+/-	+	-	+/-	+	+	-	+/-	-
Ventral medial	+	+/-	+	-	+/-	+	+/-	-	+/-	-
Posterior										
Pulvinar	+/-	+/-	-	+/-	+	+/-	+/-	-	-	-
Medial geniculate	+	+/-	+	+/-	+/-	+	+/-	-	+/-	-
Lateral geniculate	+	+/-	+/-	+	+/-	+/-	+/-	+	+/-	-
Intralaminar	+	+	-	+/-	+/-	+	+	+/-		-

Volume reductions in thalamic nuclei across the FTLD spectrum stratified by phenotype, genotype and pathological subtypes: (+) affected; (+/-) sometimes affected; (-) not affected.

6.4.1 Academic insights

The nuanced characterisation of thalamic pathology, either by imaging or histopathological examination points well beyond descriptive accounts **(Table 24)**. From a conceptual point of view, the ascertainment of focal as opposed to global thalamus degeneration mirroring selective cortical degeneration supports the notion of "what wires together, dies together" [762], namely that interconnected brain regions exhibit concomitant neurodegeneration. Conceptually, this is in line with theories of trans-synaptic spread of pTDP-43 [763] and "prion-like" propagation processes [764, 765]. This also supports observations of co-occurring deficits in interlinked clinical domains [766]. Emerging evidence from presymptomatic studies confirm that pathological change accrues long before symptom onset [184, 200, 243, 665, 767] indicating that neurodevelopmental factors may also be at play [177, 243]. Clustering strategies on large admixed imaging datasets have revealed clinically and radiologically distinct subgroups. For example, various clustering approaches have consistently captured a sub-cohort of patients with marked frontotemporal change among unselected ALS patients [768-770]. Clustering initiatives without a priori hypotheses may successfully uncover pathologically homogenous subgroups which may have distinctive genetic or clinical correlates [768]. This approach was recently applied to an FTD-ALS cohort which yielded distinct clinical phenotypes with divergent white matter tract involvement [771].

Table 24: Key academic insights and clinical relevance of thalamic involvement in FTD

Academic Insights	Focal as opposed to global thalamic atrophy Phenotype- and genotype-associated thalamic signatures Patterns of thalamic involvement mirror regional cortical pathology Evidence for "network-wise" degeneration Supports the notion of "prion-like" propagation in pTDP-43 Presymptomatic thalamic changes in mutation carriers
Clinical relevance	Thalamic alterations may precede the radiological detection of cortical change Discrimination of phenotypes Distinction of FTD from other neurodegenerative conditions such as AD, MCI Machine-learning opportunities Putative monitoring role as a biomarker - to be explored Predictive value - to be explored
Pragmatic considerations	Fast imaging data acquisition Established analysis pipelines Semi-automated methods Important metrics can be retrieved from T1-weighted MR data Opportunities for reliable single voxel spectroscopy Putative biomarker role in pharmacological trials – to be explored

6.4.2 Practical relevance

The clinical relevance of thalamic observations stem from the opportunity to capitalise on distinguishing phenotype-, genotype- and pathology-specific patterns of thalamic involvement in combination with cortical grey matter and white matter neuroimaging signatures. As evidenced by the literature, thalamic involvement can be radiologically detected, and the preferential involvement of specific regions may be computationally characterised. Thalamic signatures may help to distinguish FTD subtypes from controls [750], other phenotypes [694], genotypes [688], pathological subtypes [688] and other neurodegenerative disorders such as Alzheimer's disease [7, 716]. There are preliminary indications that using the volume of individual thalamic nuclei, rather than volume of the entire thalamus, may have better discriminating power [688, 694]. While the optimal combination of thalamic volumetric measurements is yet to be determined, a single study demonstrated that the volume of the pulvinar nuclei accurately differentiates *C9orf72* from *MAPT* genotypes; and varying combinations of anterior, lateral, medial and intralaminar nuclei volume reliably discriminates pathological subtypes [688]. The increasing availability of uniformly acquired normative datasets may help the radiological interpretation of single patients with FTD or suspected FTD [33, 42, 253]. Machine learning (ML) applications are increasingly applied to large FTD and ALS-FTD data sets [224]. MRI-based classification models use discriminatory MRI features to categorise single-subject MRI data into diagnostic groups. Feature selection in ALS-FTD spectrum disorders typically focuses on cortical grey matter thickness, volumes and white matter metrics [55, 56, 59, 90, 94, 216, 224, 772] rather than subcortical volumes; this is likely because subcortical volumes

are considered as a whole instead of the inclusion of nucleus-based metrics in the models. Thus, the addition of thalamic nuclei and thalamic radiation integrity metrics may improve the classification accuracy of such models [159]. Pre-symptomatic thalamic atrophy observed in *C9orf72* genotype may be used to ascertain and track disease-burden prior peri-diagnostic biomarker changes, such as CSF neurofilament light chain concentration alterations [209]. From a medical education point-of-view, the thalamus is continued to be predominantly linked to sensory function. The importance of thalamus mediated cognitive, behavioural, and extrapyramidal motor function needs to be emphasised at an undergraduate level and illustrated in a clinical context such as FTD for future generations of physicians. Presymptomatic studies suggest that pathological changes may be detected several years, sometimes decade before symptom onset [184, 665]. Presymptomatic insights and the observation that widespread pathological changes can be detected by the time diagnostic criteria are met, would suggest that the window for effective pharmacological intervention with true disease-modifying potential may fall into the presymptomatic or prodromal phase of the disease. The recognition of considerable disease burden around the time of diagnosis should hasten recruitment into clinical trials very early in the course of the disease and may ultimately pave the way for presymptomatic clinical trials in mutation carriers [773].

6.4.3 Study limitations

Our review also highlights the most common methodological shortcomings of thalamic studies which should be considered in the design of future research initiatives. First, heterogenous groups of different FTD

phenotypes, genotypes and pathological subtypes are sometimes admixed to boost sample sizes, but this precludes the precision characterisation of subtype-specific thalamic signatures. Despite this, sample sizes often remain relatively small, in part because of the rarity of these conditions. Second, most studies consider the volume of the entire thalamus, with only a minority of studies using emergent methods to quantify the volume of individual thalamic nuclei. Third, the majority of imaging studies adopt a single modality approach, overwhelmingly focusing on the thalamic grey matter. Multi-modal imaging strategies, integrating structural, functional, metabolic and connectivity-based observations are not only more informative but reveal more about the role of thalamic pathology in the context of thalamo-cortical circuitry dysfunction. Fourth, while several studies ascribe deficits in specific clinical domains to thalamic atrophy, direct clinico-anatomical correlations are somewhat contentious [670] as cognitive and behavioural functions are mediated by multi-synaptic networks with multiple grey and white matter components. Additionally, there is a disproportionate emphasis on the more common FTD phenotypes and thalamic pathology in low-incidence entities, such as primary lateral sclerosis associated FTD (PLS-FTD), complicated HSP, ALS-FTD or SBMA associated frontotemporal dysfunction are relatively under investigated [194, 272, 669, 774, 775] despite radiological evidence of frontotemporal pathology in PLS [776, 777], hereditary spastic paraplegia [778] and to a lesser extent in spinal bulbar muscular atrophy [255, 779]. Anatomically elusive clinical symptoms such as fatigue have been repeatedly linked to thalamic changes [780-782] but compelling evidence for direct associations are lacking [783]. Executive function, language, motivation and limbic functions are the main non-sensory

functions linked to thalamic nuclei, but thalamic nuclei also mediate social cognition and theory of mind (ToM) related functions [784, 785]. ToM deficits are increasingly recognised in a multitude of FTD phenotypes [254, 496] and the contribution of thalamic pathology should be systematically investigated in these conditions. Pseudobulbar affect is another clinical syndrome which is classically linked to corticobulbar disconnection, but more recent models implicate cortico-limbic-subcortical-thalamic-pontocerebellar network dysfunction [625, 626, 786]. Finally, the involvement of sensory nuclei is seldom appraised, despite evidence of marked ventral posterolateral and ventromedial thalamic volume loss in GGGGCC hexanucleotide repeat expansion carriers [787] in ALS and ALS-FTD [787]. From a sensory network point of view, the spinothalamic and dorsal column–medial lemniscus (DCML) pathways are rarely investigated even though the integrity of these tracts can now be reliably assessed both a spinal and cerebral level [249, 250].

6.4.4 Methodological considerations

Thalamic integrity may be evaluated with relative ease and a number of robust open-source software libraries are available to retrieve a variety of thalamus metrics. The observation that in most FTD subtypes thalamic atrophy is an early feature [767] and may precede characteristic cortical atrophy provides a strong rationale for quantitative thalamus imaging in FTD. Total thalamus volume and the volumes of specific nuclei can be estimated from high-resolution 3D T1-weighted data [788], which is routinely acquired in clinical protocols as part of the diagnostic work-up therefore there are no additional time or cost implications for acquiring raw data for post-hoc thalamic analyses. Similarly, shape deformation analyses also rely on 3D T1-weighted

images eliminating the need for additional data acquisition and scanning costs [789]. One of the challenges of cortical single-voxel MRS spectroscopy is the consistency in voxel placement [240] which is not a problem in thalamus spectroscopy as the structure is readily identified on localiser scans [790]. As the thalami are paired structures, commenting on symmetry or asymmetry based on retrieved integrity indices is very straightforward. Similarly, longitudinal statistical models are not challenging to implement [145, 172, 791]. While overall thalamic volumes are often evaluated and "overall" thalamic metabolism appraised, the thalamus consists of over 50 cytologically and functionally distinct nuclei [792] with distinguishing cortical projection patterns [663], physiological roles [793], developmental origin, [794] and vascular supply [677]. The main caveat of assessing the thalamus as a single structure, either by volumetric, [448] metabolic, [795] spectroscopic, [790] or vertex-based methods, [445] is potentially averaging imaging metrics across preferentially affected and unaffected regions, therefore reducing detection sensitivity for pathological change. A number of innovative computational strategies have been developed and validated, most of which are available as open-source pipelines, to parcellate the thalamus either by cortical connectivity patterns [792, 796-799] or based on the histological data [788]. Compared to cortical pipelines, quantitative thalamus imaging remains somewhat overlooked, despite simplicity of implementation, moderate computational time requirement and the availability of normative datasets.

6.4.5 Future directions

Given the academic and clinical relevance of thalamic measures in FTD, standard clinical imaging protocols should invariably include a high-resolution

3D T1-weighted pulse sequence and basic thalamus metrics should be routinely interrogated. A relatively short diffusion tensor imaging protocol offers ample opportunities for additional white matter analyses to evaluate the integrity of thalamic projections. It seems imperative that multimodal imaging protocols are implemented in the research setting so that the comparative detection sensitivity, prognostic value and monitoring potential of the various metrics can be contrasted and the best performing indices selected for future clinical use and as biomarkers in future pharmacological trials. Future academic studies should routinely include disease-controls in addition to healthy controls to assess the specificity of thalamic alterations to specific FTD subtype. Cross-sectional studies of patients with varied symptom duration reveal very little about the dynamic molecular process driving FTD, therefore carefully designed multi-timepoint imaging studies are required with uniform follow-up intervals to establish the natural history of disease burden propagation. As with other neurodegenerative conditions, longitudinal studies should ideally include presymptomatic mutation carriers to clarify the value of radiological metrics in predicting phenoconversion and contribute to academic debates such as neurodevelopmental versus neurodegenerative processes, and the existence of compensatory and adaptive mechanisms in neurodegeneration.

6.5 Conclusions

FTD is associated with phenotype-, genotype- and pathological subtype-specific thalamic signatures. Thalamic degeneration is likely to contribute to the diverse manifestations observed clinically as a key hub of subcortical-cortical networks. Large, pathologically and biomarker-supported

longitudinal imaging studies are required with a standardised imaging and clinical protocol for the nuance characterisation of thalamic pathology in FTD in order to develop clinically meaningful biomarkers centred on thalamic changes.

7 Focal thalamus pathology in frontotemporal dementia: phenotype-associated thalamic profiles

7.1 Introduction

Frontotemporal dementia (FTD) is an umbrella term encompassing a clinically, radiologically, genetically, and pathologically diverse set of neurodegenerative conditions with distinct clinical phenotypes: behavioural variant FTD (bvFTD), non-fluent variant primary progressive aphasia (nfvPPA), semantic variant primary progressive aphasia (svPPA) and amyotrophic lateral sclerosis-FTD (ALS-FTD). In the clinical setting, FTD phenotypes are primarily linked to cortical atrophy patterns [33], but the contribution of subcortical pathology to cognitive and behavioural dysfunction is increasingly recognised [675, 678, 679, 681-683].

Thalamic pathology may be detected several years before phenoconversion in FTD [22, 183-185, 192] and longitudinal studies readily capture progressive thalamic degeneration over time [760]. The degree of thalamic degeneration may show correlations with cognitive [759] and behavioural scores [724], but clinico-radiological correlations may be confounded by extraneous factors [670]. Whilst there is ample radiological evidence of thalamic involvement in all FTD phenotypes [663, 694, 705, 751, 761], the thalamus is typically evaluated as a single structure and the selective degeneration of specific thalamic regions are poorly characterised. Until recently, very few studies [183, 247, 688] have evaluated thalamic nuclei specifically and these differ considerably in their study design, imaging methods, and clinical focus. Relatively mild anterior, medial, lateral, and intralaminar degeneration was described in

svPPA and moderate pan-thalamic degeneration reported in bvFTD and nfvPPA [688]. Intra-thalamic [433, 489], and thalamic-cortical connectivity alterations [488, 797] have also been described in ALS, ALS-FTD and other motor neuron diseases [489, 688, 774], but thalamic disease-burden is seldom linked to specific cognitive profiles [448].Thalamic atrophy in 'genetic' FTD [688, 694, 724] is thought to be more pronounced than in sporadic FTD [688, 723, 724, 733, 759]. *C9orf72* is associated with widespread thalamic atrophy [155, 445, 724] with the involvement of most nuclear groups [183, 688]. Due to sample size differences and divergent analytical approaches, reports of genotype-associated thalamic signatures are relatively inconsistent. Pulvinar atrophy was initially proposed as a *C9orf72*-specific trait [688, 733], which was not confirmed by others [247, 758] and pulvinar involvement is also evident in *GRN* and *MAPT* genotypes [183]. The preferential laterality of findings also remains to be determined as several studies averaged thalamic changes in the left and right hemispheres [247, 758], while others suggested right-sided predominance in *C9orf72*-positive ALS-FTD [723], and relative left-predominance in *C9orf72*-associated bvFTD [723, 733]. There are also conflicting reports of ventromedial, pulvinar and medial geniculate involvement in *GRN* and accounts of posterior thalamic nuclei involvement in *MAPT* are also relatively inconsistent [183, 688].

As the involvement of specific thalamic nuclei is relatively poorly characterised post mortem [103, 160, 244, 714, 752, 755-757, 800] and significant inconsistencies exist in the thalamic imaging literature of FTD, the main objective of this study is to characterise thalamic changes in the two cerebral hemispheres separately, compare the detection sensitivity of three T1w-MR

derived imaging techniques and identify which imaging modality best distinguishes the main clinical phenotypes.

7.2 Methods

7.2.1 Participants

Following subject exclusions because of MR data quality, a total of 170 participants, 70 patients with frontotemporal dementia (FTD) and 100 healthy controls (HC) were included in a prospective, single-centre imaging study. In accordance with the Ethics Approval of this research project (Beaumont Hospital, Dublin, Ireland), all participants gave informed consent. Exclusion criteria included comorbid neoplastic, paraneoplastic or neuroinflammatory diagnoses, prior cerebrovascular events, and known traumatic brain injury. Participating FTD and ALS-FTD patients were diagnosed according to the Rascovsky and El Escorial criteria [645]. Participating patients were stratified based on their clinical phenotype into behavioural variant FTD (bvFTD, n=10), non-fluent-variant primary progressive aphasia (nfvPPA, n=15), semantic-variant primary progressive aphasia (svPPA, n=5), and ALS-FTD (n=40). Patients with ALS-FTD were further categorised into those carrying the GGGGCC hexanucleotide expansions in *C9orf72* (ALS-FTD C9+, n=20) and those without hexanucleotide repeats (ALS-FTD C9-, n=20). Methods for genetic screening for hexanucleotide repeat expansions in *C9orf72* have been previously reported [801]; repeat-primed PCR was used and expansions longer than 30 repeats were considered pathological.

7.2.2 Magnetic resonance imaging

T1-weighted (T1w) images were acquired on a 3 Tesla Philips Achieva Magnetic resonance (MR) platform with a 3D Inversion Recovery prepared

Spoiled Gradient Recalled echo (IR-SPGR) sequence with the following settings: field-of-view (FOV) of 256 x 256 x 160 mm, flip angle = 8°, spatial resolution of 1 mm^3, SENSE factor = 1.5, TR/TE = 8.5/3.9 ms, TI =1060 ms. To assess the presence of comorbid inflammatory or vascular pathologies fluid-attenuated inversion recovery (FLAIR) images were also acquired with an Inversion Recovery Turbo Spin Echo (IR-TSE) sequence: spatial resolution = 0.65 x 0.87 x 4 mm, FOV = 230 x 183 x 150 mm, TR/TE = 11000 / 125 ms, TI = 2800 ms. Imaging data from all participants were individually reviewed for incidental radiological findings prior to inclusion into quantitative analyses. Computational analyses were performed using open-source suites, running on Linux distribution and parallel processes were used when possible to expedite pre-processing.

7.2.3 Thalamic segmentation and volumetry

The thalamus was parcellated into 25 sub-regions using Bayesian inference based on a probabilistic atlas [788]. The thalamus was segmented into the following nuclei in each hemisphere: antero-ventral (AV), latero-dorsal (LD), lateral posterior (LP), ventral anterior (VA), ventral anterior magnocellular (VA mc), ventral lateral anterior (VLa), ventral lateral posterior (VLp), ventral posterolateral (VPL), ventromedial (VM), central medial (CeM), central lateral (CL), paracentral (Pc), centromedian (CM), parafascicular (Pf), paratenial (Pt), reuniens/medial ventral (MV-re), mediodorsal medial magnocellular (MDm), mediodorsal lateral parvocellular (MDl), lateral geniculate (LGN), medial geniculate (MGN), limitans/suprageniculate (L-SG), pulvinar anterior (PuA), pulvinar medial (PuM), pulvinar lateral (PuL), and pulvinar inferior (PuI). Segmentation accuracy was individually verified and 10

groups of nuclei were defined based on their functional anatomy: "Anteroventral", "Lateral geniculate", "Medial geniculate", "Pulvinar-limitans" (PuA, PuM, PuL, PuI, L-SG), "Laterodorsal", "Lateroposterior", "Mediodorsal-paratenial-reuniens" (MDm, MDl, MV-re, Pt), "Motor nuclei"/ "Motor hub" (VA, VAmc, VLa, VLp), "Sensory nuclei"/ "Sensory hub" (VPL, VM), "Intralaminar" (CeM, CL, Pc, CM, Pf). Segmentation outputs were individually verified in each participant. Three subjects were excluded because segmentation problems; on the review of their FLAIR images these patients had relatively large juxta-thalamic lacunae and were not included in the final analyses. Total intracranial volumes were estimated in each subject using FreeSurfer (v7.2) and utilised as a covariate in subsequent volumetric comparisons, morphometric and surface-based statistics.

7.2.4 Thalamic vertex analyses

Thalamic vertex analyses were performed to evaluate surface-projected atrophy patterns in each patient group with respect of healthy controls. FMRIB's (v6.0) subcortical segmentation and registration tool [789] was used to characterise thalamic shape characteristics. Vertex locations of each participant were projected on the surface of an average shape template as scalar values, positive value being outside the surface and negative values inside. Permutation based non-parametric inference was implemented for group comparisons [802], design matrices included demeaned age, sex, and total intracranial volumes as covariates [802] and family-wise error (FWE) corrections were used to account for multiple comparisons.

7.2.5 Thalamic morphometry

In order to evaluate focal thalamic pathology beyond shape deformations and nuclear volume reductions, region-of-interest morphometry was performed to detect focal density alterations. FMRIB's software library (FSL) v6.0 was used for skull removal and tissue-type segmentation. Affine registration was used to align grey-matter partial volume images to the MNI152 standard space. A study-specific grey matter template was subsequently created to which the grey matter images of individual subjects were non-linearly coregistered. A voxelwise generalised linear model and permutation-based non-parametric inference were implemented to evaluate signal alterations in a bilateral thalamus mask accounting for age, sex, and TIV [802]. The labels of the Harvard-Oxford probabilistic structural atlas [803] were used to generate the bilateral thalamus mask. The threshold-free cluster enhancement (TFCE) approach was implemented and family-wise error (FWE) corrected outputs were thresholded at $p < 0.05$. Focal intra-thalamic alterations were visualised in 3D using a semi-transparent bi-thalamic ROI mesh.

7.3 Results

The six study groups (1) ALS-FTD C9+ (n=20, age 58.650±11.2216, male: 12 right handed: 18 education: 12.3±.746) (2) ALS-FTD C9- (n=20, age 59.950±7.6741, male: 13 right handed: 18 education: 14.3±.746) (3) bvFTD (n=10, age 61.200±4.2635, male: 6 right handed: 9 education: 14.7±1.055) (4) nfvPPA (n=15, age 61.267±4.9637, male: 9 right handed: 14 education: 14.6±.861) and (5) svPPA (n=5, age 61.600±4.6690, male: 3 right handed: 5 education: 15.8±1.492) (6) healthy controls ('HC', n=100, age 59.260±10.5463,

male: 52 right handed: 94 education: 14.2±.334) were matched for age (p=0.93), sex (chi square χ2: 1.630 p=.898), handedness (chi square χ2 = 1.213 p=.944) and education (p=.0169). The C9+ and C9-ALS-FTD groups were matched for symptom duration (p=0.3) and motor disability as measured by ALSFRS-r (p=0.912).

7.3.1 Thalamic segmentation and volumetry

Volumetric analyses revealed anatomically widespread atrophy in bvFTD affecting all groups of nuclei in both hemispheres **(Table 25, Table 26)**. *C9orf72* negative ALS-FTD patients exhibited selective thalamic involvement with sparing of laterodorsal nuclei in both hemispheres and strikingly asymmetric, right-predominant pulvinar and left-predominant lateroposterior, intralaminar and sensory nuclear involvement. Interestingly, with the exception of left laterodorsal atrophy, pathological change was more widespread in C9-ALS-FTD than in hexanucleotide expansion carriers. In contrast to the C9-ALS-FTD group, medial and lateral geniculate volume loss was not observed in C9+ALS-FTD. Consistent with the clinical phenotype motor nuclei volume reductions were observed in both ALS-FTD groups. Left-predominant thalamic degeneration was observed in svPPA based on volumetric measures. More widespread thalamus pathology was observed in nfvPPA with pulvinar and intralaminar sparing in both hemispheres and sensory and motor nuclear sparing in the right hemisphere. (**Figure 12, Figure 13, Figure 14**).

7.3.2 Thalamic vertex analyses

Vertex-wise analyses did not detect shape deformations in svPPA and captured widespread, largely overlapping patterns of outline changes in the other phenotypes **(Figure 15).**

7.3.3 Thalamic morphometry

At a FWE-corrected threshold of $p < 0.05$ region-of-interest morphometry captured right sided intrathalamic changes in C9+ ALS-FTD, right-predominant, but bilateral involvement in bvFTD and svPPA, and considerable symmetric disease-burden in nfvPPA **(Figure 16)**.

Table 25: Left thalamic grey matter volumes in FTD phenotypes

LEFT Thalamic Nuclei	*Study group*	*EMM*	*Standard error*	*C9+ ALS-FTD vs HC*	*C9- ALS-FTD vs HC*	*bvFTD vs HC*	*nfvPPA vs HC*	*svPPA vs HC*
Anteroventral	ALS-FTD C9+	94.176566	4.388157	**.001***	**<.001***	**.002***	**<.001***	**.001***
	ALS-FTD C9-	93.857057	4.369024					
	bvFTD	89.336838	6.143660					
	nfvPPA	76.269693	5.008516					
	svPPA	78.402016	8.700440					
	HC	114.354730	1.945412					
Lateral geniculate	ALS-FTD C9+	151.401233	6.363185	.070	**.001***	**.009***	**<.001***	**.005***
	ALS-FTD C9-	143.325954	6.335441					
	bvFTD	138.655292	8.908807					
	nfvPPA	129.977142	7.262756					
	svPPA	123.971826	12.616348					
	HC	171.480977	2.821005					
Medial geniculate	ALS-FTD C9+	102.662335	3.984781	1.000	**.001***	**.038***	**.009***	**.005***
	ALS-FTD C9-	91.333051	3.967407					
	bvFTD	91.291808	5.578912					
	nfvPPA	92.173803	4.548114					
	svPPA	79.355346	7.900663					
	HC	109.301381	1.766582					
Pulvinar-limitans	ALS-FTD C9+	1487.004888	36.709172	.106	1.000	**.004***	.761	**.040***
	ALS-FTD C9-	1536.786264	36.549119					
	bvFTD	1397.128459	51.394850					
	nfvPPA	1508.442034	41.898792					
	svPPA	1368.838975	72.783624					
	HC	1597.118054	16.274360					
Laterodorsal	ALS-FTD C9+	16.581108	1.880173	**.019***	.086	**.007***	**.006***	**.014***
	ALS-FTD C9-	17.630101	1.871976					
	bvFTD	13.501745	2.632346					
	nfvPPA	15.042874	2.145976					
	svPPA	10.435624	3.727838					
	HC	23.352574	0.833542					
Lateroposterior	ALS-FTD C9+	96.590125	4.361024	**.001***	**.009***	**<.001***	**<.001***	**<.001***
	ALS-FTD C9-	100.150159	4.342010					
	bvFTD	83.956351	6.105673					
	nfvPPA	90.775107	4.977548					
	svPPA	76.213566	8.646644					
	HC	116.754651	1.933383					
Mediodorsal-paratenial-reuniens	ALS-FTD C9+	792.908790	27.291034	**<.001***	**<.001***	**<.001***	**<.001***	**<.001***
	ALS-FTD C9-	765.131482	27.172044					
	bvFTD	754.556508	38.208941					
	nfvPPA	718.998489	31.149201					
	svPPA	693.702377	54.110193					
	HC	969.128144	12.098996					
Motor nuclei "Motor hub"	ALS-FTD C9+	1647.447706	45.731631	**0.014***	**<.001***	**.001***	**<.001***	.070
	ALS-FTD C9-	1603.882282	45.532240					
	bvFTD	1540.928172	64.026787					
	nfvPPA	1546.486345	52.196767					
	svPPA	1550.280392	90.672540					
	HC	1817.243387	20.274308					

LEFT Thalamic Nuclei	*Study group*	*EMM*	*Standard error*	*C9+ ALS-FTD vs HC*	*C9- ALS-FTD vs HC*	*bvFTD vs HC*	*nfvPPA vs HC*	*svPPA vs HC*
Sensory Nuclei "Sensory hub"	ALS-FTD C9+	835.414533	26.307583	.085	**.006***	**.005***	**.005***	.365
	ALS-FTD C9-	813.631883	26.192881					
	bvFTD	773.471638	36.832056					
	nfvPPA	797.328115	30.026717					
	svPPA	794.710136	52.160294					
	HC	916.497338	11.663000					
Intralaminar	ALS-FTD C9+	384.479615	11.603596	.299	**.039***	**.006***	1.000	1.000
	ALS-FTD C9-	375.870245	11.553004					
	bvFTD	352.724366	16.245670					
	nfvPPA	397.531489	13.244011					
	svPPA	373.590695	23.006561					
	HC	414.474561	5.144249					
Whole thalamus	ALS-FTD C9+	5608.666900	131.514896	**<.001***	**<.001***	**<.001***	**<.001***	**.001***
	ALS-FTD C9-	5541.598479	130.941486					
	bvFTD	5235.551177	184.128052					
	nfvPPA	5373.025090	150.107315					
	svPPA	5149.500954	260.755834					
	HC	6249.705798	58.304797					

Left thalamic grey matter volumes (mm^3) in healthy controls (HC), *C9orf72* positive ALS-FTD patients (ALS-FTD C9+), *C9orf72* negative ALS-FTD patients (ALS-FTD C9-), bvFTD, nfvPPA, svPPA. Estimated marginal means and standard error are adjusted for age, gender and total intracranial volume (TIV). Significant intergroup differences at $p \leq 0.05$ after Bonferroni-corrections for multiple comparisons are flagged in bold print and an asterisk. Covariates appearing in model are evaluated at the following values: Age = 59.629, Sex = 1.44, TIV = 1536464.23305

Table 26: Right thalamic grey matter volumes in FTD phenotypes

RIGHT Thalamic Nuclei	*Study group*	*EMM*	*Standard error*	*C9+ ALS-FTD vs HC*	*C9- ALS-FTD vs HC*	*bvFTD vs HC*	*nfvPPA vs HC*	*svPPA vs HC*
Anteroventral	ALS-FTD C9+	106.843667	4.698552	**.006***	**.010***	**<.001***	**<.001***	.101
	ALS-FTD C9-	107.806973	4.678066					
	bvFTD	92.953007	6.578230					
	nfvPPA	92.979010	5.362792					
	svPPA	99.317217	9.315864					
	HC	125.583480	2.083020					
Lateral geniculate	ALS-FTD C9+	147.929840	5.732850	.208	**.001***	**.001***	**.001***	**.036***
	ALS-FTD C9-	137.981051	5.707855					
	bvFTD	129.688888	8.026304					
	nfvPPA	134.439392	6.543310					
	svPPA	127.638956	11.366576					
	HC	163.616989	2.541557					
Medial geniculate	ALS-FTD C9+	100.988939	3.443228	1.000	**.009***	**.013***	**<.001***	**.005***
	ALS-FTD C9-	94.522678	3.428215					
	bvFTD	90.386017	4.820707					
	nfvPPA	89.264759	3.930001					
	svPPA	81.911885	6.826920					
	HC	107.633156	1.526494					
Pulvinar-limitans	ALS-FTD C9+	1265.305825	34.325989	**<.001***	**.032***	**<.001***	.980	1.000
	ALS-FTD C9-	1323.925377	34.176326					
	bvFTD	1171.961616	48.058263					
	nfvPPA	1362.151856	39.178696					
	svPPA	1353.870597	68.058465					
	HC	1440.326744	15.217819					
Laterodorsal	ALS-FTD C9+	18.308572	1.918132	.700	1.000	**.001***	**0.040***	.371
	ALS-FTD C9-	19.366731	1.909769					
	bvFTD	11.168110	2.685490					
	nfvPPA	15.356123	2.189301					
	svPPA	13.684984	3.803099					
	HC	22.536846	0.850370					
Lateroposterior	ALS-FTD C9+	94.629428	4.407375	.100	.072	**<.001***	**.012***	.349
	ALS-FTD C9-	94.241970	4.388159					
	bvFTD	74.848217	6.170566					
	nfvPPA	89.474346	5.030451					
	svPPA	87.400322	8.738544					
	HC	107.954766	1.953932					
Mediodorsal-paratenial-reuniens	ALS-FTD C9+	767.550842	27.648826	**<.001***	**<.001***	**<.001***	**<.001***	**<.001***
	ALS-FTD C9-	756.080885	27.528276					
	bvFTD	682.163679	38.709869					
	nfvPPA	749.646798	31.557574					
	svPPA	706.716234	54.819590					
	HC	951.402701	12.257617					
Motor Nuclei "Motor hub"	ALS-FTD C9+	1666.405898	46.947448	**.050***	**.011***	**.001***	.500	.585
	ALS-FTD C9-	1644.023097	46.742755					
	bvFTD	1536.627336	65.728996					
	nfvPPA	1696.716423	53.584465					
	svPPA	1621.448805	93.083151					
	HC	1820.374718	20.813318					

RIGHT Thalamic Nuclei	*Study group*	*EMM*	*Standard error*	*C9+ ALS-FTD vs HC*	*C9- ALS-FTD vs HC*	*bvFTD vs HC*	*nfvPPA vs HC*	*svPPA vs HC*
Sensory Nuclei "Sensory hub"	ALS-FTD C9+	784.470686	25.095136	.726	.090	**.002***	1.000	1.000
	ALS-FTD C9-	763.397877	24.985721					
	bvFTD	695.361166	35.134564					
	nfvPPA	814.540281	28.642866					
	svPPA	772.675845	49.756365					
	HC	839.346955	11.125484					
Intralaminar	ALS-FTD C9+	369.773524	12.517554	.700	.625	**.003***	1.000	1.000
	ALS-FTD C9-	369.414889	12.462977					
	bvFTD	327.893689	17.525261					
	nfvPPA	389.691294	14.287176					
	svPPA	380.078701	24.818673					
	HC	397.362603	5.549436					
Whole thalamus	ALS-FTD C9+	5322.207222	135.483130	**<.001***	**<.001***	**<.001***	**.020***	.132
	ALS-FTD C9-	5310.761528	134.892418					
	bvFTD	4813.051727	189.683797					
	nfvPPA	5434.260282	154.636543					
	svPPA	5244.743547	268.623689					
	HC	5976.138958	60.064043					

Right thalamic grey matter volumes (mm^3) in healthy controls (HC), *C9orf72* positive ALS-FTD patients (ALS-FTD C9+), *C9orf72* negative ALS-FTD patients (ALS-FTD C9-), bvFTD, nfvPPA, svPPA. Estimated marginal means and standard error are adjusted for age, gender and total intracranial volume (TIV). Significant intergroup differences at $p \leq 0.05$ after Bonferroni-corrections for multiple comparisons are flagged in bold print and an asterisk. Covariates appearing in model are evaluated at the following values: Age = 59.629, Sex = 1.44, TIV = 1536464.23305

Figure 12: Volumetric profile of left thalamic nuclei

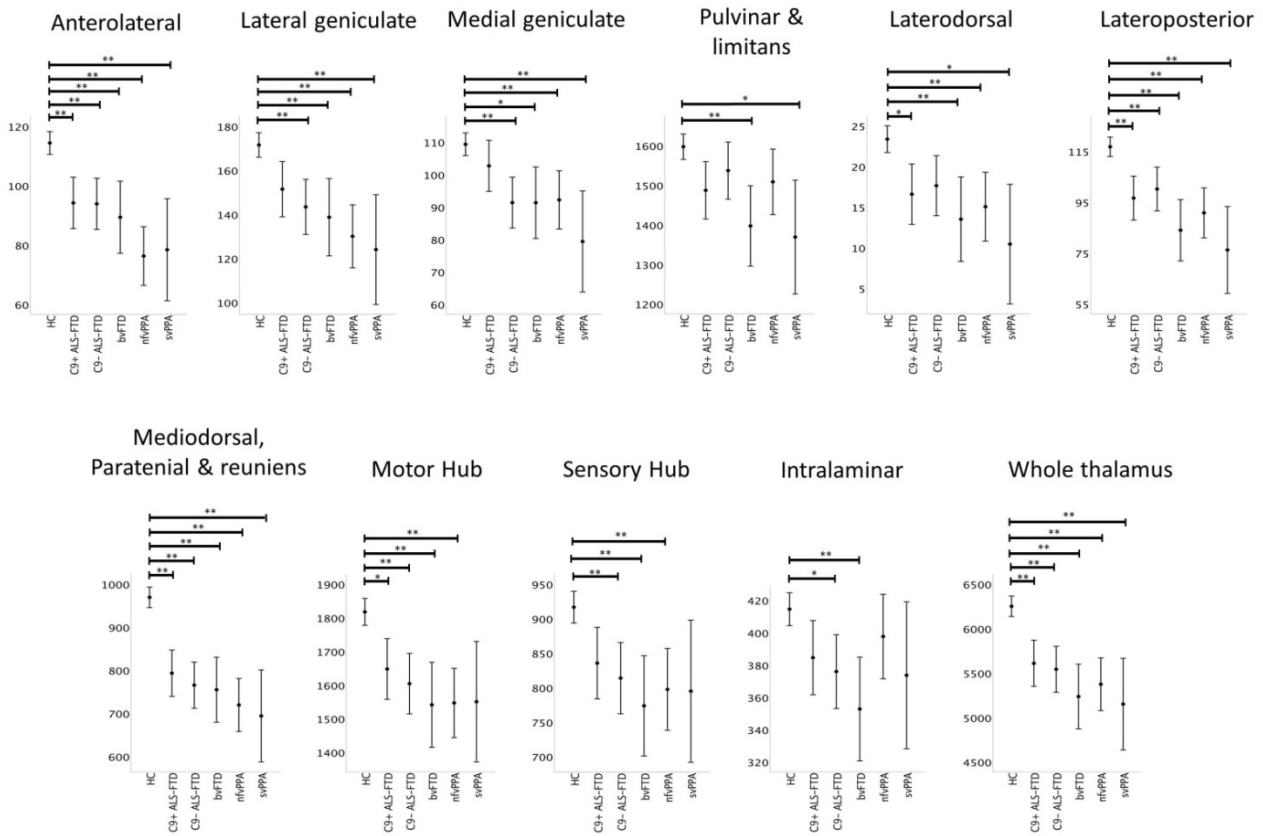

Left thalamic nuclei volumetric profile in healthy controls (HC), C9+ ALS-FTD, C9- ALS-FTD, bvFTD, nfvPPA and svPPA based on estimated marginal means adjusted for age, sex, TIV. Error bars represent 95% confidence intervals. Significant inter-group differences corrected for multiple comparisons are highlighted with asterisks * $p < 0.05$ ** $p < 0.01$

Figure 13: Volumetric profile of right thalamic nuclei

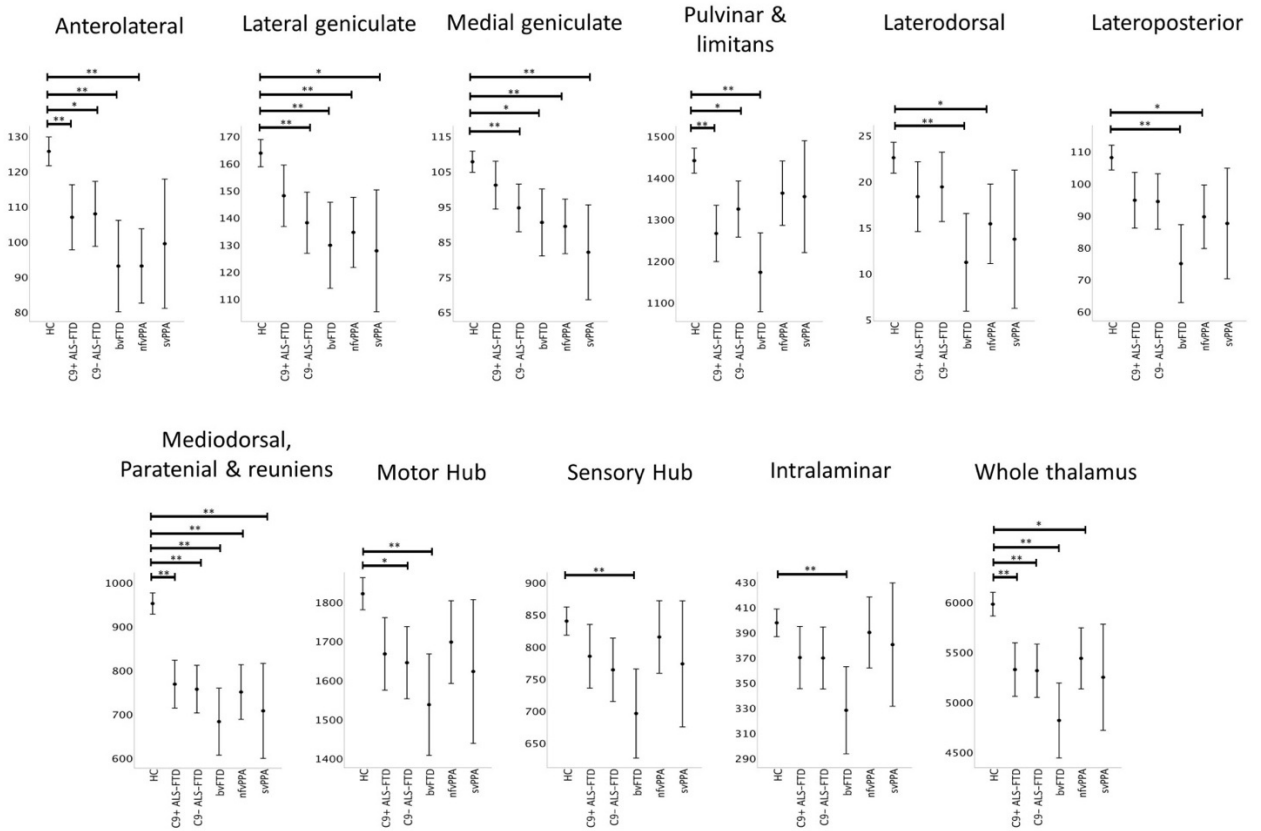

Right thalamic nuclei volumetric profile in healthy controls (HC), C9+ ALS-FTD, C9- ALS-FTD, bvFTD, nfvPPA and svPPA based on estimated marginal means adjusted for age, sex, TIV. Error bars represent 95% confidence intervals. Significant inter-group differences corrected for multiple comparisons are highlighted with asterisks * $p < 0.05$ ** $p < 0.01$

Figure 14: Preferential involvement of thalamic nuclei

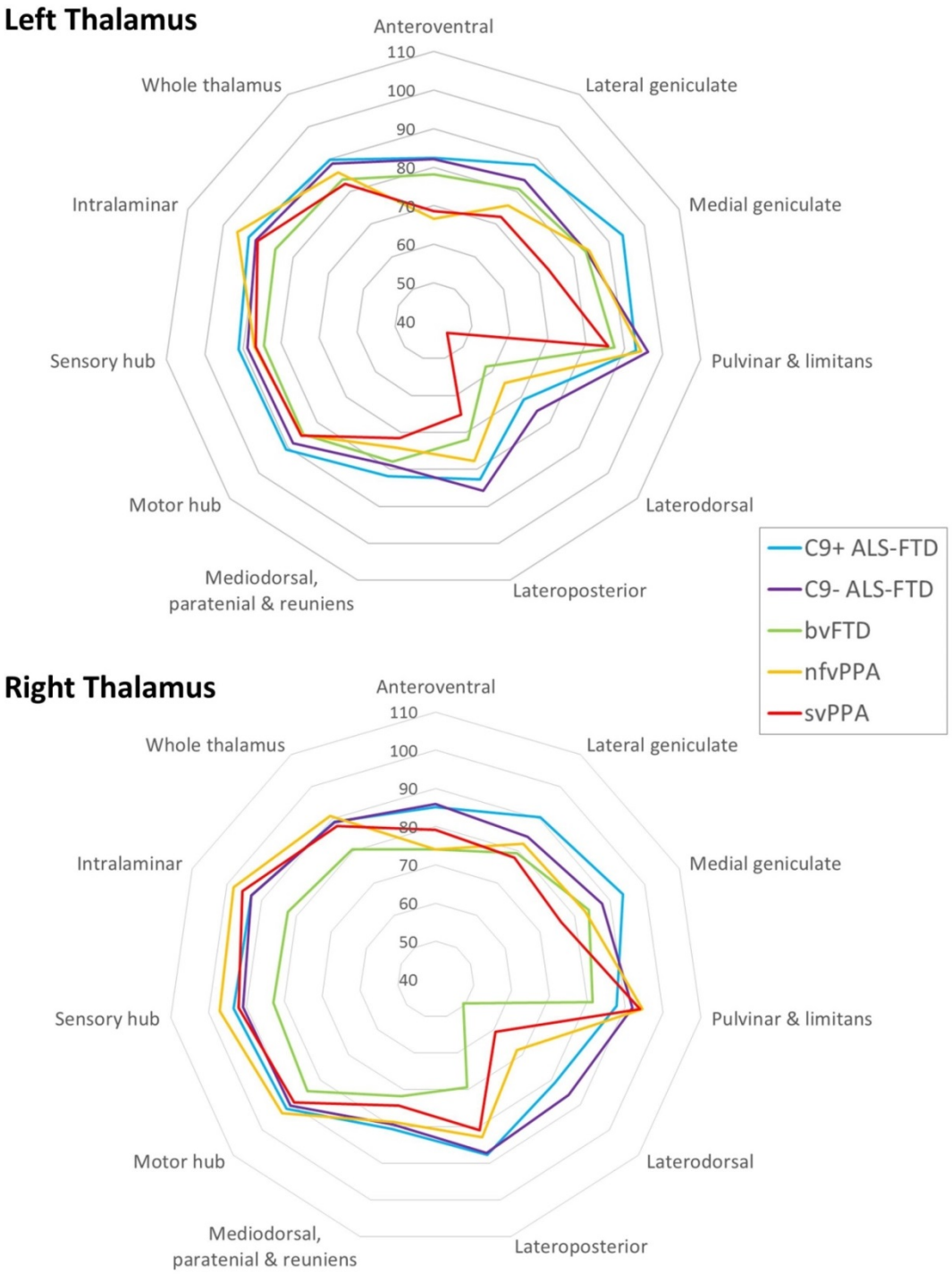

The preferential involvement of thalamic nuclei in C9+ ALS-FTD, C9- ALS-FTD, bvFTD, nfvPPA and svPPA with reference to healthy controls. 100% represents the estimated marginal mean of healthy controls for each structure. Estimated marginal means of volumes were calculated with the following values age = 59.629, sex = 1.44, TIV = 1536464.233

Figure 15: Thalamus vertex analyses

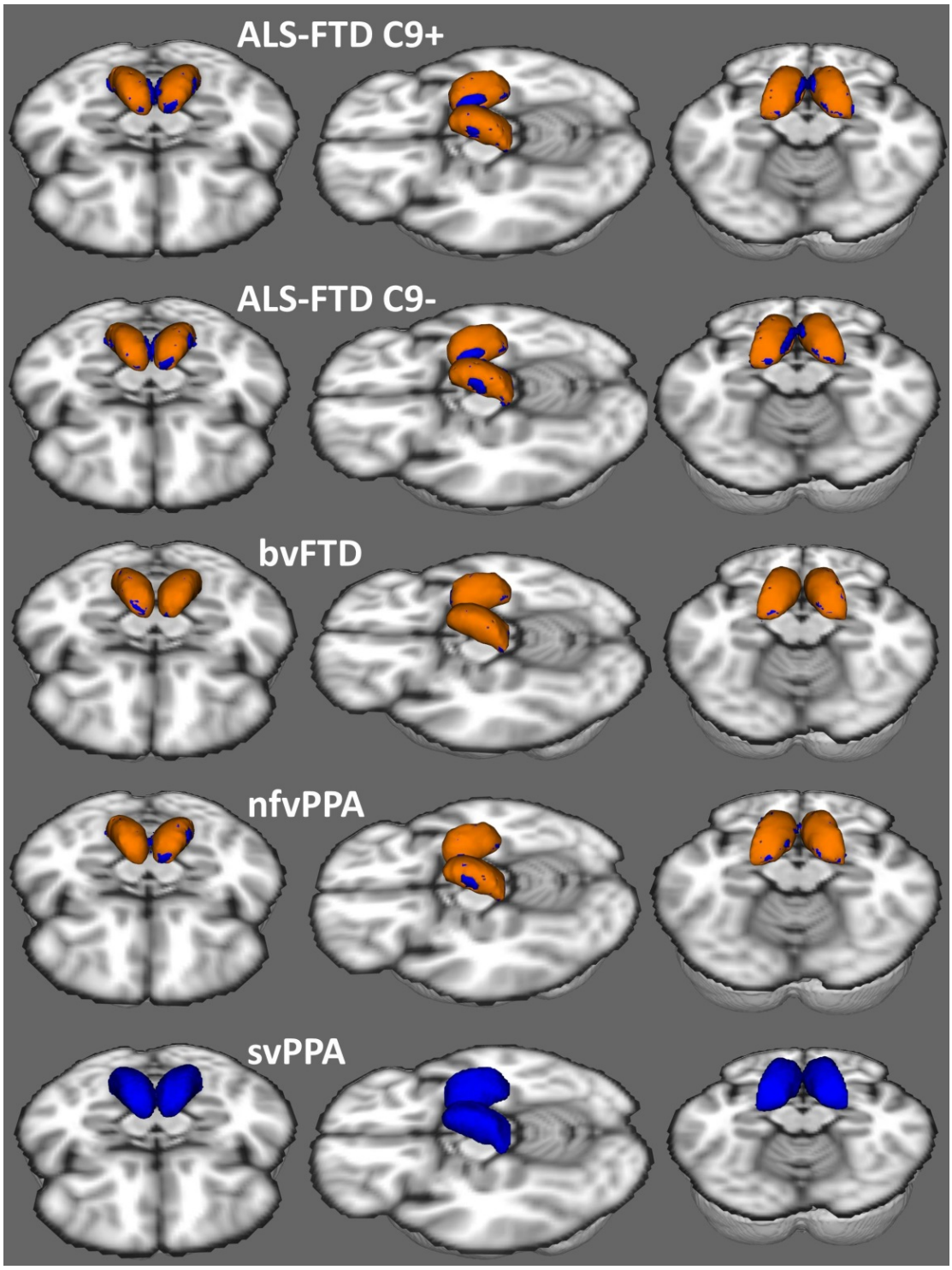

Phenotype-associated thalamic shape deformations. Vertex analyses depict surface-projected patterns of atrophy (orange colour) at $p < 0.01$ FWE-corrected and adjusted for demographic variables and TIV, projected onto a thalamic mesh mask (blue colour). Representative anterior-superior, lateral superior and posterior-superior views are shown.

Figure 16: Thalamus morphometry

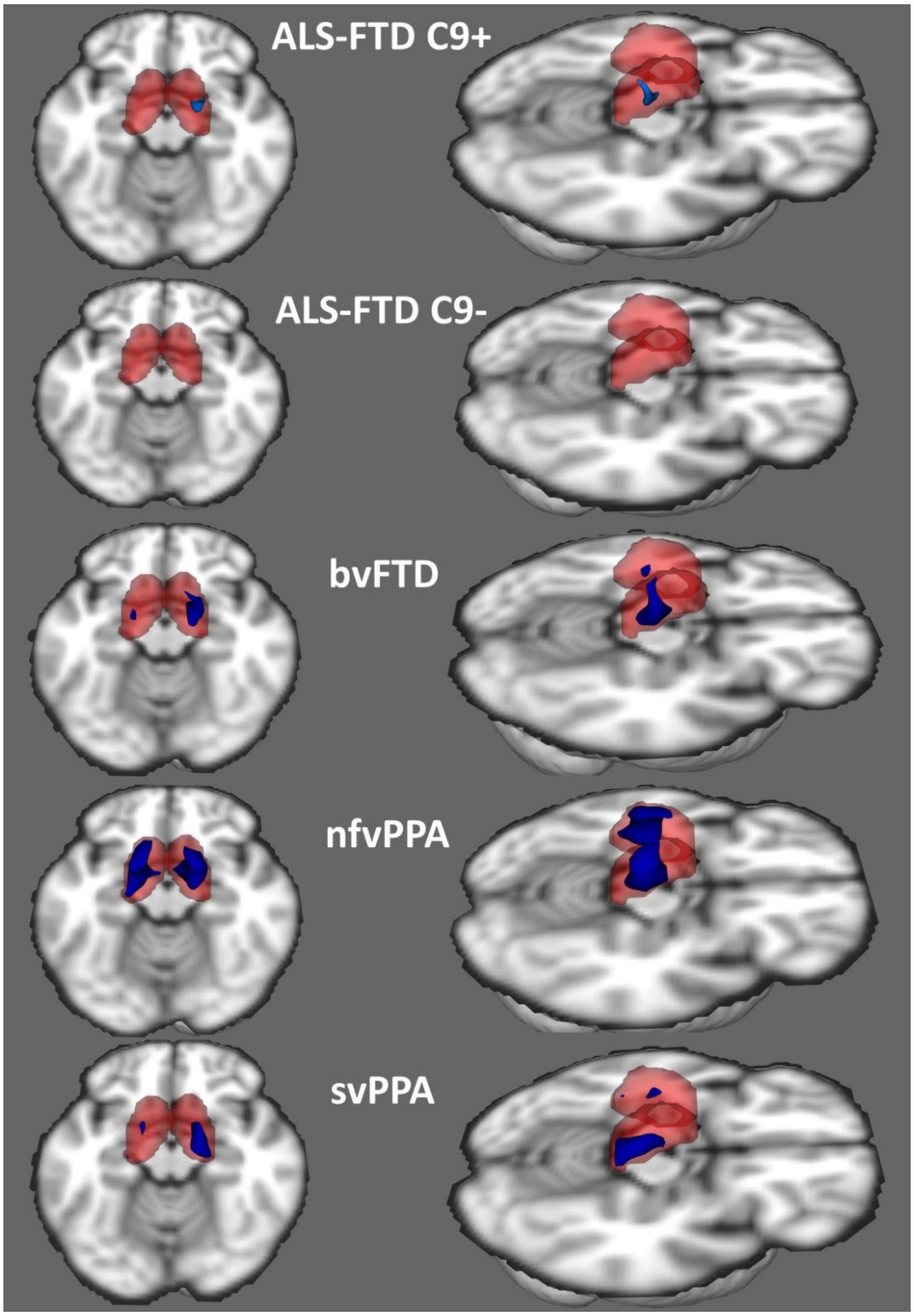

3D representation of intra-thalamic density alterations as identified by region-of-interest morphometric analyses. Focal density reductions at $p < 0.05$ FWE-corrected (TIV, age, sex adjusted) are indicated by blue colour in a transparent thalamic outline shown in pink colour.

7.4 Discussion

Our data demonstrate the selective involvement of the thalamic nuclei in FTD. The novelty of our paper is that thalamic metrics were not averaged in the left and right hemispheres, a large cohort of ALS-FTD patients were included and three independent T1w-derived MR analyses were conducted allowing the comparison of the detection sensitivity of these approaches.

In *C9orf72*-positive ALS-FTD, bilateral anteroventral and mediodorsal; left laterodorsal, lateroposterior and 'motor'; and right-predominant pulvinar degeneration was noted. Vertex analyses revealed symmetrical superior and inferior predominant surface deformations with medial and lateral sparing. Focal intra-thalamic density reductions were noted in the right hemisphere. In *C9orf72*-negative ALS-FTD, preferential volume loss was observed in the bilateral anteroventral, mediodorsal, motor, lateral and medial geniculate nuclei; left lateroposterior, sensory and intralaminar nuclei; and right-hemispheric pulvinar nuclei. Surface-mapped atrophy patterns were largely similar to those observed in C9+ALS-FTD. In bvFTD, widespread bilateral volume loss was observed involving all thalamic nuclei. Vertex analyses also confirmed widespread changes affecting the entire thalamic surface bilaterally. Morphometry analyses captured bilateral, but right-predominant intra-thalamic changes. In nfvPPA, bilateral anteroventral, mediodorsal, laterodorsal, lateroposterior, lateral and medial geniculate degeneration; and left-sided motor and sensory nuclear involvement was observed. Vertex analyses showed diffuse, symmetrical surface deformation patterns and region of interest morphometry revealed extensive intra-thalamic changes. In svPPA, left-predominant thalamic changes were noted; bilateral mediodorsal,

lateral and medial geniculate atrophy; and left-sided anteroventral, laterodorsal, lateroposterior, and pulvinar degeneration. Conversely, morphometric changes were bilateral but more pronounced in the right hemisphere.

With the exception of the bvFTD group, the above findings confirm selective thalamic involvement instead of global thalamic atrophy; with a distinctive profile of 'affected' and 'unaffected' regions. Bilateral mediodorsal atrophy was a universal finding across all FTD phenotypes which is consistent with previous reports [688]. Considerable lateral dorsal nucleus degeneration was identified bilaterally in bvFTD and on the left in svPPA. Both of these regions project to cortical and subcortical limbic structures [804] that are critical for memory, motivation and the regulation of emotion and behaviour [677, 688]. The marked involvement of this region, amongst other limbic thalamic nuclei, is in keeping with the clinical spectrum of limbic dysfunction observed in all FTD phenotypes. The involvement of thalamic regions associated with language is of particular interest in the nfvPPA and svPPA cohorts. Language is relatively poorly localised within the thalamus, with potential deficits arising from pathology in most regions [805]. It tends to be lateralised to the dominant thalamic hemisphere, akin to the cortical localisation of language [805, 806]. The thalamic regions that are most frequently implicated in language deficits include the pulvinar, intralaminar and ventrolateral nuclei [805, 807]. Our understanding of the role of the thalamus in language stems from lesion studies, neurovascular observations, fMRI experiments and the effects of deep brain stimulation on language [808]. In nfvPPA, left-lateralised ventrolateral nuclei were affected; the involvement of this region is

associated with perseveration, naming, fluency and articulation errors [805, 807-809]. In svPPA, left-lateralised pulvinar nuclei were affected; the involvement of this region is associated with naming errors [677, 805, 809]. These thalamic nuclei are key components of complex thalamocortical networks that mediate language function [806]. While ALS-FTD is primarily dominated by behavioural, executive and language deficits [441], there is increasing evidence of considerable deficits in social cognition ALS [254, 496], which may be exacerbated by subcortical grey matter changes [785].

Our data indicate that pulvinar atrophy is not unique to the *C9orf72* genotype [688, 733]. We found bilateral pulvinar atrophy in bvFTD, left-lateralised in svPPA and right lateralised in *C9orf72*-positive ALS-FTD and *C9orf72*-negative ALS-FTD. This region plays diverse limbic and associative roles modulating language, memory, somatosensory and visual information [677, 688]. Some of these functions are relatively lateralised [677]. Most patients with nfvPPA eventually develop symptoms consistent with progressive supranuclear palsy (PSP) or corticobasal syndrome (CBS), conditions associated with similar thalamic profiles [810, 811]. In CBS, there is early severe focal involvement of the ventral anterior and ventral lateral thalamic motor nuclei, just as seen in our nfvPPA cohort [810, 811]. Our observations not only reiterate the importance of evaluating thalamic nuclei separately rather than evaluating 'overall' thalamic volumes as a single structure, but also highlight the importance of assessing integrity measures in the two hemispheres separately. This approach permits the nuanced characterisation of focal changes, and also enables detecting asymmetric involvement, analogous to the asymmetric cortical signatures observed in PPA and svPPA. In contrast to

previous thalamus studies in FTD, we have conducted three independent T1w-derived MR analysis streams to highlight the relative advantages and limitations of each method. This may inform the methodological design of future thalamus studies. For example, while vertex analyses are commonly performed, we demonstrate their limited utility in symptomatic FTD cases where nearly the entire thalamic convexity is deformed, irrespective of the underlying clinical diagnosis. The morphometric approach offers additional benefits to volumetric outputs. Contrary to the post hoc statistics necessary for the interpretation of volumetric outputs, covariates can be directly incorporated in the design-matrices, non-parametric permutation testing can be readily performed accounting for family wise error, spatial coordinates of maxima can be established, and as illustrated in **Figure 16**, intra-thalamic changes can be visualised in 2D or 3D. The inclusion of additional MRI techniques such as intra-thalamic diffusivity alterations [200], thalamic parcellation based on cortical projection patterns [663], or thalamic spectroscopy [790] may also contribute to the multifaceted characterisation of thalamic degeneration in FTD and ALS-FTD. The widespread structural changes identified in this study are largely consistent with previous metabolic and functional studies. It has been proposed that metabolic and functional findings may precede frank grey matter atrophy in FTD and ALS-FTD [202, 231]. [^{18}F] FDG-PET studies revealed thalamic hypometabolism in both pre-symptomatic [202] and symptomatic [740] hexanucleotide repeat carriers and to a lesser extent sporadic FTD [740]. Functional connectivity studies have consistently shown thalamus mediated network disruption [491, 733]; medial

pulvinar nuclei atrophy has been linked to salience network disruption in both pre-symptomatic *C9orf72* [185] and symptomatic bvFTD [733].

Accurate early diagnosis in FTD is hugely important for individual patients, genetic counselling, resource allocation, care planning, but also for early recruitment into clinical trials. One of the practical implications of describing phenotype-specific imaging traits lies in its potential to discriminate disease phenotypes early in the course of the disease and capitalise on distinguishing MR signatures in automated machine learning algorithms [55]. A multitude of ML approaches have been applied to FTD [79, 128], ALS [58, 60, 159], and mixed ALS-FTD datasets [75] with varying classification accuracy. Preliminary discriminant analyses confirmed the value of evaluating individual thalamic nuclei rather than the entire thalamus in distinguishing FTD subgroups [688]. The distinction between AD and early FTD can also be challenging on clinical grounds. There is evidence of relatively selective thalamic nuclei involvement along the clinical continuum of AD [812]. Post-mortem studies have shown preferential involvement of the anterior thalamic nuclei with relative sparing of the medial dorsal nuclei even in the later stages [813], which is particularly interesting given our contrary finding of mediodorsal nuclei atrophy in FTD.

Our study demonstrates the structural degeneration of thalamic hubs of key corticobasal circuits in FTD [675], complementing existing insights from functional imaging studies [521, 733, 814]. As both presymptomatic cortical and thalamic changes have been described [184], the chronology of cortical and thalamic changes are not clear at present and disease propagation patterns remain disputed [815]. Robust longitudinal studies with asymptomatic mutation carriers are required to elucidate anatomical propagation patterns [145].

This study is not without limitations; as asymptomatic hexanucleotide expansion carriers have not been included, early thalamic changes could not be evaluated. Imaging studies of GGGGCC repeat carriers suggest structural alterations long before symptom manifestation [184, 248, 665], and thalamic analyses in these cohorts are likely to reveal more focal signatures than the ones observed in our study. Furthermore, the integrity of thalamic white matter projections was not characterised despite their likely involvement. Finally, in the absence of post mortem data, we are unfortunately not in a position to describe the microscopic and molecular underpinnings of the changes detected in vivo. Notwithstanding these limitations our data demonstrate focal thalamic involvement across the clinical spectrum of FTD and confirm that intra-thalamic neurodegenerative change can be reliably captured based on high-resolution T1-weighted datasets. Thalamic degeneration is a likely contributor to phenotype-specific clinical manifestations and large future studies are required to verify proposed genotype-associated atrophy patterns.

7.5 Conclusions

FTD is associated with focal rather than global thalamus degeneration. The main clinical subtypes exhibit phenotype-specific thalamic traits. Thalamic degeneration, while difficult to ascertain on visual inspection, is readily detected and characterised through computational image analyses. Thalamus degeneration is likely to contribute to the diverse manifestations observed clinically as a central hub of corticobasal and corticocortical circuits.

8 Mapping cortical disease-burden at individual-level in frontotemporal dementia: implications for clinical care and pharmacological trials

8.1 Introduction

The majority of imaging studies in FTD stratifies patients based on clinical, molecular or genetic categories and describes group-specific radiological traits [26, 643, 816-818]. These data however are difficult to apply to individual patients is everyday clinical practice. The current role of MR imaging in the diagnostic pathway of FTD is limited to 'ruling-out' structural mimics and alternative diagnoses. MR images acquired in a clinical setting are typically only subjectively and qualitatively interpreted with regards to atrophy [819-833]. This is a missed opportunity, as raw MRI datasets contain rich, spatially coded information with regards to cortical thickness, subcortical volumes and white matter integrity that cannot be meaningfully appraised on visual inspection. In contrast, computational imaging offers objective, observer-independent, reference-based quantitative image interpretation [669]. The potential translation of quantitative MR analysis frameworks to routine clinical practice may offer a number of practical benefits, including the generation of individualised atrophy maps, the objective assessment of longitudinal changes, and the classification of single scans into likely phenotypic categories. Ultimately, quantitative imaging may enable 'ruling-in' patients into specific groups, as opposed to merely 'ruling-out' differential diagnoses [55, 834]. From a practical point of view, MR platforms are widely available, MR imaging is non-invasive, relatively cheap, and a multitude of open-source

software are available for computational data analyses [25]. Access to [^{18}F] FDG PET-CT imaging on the other hand may be limited and the costs of routine PET imaging may be prohibitive in some health care systems [835, 836].

The current diagnostic approach to FTD subtypes – bvFTD, ALS-FTD, nfvPPA, svPPA - requires meeting specific clinical criteria and a definitive diagnosis may only be confirmed in vivo by identifying a pathogenic genetic mutation or typical histopathological findings [71, 73, 162, 411, 505, 506, 837-839]. The recent development, optimisation and validation of serum and CSF biomarkers panels will not only aid diagnostic classification but help the exclusion of alternative neurodegenerative diagnoses such as Alzheimer's pathology [73, 158, 169, 503, 840-843]. As with all diagnostic criteria, there are practical shortcomings with regards to sensitivity and specificity: some symptomatic patients do not meet proposed thresholds for diagnosis, despite subsequent pathological confirmation. In a subset of FTD cases, the diagnosis may never be reached in vivo, or a considerable diagnostic delay is experienced [844, 845]. Diagnostic uncertainty often creates undue stress for the patient and their family. The insidious onset of apathy, lack of interest and social withdrawal may be mistaken for depression, amongst other misdiagnoses [269, 846]. Early behavioural symptoms may be difficult to articulate, which is further complicated by the disparity in those perceived by the patients and their caregivers. Early cognitive deficits may also be difficult to identify, particularly due to the masking effect of cognitive reserve and the lack of sensitivity of generic screening instruments [269, 847]. Primary care physicians may reassure patients and caregivers based on neuropsychological screening tests and a 'grossly' normal MR imaging whilst awaiting lengthy specialist referrals [269].

Diagnostic delay in neurodegenerative conditions has a number of adverse implications. From a patients' perspective, timely diagnosis is important to inform realistic expectations over coming years [848]. It helps to guide targeted genetic testing that may be of significance to other family members. Accurate and early diagnostic classification enables prompt multidisciplinary team referrals and appropriate lifestyle adjustments with regards to employment, finances, driving, and childcare [848]. In those with language impairment, there is a critical time-window to explore alternative communication options e.g. 'voice-banking' to create a digital library for assisted communication devices [849]. A timely diagnosis is also important for resource allocation and advanced care planning to ensure that the patients' end-of-life preferences are recognised [850]. Early diagnostic categorisation is also indispensable for the timely inclusion of patients in clinical trials, which in turns enables longer follow-up [667]. Based on these considerations, we have undertaken a quantitative imaging study across the spectrum of FTD phenotypes to test a framework to interpret cortical atrophy patterns at both individual- and group-level.

8.2 Methods

8.2.1 Recruitment

A total of 227 participants were included in this study; 12 patients with non-fluent variant primary progressive aphasia ('nfvPPA' 6 females, mean age 61.50±2.97), 3 patients with semantic variant primary progressive aphasia ('svPPA' 1 female, mean age 61.67±6.43), 7 patients with behavioural variant FTD ('bvFTD' 3 females, mean age 60.71±3.30 years, 20 ALS-FTD patients with *C9orf72* hexanucleotide expansions ('C9+ALSFTD' 8 females, mean age

58.65±11.22), 20 ALS-FTD patients without *C9orf72* hexanucleotide expansions ('C9–ALSFTD' 7 females, mean age 59.95±7.67), 40 ALS patients with no cognitive impairment ('ALS-nci' 21 females, mean age 58.70±11.33) as disease controls and 125 healthy controls (HC). Methods for screening for GGGGCC hexanucleotide repeat expansions in *C9orf72* have been previously described [801, 851]. All participants provided written informed consent in accordance with the ethics approval of the Ethics Medical Research Committee of Beaumont Hospital, Dublin, Ireland. 651 additional HCs were also included from the Cambridge Centre for Ageing and Neuroscience (Cam-CAN) data base resulting in a total of 776 healthy controls (HC: 393 females, mean age 55.08±17.63 years) [852].

8.2.2 Imaging pulse sequences

All local participants were scanned with uniform scanning parameters on a 3 Tesla Philips Achieva scanner using an 8-channel receiver head coil. As described previously [449], a 3D Inversion Recovery Prepared Spoiled Gradient Recalled Echo (IP-SPGR) pulse sequence was utilised to acquire T1-weighted images. Acquisition details: repetition time (TR) / echo time (TE) = 8.5/3.9 ms, inversion time (TI) = 1060 ms, field-of-view (FOV): 256 x 256 x 160 mm, spatial resolution: 1 mm3. To assess vascular white matter lesion load FLAIR images were also acquired from each participant. The Cam-CAN control subjects were scanned with a T1-weighted MPRAGE sequence on a 3T Siemens Magnetom TrioTrim scanner at the University of Cambridge, using the following image acquisition parameters: TR/TE 2.25/2.99 ms, TI 900 ms, FOV= 256 x 240 x 192 mm; spatial resolution 1 mm^3 [852].

8.2.3 Pre-processing

All subjects' T1-weighted data were first pre-processed with FreeSurfer's *recon-all* pipeline to reconstruct and parcellate the cortical surface and generate a cortical thickness (CT) map, which estimates CT at each vertex point of the cortical surface. All CT maps were subsequently transformed to the CIFTI file format at a 32k resolution per hemisphere (Connectivity Informatics Technology Initiative[853, 854]) using the *Ciftify* toolbox[855]. Finally, each subject's CT map was parcellated into 1000 equally-sized patches, or 'mosaics', using a local-global cortical parcellation scheme [856], which further refines a previously published 7-brain-network cortical parcellation framework[857].

8.2.4 Statistical analyses: the standard approach

A one-factorial, two-level, between-subjects comparison was first conducted between each patient group and controls controlling for age and gender. To correct for alpha-level inflation, we used a Monte-Carlo permutation procedure to obtain family-wise error-corrected (FWER) p-values (5000 permutations; thresholded at the voxel-level). These analyses were ran within the SPM-based toolbox (http://www.fil.ion.ucl.ac.uk) *Multivariate and repeated measures* [858].

8.2.5 Statistical analyses: the 'mosaic' approach

To appraise cortical thinning at an individual level, each CT map was rated with respect to an age- and sex-matched control group. Since neurite density varies significantly across the cortex[859], CT was averaged across small 'mosaics', defined by a 1000-patch atlas. For each mosaic, null distributions were built non-parametrically as follows: First, the average CT value of each

HC was z-scored with respect to all remaining controls to obtain a distribution at the size of the control group. Likewise, an individual patient's CT was z-scored with respect to all HC. P-values reflecting expected probabilities of cortical thinning were then calculated by counting how many values in the control distribution were smaller than the observed patient's and dividing that count by the number of subjects in the control group. We considered mosaics with p-values ≤ 0.05 as significantly thin or 'atrophic'. To account for confounding effects of age and gender [860], we customised the reference groups: For each patient, we only included age- and gender-matched controls from the mixed control cohort (in total 776 HC). 'Age-matched' was defined as +/– 2 years from the patients' age. As demonstrated before [673], this strategy successfully corrects for variance introduced by demographic confounders. This strategy generates a binary atrophic/not-atrophic label to each cortical mosaic with reference to demographically matched controls, enables the calculation of the number of 'significantly thin' mosaics throughout the cortex, as well as its fraction with respect to all evaluated mosaics. To co-validate the output of this method with the 'gold standard' approach we juxtaposed our findings with standard cortical thickness analyses.

8.2.6 Inferential statistics of 'mosaic' maps

The output maps of the mosaic approach can be readily visualised for individual patients indicating whether a cortical region (mosaic) is atrophic ('hit') or not with respect of demographically matched controls. However, these outputs can also be at group level; we employed a Monte-Carlo permutation testing scheme to compare each of the clinical groups to HCs. In brief, we first generated a matrix with the dimensions of $n_{Patients}$ x $n_{mosaics}$ for

each clinical group, indicating for each element either the presence (‘1’) or absence (‘0’) of regional atrophy. We then shuffled that matrix 100,000 times across mosaics, whereby we saved the count of patients with 1s at each iteration. As a result, we obtained non-parametric distributions, comprised of 100,000 values per mosaic, based on which FWER p-values can be calculated by counting the number of values exceeding the observed number of hits in the data and dividing that count by the number of iterations. We considered p-values ≤ 0.05 as statistically significant. Mathematical analyses were conducted within MATLAB version R2019b (The Mathworks, Natick, MA, USA).

8.2.7 Between group contrasts

Based on the ‘mosaic’ approach, a one-way, six-level analysis of variance (ANOVA) was conducted to ascertain differences among means of whole-brain thin-patch-fractions between the clinical groups. Based on the ‘standard’ approach, the means of raw CT values were also compared with the inclusion of age and gender as covariates (ANCOVA), since, as opposed to the mosaic approach, these are not inherently accounted for. As the ANOVA/ANCOVA revealed statistically significant effects, post-hoc testing was conducted. Tukey’s honestly significant difference testing (HSD) using type III errors were utilised for pairwise comparisons. For post-hoc testing, age was converted into a categorical variable by assigning each patient to one of six separate age groups, since only categorical confounders can be accounted for in Tukey HSD. All statistical analyses were conducted within RStudio (version 1.3.1093, R Core Team, R Foundation for Statistical Computing, Vienna, Austria).

8.2.8 Region-of-interest statistics

To further characterise regional disease-burden, we calculated fractional thin-patch-counts for four large regions of interest (ROIs): motor cortex (i.e. pre-/paracentral gyri), parietal, temporal and frontal cortices. The 1000-patch mosaic-parcellation was overlaid the anatomically-defined Desikan-Killiany atlas resulting in 122 mosaics in the motor, 185 in the parietal, 150 in the temporal and 200 in the frontal cortices. For each patient, we calculated the fraction of atrophic mosaics, and averaged that fraction across subjects in each clinical subgroup. To highlight the preferential involvement of main brain regions in each phenotype, we generated radar plots in which whole-brain fractional thin-patch-counts were also incorporated. Regional radar plots were also generated to characterise regional involvement in individual patients.

8.3 Results

Standard cortical thickness analyses confirmed subgroup-specific patterns of cortical atrophy consistent with the clinical diagnosis **(Figure 17).** The 'mosaic-based' approach has successfully generated individual atrophy maps for each patient with reference to controls **(Figure 18).** Group-level observations could also be inferred from the 'mosaic-based' approach following permutation testing **(Figure 19).** These results were anatomically consistent with the outputs of the 'standard approach' **(Figure 17).** Group-level traits deduced from the 'mosaic-based' approach produced more focal and better demarcated atrophy maps than those generated by the standard approach. This is best demonstrated by the C9+ALS-FTD group where atrophy is not just more widespread than the C9–ALS-FTD group, but the precentral

gyrus is more affected. Cortical atrophy patterns derived from the 'mosaic-approach' are also more focal and less noisy in the nfvPPA group than the in the maps generated by the standard approach.

Figure 17: ‘Standard’ cortical thickness analyses

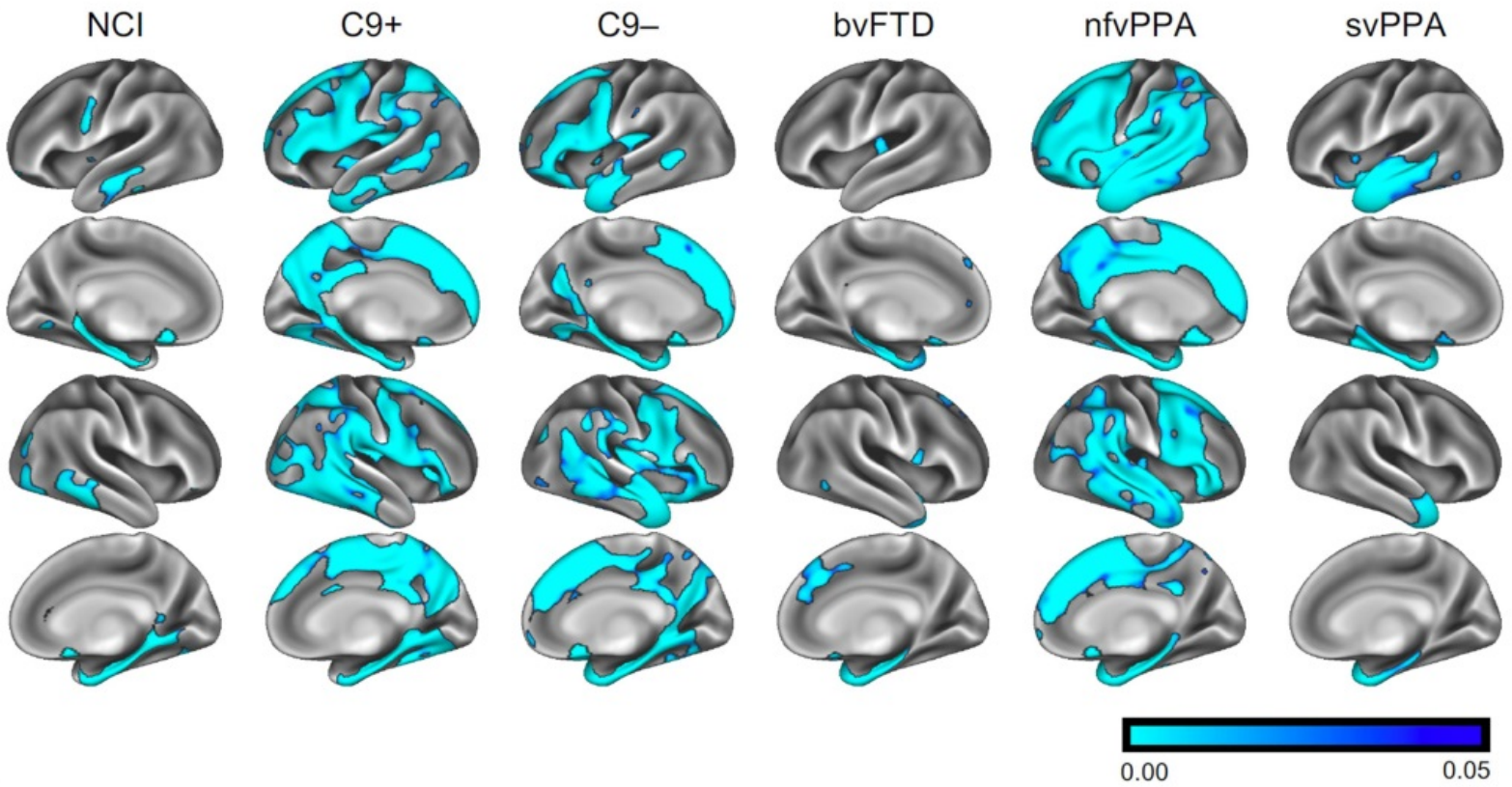

’Standard’ cortical thickness analyses using voxelwise permutation testing, corrected for age and gender; family-wise error corrected p-maps are presented for the six clinical groups with reference to healthy controls. NCI: ALS patients with no cognitive impairment, C9+: ALS-FTD patients with *C9orf72* hexanucleotide expansions, C9-: ALS-FTD patients without *C9orf72* hexanucleotide expansions, bvFTD: behavioural variant FTD, nfvPPA: non-fluent variant primary progressive aphasia, svPPA: semantic variant primary progressive aphasia

Figure 18: 'Mosaic-based' individualised brain atrophy maps

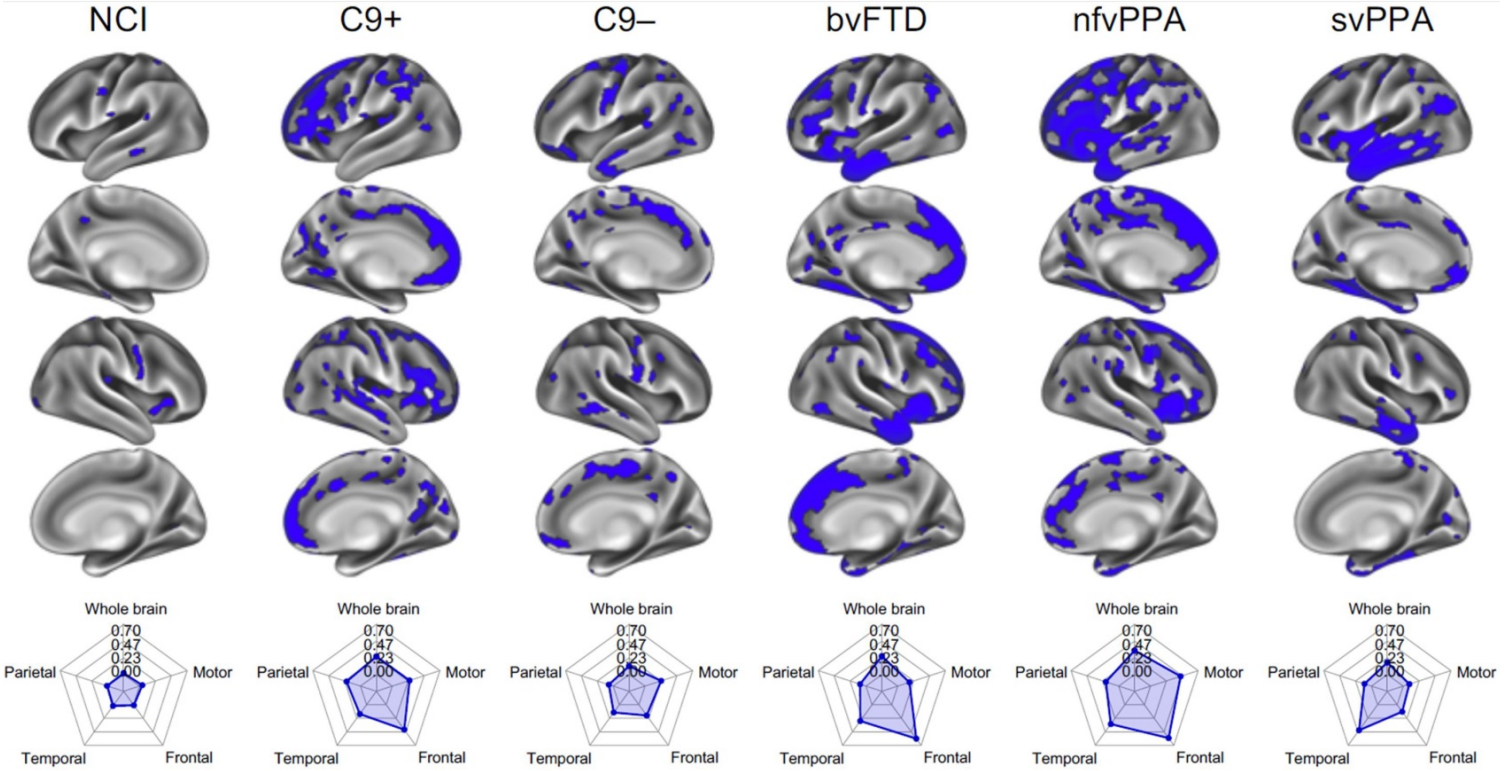

Individual data interpretation in single patients using the 'mosaic' pipeline; representative examples are shown from each clinical groups. Blue colour indicates cortical thinning with respect to demographically matched controls. Radar charts indicate the fraction of affected 'mosaics' in frontal, parietal, temporal and motor cortices as well as over the entire cortex.
NCI: ALS patients with no cognitive impairment, C9+: ALS-FTD patients with *C9orf72* hexanucleotide expansions, C9-: ALS-FTD patients without *C9orf72* hexanucleotide expansions, bvFTD: behavioural variant FTD, nfvPPA: non-fluent variant primary progressive aphasia, svPPA: semantic variant primary progressive aphasia

Figure 19: 'Mosaic-based' group-level brain atrophy maps

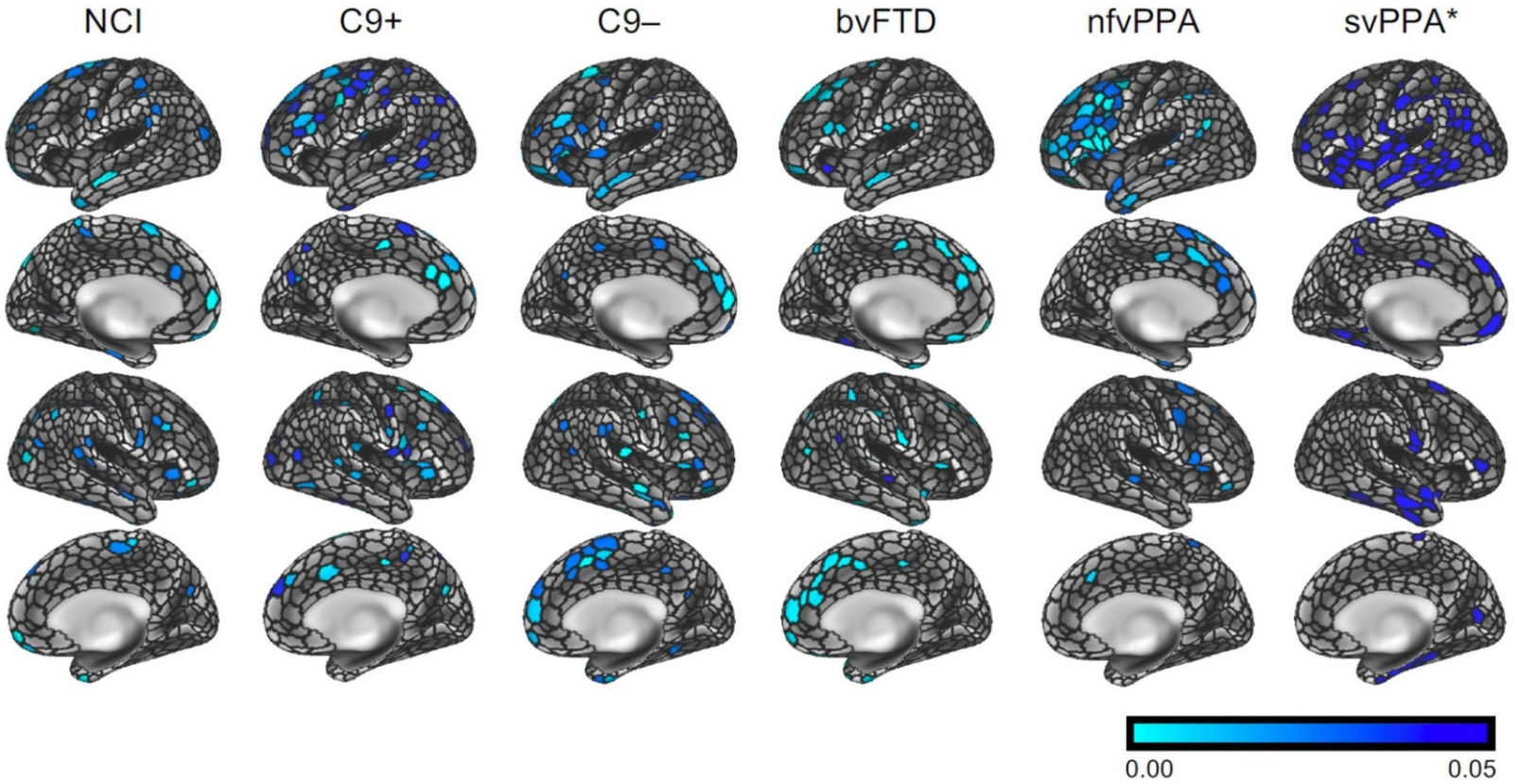

Inferential statistics; group-level atrophy patterns derived from the 'mosaic' approach. Family-wise error-corrected p-maps are presented at p<.05. For svPPA a threshold of p<.06 is shown.
NCI: ALS patients with no cognitive impairment, C9+: ALS-FTD patients with *C9orf72* hexanucleotide expansions, C9-: ALS-FTD patients without *C9orf72* hexanucleotide expansions,
bvFTD: behavioural variant FTD, nfvPPA: non-fluent variant primary progressive aphasia, svPPA: semantic variant primary progressive aphasia

Both the 'mosaic' and the 'standard' approach indicated intergroup differences **(Figure 20a/ Figure 20c)** (mosaic approach: $F(5) = 14.86$, $p = 8.73e\text{-}11$; standard approach: $F(5) = 14.89$, $p = 9.50e\text{-}11$). Post-hoc testing revealed that least affected study group was ALS-nci compared to all the other diagnostic categories. **(Figure 20b)** ALS-nci vs. C9–(0.202 +/– 0.132), $p_{adj} = 1.76e\text{-}04$; ALS-nci vs. C9+(0.214 +/– 0.100), $p_{adj} = 2.54e\text{-}05$; ALS-nci vs. bvFTD (0.208 +/– 0.076), $p_{adj} = 2.01e\text{-}02$; ALS-nci vs. nfvPPA (0.321 +/– 0.121), $p_{adj} < 0.0001$. The same pattern was observed for the standard approach **(Figure 20d)**, where the ALS-nci group exhibited higher CT in the pairwise comparisons than all other groups: ALS-nci vs. C9– (2.24 mm +/–0.11 mm), $p_{adj} = 1.85e\text{-}04$; ALS-nci vs. C9+ (2.23 mm +/–0.10 mm), $p_{adj} = 2.86e\text{-}05$; ALS-nci vs. bvFTD (2.22 mm +/–0.09 mm), $p_{adj} = 4.30e\text{-}03$; ALS-nci vs. nfvPPA (2.13 mm +/–0.11 mm), $p_{adj} < 0.0001$; ALS-nci vs. svPPA (2.17 mm +/–0.07 mm), $p_{adj} = 1.61e\text{-}02$. In contrast, the most affected clinical group was nfvPPA, where the mean thin-patch-count fraction was not only higher than that of the ALS-nci group, but also the C9–ALSFTD ($p_{adj} = 9.45e\text{-}03$) and the C9+ALSFTD ($p_{adj} = 2.80e\text{-}02$). Again, this pattern was mirrored by the standard approach, where the ALS-nci group not only showed higher mean values than the nfvPPA group, but just as in the mosaic approach, also the C9–ALSFTD ($p_{adj} = 1.72e\text{-}02$) and the C9+ALSFTD ($p_{adj} = 4.66e\text{-}02$) groups.

Our region-of-interest statistics evaluated thin-patch-count fraction per 'ROI' **(Figure 21a)** and confirmed the preferential involvement of ROIs in the study groups **(Figure 21b).** The most anatomically widespread disease-burden was detected in nfvPPA (largest radius), the least pathology in ALS-nci (smallest radius) and the most focal involvement in svPPA (temporal cortex).

Figure 20: A comparison of 'standard-' and 'mosaic-approach' group profiles

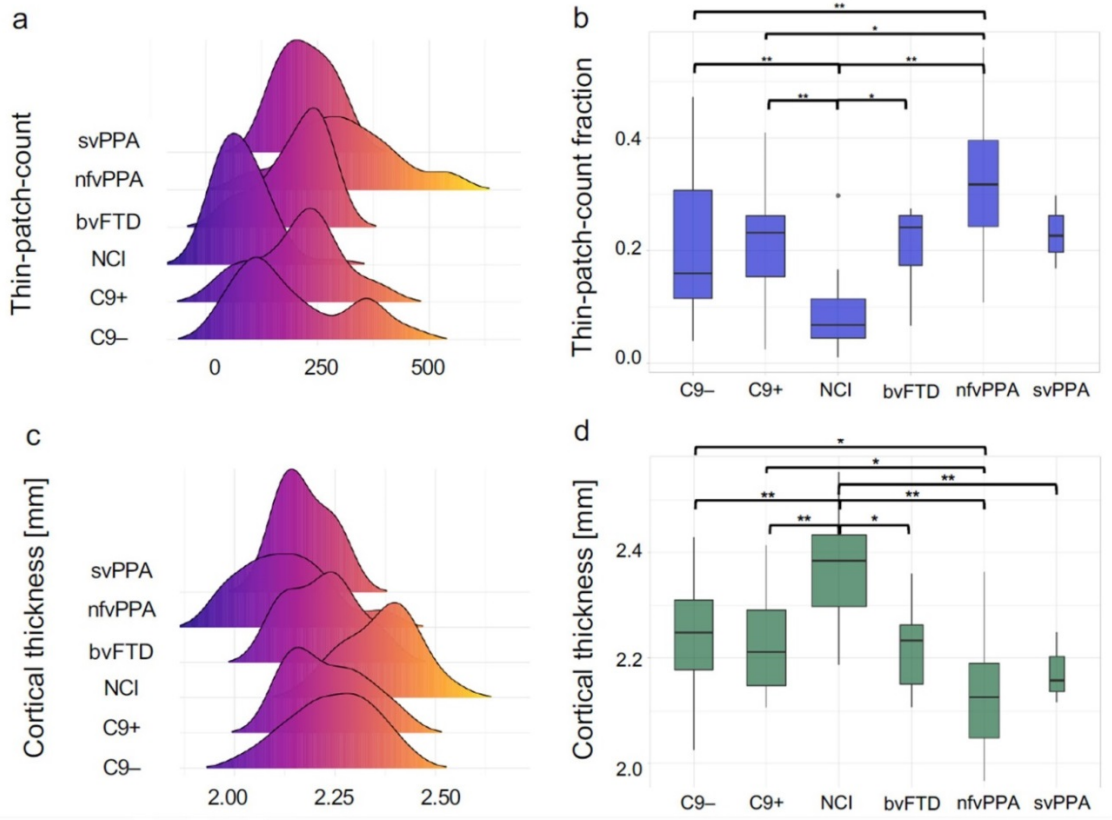

The comparison of group profiles; distribution of the number of thin patches derived from the 'mosaic approach' (a) and cortical thickness values as calculated by the 'standard approach' (c). Group differences in the number of thin patches (b) and mean cortical thickness (d). * indicates post hoc intergroup difference at $p_{adj} \leq 0.05$, (**) at $p_{adj} \leq 0.001$ following Tukey HSD testing. The widths of box plots indicate sample size and error bars represent 1.5 times the interquartile range. NCI: ALS patients with no cognitive impairment, C9+ALS-FTD patients with *C9orf72* hexanucleotide expansions, C9-ALS-FTD patients without *C9orf72* hexanucleotide expansions, bvFTD: behavioural variant FTD, nfvPPA: non-fluent variant primary progressive aphasia, svPPA: semantic variant primary progressive aphasia.

Figure 21: Regional disease burden in frontotemporal dementia

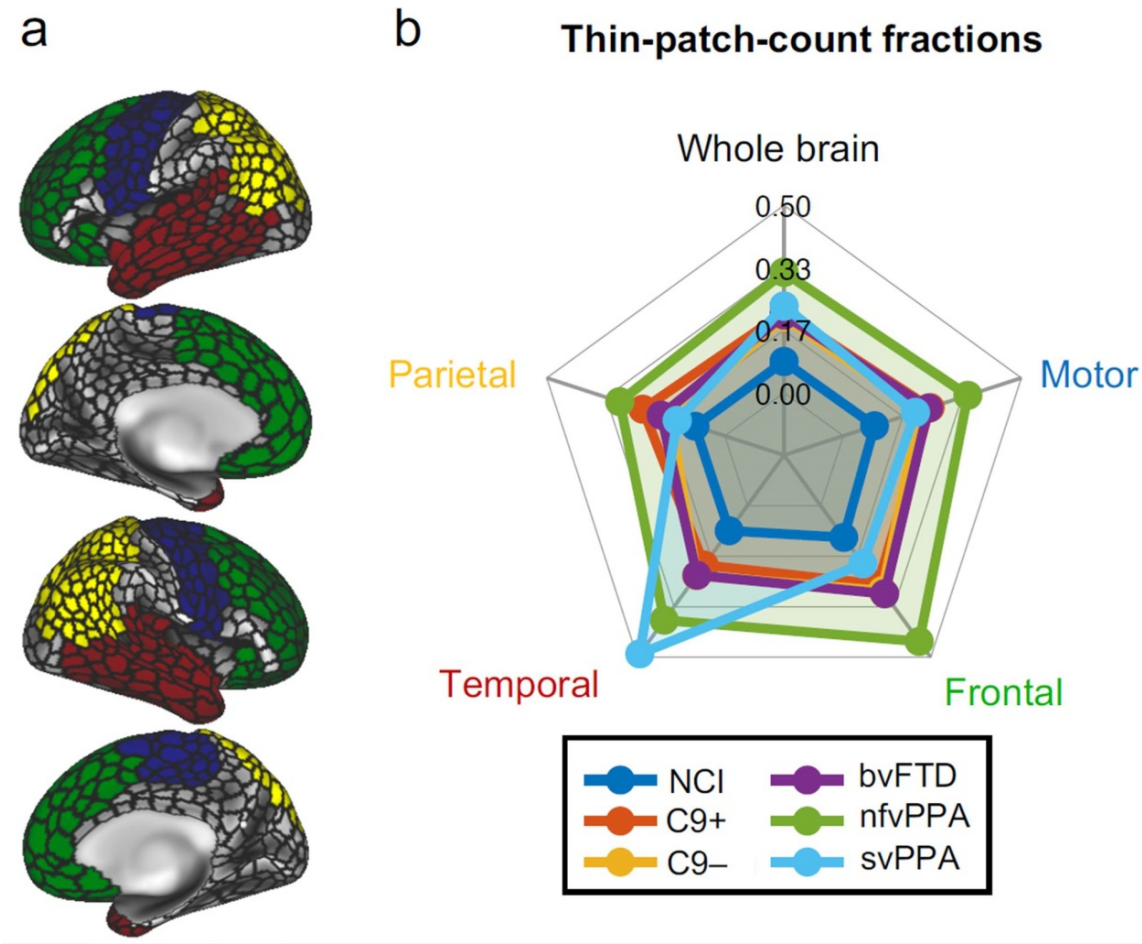

Regional disease burden; cortical thinning was further evaluated in four atlas-defined regions-of-interest (ROIs) in the motor (blue), parietal (yellow), temporal (red) and frontal (green) cortices and over the entire cerebral cortex (a). The fraction of atrophic 'mosaics' was calculated in each patient within each ROI with respect to the total number of mosaics comprising the given ROI. The distribution of disease burden in the patient groups is presented as radar charts (b). NCI: ALS patients with no cognitive impairment, C9+: ALS-FTD patients with *C9orf72* hexanucleotide expansions, C9-: ALS-FTD patients without *C9orf72* hexanucleotide expansions, bvFTD: behavioural variant FTD, nfvPPA: non-fluent variant primary progressive aphasia, svPPA: semantic variant primary progressive aphasia

8.4 Discussion

Our findings demonstrate the feasibility of interpreting single T1-weighted images from individual patients to generate maps of atrophy. We have shown that cortical regions can be successfully categorised as atrophic or unaffected in single subjects with respect to a databank of controls. A z-score based approach not only enables the appraisal of cortical disease-burden in individual-subjects, but group-level patterns may also be inferred. The output maps of the proposed 'mosaic' approach are anatomically concordant with gold standard cortical thickness analyses. The topography of cortical thinning can be reported visually, numerically and in an ROI-based representation at both individual- and group-level. The pipeline is based on quantitative cortical thickness measurements, an atlas-based parcellation and is fully observer independent. In its current form it is computationally demanding, but all the mathematical steps utilised could be integrated into a single computer script and run either as a cloud-based solution or installed locally on the MR platform or data server.

In this paper we have demonstrated the utility of this approach in FTD phenotypes, but this method could potentially also be utilised in neurodegenerative conditions where the ascertainment of cortical atrophy patterns is clinically relevant [272, 441, 488, 493, 861]. The technique relies on the binary labelling of cortical regions as 'atrophic' or 'normal'. This is fundamentally a reductionist approach, but given the very high number of cortical regions (mosaics), it is a successful strategy as demonstrated by the detection of confluent cortical areas. The generation of putative atrophy maps provides an instant representation of the anatomical expansion, focality and

lobar predominance of disease burden. These colour coded maps are potentially useful to illustrate affected regions to patients, caregivers and members of the multidisciplinary team. This starkly contrasts with the current practice of pointing at presumed regions of atrophy on black and white 2D images which are difficult to decipher by laypeople [833]. The *z*-score derived, 'mosaic' method may not only be applied to those with an established diagnosis, but also to those with a suspected diagnosis or pre-symptomatic mutation carriers to characterise disease burden distribution.

In a clinical setting, progressive frontotemporal pathology is often monitored by validated neuropsychological tests [496, 847, 862]. Cognitive assessment however may be particularly challenging in certain FTD phenotypes, especially in ALS-FTD where motor disability and dysarthria may preclude the use of certain tests [500, 668, 670]. In other FTD phenotypes, performance on neuropsychological testing may be confounded by mood, apathy, cognitive reserve and practice-effects which highlight the role of neuroimaging in tracking progressive changes [229, 516].

Quantitative cortical thickness mapping may also give additional reassurance to those who fear a particular diagnosis despite scoring high on neuropsychological tests [637]. This is often a significant source of anxiety for patients, particularly for those who have first-hand witnessed a family member or close friend carrying a certain a diagnosis. Immediate answers would provide early reassurance, alleviating the sense of heightened stress and anxiety. The implementation of this method may be relatively straightforward as most patients undergo a routine MRI brain scan as part of the current diagnostic pathway [833].

Despite the clinical rationale to devise such frameworks, our study has a number of limitations. The sample size of the various patient groups in this pilot study is relatively small necessitating validation in larger external datasets. All patients in our study had an established diagnosis; thus, the sensitivity of this method needs to be further evaluated in those with a suspected diagnosis, early-stage disease or in asymptomatic mutation carriers [154, 155, 665]. Moreover, only grey matter analyses were conducted, despite the contribution of white matter pathology to the clinical manifestations of these phenotypes [50, 433, 663, 863, 864]. Finally, while our approach provides individualised atrophy maps, supervised and unsupervised machine learning approaches offer direct individual patient categorisation into diagnostic and prognostic groups [56, 57, 60, 157, 865].

We envisage future applications for this methodological approach in both clinical practice and potentially in clinical trials. Consecutive MR datasets could be compared to the patients' initial scan; allowing for the objective measurement of disease-burden accumulation and the evaluation of progression rates [145, 172, 866]. Alternative imaging metrics such as spinal cord measures, network integrity indices, white matter diffusivity parameters or subcortical grey matter metrics could also be readily investigated in a similar z-score based framework [231, 249, 256, 491, 671]. Future applications would require the validation of our findings in large multicentre studies, ideally incorporating diverse patient populations across a variety of neurodegenerative disorders.

8.5 Conclusions

Our preliminary findings indicate that T1-weighted MRI data from individual patients may be meaningfully interpreted and maps of cortical

atrophy can be readily generated. The outputs of our analyses are anatomically analogous with gold standard methods. This is a promising approach to interpret single subject scans with viable clinical and clinical trial utility.

9 White matter microstructure alterations in frontotemporal dementia: phenotype-associated signatures and single-subject interpretation

9.1 Introduction

White matter changes in frontotemporal dementia (FTD) have been extensively studied and both clinical subtypes [13, 14, 16, 36, 867, 868] and genotypes [21, 140, 150] have been linked to relatively specific white matter signatures. The most commonly utilised white matter technique is diffusion tensor imaging (DTI), but a variety of non-Gaussian techniques such as diffusion kurtosis imaging (DKI), neurite orientation dispersion and density imaging (NODDI) have also been successfully utilised. [200] White matter (WM) alterations in FTD can already be detected in the presymptomatic phase of the disease and white matter alterations are relatively marked by the time the diagnosis can be established.[200] WM changes can also be readily tracked longitudinally across multiple timepoints to appraise the rate of progression and patterns of anatomical propagation. A shortcoming of descriptive imaging studies in FTD is that often only group-level inferences are presented i.e. shared patterns of white matter disease burden in specific phenotypes or genotypes. The demands of clinical imaging differ significantly from the deliverables of academic radiology. [834] The emphasis in the clinical setting is the accurate categorisation of a suspected patient into a diagnostic subgroup, the evaluation of an asymptomatic mutation carrier with regards to presymptomatic disease burden, or the follow-up of a specific patient with an established diagnosis to verify if further pathology has been accrued. [154, 172]

The gap between group-level imaging and single-subject imaging is considerable in terms of practical utility, methodological challenges, and academic relevance. [670] While patterns of grey matter atrophy can be assessed in a variety of ways, the interpretation of single subject white matter profiles is particularly challenging. The visual inspection of FLAIR and T2-weighted images offers limited information and the visual review of DTI data only permits the appreciation of movement, susceptibility or eddy-current related artefacts. In current clinical practice, the primary role of MR imaging is the exclusion of neoplastic, paraneoplastic, inflammatory and structural mimics rather than the confirmation of FTD-associated changes. Existing frameworks for single-subject categorisation rely on various machine learning algorithms to classify single-individuals into groups. A variety of supervised and unsupervised methods have been previously implemented across the spectrum of ALS-FTD. Models such as support-vector machines, decision trees, neural networks, discriminant function analyses have been applied to imaging datasets with varying accuracy. [55-57, 59, 62-64, 67, 68, 75, 79, 80, 85, 88, 90, 100, 114, 115, 122, 130, 869] A common application of these approaches is the categorisation of patients into FTD versus AD diagnostic groups. [53, 54, 65, 92-94, 99, 107, 123, 131] A key barrier to the development of successful machine learning algorithms in neurodegenerative conditions is the scarcity of uniformly acquired training data, especially in low-incidence phenotypes such as ALS-FTD, PLS-FTD, post-polio syndrome etc. [260, 472, 751, 774, 870-876] Accordingly, the objective of this study is piloting an alternative quantitative white matter rating framework for single-subject diffusion data interpretation based on tractwise *z*-scoring of diffusivity metrics with reference to demographically-matched controls.

9.2 Methods

9.2.1 Participants

A total of 160 subjects were enrolled in this study. Sixty patients were included from across the clinical spectrum of FTD: 7 patients with behavioural variant FTD (bvFTD, 4 males, mean age = 60.71 yrs +/– 3.30 yrs), 9 patients with non-fluent variant primary progressive aphasia (nfvPPA, 5 males, mean age = 62.22 yrs +/– 3.03 yrs), 3 patients with semantic-variant PPA (svPPA, 2 males, mean age = 61.67 yrs +/– 6.43 yrs), 21 patients with ALS-FTD carrying hexanucleotide repeat expansions in *C9orf72* (ALSFTD-C9+, 13 males, mean age = 58.95 yrs +/– 9.95 yrs), and 20 ALS-FTD patients who tested negative for *C9orf72* (ALSFTD-C9-, 13 males, mean age = 60.65 yrs +/– 8.73 yrs). The imaging profiles of patients were interpreted based on radiological data from 100 healthy controls (HC, 50 males, mean age = 58.95 yrs +/– 9.95 yrs). Patients were diagnosed according to the Rascovsky[73] and El Escorial [877] criteria. The *z*-scoring strategy implemented in this study relies on the rating of single subjects' data with respect to a demographically-matched control population. Accordingly, control selection for normative data generation was defined based on age to ensure age-matching between each male / female patient and the corresponding male / female control group. Two-sample t-tests were performed to verify successful age-matching. Sex-matching was ensured by contrasting each male / female patient only to male / female controls. Given the available number of total controls, only one male and one female control group were defined, each of size $n = 50$. Relevant demographic data are presented in **Table 27.** Methods for ascertaining GGGGCC hexanucleotide repeat expansion in *C9orf72* by repeat-primed PCR have been

described previously, [801, 878] expansions longer than 30 hexanucleotide repeats were considered pathological.

Table 27: Demographic data of study participants

Patient group	Male		Female	
	Mean age (*SD*) [years], sample size (*n*)	***t*-score from two-sample *t*-test (DOF), *p*-value [HC vs. patients]**	**Mean age (*SD*) [years], sample size (*n*)**	***t*-score from two-sample *t*-test (DOF), *p*-value [HC vs. patients]**
ALSFTD-C9+	55.92 (8.11), *n* = 13	*t*(61) = 1.73, *p* = 0.09	58.50 (9.61), *n* = 8	*t*(56) = -0.42, *p* = 0.68
ALSFTD-C9-	62.00 (9.11), *n* = 13	*t*(61) = –0.35, *p* = 0.73	58.14 (7.98), *n* = 7	*t*(55) = –0.31, *p* = 0.76
bvFTD	59.25 (3.50), *n* = 4	*t*(52) = 0.35, *p* = 0.73	62.67 (2.98), *n* = 3	*t*(51) = –0.99, *p* = 0.33
nfvPPA	63.60 (2.97), *n* = 5	*t*(53) = –0.60, *p* = 0.55	60.50 (3.42), *n* = 4	*t*(52) = –0.71, *p* = 0.48
svPPA	58.00 (1.41), *n* = 2	*t*(50) = 0.43, *p* = 0.67	69.00 (0.00), *n* = 1	*t*(49) = –1.21, *p* = 0.23
HC	60.96 (9.68), *n* = 50		56.94 (9.91), *n* = 50	

ALSFTDC9-: ALS-FTD patients without *C9orf72* hexanucleotide expansions, ALSFTDC9+: ALS-FTD patients with *C9orf72* hexanucleotide expansions, bvFTD: behavioural variant FTD, DOF: degrees of freedom, HC: healthy controls, nfvPPA: non-fluent variant primary progressive aphasia, SD: standard deviation, svPPA: semantic variant primary progressive aphasia

9.2.2 Data acquisition

A spin-echo echo planar imaging (SE-EPI) pulse sequence with a 32-direction Stejskal-Tanner diffusion encoding scheme was used to acquire diffusion tensor imaging (DTI) data on a 3 Tesla Philips Achieva Magnetic resonance (MR) platform. The key parameters included: TR/TE = 7639 / 59 ms, b-values = 0, 1100 s/mm2, FOV = 245 x 245 x 150 mm, spatial resolution = 2.5 mm3, 60 axial slices with no interslice gaps, SENSE factor = 2.5, dynamic stabilisation and spectral presaturation with inversion recovery (SPIR) fat suppression. For the visual assessment of co-morbid white matter pathology, FLAIR images were also reviewed of each participant. FLAIR data were acquired in the axial orientation using an Inversion Recovery Turbo Spin Echo (IR-TSE) sequence: FOV = 230 x 183 x 150 mm, spatial resolution = 0.65 x 0.87 x 4 mm, TR/TE = 11000 / 125 ms, TI = 2800 ms, 120° refocusing pulse, with flow compensation and motion smoothing and a saturation slab covering the neck region. T1-weighted (T1w) images were acquired with a 3D Inversion Recovery prepared Spoiled Gradient Recalled echo (IR-SPGR) sequence with a field-of-view (FOV) of 256 x 256 x 160 mm, spatial resolution of 1 mm3, TR/TE = 8.5/3.9 ms, TI =1060 ms, flip angle = 8°, SENSE factor = 1.5.

9.2.3 Diffusion-weighted data processing

Diffusion-weighted (DW) data were pre-processed within *MRtrix3*, including noise removal and removal of Gibb's Ringing Artifacts. The *topup-eddy* algorithm was utilised for corrections for eddy-induced distortions and subject movements as implemented in FSL. Bias-corrections was performed with the ANTs1.9 *N4* method. Diffusion tensors were fitted within *MRtrix3* and maps of fractional anisotropy (FA), and radial diffusivity (RD) were

generated. Anatomical images were pre-processed using FMRIB's FSL6.0's *fsl-anat* algorithm, including brain-extraction and biasfield-corrections.

9.2.4 Tract segmentation

As the main objective of the study was the detection of WM microstructure integrity changes in individual patients, our analyses were restricted to regions of FA reductions and foci of increased RD as these diffusivity shifts indicate pathologic processes. Tract-wise probabilities of presumed pathology in individual subjects were estimated based on reference normative data. First, each patient's and control's DW data were segmented into 50 WM tracts using a neural-network based algorithm, *TractSeg*, which, as opposed to atlas-based approaches, does not assume a common anatomy between subjects and relies on individual WM fibre bundles anatomy. Peaks of the spherical harmonic function were extracted at each voxel to inform *TractSeg*, which were calculated from fitting voxelwise constrained spherical deconvolution (CSD). CSD is an alternative to the tensor model to perform tractography, which has been shown to outperform the tensor model in regions of crossing fibres, among others. Response functions were estimated using the *dhollander* method as implemented in *MRtrix3* from which fibre orientation distributions (fODF) could be calculated. Given that DW shells were acquired (b = 1000 and b = 0), a multi-shell approach could be implemented. Resulting fODFs were normalised according to Raffelt et al.[879]; spherical harmonic peaks were retrieved from the normalised measures, which then served as input values into *TractSeg*.

9.2.5 *z*-score based tract integrity evaluation

The concept behind the *z*-scored-based strategy is the ascertainment of affected fibre bundles in individual patients. WM tracts were rated in individual patients with reference to age-/ sex-matched HCs. Only tracts exhibiting significant FA reductions and increased RD were considered 'affected'. First, subject-specific FA and RD maps were created for the segmented tracts by inputting each subjects' individual FA / RD map into *TractSeg* and averaging the estimated values across each tract. Normative data from HCs were *z*-scored and patient data were normalised with respect to the relevant control group. Single patients' tract profiles were then contrasted to normative data using nonparametric statistics. First, the number of HCs exhibiting lower FA and higher RD than the observed value in the patient was determined for each patient and each tract. This value was then divided by the number of HCs (i.e. 50 both for males and females) to obtain *p*-values. Given that two tests were run (decreased FA / increased RD), tracts with $p < 0.025$ were considered significantly different.

Finally, group-level statistics were also derived from the *z*-score-based strategy to aid cross-validation against the standard approach. We tested which tracts were preferentially affected across the entire patient group. To quantify this probability, probability distributions were first created reflecting the number of false positives across the patient group (i.e. *p*-values of < 0.025 provided a random event). This was modelled as a Binomial process:

1. $X \sim B(n, p)$,

where X is the random variable (a scalar), n is the number of correctly segmented tracts in the control distribution and p is the probability of

assigning significance to a tract's *p*-value (in our case 0.025). This process was repeated 100,000 times to provide a dense probability distribution. *p*-values were then derived for each tract by counting how many values in the null distribution exceeded the sum of significant observations across the patient group and dividing that count by the number of iterations. To match the threshold used in the validation arm of the study, the most affected tracts were identified using a relatively stringent alpha-threshold of $p < 0.01$.

9.2.6 Cross-validation by standard tract-based statistics

To validate the *z*-score-based approach, the group-level outputs were compared to those of an established analysis pipeline, FMRIB FSL's tract-based spatial statistics (TBSS). The voxelwise diffusivity profile of the five FTD group was contrasted to controls. In accordance with FSL's TBSS recommendations, processing included outliner removal, non-linear registration to the FMRIB58FA template and application of that transformation to align all subjects' FA / RD images to the MNI152 1mm standard space. Voxelwise group-comparisons were computed using FSL's *randomise* algorithm, a non-parametric permutation testing scheme, with 2D-optimised threshold-free cluster enhancement (TFCE) to control for the family-wise error rate (FWER). To highlight the most pertinent WM changes, a stringent alpha-threshold of $p_{FWER} < 0.01$ was applied.

9.3 Results

9.3.1 Demographics

Two-sample *t*-tests were run between each male / female patient group vs. the male / female control groups to confirm age-matching. No statistical difference was found between any of the patient and control

groups suggesting appropriate age-matching. Relevant descriptive and inferential statistics are provided in **Table 27.**

9.3.2 *z*-score-based subject-level inferences

The *z*-score-based strategy has successfully captured relevant white matter pathology in individual subjects in each of the 60 FTD patients. A dual-output scheme was utilised, affected white matter tracts can be depicted in 3D and a text file was also generated listing the affected tract with the relevant *z*- and *p*-values. To showcase the potential utility of single-subject white matter profile interpretation we provide representative individual examples from the five patient groups **(Figure 22).** As described in the methods section, the *z*-score-based strategy also permits the description of group-level findings. An overview of affected tracts at a group-level is provided in **Table 28** and **Table 29** for each FTD cohort. More tracts were detected exhibiting increased RD than tracts with FA reductions suggesting that RD may be more sensitive to capture relevant white matter degeneration. Our approach detected left-hemisphere dominant changes in language variant phenotypes (nfvPPA and svPPA) compared to the relatively symmetric pathology in bvFTD and ALS-FTD groups. Relative sparing of posterior white matter bundles was observed across the entire spectrum of subgroups.

Figure 22: White matter alterations in individual FTD subjects

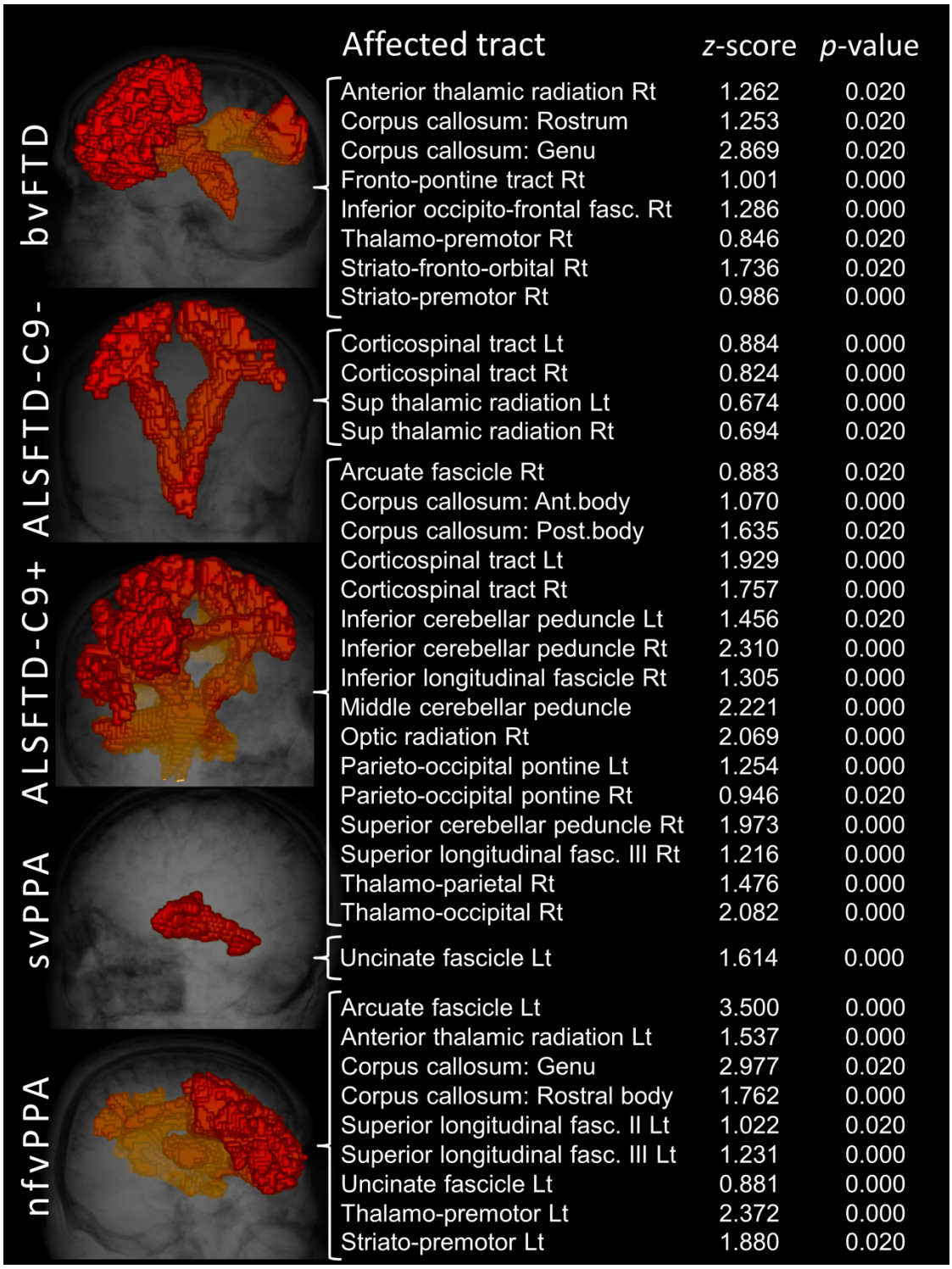

White matter alterations in individual subjects based on single DTI datasets and normative data. Illustrative outputs from single patients with behavioural variant FTD (bvFTD), ALS-FTD patients without *C9orf72* hexanucleotide expansions (ALSFTD-C9-), ALS-FTD patients with *C9orf72* hexanucleotide expansions (ALSFTD-C9+), semantic variant primary progressive aphasia (svPPA) and non-fluent variant primary progressive aphasia (nfvPPA).

Table 28: Affected white matter tracts at group-level in ALS-FTD

ALS-FTD with GGGGCC hexanucleotide repeat expansions in *C9orf72* (*C9orf72*+)					
FA reductions		**Increased RD**		**Increased RD (continued)**	
Tract name	**p_{FWER}**	**Tract name**	**p_{FWER}**	**Tract name**	**p_{FWER}**
Arcuate fascicle right	0.0011	Arcuate fascicle left	0.0001	Optic radiation right	<0.0001
Corpus callosum: Rostrum	0.0096	Arcuate fascicle right	<0.0001	Parieto-occipital pontine left	<0.0001
Corpus callosum: Genu	0.0009	Corpus callosum: Rostrum	<0.0001	Parieto-occipital pontine left	0.0008
Corpus callosum: Anterior midbody	0.0001	Corpus callosum: Genu	0.0010	Superior cerebellar peduncle right	0.0008
Corpus callosum: Posterior midbody	<0.0001	Corpus callosum: Rostral body	0.0029	Sup. longitudinal fascicle I left	<0.0001
Corpus callosum: Isthmus	0.0011	Corpus callosum: Anterior midbody	<0.0001	Sup. longitudinal fascicle I right	0.0001
Corpus callosum: Splenium	<0.0001	Corpus callosum: Posterior midbody	0.0001	Sup. longitudinal fascicle II left	0.0012
Cingulum left	0.0012	Corpus callosum: Isthmus	0.0011	Sup. longitudinal fascicle II right	0.0009
Cingulum right	0.0013	Corpus callosum: Splenium	0.0010	Sup. longitudinal fascicle III left	0.0084
Corticospinal tract left	0.0073	Cingulum left	<0.0001	Sup. longitudinal fascicle III right	0.0001
Corticospinal tract right	<0.0001	Cingulum right	0.0013	Sup. thalamic radiation left	<0.0001
Fronto-pontine tract right	0.0082	Corticospinal tract left	<0.0001	Sup. thalamic radiation right	<0.0001
Optic radiation left	0.0008	Corticospinal tract right	<0.0001	Uncinate fascicle left	<0.0001
Parieto-occipital pontine right	0.0095	Fronto-pontine tract left	0.0085	Uncinate fascicle right	0.0004
Superior longitudinal fascicle I left	0.0001	Fronto-pontine tract right	0.0082	Thalamo-parietal right	0.0001
Superior longitudinal fascicle I right	<0.0001	Inf. cerebellar peduncle left	0.0001	Thalamo-occipital left	<0.0001
Superior longitudinal fascicle II left	0.0010	Inf. cerebellar peduncle right	0.0053	Thalamo-occipital right	<0.0001
Superior longitudinal fascicle II right	0.0007	Inf. occipito-frontal fascicle left	0.0001	Striato-fronto-orbital right	<0.0001
Superior longitudinal fascicle III right	<0.0001	Inf. occipito-frontal fascicle right	<0.0001		
Superior thalamic radiation right	0.0005	Inf. longitudinal fascicle left	<0.0001		
Thalamo-occipital left	0.0009	Inf. longitudinal fascicle right	<0.0001		
Striato-fronto-orbital right	0.0095	Optic radiation left	<0.0001		

ALS-FTD without GGGGCC hexanucleotide repeat expansions in *C9orf72* (*C9orf72*-)					
FA reductions		**Increased RD**		**Increased RD (continued)**	
Tract name	**p_{FWER}**	**Tract name**	**p_{FWER}**	**Tract name**	**p_{FWER}**
Arcuate fascicle left	0.0097	Arcuate fascicle left	0.0001	Parieto-occipital pontine right	0.0055
Corpus callosum: Genu	0.0007	Arcuate fascicle right	0.0009	Sup. cerebellar peduncle left	0.0006
Corpus callosum: Splenium	0.0005	Corpus callosum: Rostrum	<0.0001	Sup. cerebellar peduncle right	0.0059
Cingulum left	0.0009	Corpus callosum: Genu	<0.0001	Sup. longitudinal fascicle I left	<0.0001
Corticospinal tract right	0.0002	Corpus callosum: Rostral body	0.0013	Sup. longitudinal fascicle I right	0.0007
Inferior occipito-frontal fascicle right	0.0068	Corpus callosum: Isthmus	<0.0001	Sup. longitudinal fascicle II left	<0.0001
Middle cerebellar peduncle	0.0068	Corpus callosum: Splenium	0.0080	Sup. longitudinal fascicle III left	0.0060
Superior longitudinal fascicle III right	0.0072	Cingulum left	0.0001	Sup. longitudinal fascicle III right	0.0067
		Cingulum right	0.0070	Sup. thalamic radiation left	<0.0001
		Corticospinal tract left	<0.0001	Sup. thalamic radiation right	0.0047
		Corticospinal tract right	0.0002	Uncinate fascicle left	<0.0001
		Fronto-pontine tract right	0.0003	Uncinate fascicle right	<0.0001
		Inf. cerebellar peduncle left	0.0071	Thalamo-parietal left	0.0064
		Inf. cerebellar peduncle right	0.0075	Thalamo-occipital right	0.0004
		Inf. occipito-frontal fasc. right	0.0005	Striato-fronto-orbital left	0.0069
		Middle cerebellar peduncle	0.0067	Striato-premotor left	0.0060
		Optic radiation right	0.0004		

Table 29: Affected white matter tracts at group-level in bvFTD, nfvPPA, svPPA

Decreased FA		**Increased RD**	
Tract name	**p_{FWER}**	**Tract name**	**p_{FWER}**
bvFTD			
Corpus callosum: Genu	<0.0001	Arcuate fascicle left	0.0004
		Corpus callosum: Rostrum	<0.0001
		Corpus callosum: Genu	<0.0001
		Corticospinal tract right	0.0005
		Fronto-pontine tract right	0.0003
		Inferior occipito-frontal fascicle right	0.0006
		Superior thalamic radiation left	0.0002
		Superior thalamic radiation right	0.0006
		Uncinate fascicle right	0.0006
		Thalamo-premotor right	0.0006
		Striato-fronto-orbital left	0.0005
		Striato-fronto-orbital right	0.0005
		Striato-premotor right	0.0005
nfvPPA			
Corpus callosum: Genu	<0.0001	Arcuate fascicle left	<0.0001
Cingulum left	0.0014	Arcuate fascicle right	0.0014
Superior longitudinal fascicle I left	0.0008	Anterior thalamic radiation left	0.0005
Superior longitudinal fascicle II left	0.0006	Anterior thalamic radiation right	<0.0001
Thalamo-premotor left	0.0059	Corpus callosum: Rostrum	0.0001
		Corpus callosum: Genu	<0.0001
		Corpus callosum: Rostral body	0.0018
		Corpus callosum: Post. midbody	0.0007
		Cingulum left	<0.0001
		Cingulum right	0.0011
		Fronto-pontine tract left	0.0004
		Fronto-pontine tract right	0.0005
		Inf. occipito-frontal fascicle left	<0.0001
		Inf. occipito-frontal fascicle right	<0.0001
		Inf. longitudinal fascicle right	0.0011
		Optic radiation left	<0.0001
		Optic radiation right	0.0001
		Sup. longitudinal fascicle I left	<0.0001
		Sup. longitudinal fascicle I right	0.0001
		Sup. longitudinal fascicle II left	<0.0001
		Sup. longitudinal fascicle II right	0.0008
		Sup. longitudinal fascicle III left	<0.0001
		Sup. longitudinal fascicle III right	0.0012
		Uncinate fascicle left	0.0007
		Thalamo-premotor left	0.0002
		Thalamo-parietal left	0.0013
		Thalamo-parietal right	0.0001
		Thalamo-occipital left	0.0008
		Thalamo-occipital right	0.0001
		Striato-fronto-orbital left	<0.0001
		Striato-fronto-orbital right	<0.0001

Decreased FA		Increased RD	
Tract name	**p_{FWER}**	**Tract name**	**p_{FWER}**
svPPA			
Inferior occipito-frontal fascicle left	0.0018	Arcuate fascicle left	0.0023
Superior longitudinal fascicle III left	0.0017	Arcuate fascicle right	0.0018
		Corpus callosum: Rostrum	0.0019
		Corpus callosum: Genu	0.0018
		Corpus callosum: Isthmus	0.0020
		Cingulum left	0.0016
		Inf. occipito-frontal fascicle left	0.0021
		Inf. occipito-frontal fascicle right	0.0016
		Inf. longitudinal fascicle left	0.0007
		Inf. longitudinal fascicle right	0.0005
		Optic radiation left	0.0015
		Optic radiation right	0.0018
		Sup. longitudinal fascicle I left	0.0017
		Sup. longitudinal fascicle I right	0.0020
		Sup. longitudinal fascicle II left	0.0015
		Sup. longitudinal fascicle II right	0.0019
		Sup. longitudinal fascicle III left	0.0019
		Sup. thalamic radiation right	0.0019
		Uncinate fascicle left	<0.0001
		Thalamo-parietal left	0.0017
		Thalamo-parietal right	0.0018
		Thalamo-occipital left	0.0018
		Thalamo-occipital right	0.0019
		Striato-fronto-orbital left	0.0019
		Striato-fronto-orbital right	0.0019

9.3.3 Validation

For validation purposes, standard TBSS analyses were performed to contrast each of the five FTD groups to healthy controls. Widespread, multi-lobar FA reductions were detected in both ALS-FTD groups irrespective of *C9orf72* status **(Figure 23).** Anterior frontal and left hemisphere predominant FA reductions were identified in the nfvPPA group. At $p < 0.01$ no significant FA reductions were identified in the svPPA and bvFTD groups. At the same statistical threshold, areas of increased RD were detected in each FTD group: orbitofrontal and forceps minor predominant changes in bvFTD, left superior temporal and insular white matter alterations in svPPA, and extensive multi-lobar white matter degeneration in nfvPPA, ALS-FTD-C9+ and ALS-FTD-C9- **(Figure 24).** While RD was more sensitive in detecting white matter pathology in bvFTD and svPPA, FA was more sensitive in detecting cerebellar changes in the two ALS-FTD groups compared to RD. Occipital involvement was relatively limited in the nfvPPA group.

Figure 23: Fractional anisotropy reductions in FTD at group-level

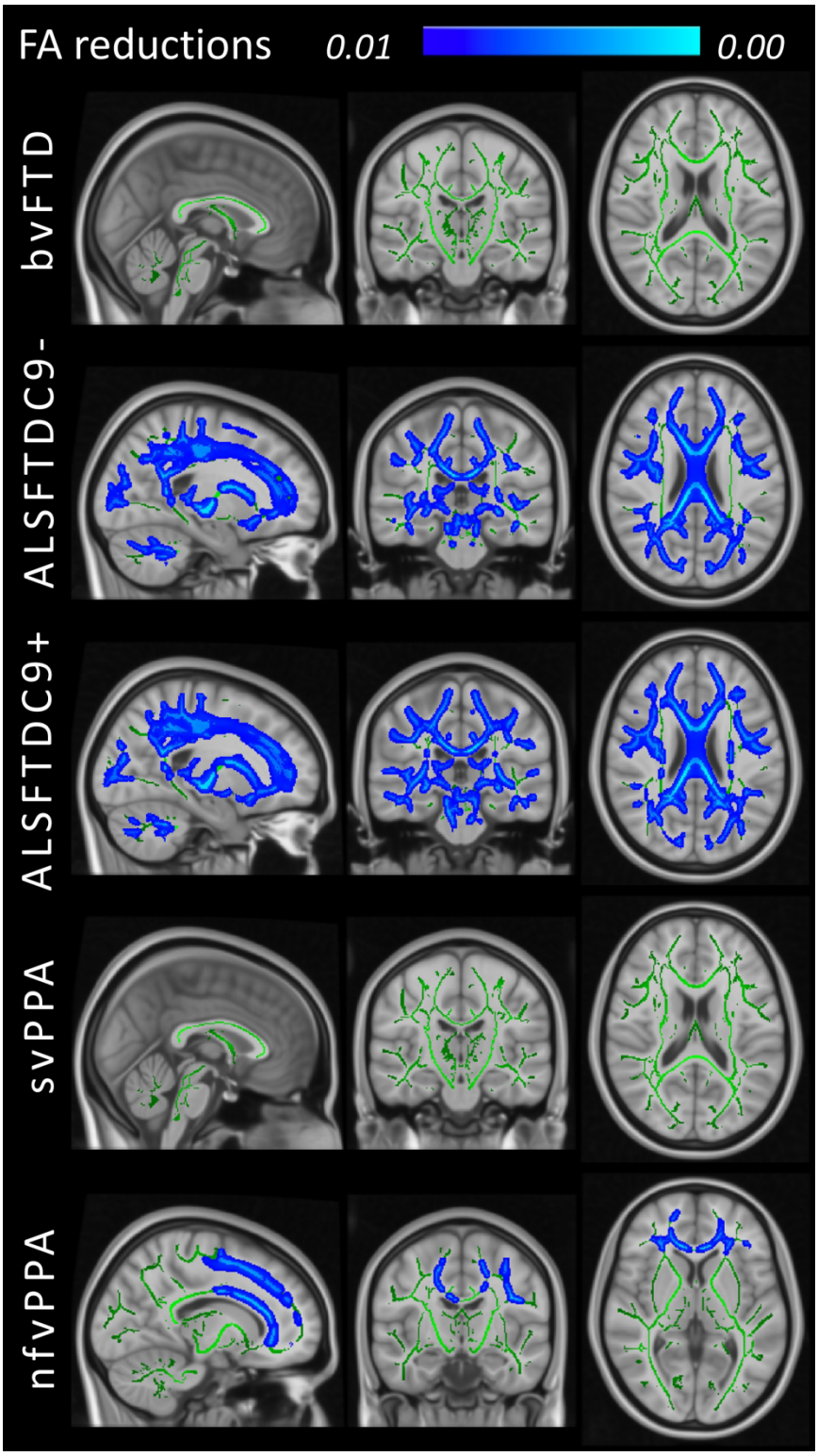

Fractional anisotropy (FA) reductions at group-level in patients with behavioural variant FTD (bvFTD), ALS-FTD patients without *C9orf72* hexanucleotide expansions (ALSFTDC9-), ALS-FTD patients with *C9orf72* hexanucleotide expansions (ALSFTDC9+), semantic variant primary progressive aphasia (svPPA) and non-fluent variant primary progressive aphasia (nfvPPA) compared to healthy controls at $p < 0.01$ controlling for age, sex and family-wise error.

Figure 24: Increased radial diffusivity in FTD at group-level

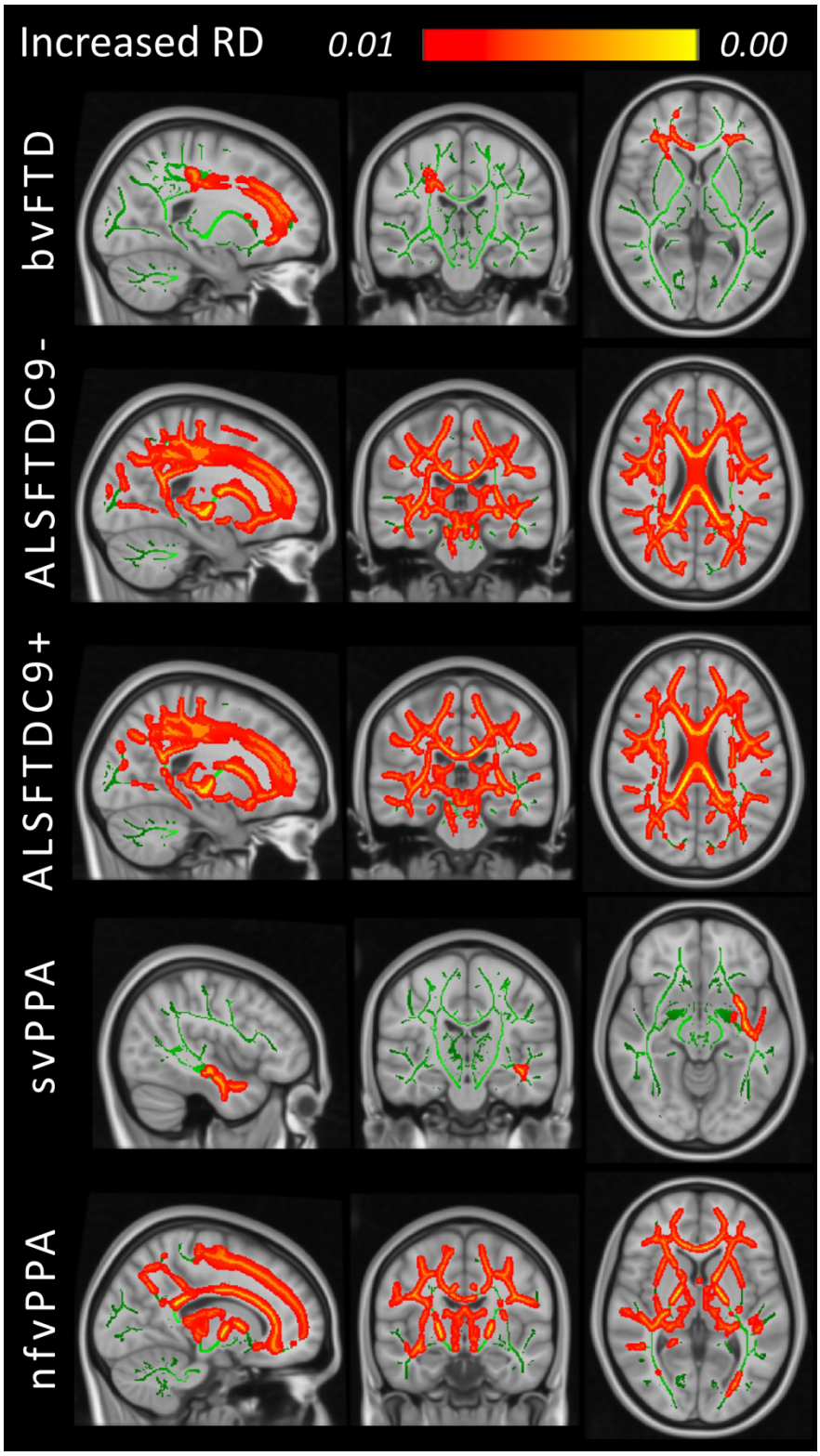

Increased radial diffusivity (RD) at group-level in patients with behavioural variant FTD (bvFTD), ALS-FTD patients without *C9orf72* hexanucleotide expansions (ALSFTDC9-), ALS-FTD patients with *C9orf72* hexanucleotide expansions (ALSFTDC9+), semantic variant primary progressive aphasia (svPPA) and non-fluent variant primary progressive aphasia (nfvPPA) compared to healthy controls at $p < 0.01$ controlling for age, sex and family-wise error.

9.4 Discussion

We have successfully captured phenotype-specific white matter alterations in individual FTD patients using a *z*-scored based strategy. The group-level findings inferred from the trialled white matter rating scheme were consistent with the outputs of established pipelines. Our results indicate that it is feasible to interpret single DTI datasets if large reference datasets are available with uniform scanning parameters.

In a clinical setting, grey matter atrophy can often be qualitatively appreciated in patients with FTD. [637] In contrast, white matter changes cannot be meaningfully commented upon beyond the exclusion of demyelination, inflammatory or vascular changes. WM changes are typically reviewed visually on T2w, FLAIR and DWI to make sure the suspected diagnosis is not confounded by coexisting vascular, inflammatory or neoplastic, or paraneoplastic pathology. In established cases of FTD, FLAIR and T2w images often look relatively normal and white matter 'atrophy' cannot be ascertained on visual inspection. While most FTD phenotypes are associated with the selective degeneration of specific white matter tracts, these patterns are not visible on standard clinical sequences. It is also noteworthy that clinical pulse-sequences are typically optimised for speed of acquisition, often include slice gaps and operate with large voxel sizes, especially for FLAIR and T2w.

In a research setting, imaging traits are typically derived from contrasting a group of patients with a specific clinical profile or a specific mutation to a group of demographically-matched controls. In bvFTD, progressive WM changes have been described in the uncinate fasciculus, cingulum and corpus callosum; and to a lesser extent in the anterior thalamic

radiation, fornix and superior and inferior longitudinal fasciculus in both hemispheres [13, 14, 16, 36, 867]. Studies in nfvPPA captured preferential left-sided changes in the anterior thalamic radiation, uncinate and superior longitudinal fasciculus [13, 14, 868], which become more prominent in the right hemisphere over time [867]. In svPPA, left-hemispheric uncinate, arcuate and inferior longitudinal fasciculus [13, 14, 16, 868] degeneration has been consistently detected which remain relatively focal on longitudinal follow-up with some interval involvement of right frontotemporal regions [13, 867]. In *MAPT* mutation carriers, early parahippocampal, cingulate and uncus involvement can be detected [21, 140, 150] accompanied by corpus callosum, inferior and superior longitudinal fasciculus and fornix degeneration [36, 140, 150]. In association with *GRN*, early corpus callosum and internal capsule changes have been described, followed by left-hemisphere predominant cingulum, inferior fronto-occipital, superior- and inferior longitudinal fasciculus degeneration [21, 140, 150]. *C9orf72* repeats have been linked to corticospinal tract, corpus callosum, thalamic radiation, cingulum, uncinate, superior and inferior longitudinal fasciculus degeneration [36, 150]. The imaging signatures of rare genotypes – such as *TARDBP* and *VCP* - are poorly characterised as these have been predominantly evaluated in smaller case series [532].

The group comparisons of academic imaging have relatively little to offer, when the priority is the appraisal of cerebral pathology in individual patients; either in those with a suspected diagnosis, or, on follow-up of patients with an established diagnosis. While machine learning (ML) applications show promise in accurate patient categorisation, they work best when ample training data are available which pertains to more common

neurodegenerative conditions. [157, 865] An advantage of the presented method is that, contrary to ML applications, it does not impose a possible diagnostic label (category), but merely lists the tracts which are 'affected' compared to normative controls. This leaves the interpretation of the output text file to the clinicians to be judiciously integrated with clinical findings and the broader clinical context, family history, comorbid conditions, genetic susceptibility etc. As shown in **Figure 22**, the algorithm offers a list of affected tracts based on a single DWI scan which can be depicted visually if need, but the main output is the text file with the relevant *z*-scores and *p*-values.

Another advantage of the approach is the detection of white matter abnormalities in each hemisphere separately. The laterality of findings can then be interpreted in single subjects based on handedness which is particularly important in language variant FTDs. Our findings indicate left hemispheric dominant WM pathology in svPPA and nfvPPA both at individual and group-level. This is in striking contrast to the relatively symmetric WM degeneration observed in ALS-FTD. Academic studies using group comparisons typically pool data across right- and left-handed subjects which makes the interpretation of the laterality of findings more challenging. The quantitative evaluation of single subjects has other advantages. Pooled group-level data not only introduce undue heterogeneity in terms of handedness but also with regards to symptom duration and disease severity which undermines the value of group-level inferences and rendering them less pertinent to single participants. This study has exclusively focused on whiter matter alterations. The assessment of cortical grey matter changes has been previously tested in a similar framework. [673, 880] It is conceivable that

additional imaging measures, such as basal ganglia volumes normalised for total intracranial volume (TIV), alternative white matter metrics, metabolite ratios, and network coherence indices could be interpreted in a similar framework with reference to normative data [231, 488, 489, 491, 493, 881] as well as cord parameters in ALS-FTD cohorts. [60, 249, 250, 665, 882] Finally, it is plausible that statistical outputs from imaging modalities can be integrated into larger biomarker panels, which would include quantitative serum, cerebrospinal fluid, EEG, MEG, proteomic and neuropsychological indices. [158, 231, 441, 491, 493, 496, 500, 503] While the group-level outputs of the *z*-scored based strategy and TBSS are anatomically concordant, their sensitivity in detecting WM changes are different. It is noteworthy that FA on TBSS does not capture WM degeneration in svPPA and bvFTD even at $p < 0.01$ using the appropriate covariates. Using the tract-wise approach, FA reductions are readily detected in the anterior corpus callosum in bvFTD and in the left inferior occipito-frontal and left superior longitudinal fascicles in svPPA **(Table 29).** At an individual level, the *z*-score-based approach readily detects the degeneration of relevant WM tracts in these two groups, which may be 'averaged out' by less severe cases in the group comparisons **(Figure 22).** TBSS generates voxelwise statistical maps projected on a white matter skeleton which can be thresholded at a specific *p*-value, but it is typically reviewed visually i.e. anything below that threshold is highlighted as 'affected' with a colour spectrum map. In contrast, the text outputs from the *z*-score-approach offer a list of 'affected tracts' which can be ranked in order of 'severity' based on associated *p*-values.

Both the tractwise analyses and TBSS suggest that RD is more sensitive to detect white matter alterations in FTD. Based on RD profiles, affected tracts in bvFTD include corpus callosum, corticospinal tract and a number of subcoritco-cortical projections such as the superior thalamic radiation, thalamo-premotor, and striato-premotor fibres. The involvement of the corticospinal tract in bvFTD is of interest as another shared feature between ALS and FTD. The involvement of bundles linking subcortical and cortical regions supports previous findings, [247] and highlight the contribution of subcortical pathology to clinical manifestations. [669] White matter degeneration in svPPA not only includes the corpus callosum, cingulum and arcuate degeneration, but the left-hemisphere predominant involvement of long association fibres and projections from the thalamus and striatum **(Table 29).** The nfvPPA cohort exhibits widespread degeneration of both commissural and long association fibres with slight left hemispheric predominance in addition to thalamic and striatal projections. The *C9orf72* negative ALS-FTD cohort not only exhibits widespread white matter pathology in core ALS-associated regions such as the corticospinal tracts and corpus callosum, but in line with more recent studies, in the cerebellar peduncles, long association fibres, arcuate fasciculus, uncinate and cingulum [34, 883, 884] **(Table 28).** White matter degeneration in ALS-FTD patients carrying the GGGGCC hexanucleotide expansion is comparable to the anatomical patterns observed in *C9orf72* negative patients, but is more readily detected by FA reductions (**Table 28**). These observations highlight that contrary to previous suggestions, severe frontotemporal degeneration and subcortical involvement in ALS are not unique to the *C9orf72* genotype.

In the absence of accompanying post mortem and CSF data, the participants of this study were merely categorised clinically. FTD phenotypes arise from different underlying proteinopathies; [839, 885, 886] ALS-FTD is primarily linked to pTDP-43, [887] svPPA is nearly always associated with underlying TDP-43-C pathological aggregates, [888] nfvPPA is commonly associated with 4R tau, [889] and molecular findings in bvFTD are thought to be heterogeneous. [162] There are a number of study limitations we need to acknowledge, chief of which is the limited normative data at our disposal. Larger reference datasets stratified for narrow age brackets would permit more precise data interpretation. In this pilot study, we have only evaluated two diffusivity indices, but other diffusivity metrics, such as AD [142] or non-Gaussian diffusivity measures [524], could also be incorporated in *z*-score models. Finally, this is merely a cross-sectional study to test a quantitative, single-subject data interpretation framework. The natural expansion of this study would be tracking single subjects longitudinally to test whether our approach captures expanding white matter pathology in single subjects over time. Notwithstanding these limitations, our findings indicate that our strategy offers valuable clinical insights in single subjects and may be potentially developed into a viable clinical and pharmaceutical trial applications.

9.5 Conclusions

Frontotemporal dementia is associated with subtype-specific white matter signatures and regional white matter degeneration is a key contributor to phenotype-defining clinical manifestations. The early diagnosis of FTD soon after symptom onset is challenging, and the current clinical role of imaging is limited to the exclusion of alternative structural, inflammatory or neoplastic

pathologies. As demonstrated, carefully designed computational pipelines enable the interpretation of individual diffusion datasets and the ascertainment of anatomical patterns of white matter degeneration in vivo. The development, optimisation and validation of similar imaging frameworks that categorise individual patients based on raw MR data should be a key research priority. These initiatives signal a departure from describing group-level signature, and herald a paradigm shift to precision, individualised, computational radiology.

10 A case series of semantic behavioural variant frontotemporal dementia

10.1 Introduction

Frontotemporal dementia (FTD) encompasses a wide spectrum of neurodegenerative disorders that may be further stratified according to clinical phenotype, genotype or pathology. Semantic variant primary progressive aphasia (svPPA) is an FTD phenotype that clinically manifests as anomia and impaired single-word comprehension[890]; radiologically defined by dominant anterior temporal lobe atrophy[890]; and pathologically characterised by frontotemporal lobar degeneration transactive response DNA binding protein 43 (FTLD-TDP-43) pathology type C in the majority of cases[724]. In recent times, it has become apparent that non-dominant anterior temporal lobe atrophy presents with a distinct clinical phenotype that initially does not meet the classification criteria for svPPA[890, 891]. A vast range of alternative nomenclature has been used to describe this entity: 'right temporal variant FTD', 'right temporal semantic dementia', 'right temporal svPPA' and 'right temporal behavioural variant FTD (bvFTD)'. Clinical algorithms have been proposed to differentiate this presentation from other FTD phenotypes and other neurodegenerative disorders [892]. A recent study outlined the longitudinal clinical characteristics of this cohort, proposing a dedicated classification criteria with streamlined nomenclature highlighting the main symptomatology: 'semantic behavioural variant FTD' (sbvFTD)[893].

The proposed classification criteria for sbvFTD requires at least 2 core criteria: loss of empathy; difficulty identifying and naming people; rigid

thought processes or complex compulsions; and at least 2 supportive criteria: object naming difficulties; spared visuospatial functions; and spared motor speech and phonology[893]. It may be difficult to diagnose in early disease, often being mistaken for psychiatric illnesses[893]. The behavioural and language manifestations later progress and overlap with other FTD phenotypes, particularly svPPA and bvFTD[894-897]. It is radiologically defined by non-dominant anterior temporal lobe atrophy with progressive bilateral orbitofrontal cortex, anterior cingulate and contralateral anterior temporal lobe atrophy[894]. FTLD TDP-43 type C is the most commonly reported pathology[891, 893, 895]. The clinical symptoms, neuropsychological and radiological findings of sbvFTD are highlighted in the following case series. We have also included exploratory quantitative analyses of MRI brain scans of 4 different patients with sbvFTD to illustrate the radiological findings.

10.2 Methods

10.2.1 Grey and white matter analyses

In an exploratory analysis, anatomical patterns of grey and white matter degeneration were investigated in 4 patients with right-sided semantic behavioural variant frontotemporal dementia (sbvFTD) compared to fifty age-, sex-, education-matched healthy controls. The standard voxel-based morphometry (VBM) and tract-based spatial statistics (TBSS) pipelines of the FMRIB's software library were used as described previously. Resulting statistical maps were thresholded at $p < 0.05$, TFCE corrected and adjusted for age, sex, education and total intracranial volumes.

10.3 Results

10.3.1 Case series

The patients' ages and occupations are omitted from the case series to avoid identification. The mean age of first symptoms was 62 (57-70) years.

10.3.1.1 Case 1

A right-handed man presented with a 2-year history of indifference, lack of interest and lack of motivation. This was initially mistaken for a depressive episode. He had a history of a coronary-artery bypass graft in 2016. Over the next 2-years, he developed an increasingly rigid routine: repetitively watching the same movie; going for long drives listening to the same music; and taking the train to the same destination to get an ice-cream every day. He lost interest in playing golf, reading and gardening. He spent most of his time lying in bed. He stopped socialising, partly because he had difficulty recognising people. He found it difficult to use his mobile phone and laptop. His impaired judgement led to him being a victim of online fraud. He developed a preference for sweet foods. He made inappropriate comments, mostly referring to a passive death wish. He also had perseverative thoughts ruminating on previous work issues.

On examination, there was subtle behavioural impairment: mildly inappropriate affect; insensitivity to social cues; cognitive rigidity; and lacked empathy when his wife was tearful. He also had difficulty identifying and explaining his feelings. He had insight, and found these changes upsetting: 'I'm not the person that I was'. Neuropsychological testing revealed impaired processing speed, attention, language and subtle executive dysfunction relative to his expected level of pre-morbid functioning. MRI brain scans

showed progressive bilateral frontotemporal atrophy with marked right temporal lobe atrophy **(Figure 25A).** [^{18}F] FDG PET-CT brain revealed right temporal lobe hypometabolism **(Figure 25E).** CSF biomarkers were not compatible with Alzheimer's disease.

Figure 25: Case series MRI brain and [^{18}F] FDG PET-CT brain scans

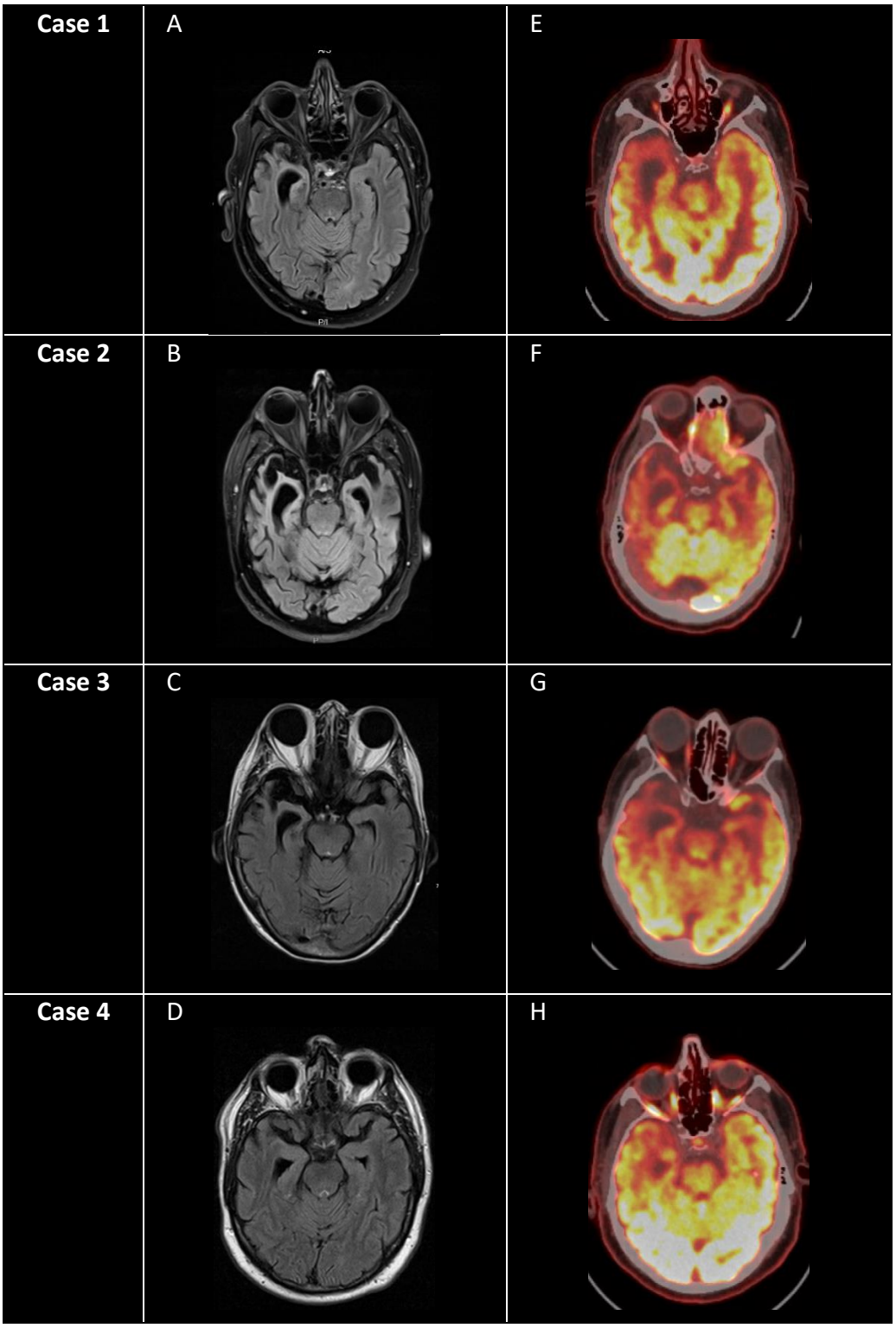

10.3.1.2 Case 2

A right handed man presented with a 10-year history of initial difficulty recognising people, naming objects and behavioural impairment. He had a background of anxiety and suspected autism spectrum disorder. His wife first noticed that he could not recognise a famous politician in the newspaper. He later developed difficulty naming high- and low-frequency objects, with variable levels of understanding. He always had a regimented routine, but had developed increasingly rigid, precise and obsessive behaviours e.g. only charging his mobile phone to exactly 100%. His self-soothing movements in anxious settings were increasingly disinhibited e.g. tapping his head or flapping his hands in busy crowds. He had difficulty planning, organising and completing his collaborative academic projects. His preferred music choice had evolved from classical to traditional Irish folk music.

On examination, he had fluent speech with limited content, frequent circumlocution and perseveration. He had difficulty identifying and explaining his feelings. He had initial insight into these changes. Neuropsychological testing revealed marked anomia with variable comprehension (e.g. he was unable to name an 'elastic band' but knew that it was used 'to put things together'); marked prosopagnosia (e.g. he was unable to name King Charles); surface dyslexia (e.g. he could not correctly pronounce 'dough' or 'pint'); and impaired verbal fluency. He also had impaired abstract thought and proverb interpretation, but his wife said that this was a lifelong trait. MRI brain scans showed progressive bilateral temporal atrophy, greater on the right-side **(Figure 25B).** [^{18}F] FDG PET-CT brain scan showed bilateral frontotemporal hypometabolism, most marked in the right temporal region **(Figure 25F).**

10.3.1.3 Case 3

A right-handed woman presented with an 8-year history of forgetfulness, difficulty recognising people and naming objects. She had a background of hypertension, type 2 diabetes, hypercholesterolaemia, age-related macular degeneration and hypothyroidism secondary to radioactive iodine therapy for hyperthyroidism. She first noticed that she needed increased effort to prepare her lectures. She felt that it was because of a lack of attention and concentration from a highly-functioning baseline. She later noticed difficulty recognising familiar faces, mostly identifying people by their voices. Over the next few years, she described progressive forgetfulness e.g. not retaining detailed current affairs information and sometimes forgetting to take her medications. Collateral history from her husband reported difficulty naming objects, mild irritability and subtle increasingly rigid and obsessive behaviours; however, he acknowledges that she has always been quite rigid. She continued to enjoy assisting her former students in preparing manuscripts for publication.

On examination, she had fluent speech with occasional tangential anecdotes. Neuropsychological testing revealed executive dysfunction, impaired verbal fluency, and marked prosopagnosia and anomia (e.g. when shown an image of a 'volcano', she named it a 'sand-dune'). She had insight and described it 'like an Olympic athlete losing their talent'. MRI brain scan show bilateral temporal atrophy, greater on the right-side **(Figure 25C).** [^{18}F] FDG PET-CT brain scan showed hypometabolism of the bilateral frontal lobes and right temporal lobe (**Figure 25G).** CSF biomarkers were not compatible with Alzheimer's disease.

10.3.1.4 Case 4

A left-handed man presented with a 7-year history of lack of motivation, forgetfulness, and negative behavioural changes. He had a background of epilepsy, depression and a few concussions without loss of consciousness during his 20-year boxing career. He lacked motivation at work and in his personal life. He lost interest in keeping fit and meeting up with his friends. He was increasingly forgetful e.g. unable to recall previous projects, content of conversations and misplacing items. He had difficulty remembering peoples' names and sometimes recognizing peoples' faces. He had low mood, poor attention and less spontaneous verbal output. His wife noticed new emotional indifference, inflexibility and irritation. He needed prompting for personal hygiene e.g. showering. His work partner noticed that he was newly disorganised and had some subtle impaired comprehension e.g. not sure what to do with his set of tools.

Neuropsychological testing revealed attentional deficits, anomia with preserved semantic knowledge e.g. he was unable to name a 'tricycle' but knew what is was used for. He had prosopagnosia for less familiar faces but had retained person-specific knowledge e.g. he was unable to name 'Mary MacAleese', but he knew that she was previously the President of Ireland. He had insight into his deficits, and found it upsetting. MRI brain scans showed a small septum pellucidum and progressive bitemporal atrophy, greater on the right-side **(Figure 25D).** [^{18}F] FDG PET-CT brain scan showed bitemporal hypometabolism, greater on the right side **(Figure 25H).** CSF biomarkers were not compatible with Alzheimer's disease.

10.3.2 Grey- and white-matter analyses

Our voxelwise analyses confirmed right-hemisphere predominant temporal grey matter atrophy and white matter degeneration as evidenced by focal morphometric changes and decreased fractional anisotropy **(Figure 26**, **Figure 27).** While the radiological findings were mostly in the right hemisphere, left hemispheric findings were also revealed.

Figure 26: Grey-matter analyses in sbvFTD

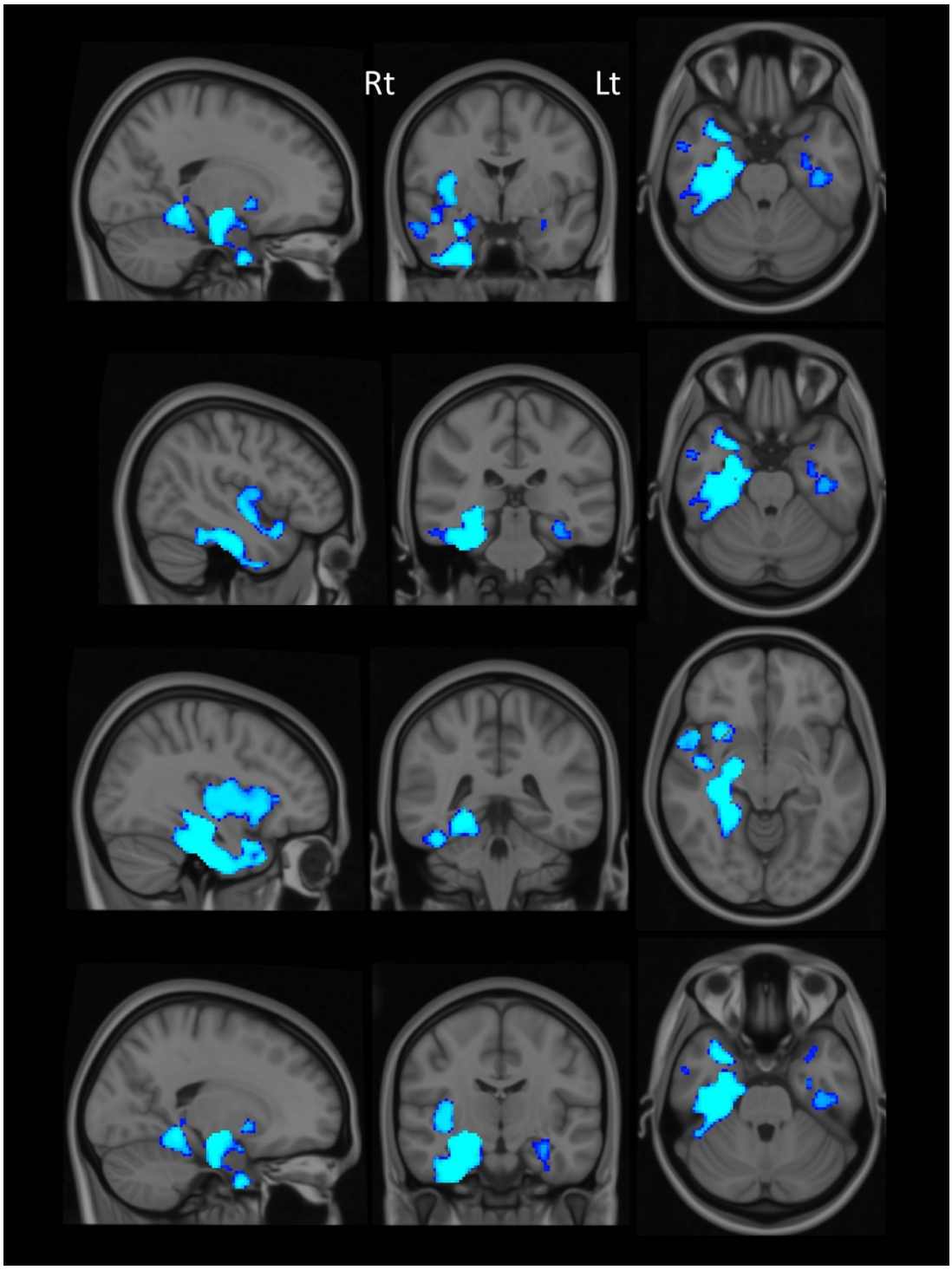

Patterns of grey matter volume reductions in right-sided semantic behavioural variant frontotemporal dementia (sbvFTD) patients compared to age-matched healthy controls as evidence by voxel-based morphometry, statistical map shown in radiological convention thresholded at $p < 0.05$ TFCE corrected and adjusted for age, sex, education and total intracranial volumes.

Figure 27: White-matter analyses in sbvFTD

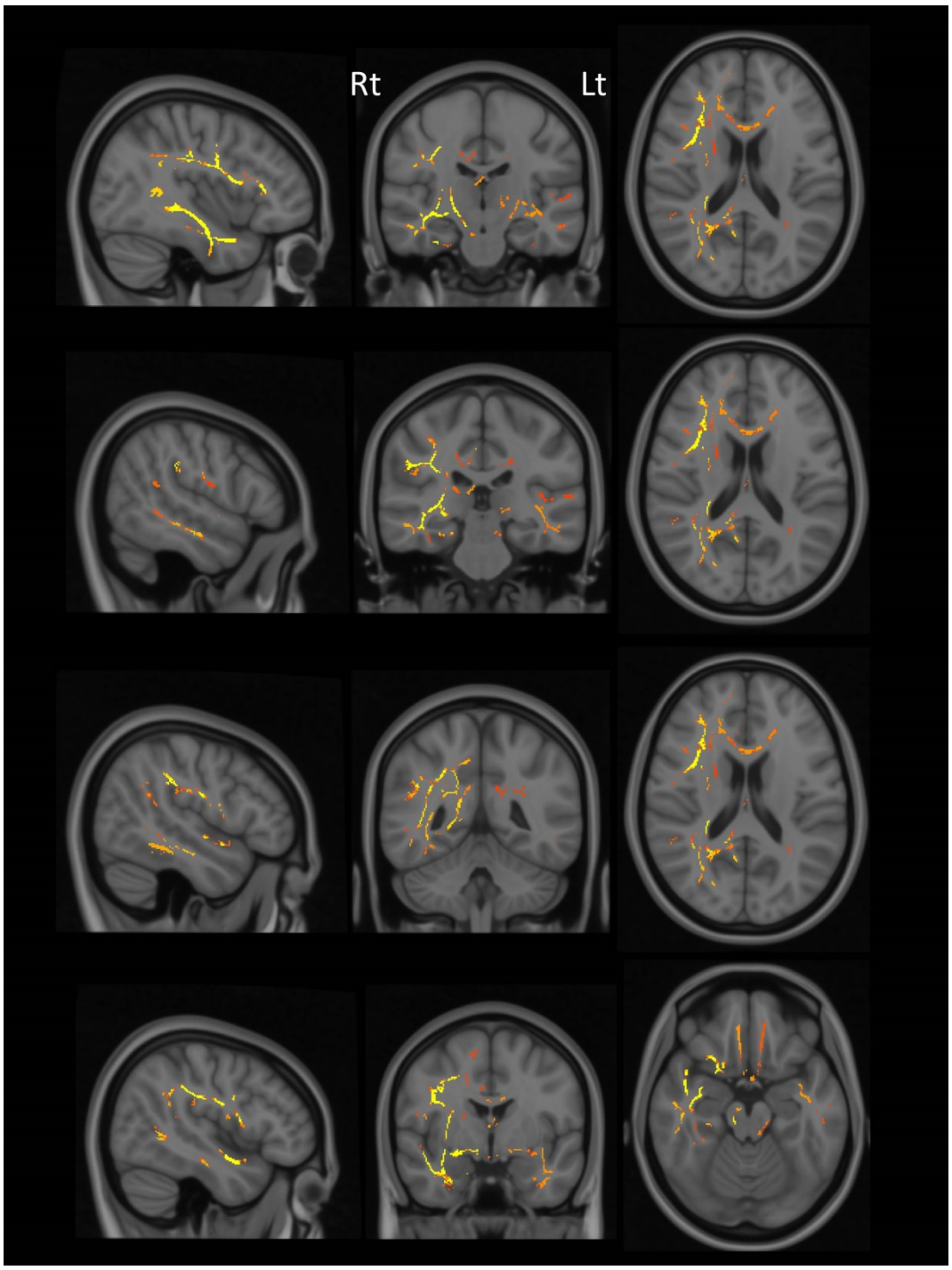

Tract-based patterns of fractional anisotropy reductions in right-sided semantic behavioural variant frontotemporal dementia (sbvFTD) patients compared to age-matched controls as evidence by tract-based spatial statistics, statistical map shown in radiological convention thresholded at $p < 0.05$ TFCE corrected and adjusted for age, sex, education and total intracranial volumes.

10.4 Discussion

This case series highlights the clinical presentation and radiological features of sbvFTD **(Table 30).** There were 3 men and 1 woman; 3 of whom were right-handed and 1 was left-handed. The majority had completed 3rd level education. The mean age of first symptom onset was 62 years (range 57-70). The mean duration of symptoms at the time of clinical assessment was 7 years (range 2-10 years). All cases had initial insight into their deficits. All cases presented with rigid thought processes, executive dysfunction and varying degrees of prosopagnosia; the majority had verbal semantic loss, obsessive repetitive behaviours, and episodic memory impairment; and some also had loss of empathy, apathy, disinhibition, alexithymia and dietary changes. The main cognitive domains affected were executive, language, fluency and memory. Most cases had anomia with varying levels of impaired comprehension. Surface dyslexia was also observed. All cases had bilateral anterior temporal lobe atrophy and hypometabolism, that was more pronounced in the right anterior temporal lobe. This radiological pattern was illustrated in exploratory quantitative analyses in 4 different patients with sbvFTD that captured right temporal predominant grey matter atrophy and white matter degeneration **(Figure 26**, **Figure 27)**. Some cases also had structural and metabolic involvement of the frontal regions.

These case studies were consistent with the existing sbvFTD literature. The average age of symptom onset is early 60's [893]. It typically affects a highly-educated cohort [893]. It presents with early behavioural symptoms: loss of empathy, rigid thought processes and loss of person-specific knowledge[893, 897]. It is suggested that 'loss of person-specific semantic knowledge' better

captures the multi-modal loss of person-specific concepts – faces, voices, names or biographical information - rather than 'prosopagnosia' which only refers to difficulty recognising faces[891, 893]. This tends to precede loss of verbal semantic knowledge which corresponds with the anatomical progression of the disease to the contralateral anterior temporal lobe. In addition to 'loss of person-specific semantic knowledge'[892], there are some early clinical features that help to distinguish sbvFTD from other FTD phenotypes, despite subsequent considerable clinical overlap[892-894]. In contrast with svPPA[71], sbvFTD presents with early behavioural rather than language impairment[895]. Compulsive behaviours tend to be driven by verbal (words and symbols e.g. Case 2 was fixated on charging his phone to 100%) rather than visual targets[895] (e.g. cleaning dishes). These behaviours include ritualistic preoccupations[892] e.g. Case 1 gets an ice-cream in the same place every day. In contrast with bvFTD[73, 84], insight is initially preserved[897] , episodic memory is often impaired[892, 897], language dysfunction is more marked[898], dietary changes are less frequent[892], and disinhibition tends to be more subtle in sbvFTD[893] e.g. insensitivity to social cues telling long tangential stories - as seen in Case 1 and Case 3. The lateralisation of language may also influence the clinical phenotype. Most people are left hemispheric dominant irrespective of their handedness[899]. Indeed, in the largest case series of sbvFTD, 15% of cases were left-handed or ambidextrous [893].

From a radiological perspective, there is striking anterior non-dominant temporal lobe atrophy and hypometabolism. There is progressive medial-to-lateral gradient anterior temporal lobe [892, 897, 900] atrophy associated with ipsilateral insula[892], hippocampal [897, 900], amygdala [897 895, 900 901] and

fusiform gyrus [892, 900] atrophy. Non-dominant temporal lobe atrophy correlates with loss of socioemotional non-verbal semantic knowledge[893] e.g. recognizing emotion[898, 901-905], peoples' faces[892, 894] and social cues[905, 906]; and hypometabolism correlates with psychiatric symptoms of low mood and anxiety[907]. The disease later progresses to involve the contralateral anterior temporal lobe[892, 893, 895, 897, 900], hippocampus [897, 900], amygdala [897, 900], fusiform gyrus [900], bilateral anterior cingulate[894] and orbitofrontal regions[891, 892, 894, 895, 901 892]. The degree of atrophy inversely correlates with disease duration [895].

Similar to svPPA, FTLD-TDP43 type C is the most commonly reported pathology[891, 908]; however FTLD-tau, FTLD TDP43 type A and B are also described [908, 909]. The different pathologies demonstrate distinct patterns of progression at the end stage of the disease: FTLD-TDP43 type C demonstrate predominant temporal atrophy which is associated with prominent semantic impairment; whereas FTLD-tau, FTLD-TDP43 types A and B demonstrate predominant frontal atrophy which is associated with prominent behavioural impairment [908, 909].

10.5 Conclusions

Despite shared clinical, neuroanatomical and pathological features, it is suggested that sbvFTD should be considered a distinct clinical phenotype along the FTLD continuum[892, 893, 897] . This facilitates early diagnosis; helping patients and their families better understand the disease[893]; and developing research frameworks to accurately stratify FTD phenotypes[891].

Table 30: Case series of semantic behavioural variant FTD

	Case 1	Case 2	Case 3	Case 4
Handedness	RHD	RHD	RHD	LHD
Sex	M	M	F	M
Education	3rd Level	3rd Level	3rd Level	Left school aged 15-years
Duration of symptom onset	2-years	10-years	8-years	7-years
Symptoms	Prosopagnosia Rigid thought process Dysexecutive Obsessive repetitive behaviours - - Disinhibition Loss of empathy Apathy Dietary changes Alexithymia	Prosopagnosia Rigid thought process Dysexecutive Obsessive repetitive behaviours Verbal semantic loss Episodic memory impairment Disinhibition - - - Alexithymia	Prosopagnosia Rigid thought process Dysexecutive Obsessive repetitive behaviours Verbal semantic loss Episodic memory impairment Disinhibition - - - -	Prosopagnosia Rigid thought process Dysexecutive - Verbal semantic loss Episodic memory impairment - Loss of empathy Apathy - -
Cognitive Testing				
ACE-III	97/100	41/100	91/100	88/100
ECAS	120/136	-	109/136	92/136
BNT	25/30	-	14/30	21/30
FBI	-	-	2 (Negative 1; Disinhibition 1)	30 (Negative 24; Disinhibition 6)
FAB	18/18	'Impaired'	-	-
Main domains affected	Executive Language Memory - Attention	Executive Language Memory Fluency -	Executive Language Memory Fluency -	Executive Language Memory Fluency Attention
CSF	Not compatible with AD	-	Not compatible with AD	Not compatible with AD
AB42 (591-997pg/mL)	835	-	959.6	722.2
Total Tau (135-345pg/mL)	602.7	-	249	302
P-Tau (35.0-64.0pg/mL)	116.5	-	46	67.3

List of Abbreviations

l-[β-^{11}C] dopa PET	Pre-synaptic dopamine synthesis PET tracer	***ATXN2***	Ataxin-2
[^{11}C] ABP688 PET	mGluR5 PET tracer	**AUC**	Area under the receiving operating characteristic curve
[^{11}C] DAA1106 PET	Peripheral benzodiazepine receptors PET tracer	**AV**	Anterior ventral
[^{11}C] flumazenil PET	GABA-A PET tracer	**AxD**	Axial diffusivity
[^{11}C] PBR28 PET	PET tracer; 18 kDa translocator protein	**BET**	Brain extraction tool
[^{11}C] UCB-J PET	Synaptic vesicle glycoprotein 2A PET tracer	**BNT**	Boston naming test
[^{18}F] AV-1451 PET	Tau PET tracer	**bvFTD**	Behavioural variant FTD
[^{18}F] FDG PET-CT	18F-fluorodeoxyglucose positron emission tomography computed tomography	***C21orf2***	Cilia and flagella associated protein 410
[^{18}F] THK5351 PET	Tau PET-tracer	***C9orf72***	Chromosome 9 open reading frame 72
^{1}H-MRS	Proton MR spectroscopy	**CAG**	Cytosine-adenine-guanine
ABCD1	ATP binding cassette subfamily D member 1	**CBD**	Corticobasal degeneration
ACE-III	Addenbrooke's cognitive examination III	**CBS**	Corticobasal syndrome
AD	Alzheimer's disease	**CC**	Corpus callosum
ALD	Adrenoleukodystrophy	**CeM**	Central medial
ALS	Amyotrophic lateral sclerosis	***CHCHD10***	Coiled-coil-helix-coiled-coil-helix domain containing 10
ALS2	Amyotrophic lateral sclerosis 2	***CHMP2B***	Charged multivesicular body protein 2B
ALS-bi	ALS with behavioural impairment	**Cho**	Choline
ALS-ci	ALS with cognitive impairment	**Cho/Cr**	Choline/creatine
ALSFRS-R	Amyotrophic lateral sclerosis functional rating scale revised	**cHSP**	Complicated HSP
ALS-FTD	Amyotrophic lateral sclerosis frontotemporal dementia	**CL**	Central lateral
ALS-FTD C9+	*C9orf72* positive ALS-FTD	**CM**	Centromedian
ALS-FTD C9-	*C9orf72* negative ALS-FTD	**Cr**	Creatine
ALS-nc/ALS-nci	ALS with normal cognition / no cognitive impairment	**CSA**	Cross-sectional area
ANCOVA	Analysis of covariance	**CSD**	Constrained spherical deconvolution
ANG	Angiogenin	**CSF**	Cerebrospinal fluid
ANN	Artificial neural networks	**CST**	Corticospinal tracts
ANOVA	Analysis of variance	**CT**	Cortical thickness
AP	Anteroposterior	***DAO***	D-Amino Acid Oxidase
AR	Androgen receptor	**DCML**	Dorsal column-medial lemniscus
ARCA	Autosomal recessive cerebellar ataxia	***DCTN1***	Dynactin Subunit 1
ASIA	American spinal cord injury association	**DKI**	Diffusion kurtosis imaging
ASL	Arterial spin labelling	**DLB**	Dementia with Lewy bodies
ASO	Antisense oligonucleotide	**DLPFC**	Dorsolateral prefrontal cortex

DRG	Dorsal root ganglion	***HNRNPA1***	Heterogeneous nuclear ribonucleoprotein A1
DSI	Diffusion spectrum imaging	**HSD**	Honestly significant difference testing
DSM	Diagnostic and statistical manual of mental disorders	**HSP**	Hereditary spastic paraplegia
DTI	Diffusion tensor imaging	**HTLV1**	Human T-lymphotropic virus 1
DW	Diffusion weighted	**IC**	Internal capsule
DWI	Diffusion weighted imaging	**ihMT**	Inhomogeneous magnetization transfer
ECAS	Edinburgh cognitive and behavioural ALS screen	**ihMTR**	Inhomogeneous magnetization transfer ratio
EEG	Electroencephalogram	**IR-SPGR**	Inversion recovery prepared spoiled gradient recalled echo
ELP3	Elongator Acetyltransferase Complex Subunit 3	**IR-TSE**	Inversion Recovery Turbo Spin Echo
EMM	Estimated marginal means	**IWG**	International Working Group
EOAD	Early onset Alzheimer's disease	**KNN**	K-nearest neighbour
EPI	Echo-planar imaging	**LBD**	Lewy body dementia
ERBB4	Erb-B2 Receptor Tyrosine Kinase 4	**LD**	Lateral dorsal
FA	Fractional anisotropy	**LGN**	Lateral geniculate
FAB	Frontal assessment battery	**LMN**	Lower motor neuron
FARS	Friedreich's ataxia rating scale	***LMNB1***	Lamin B1
FAST	FMRIB's Automated Segmentation Tool	**LMND**	Lower motor neuron disease
FBI	Frontal behavioural inventory	**LOAD**	Late-onset Alzheimer's disease
FDR	False discovery rate	**LoCo**	Loss in connectivity
FDRA	Friedreich's ataxia	**LP**	Lateral posterior
FIG4	Factor-induced gene	**L-SG**	Limitans/suprageniculate
FLAIR	Fluid-attenuated inversion recovery	**Lt**	Left
FLIRT	FMRIB's Linear Image Registration Tool	**lvPPA**	Logopaenic primary progressive aphasia
fMRI	Functional magnetic resonance imaging	***LY6G6F***	Lymphocyte antigen 6 family member G6F
fODF	Fibre orientation distributions	**MANCOVA**	Multivariate analysis of covariance
FOV	Field-of-view	***MAPT***	Microtubule associated protein tau
FSL	FMRIB Software Library	***MATR3***	Matrin 3
FSLeyes	FSL image viewer	**mcDESPOT**	Multi-component driven equilibrium single pulse observation
FTD	Frontotemporal dementia	**MCI**	Mild cognitive impairment
FTDP-17	Frontotemporal dementia with parkinsonism-17	**MD**	Medial dorsal
FTLD	Frontotemporal lobar degeneration	**MD**	Mean diffusivity
FUS	Fused in sarcoma	**MDI**	Mediodorsal lateral parvocellular
FWE	Family-wise error	**MDm**	Mediodorsal medial magnocellular
FWER	Family-wise error connected	**MEDIC**	Multiple echo data image combination
GAN	Generative adversarial neural network	**MEG**	Magnetoencephalography
GM	Grey matter	**MGN**	Medial geniculate
GMD	Grey matter density	**MGUS**	Monoclonal gammopathy of uncertain significance
GRASE	Gradient and spin echo sequence	**m-Ins**	Myo-inositol
GRN	Progranulin	**m-Ins/Cr**	Myo-inositol/creatine
HAM/TSP	HTLV1 associated myelitis/tropical spastic paraparesis	**ML**	Machine learning
HC	Healthy control	**mm**	millimetres
HD	Huntington's disease	**MNI**	Montreal Neurological Institute
HIV	Human immunodeficiency virus	**MNI152**	Montreal Neurological Institute 152 Standard Space

MND	Motor neuron disease	***PSEN2***	Presenilin 2
MPRAGE	Magnetization-Prepared Rapid Acquisition Gradient Echo.	**Pt**	Paratenial
MR	Magnetic resonance	**PuA**	Pulvinar anterior
MRI	Magnetic resonance imaging	**PuI**	Pulvinar inferior
MRS	Magnetic resonance spectroscopy	**PuL**	Pulvinar lateral
MS	Multiple sclerosis	**PuM**	Pulvinar medial
MT	Magnetization transfer	**PPA**	Primary progressive aphasia
MTI	Magnetization transfer imaging	**PPMS**	Primary progressive multiple sclerosis
MTR	Magnetization transfer ratio	**PPS**	Post-polio syndrome
MV-re	Medial ventral/reunions	**PSIR**	Phase sensitive inversion recovery
MWI	Myelin water imaging	**PSP**	Progressive supranuclear palsy
NAA	N-acetyl-aspartate	**p-tau**	Phosphorylated tau
NAA/Cho	N-acetyl-aspartate/choline	**pTDP-43**	Phosphorylated transactive response DNA binding protein 43 kDa
NAA/Cr	N-acetyl-aspartate/creatine	**RD**	Radial diffusivity
NAA/m-Ins	N-acetyl aspartate/myo-inositol	**ROI**	Region-of-interest
NCI	No cognitive impairment	**RRMS**	Relapsing remitting multiple sclerosis
NEFH	Neurofilament heavy chain	**rs-fMRI**	Resting state functional magnetic resonance imaging
NEK1	NIMA Related Kinase 1	**Rt**	Right
nfvPPA	Non-fluent variant PPA	**RUSBoost**	Random undersampling boosting
NIAA-AA	National Institute on Ageing and the Alzheimer's Association	**SACD**	Subacute combined degeneration
NINCDS-ADRDA	National Institute of Neurological and Communicative Disorders and Stroke and Alzheimer's Disease and Related Disorders Association	**SARA**	Scale for the assessment and rating of ataxia
NINDS-AIREN	National Institute of Neurological Disorders and Stroke and Association Internationale pour la Recherche et l'Enseignement en Neurosciences	***SARM1***	Sterile Alpha And TIR Motif Containing 1
NINDS-SPSP	National Institute of Neurological Disorders and Stroke and Society of Progressive Supranuclear Palsy	**SBMA**	Spinal bulbar muscular atrophy
NMO	Neuromyelitis optica	**sbvFTD**	Semantic behavioural variant FTD
NODDI	Neurite orientation dispersion and density imaging	**SCA**	Spinocerebellar ataxia
OPTN	Optineurin	**SCAFI**	Spinocerebellar Ataxia Functional Index
Pc	Paracentral	**SD**	Standard deviation
PCA	Principal component analysis	**SE**	Standard error
PET	Positron emission tomography	**SE-EPI**	Spin-echo echo planar imaging
PF	Parafascicular	**SENSE**	Sensitivity encoding
PFN1	Profilin-1	***SETX***	Senataxin
pHSP	Pure HSP	***SIGMAR1***	Sigma non-opioid intracellular receptor 1
PIB-PET	Pittsburgh compound B positron emission tomography	**SMA**	Spinal muscular atrophy
PLS	Primary lateral sclerosis	**SMC**	Subjective memory complaints
PLS-FTD	Primary lateral sclerosis-FTD	**SMN**	Survival motor neuron
PMA	Progressive muscular atrophy	***SMN1***	Survival motor neuron 1
PRISMA	Preferred Reporting Items for Systematic Reviews and Meta-Analyses	***SMN2***	Survival motor neuron 2
PRPH	Peripherin	***SOD1***	Superoxide dismutase type 1
PSEN1	Presenilin 1	***SPAST***	Spastin

SPG	Spastic paraplegia	**VM**	Ventral medial
SPIR	Spectral pre-saturation with inversion recovery	**VOI**	Volumes of interest
SQSTM1	Sequestosome-1	**VOL**	Volumetry
STAND	Structural abnormality in neurodegeneration	**VPL**	Ventral posterolateral
SuStaIn	Subtype and stage inference	**WM**	White matter
SVD	Singular value decomposition	**WMD**	White matter density
SVM	Support vector machine	**WMH**	White matter hyperintensity
svPPA	Semantic variant PPA	**wSDM**	Weighted symbolic dependence metric
SYNE1	Synaptic nuclear envelope protein 1		
T	Tesla		
T1W	T1-weighted		
T2W	T2-weighted		
TAF15	TATA-Box Binding Protein Associated Factor 15		
TARDBP	TAR DNA binding protein		
TBK1	TANK binding kinase 1		
TBM	Tensor-based morphometry		
TBM-Syn	Tensor-based morphometry symmetric diffeomorphic image normalization		
TBSS	Tract based spatial statistics		
TDP-43	Transactive response DNA binding protein 43 kDa		
TE	Echo time		
TFCE	Threshold-free cluster enhancement		
TI	Inversion time		
TIV	Total Intracranial volume		
TMEM106B	Transmembrane protein 106B		
TMEM40	Transmembrane protein 40		
tNAA	Total N-acetyl aspartate		
tNAA/m-Ins	Total N-acetyl aspartate/myo-inositol		
ToM	Theory of mind		
TR	Repetition time		
TREM2	Triggering Receptor Expressed On Myeloid Cells 2		
TRIM	Turbo inversion recovery magnitude		
t-tau	Total tau		
UBQLN2	Ubiquilin-2		
UMN	Upper motor neuron		
UNC13A	Unc-13 Homolog A		
VA	Ventral anterior		
VA mc	Ventral anterior magnocellular		
VAPB	Vesicle-associated membrane protein-associated protein B/C		
VB12	Vitamin B12		
VBM	Voxel based morphometry		
VCP	Valsoin containing protein		
VD	Vascular dementia		
VLa	Ventral lateral anterior		
VLp	Ventral lateral posterior		

References

1. Couto B, Manes F, Montañés P, Matallana D, Reyes P, Velasquez M, et al. Structural neuroimaging of social cognition in progressive non-fluent aphasia and behavioral variant of frontotemporal dementia. Front Hum Neurosci. 2013;7:467-.
2. Grossman M, McMillan C, Moore P, Ding L, Glosser G, Work M, et al. What's in a name: voxel-based morphometric analyses of MRI and naming difficulty in Alzheimer's disease, frontotemporal dementia and corticobasal degeneration. Brain. 2004;127(Pt 3):628-49.
3. Rosen HJ, Gorno-Tempini ML, Goldman WP, Perry RJ, Schuff N, Weiner M, et al. Patterns of brain atrophy in frontotemporal dementia and semantic dementia. Neurology. 2002;58(2):198-208.
4. Nestor PJ, Graham NL, Fryer TD, Williams GB, Patterson K, Hodges JR. Progressive non-fluent aphasia is associated with hypometabolism centred on the left anterior insula. Brain. 2003;126(Pt 11):2406-18.
5. Nestor PJ, Fryer TD, Hodges JR. Declarative memory impairments in Alzheimer's disease and semantic dementia. Neuroimage. 2006;30(3):1010-20.
6. Mummery CJ, Patterson K, Price CJ, Ashburner J, Frackowiak RS, Hodges JR. A voxel-based morphometry study of semantic dementia: relationship between temporal lobe atrophy and semantic memory. Ann Neurol. 2000;47(1):36-45.
7. Möller C, Hafkemeijer A, Pijnenburg YAL, Rombouts SARB, van der Grond J, Dopper E, et al. Joint assessment of white matter integrity, cortical and subcortical atrophy to distinguish AD from behavioral variant FTD: A two-center study. Neuroimage Clin. 2015;9:418-29.
8. Hornberger M, Geng J, Hodges JR. Convergent grey and white matter evidence of orbitofrontal cortex changes related to disinhibition in behavioural variant frontotemporal dementia. Brain. 2011;134(Pt 9):2502-12.
9. Zhang Y, Schuff N, Ching C, Tosun D, Zhan W, Nezamzadeh M, et al. Joint assessment of structural, perfusion, and diffusion MRI in Alzheimer's disease and frontotemporal dementia. Int J Alzheimers Dis. 2011;2011:546871-.
10. Lu PH, Mendez MF, Lee GJ, Leow AD, Lee HW, Shapira J, et al. Patterns of brain atrophy in clinical variants of frontotemporal lobar degeneration. Dementia and geriatric cognitive disorders. 2013;35(1-2):34-50.
11. Agosta F, Galantucci S, Magnani G, Marcone A, Martinelli D, Antonietta Volonte M, et al. MRI signatures of the frontotemporal lobar degeneration continuum. Human brain mapping. 2015;36(7):2602-14.
12. Bocti C, Rockel C, Roy P, Gao F, Black SE. Topographical patterns of lobar atrophy in frontotemporal dementia and Alzheimer's disease. Dementia and geriatric cognitive disorders. 2006;21(5-6):364-72.
13. Agosta F, Scola E, Canu E, Marcone A, Magnani G, Sarro L, et al. White matter damage in frontotemporal lobar degeneration spectrum. Cereb Cortex. 2012;22(12):2705-14.
14. Whitwell JL, Avula R, Senjem ML, Kantarci K, Weigand SD, Samikoglu A, et al. Gray and white matter water diffusion in the syndromic variants of frontotemporal dementia. Neurology. 2010;74(16):1279-87.
15. Agosta F, Galantucci S, Canu E, Cappa SF, Magnani G, Franceschi M, et al. Disruption of structural connectivity along the dorsal and ventral language pathways in patients with nonfluent and semantic variant primary progressive aphasia: a DT MRI study and a literature review. Brain Lang. 2013;127(2):157-66.
16. Borroni B, Brambati SM, Agosti C, Gipponi S, Bellelli G, Gasparotti R, et al. Evidence of White Matter Changes on Diffusion Tensor Imaging in Frontotemporal Dementia. Archives of Neurology. 2007;64(2):246-51.
17. Janssen JC, Schott JM, Cipolotti L, Fox NC, Scahill RI, Josephs KA, et al. Mapping the onset and progression of atrophy in familial frontotemporal lobar degeneration. J Neurol Neurosurg Psychiatry. 2005;76(2):162-8.
18. Rohrer JD, Warren JD, Barnes J, Mead S, Beck J, Pepple T, et al. Mapping the progression of progranulin-associated frontotemporal lobar degeneration. Nature Clinical Practice Neurology. 2008;4(8):455-60.
19. Cruchaga C, Fernández-Seara MA, Seijo-Martínez M, Samaranch L, Lorenzo E, Hinrichs A, et al. Cortical atrophy and language network reorganization associated with a novel progranulin mutation. Cereb Cortex. 2009;19(8):1751-60.
20. Pievani M, Paternicò D, Benussi L, Binetti G, Orlandini A, Cobelli M, et al. Pattern of structural and functional brain abnormalities in asymptomatic granulin mutation carriers. Alzheimer's & Dementia. 2014;10(5S):S354-S63.e1.
21. Jiskoot LC, Panman JL, Meeter LH, Dopper EGP, Donker Kaat L, Franzen S, et al. Longitudinal multimodal MRI as prognostic and diagnostic biomarker in presymptomatic familial frontotemporal dementia. Brain. 2019;142(1):193-208.
22. Rohrer JD, Nicholas JM, Cash DM, van Swieten J, Dopper E, Jiskoot L, et al. Presymptomatic cognitive and neuroanatomical changes in genetic frontotemporal dementia in the Genetic

Frontotemporal dementia Initiative (GENFI) study: a cross-sectional analysis. The Lancet Neurology. 2015;14(3):253-62.
23. Dopper EGP, Rombouts SARB, Jiskoot LC, den Heijer T, de Graaf JRA, de Koning I, et al. Structural and functional brain connectivity in presymptomatic familial frontotemporal dementia. Neurology. 2014;83(2):e19.
24. Rabinovici GD, Miller BL. Frontotemporal lobar degeneration: epidemiology, pathophysiology, diagnosis and management. CNS Drugs. 2010;24(5):375-98.
25. Du A-T, Schuff N, Kramer JH, Rosen HJ, Gorno-Tempini ML, Rankin K, et al. Different regional patterns of cortical thinning in Alzheimer's disease and frontotemporal dementia. Brain. 2007;130(4):1159-66.
26. Whitwell JL, Josephs KA, Rossor MN, Stevens JM, Revesz T, Holton JL, et al. Magnetic Resonance Imaging Signatures of Tissue Pathology in Frontotemporal Dementia. Archives of Neurology. 2005;62(9):1402-8.
27. Pereira JM, Williams GB, Acosta-Cabronero J, Pengas G, Spillantini MG, Xuereb JH, et al. Atrophy patterns in histologic vs clinical groupings of frontotemporal lobar degeneration. Neurology. 2009;72(19):1653-60.
28. Avants BB, Cook PA, Ungar L, Gee JC, Grossman M. Dementia induces correlated reductions in white matter integrity and cortical thickness: a multivariate neuroimaging study with sparse canonical correlation analysis. NeuroImage. 2010;50(3):1004-16.
29. McMillan CT, Brun C, Siddiqui S, Churgin M, Libon D, Yushkevich P, et al. White matter imaging contributes to the multimodal diagnosis of frontotemporal lobar degeneration. Neurology. 2012;78(22):1761-8.
30. Seeley WW, Crawford R, Rascovsky K, Kramer JH, Weiner M, Miller BL, et al. Frontal paralimbic network atrophy in very mild behavioral variant frontotemporal dementia. Arch Neurol. 2008;65(2):249-55.
31. Rabinovici GD, Seeley WW, Kim EJ, Gorno-Tempini ML, Rascovsky K, Pagliaro TA, et al. Distinct MRI atrophy patterns in autopsy-proven Alzheimer's disease and frontotemporal lobar degeneration. Am J Alzheimers Dis Other Demen. 2007;22(6):474-88.
32. Pan P, Song W, Yang J, Huang R, Chen K, Gong QY, et al. Gray Matter Atrophy in Behavioral Variant Frontotemporal Dementia: A Meta-Analysis of Voxel-Based Morphometry Studies. Dementia and geriatric cognitive disorders. 2012;33(2-3):141-8.
33. McKenna MC, Tahedl M, Lope J, Chipika RH, Li Hi Shing S, Doherty MA, et al. Mapping cortical disease-burden at individual-level in frontotemporal dementia: implications for clinical care and pharmacological trials. Brain imaging and behavior. 2021.
34. McKenna MC, Chipika RH, Li Hi Shing S, Christidi F, Lope J, Doherty MA, et al. Infratentorial pathology in frontotemporal dementia: cerebellar grey and white matter alterations in FTD phenotypes. Journal of neurology. 2021.
35. Zhang Y, Schuff N, Du A-T, Rosen HJ, Kramer JH, Gorno-Tempini ML, et al. White matter damage in frontotemporal dementia and Alzheimer's disease measured by diffusion MRI. Brain. 2009;132(9):2579-92.
36. Mahoney CJ, Ridgway GR, Malone IB, Downey LE, Beck J, Kinnunen KM, et al. Profiles of white matter tract pathology in frontotemporal dementia. Human brain mapping. 2014;35(8):4163-79.
37. Chen TF, Lin CC, Chen YF, Liu HM, Hua MS, Huang YC, et al. Diffusion tensor changes in patients with amnesic mild cognitive impairment and various dementias. Psychiatry Res. 2009;173(1):15-21.
38. Matsuo K, Mizuno T, Yamada K, Akazawa K, Kasai T, Kondo M, et al. Cerebral white matter damage in frontotemporal dementia assessed by diffusion tensor tractography. Neuroradiology. 2008;50(7):605-11.
39. Jakabek D, Power BD, Macfarlane MD, Walterfang M, Velakoulis D, van Westen D, et al. Regional structural hypo- and hyperconnectivity of frontal-striatal and frontal-thalamic pathways in behavioral variant frontotemporal dementia. Human brain mapping. 2018;39(10):4083-93.
40. Daianu M, Mendez MF, Baboyan VG, Jin Y, Melrose RJ, Jimenez EE, et al. An advanced white matter tract analysis in frontotemporal dementia and early-onset Alzheimer's disease. Brain imaging and behavior. 2016;10(4):1038-53.
41. Galantucci S, Tartaglia MC, Wilson SM, Henry ML, Filippi M, Agosta F, et al. White matter damage in primary progressive aphasias: a diffusion tensor tractography study. Brain. 2011;134(10):3011-29.
42. McKenna MC, Tahedl M, Murad A, Lope J, Hardiman O, Hutchinson S, et al. White matter microstructure alterations in frontotemporal dementia: Phenotype-associated signatures and single-subject interpretation. Brain and behavior. 2022:e2500.
43. Seelaar H, Klijnsma KY, de Koning I, van der Lugt A, Chiu WZ, Azmani A, et al. Frequency of ubiquitin and FUS-positive, TDP-43-negative frontotemporal lobar degeneration. Journal of neurology. 2010;257(5):747-53.
44. Neumann M, Rademakers R, Roeber S, Baker M, Kretzschmar HA, Mackenzie IR. A new subtype of frontotemporal lobar degeneration with FUS pathology. Brain. 2009;132(Pt 11):2922-31.

45. Looi JCL, Lindberg O, Zandbelt BB, Ostberg P, Andersen C, Botes L, et al. Caudate nucleus volumes in frontotemporal lobar degeneration: differential atrophy in subtypes. AJNR Am J Neuroradiol. 2008;29(8):1537-43.
46. Halabi C, Halabi A, Dean DL, Wang P-N, Boxer AL, Trojanowski JQ, et al. Patterns of striatal degeneration in frontotemporal dementia. Alzheimer Dis Assoc Disord. 2013;27(1):74-83.
47. Looi JCL, Svensson L, Lindberg O, Zandbelt BB, Ostberg P, Orndahl E, et al. Putaminal volume in frontotemporal lobar degeneration and Alzheimer disease: differential volumes in dementia subtypes and controls. AJNR Am J Neuroradiol. 2009;30(8):1552-60.
48. van de Pol LA, Hensel A, van der Flier WM, Visser PJ, Pijnenburg YAL, Barkhof F, et al. Hippocampal atrophy on MRI in frontotemporal lobar degeneration and Alzheimer's disease. J Neurol Neurosurg Psychiatry. 2006;77(4):439-42.
49. Muñoz-Ruiz MÁ, Hartikainen P, Koikkalainen J, Wolz R, Julkunen V, Niskanen E, et al. Structural MRI in frontotemporal dementia: comparisons between hippocampal volumetry, tensor-based morphometry and voxel-based morphometry. PLoS One. 2012;7(12):e52531-e.
50. Zhou J, Greicius MD, Gennatas ED, Growdon ME, Jang JY, Rabinovici GD, et al. Divergent network connectivity changes in behavioural variant frontotemporal dementia and Alzheimer's disease. Brain : a journal of neurology. 2010;133(Pt 5):1352-67.
51. Filippi M, Agosta F, Scola E, Canu E, Magnani G, Marcone A, et al. Functional network connectivity in the behavioral variant of frontotemporal dementia. Cortex; a journal devoted to the study of the nervous system and behavior. 2013;49(9):2389-401.
52. Hafkemeijer A, Möller C, Dopper EG, Jiskoot LC, Schouten TM, van Swieten JC, et al. Resting state functional connectivity differences between behavioral variant frontotemporal dementia and Alzheimer's disease. Front Hum Neurosci. 2015;9:474.
53. Bouts MJRJ, Möller C, Hafkemeijer A, van Swieten JC, Dopper E, van der Flier WM, et al. Single Subject Classification of Alzheimer's Disease and Behavioral Variant Frontotemporal Dementia Using Anatomical, Diffusion Tensor, and Resting-State Functional Magnetic Resonance Imaging. Journal of Alzheimer's Disease. 2018;62:1827-39.
54. Canu E, Agosta F, Mandic-Stojmenovic G, Stojković T, Stefanova E, Inuggi A, et al. Multiparametric MRI to distinguish early onset Alzheimer's disease and behavioural variant of frontotemporal dementia. NeuroImage: Clinical. 2017;15:428-38.
55. Grollemund V, Pradat PF, Querin G, Delbot F, Le Chat G, Pradat-Peyre JF, et al. Machine Learning in Amyotrophic Lateral Sclerosis: Achievements, Pitfalls, and Future Directions. Frontiers in neuroscience. 2019;13:135.
56. Schuster C, Hardiman O, Bede P. Development of an Automated MRI-Based Diagnostic Protocol for Amyotrophic Lateral Sclerosis Using Disease-Specific Pathognomonic Features: A Quantitative Disease-State Classification Study. PLoS One. 2016;11(12):e0167331.
57. Bede P, Iyer PM, Finegan E, Omer T, Hardiman O. Virtual brain biopsies in amyotrophic lateral sclerosis: Diagnostic classification based on in vivo pathological patterns. Neuroimage Clin. 2017;15:653-8.
58. Grollemund V, Le Chat G, Secchi-Buhour MS, Delbot F, Pradat-Peyre JF, Bede P, et al. Manifold learning for amyotrophic lateral sclerosis functional loss assessment : Development and validation of a prognosis model. Journal of neurology. 2021;268(3):825-50.
59. Schuster C, Hardiman O, Bede P. Survival prediction in Amyotrophic lateral sclerosis based on MRI measures and clinical characteristics. BMC neurology. 2017;17(1):73.
60. Querin G, El Mendili MM, Bede P, Delphine S, Lenglet T, Marchand-Pauvert V, et al. Multimodal spinal cord MRI offers accurate diagnostic classification in ALS. J Neurol Neurosurg Psychiatry. 2018;89(11):1220-1.
61. Feis RA, Bouts MJRJ, Dopper EGP, Filippini N, Heise V, Trachtenberg AJ, et al. Multimodal MRI of grey matter, white matter, and functional connectivity in cognitively healthy mutation carriers at risk for frontotemporal dementia and Alzheimer's disease. BMC neurology. 2019;19(1):343-.
62. Feis RA, Bouts MJRJ, Panman JL, Jiskoot LC, Dopper EGP, Schouten TM, et al. Single-subject classification of presymptomatic frontotemporal dementia mutation carriers using multimodal MRI. NeuroImage: Clinical. 2019;22:101718.
63. Feis RA, Bouts MJRJ, de Vos F, Schouten TM, Panman JL, Jiskoot LC, et al. A multimodal MRI-based classification signature emerges just prior to symptom onset in frontotemporal dementia mutation carriers. Journal of Neurology, Neurosurgery & Psychiatry. 2019;90(11):1207.
64. Feis RA, van der Grond J, Bouts MJRJ, Panman JL, Poos JM, Schouten TM, et al. Classification using fractional anisotropy predicts conversion in genetic frontotemporal dementia, a proof of concept. Brain Communications. 2020;2(2).
65. Bron EE, Smits M, Papma JM, Steketee RME, Meijboom R, de Groot M, et al. Multiparametric computer-aided differential diagnosis of Alzheimer's disease and frontotemporal dementia using structural and advanced MRI. European Radiology. 2017;27(8):3372-82.
66. Raamana PR, Rosen H, Miller B, Weiner MW, Wang L, Beg MF. Three-Class Differential Diagnosis among Alzheimer Disease, Frontotemporal Dementia, and Controls. Frontiers in Neurology. 2014;5(71).

67. Klöppel S, Peter J, Ludl A, Pilatus A, Maier S, Mader I, et al. Applying Automated MR-Based Diagnostic Methods to the Memory Clinic: A Prospective Study. Journal of Alzheimer's Disease. 2015;47:939-54.
68. Koikkalainen J, Rhodius-Meester H, Tolonen A, Barkhof F, Tijms B, Lemstra AW, et al. Differential diagnosis of neurodegenerative diseases using structural MRI data. NeuroImage: Clinical. 2016;11:435-49.
69. Meyer S, Mueller K, Stuke K, Bisenius S, Diehl-Schmid J, Jessen F, et al. Predicting behavioral variant frontotemporal dementia with pattern classification in multi-center structural MRI data. NeuroImage: Clinical. 2017;14:656-62.
70. Agosta F, Ferraro PM, Canu E, Copetti M, Galantucci S, Magnani G, et al. Differentiation between Subtypes of Primary Progressive Aphasia by Using Cortical Thickness and Diffusion-Tensor MR Imaging Measures. Radiology. 2015;276(1):219-27.
71. Gorno-Tempini ML, Hillis AE, Weintraub S, Kertesz A, Mendez M, Cappa SF, et al. Classification of primary progressive aphasia and its variants. Neurology. 2011;76(11):1006-14.
72. Bachli MB, Sedeño L, Ochab JK, Piguet O, Kumfor F, Reyes P, et al. Evaluating the reliability of neurocognitive biomarkers of neurodegenerative diseases across countries: A machine learning approach. Neuroimage. 2020;208:116456.
73. Rascovsky K, Hodges JR, Knopman D, Mendez MF, Kramer JH, Neuhaus J, et al. Sensitivity of revised diagnostic criteria for the behavioural variant of frontotemporal dementia. Brain : a journal of neurology. 2011;134(Pt 9):2456-77.
74. McKhann GM, Knopman DS, Chertkow H, Hyman BT, Jack CR, Jr., Kawas CH, et al. The diagnosis of dementia due to Alzheimer's disease: recommendations from the National Institute on Aging-Alzheimer's Association workgroups on diagnostic guidelines for Alzheimer's disease. Alzheimer's & dementia : the journal of the Alzheimer's Association. 2011;7(3):263-9.
75. Bede P, Murad A, Hardiman O. Pathological neural networks and artificial neural networks in ALS: diagnostic classification based on pathognomonic neuroimaging features. Journal of neurology. 2021.
76. Brooks BR, Miller RG, Swash M, Munsat TL, Gr WFNR. El Escorial revisited: Revised criteria for the diagnosis of amyotrophic lateral sclerosis. Amyotroph Lateral Sc. 2000;1(5):293-9.
77. Bisenius S, Mueller K, Diehl-Schmid J, Fassbender K, Grimmer T, Jessen F, et al. Predicting primary progressive aphasias with support vector machine approaches in structural MRI data. Neuroimage Clin. 2017;14:334-43.
78. Canu E, Agosta F, Imperiale F, Fontana A, Caso F, Spinelli EG, et al. Added value of multimodal MRI to the clinical diagnosis of primary progressive aphasia variants. Cortex; a journal devoted to the study of the nervous system and behavior. 2019;113:58-66.
79. Cajanus A, Hall A, Koikkalainen J, Solje E, Tolonen A, Urhemaa T, et al. Automatic MRI Quantifying Methods in Behavioral-Variant Frontotemporal Dementia Diagnosis. Dement Geriatr Cogn Dis Extra. 2018;8(1):51-9.
80. Chagué P, Marro B, Fadili S, Houot M, Morin A, Samper-González J, et al. Radiological classification of dementia from anatomical MRI assisted by machine learning-derived maps. J Neuroradiol. 2020.
81. Dubois B, Feldman H, Jacova C, DeKosky S, Barberger-Gateau P, Cummings J, et al. Research criteria for the diagnosis of Alzheimer's disease: Revising the NINCDS-ADRDA criteria. Lancet neurology. 2007;6:734-46.
82. Association AP. Diagnostic and statistical manual of mental disorders : DSM-5™. 5th edition. ed. Washington, DC ;: American Psychiatric Publishing, a division of American Psychiatric Association; 2013.
83. Chow TW, Binns MA, Freedman M, Stuss DT, Ramirez J, Scott CJ, et al. Overlap in frontotemporal atrophy between normal aging and patients with frontotemporal dementias. Alzheimer Dis Assoc Disord. 2008;22(4):327-35.
84. Neary D, Snowden JS, Gustafson L, Passant U, Stuss D, Black S, et al. Frontotemporal lobar degeneration. Neurology. 1998;51(6):1546.
85. Davatzikos C, Resnick SM, Wu X, Parmpi P, Clark CM. Individual patient diagnosis of AD and FTD via high-dimensional pattern classification of MRI. Neuroimage. 2008;41(4):1220-7.
86. McKhann GM, Albert MS, Grossman M, Miller B, Dickson D, Trojanowski JQ. Clinical and pathological diagnosis of frontotemporal dementia: report of the Work Group on Frontotemporal Dementia and Pick's Disease. Arch Neurol. 2001;58(11):1803-9.
87. McKhann G, Drachman D, Folstein M, Katzman R, Price D, Stadlan EM. Clinical diagnosis of Alzheimer's disease: report of the NINCDS-ADRDA Work Group under the auspices of Department of Health and Human Services Task Force on Alzheimer's Disease. Neurology. 1984;34(7):939-44.
88. Donnelly-Kehoe PA, Pascariello GO, García AM, Hodges JR, Miller B, Rosen H, et al. Robust automated computational approach for classifying frontotemporal neurodegeneration: Multimodal/multicenter neuroimaging. Alzheimers Dement (Amst). 2019;11:588-98.
89. Du AT, Jahng GH, Hayasaka S, Kramer JH, Rosen HJ, Gorno-Tempini ML, et al. Hypoperfusion in frontotemporal dementia and Alzheimer disease by arterial spin labeling MRI. Neurology. 2006;67(7):1215-20.

90. Egger K, Rau A, Yang S, Klöppel S, Abdulkadir A, Kellner E, et al. Automated voxel- and region-based analysis of gray matter and cerebrospinal fluid space in primary dementia disorders. Brain Res. 2020;1739:146800.
91. Ludolph A, Drory V, Hardiman O, Nakano I, Ravits J, Robberecht W, et al. A revision of the El Escorial criteria - 2015. Amyotrophic lateral sclerosis & frontotemporal degeneration. 2015;16(5-6):291-2.
92. Frings L, Yew B, Flanagan E, Lam BYK, Hüll M, Huppertz H-J, et al. Longitudinal Grey and White Matter Changes in Frontotemporal Dementia and Alzheimer's Disease. PLoS One. 2014;9(3):e90814.
93. Hu J, Qing Z, Liu R, Zhang X, Lv P, Wang M, et al. Deep Learning-Based Classification and Voxel-Based Visualization of Frontotemporal Dementia and Alzheimer's Disease. Frontiers in neuroscience. 2020;14:626154.
94. Kim JP, Kim J, Park YH, Park SB, Lee JS, Yoo S, et al. Machine learning based hierarchical classification of frontotemporal dementia and Alzheimer's disease. Neuroimage Clin. 2019;23:101811.
95. McKeith IG, Dickson DW, Lowe J, Emre M, Brien JT, Feldman H, et al. Diagnosis and management of dementia with Lewy bodies. Neurology. 2005;65(12):1863.
96. Román GC, Tatemichi TK, Erkinjuntti T, Cummings JL, Masdeu JC, Garcia JH, et al. Vascular dementia: diagnostic criteria for research studies. Report of the NINDS-AIREN International Workshop. Neurology. 1993;43(2):250-60.
97. McKeith IG, Galasko D, Kosaka K, Perry EK, Dickson DW, Hansen LA, et al. Consensus guidelines for the clinical and pathologic diagnosis of dementia with Lewy bodies (DLB): report of the consortium on DLB international workshop. Neurology. 1996;47(5):1113-24.
98. Kuceyeski A, Zhang Y, Raj A. Linking white matter integrity loss to associated cortical regions using structural connectivity information in Alzheimer's disease and fronto-temporal dementia: The Loss in Connectivity (LoCo) score. NeuroImage. 2012;61(4):1311-23.
99. Ma D, Lu D, Popuri K, Wang L, Beg MF. Differential Diagnosis of Frontotemporal Dementia, Alzheimer's Disease, and Normal Aging Using a Multi-Scale Multi-Type Feature Generative Adversarial Deep Neural Network on Structural Magnetic Resonance Images. Frontiers in neuroscience. 2020;14:853.
100. Manera AL, Dadar M, Van Swieten JC, Borroni B, Sanchez-Valle R, Moreno F, et al. MRI data-driven algorithm for the diagnosis of behavioural variant frontotemporal dementia. J Neurol Neurosurg Psychiatry. 2021.
101. Murray R, Neumann M, Forman MS, Farmer J, Massimo L, Rice A, et al. Cognitive and motor assessment in autopsy-proven corticobasal degeneration. Neurology. 2007;68(16):1274-83.
102. Mackenzie IR, Neumann M, Bigio EH, Cairns NJ, Alafuzoff I, Kril J, et al. Nomenclature and nosology for neuropathologic subtypes of frontotemporal lobar degeneration: an update. Acta Neuropathol. 2010;119(1):1-4.
103. Mackenzie IRA, Neumann M, Baborie A, Sampathu DM, Du Plessis D, Jaros E, et al. A harmonized classification system for FTLD-TDP pathology. Acta Neuropathologica. 2011;122(1):111-3.
104. McMillan C, Avants B, Cook P, Ungar L, Trojanowski J, Grossman M. The Power of Neuroimaging Biomarkers for Screening Frontotemporal Dementia. Human brain mapping. 2014;35.
105. Armstrong MJ, Litvan I, Lang AE, Bak TH, Bhatia KP, Borroni B, et al. Criteria for the diagnosis of corticobasal degeneration. Neurology. 2013;80(5):496-503.
106. Litvan I, Agid Y, Calne D, Campbell G, Dubois B, Duvoisin RC, et al. Clinical research criteria for the diagnosis of progressive supranuclear palsy (Steele-Richardson-Olszewski syndrome): report of the NINDS-SPSP international workshop. Neurology. 1996;47(1):1-9.
107. Möller C, Pijnenburg YA, van der Flier WM, Versteeg A, Tijms B, de Munck JC, et al. Alzheimer Disease and Behavioral Variant Frontotemporal Dementia: Automatic Classification Based on Cortical Atrophy for Single-Subject Diagnosis. Radiology. 2016;279(3):838-48.
108. Moguilner S, García AM, Mikulan E, Hesse E, García-Cordero I, Melloni M, et al. Weighted Symbolic Dependence Metric (wSDM) for fMRI resting-state connectivity: A multicentric validation for frontotemporal dementia. Sci Rep. 2018;8(1):11181-.
109. Moguilner S, García AM, Perl YS, Tagliazucchi E, Piguet O, Kumfor F, et al. Dynamic brain fluctuations outperform connectivity measures and mirror pathophysiological profiles across dementia subtypes: A multicenter study. Neuroimage. 2021;225:117522.
110. Association AP. Diagnostic and statistical manual of mental disorders : DSM-IV: Fourth edition. Washington, DC : American Psychiatric Association, [1994] ©1994; 1994.
111. Petersen RC, Smith GE, Waring SC, Ivnik RJ, Kokmen E, Tangelos EG. Aging, memory, and mild cognitive impairment. Int Psychogeriatr. 1997;9 Suppl 1:65-9.
112. Staffaroni AM, Cobigo Y, Goh S-YM, Kornak J, Bajorek L, Chiang K, et al. Individualized atrophy scores predict dementia onset in familial frontotemporal lobar degeneration. Alzheimer's & dementia : the journal of the Alzheimer's Association. 2020;16(1):37-48.
113. Tahmasian M, Shao J, Meng C, Grimmer T, Diehl-Schmid J, Yousefi BH, et al. Based on the Network Degeneration Hypothesis: Separating Individual Patients with Different Neurodegenerative Syndromes in a Preliminary Hybrid PET/MR Study. J Nucl Med. 2016;57(3):410-5.
114. Tong T, Ledig C, Guerrero R, Schuh A, Koikkalainen J, Tolonen A, et al. Five-class differential diagnostics of neurodegenerative diseases using random undersampling boosting. Neuroimage Clin. 2017;15:613-24.

115. Torso M, Bozzali M, Cercignani M, Jenkinson M, Chance SA. Using diffusion tensor imaging to detect cortical changes in fronto-temporal dementia subtypes. Sci Rep. 2020;10(1):11237-.
116. Torso M, Ridgway GR, Jenkinson M, Chance S. Intracortical diffusion tensor imaging signature of microstructural changes in frontotemporal lobar degeneration. Alzheimers Res Ther. 2021;13(1):180.
117. Höglinger GU, Respondek G, Stamelou M, Kurz C, Josephs KA, Lang AE, et al. Clinical diagnosis of progressive supranuclear palsy: The movement disorder society criteria. Mov Disord. 2017;32(6):853-64.
118. Vemuri P, Simon G, Kantarci K, Whitwell JL, Senjem ML, Przybelski SA, et al. Antemortem differential diagnosis of dementia pathology using structural MRI: Differential-STAND. NeuroImage. 2011;55(2):522-31.
119. Boeve BF, Lang AE, Litvan I. Corticobasal degeneration and its relationship to progressive supranuclear palsy and frontotemporal dementia. Ann Neurol. 2003;54 Suppl 5:S15-9.
120. Mackenzie IR, Baborie A, Pickering-Brown S, Du Plessis D, Jaros E, Perry RH, et al. Heterogeneity of ubiquitin pathology in frontotemporal lobar degeneration: classification and relation to clinical phenotype. Acta Neuropathol. 2006;112(5):539-49.
121. Group NIoAaRIW. Consensus recommendations for the postmortem diagnosis of Alzheimer's disease. The National Institute on Aging, and Reagan Institute Working Group on Diagnostic Criteria for the Neuropathological Assessment of Alzheimer's Disease. Neurobiol Aging. 1997;18(4 Suppl):S1-2.
122. Vernooij MW, Jasperse B, Steketee R, Koek M, Vrooman H, Ikram MA, et al. Automatic normative quantification of brain tissue volume to support the diagnosis of dementia: A clinical evaluation of diagnostic accuracy. Neuroimage Clin. 2018;20:374-9.
123. Wang J, Redmond SJ, Bertoux M, Hodges JR, Hornberger M. A Comparison of Magnetic Resonance Imaging and Neuropsychological Examination in the Diagnostic Distinction of Alzheimer's Disease and Behavioral Variant Frontotemporal Dementia. Front Aging Neurosci. 2016;8:119-.
124. Whitwell JL, Jack CR, Jr., Przybelski SA, Parisi JE, Senjem ML, Boeve BF, et al. Temporoparietal atrophy: a marker of AD pathology independent of clinical diagnosis. Neurobiology of aging. 2011;32(9):1531-41.
125. Caselli RJ, Windebank AJ, Petersen RC, Komori T, Parisi JE, Okazaki H, et al. Rapidly progressive aphasic dementia and motor neuron disease. Ann Neurol. 1993;33(2):200-7.
126. Josephs KA, Whitwell JL, Duffy JR, Vanvoorst WA, Strand EA, Hu WT, et al. Progressive aphasia secondary to Alzheimer disease vs FTLD pathology. Neurology. 2008;70(1):25-34.
127. Dickson DW, Bergeron C, Chin SS, Duyckaerts C, Horoupian D, Ikeda K, et al. Office of Rare Diseases neuropathologic criteria for corticobasal degeneration. J Neuropathol Exp Neurol. 2002;61(11):935-46.
128. Wilson SM, Ogar JM, Laluz V, Growdon M, Jang J, Glenn S, et al. Automated MRI-based classification of primary progressive aphasia variants. Neuroimage. 2009;47(4):1558-67.
129. Gorno-Tempini ML, Brambati SM, Ginex V, Ogar J, Dronkers NF, Marcone A, et al. The logopenic/phonological variant of primary progressive aphasia. Neurology. 2008;71(16):1227-34.
130. Young AL, Marinescu RV, Oxtoby NP, Bocchetta M, Yong K, Firth NC, et al. Uncovering the heterogeneity and temporal complexity of neurodegenerative diseases with Subtype and Stage Inference. Nature communications. 2018;9(1):4273.
131. Yu Q, Mai Y, Ruan Y, Luo Y, Zhao L, Fang W, et al. An MRI-based strategy for differentiation of frontotemporal dementia and Alzheimer's disease. Alzheimers Res Ther. 2021;13(1):23.
132. Zhang Y, Tartaglia MC, Schuff N, Chiang GC, Ching C, Rosen HJ, et al. MRI signatures of brain macrostructural atrophy and microstructural degradation in frontotemporal lobar degeneration subtypes. J Alzheimers Dis. 2013;33(2):431-44.
133. Zhutovsky P, Vijverberg EGB, Bruin WB, Thomas RM, Wattjes MP, Pijnenburg YAL, et al. Individual Prediction of Behavioral Variant Frontotemporal Dementia Development Using Multivariate Pattern Analysis of Magnetic Resonance Imaging Data. J Alzheimers Dis. 2019;68(3):1229-41.
134. Krueger CE, Dean DL, Rosen HJ, Halabi C, Weiner M, Miller BL, et al. Longitudinal rates of lobar atrophy in frontotemporal dementia, semantic dementia, and Alzheimer's disease. Alzheimer Dis Assoc Disord. 2010;24(1):43-8.
135. Gordon E, Rohrer JD, Kim LG, Omar R, Rossor MN, Fox NC, et al. Measuring disease progression in frontotemporal lobar degeneration: a clinical and MRI study. Neurology. 2010;74(8):666-73.
136. Frings L, Yew B, Flanagan E, Lam BYK, Hüll M, Huppertz H-J, et al. Longitudinal grey and white matter changes in frontotemporal dementia and Alzheimer's disease. PloS one. 2014;9(3):e90814-e.
137. Möller C, Hafkemeijer A, Pijnenburg YAL, Rombouts S, van der Grond J, Dopper E, et al. Different patterns of cortical gray matter loss over time in behavioral variant frontotemporal dementia and Alzheimer's disease. Neurobiol Aging. 2016;38:21-31.
138. Frings L, Mader I, Landwehrmeyer BG, Weiller C, Hüll M, Huppertz H-J. Quantifying change in individual subjects affected by frontotemporal lobar degeneration using automated longitudinal MRI volumetry. Human brain mapping. 2012;33(7):1526-35.
139. Whitwell JL, Jack CR, Jr., Boeve BF, Senjem ML, Baker M, Rademakers R, et al. Voxel-based morphometry patterns of atrophy in FTLD with mutations in MAPT or PGRN. Neurology. 2009;72(9):813-20.

140. Rohrer JD, Ridgway GR, Modat M, Ourselin S, Mead S, Fox NC, et al. Distinct profiles of brain atrophy in frontotemporal lobar degeneration caused by progranulin and tau mutations. NeuroImage. 2010;53(3):1070-6.
141. McMillan CT, Irwin DJ, Avants BB, Powers J, Cook PA, Toledo JB, et al. White matter imaging helps dissociate tau from TDP-43 in frontotemporal lobar degeneration. J Neurol Neurosurg Psychiatry. 2013;84(9):949-55.
142. Omer T, Finegan E, Hutchinson S, Doherty M, Vajda A, McLaughlin RL, et al. Neuroimaging patterns along the ALS-FTD spectrum: a multiparametric imaging study. Amyotrophic lateral sclerosis & frontotemporal degeneration. 2017;18(7-8):611-23.
143. Rohrer JD, Warren JD, Fox NC, Rossor MN. Presymptomatic studies in genetic frontotemporal dementia. Revue Neurologique. 2013;169(10):820-4.
144. Illán-Gala I, Montal V, Borrego-Écija S, Vilaplana E, Pegueroles J, Alcolea D, et al. Cortical microstructure in the behavioural variant of frontotemporal dementia: looking beyond atrophy. Brain. 2019;142(4):1121-33.
145. Schuster C, Elamin M, Hardiman O, Bede P. Presymptomatic and longitudinal neuroimaging in neurodegeneration--from snapshots to motion picture: a systematic review. J Neurol Neurosurg Psychiatry. 2015;86(10):1089-96.
146. Seeley WW, Menon V, Schatzberg AF, Keller J, Glover GH, Kenna H, et al. Dissociable intrinsic connectivity networks for salience processing and executive control. J Neurosci. 2007;27(9):2349-56.
147. Hafkemeijer A, Möller C, Dopper EG, Jiskoot LC, van den Berg-Huysmans AA, van Swieten JC, et al. Differences in structural covariance brain networks between behavioral variant frontotemporal dementia and Alzheimer's disease. Human brain mapping. 2016;37(3):978-88.
148. Whitwell JL, Josephs KA, Avula R, Tosakulwong N, Weigand SD, Senjem ML, et al. Altered functional connectivity in asymptomatic MAPT subjects: a comparison to bvFTD. Neurology. 2011;77(9):866-74.
149. Hu WT, Wang Z, Lee VM, Trojanowski JQ, Detre JA, Grossman M. Distinct cerebral perfusion patterns in FTLD and AD. Neurology. 2010;75(10):881-8.
150. Jiskoot LC, Bocchetta M, Nicholas JM, Cash DM, Thomas D, Modat M, et al. Presymptomatic white matter integrity loss in familial frontotemporal dementia in the GENFI cohort: A cross-sectional diffusion tensor imaging study. Annals of Clinical and Translational Neurology. 2018;5(9):1025-36.
151. Borroni B, Alberici A, Premi E, Archetti S, Garibotto V, Agosti C, et al. Brain magnetic resonance imaging structural changes in a pedigree of asymptomatic progranulin mutation carriers. Rejuvenation Res. 2008;11(3):585-95.
152. Jiskoot LC, Panman JL, van Asseldonk L, Franzen S, Meeter LHH, Donker Kaat L, et al. Longitudinal cognitive biomarkers predicting symptom onset in presymptomatic frontotemporal dementia. Journal of neurology. 2018;265(6):1381-92.
153. Meeter LH, Dopper EG, Jiskoot LC, Sanchez-Valle R, Graff C, Benussi L, et al. Neurofilament light chain: a biomarker for genetic frontotemporal dementia. Annals of Clinical and Translational Neurology. 2016;3(8):623-36.
154. Chipika RH, Siah WF, McKenna MC, Li Hi Shing S, Hardiman O, Bede P. The presymptomatic phase of amyotrophic lateral sclerosis: are we merely scratching the surface? Journal of neurology. 2020.
155. Li Hi Shing S, McKenna MC, Siah WF, Chipika RH, Hardiman O, Bede P. The imaging signature of C9orf72 hexanucleotide repeat expansions: implications for clinical trials and therapy development. Brain imaging and behavior. 2021.
156. Cash DM, Bocchetta M, Thomas DL, Dick KM, van Swieten JC, Borroni B, et al. Patterns of gray matter atrophy in genetic frontotemporal dementia: results from the GENFI study. Neurobiology of aging. 2018;62:191-6.
157. Grollemund V, Chat GL, Secchi-Buhour MS, Delbot F, Pradat-Peyre JF, Bede P, et al. Development and validation of a 1-year survival prognosis estimation model for Amyotrophic Lateral Sclerosis using manifold learning algorithm UMAP. Sci Rep. 2020;10(1):13378.
158. Blasco H, Patin F, Descat A, Garcon G, Corcia P, Gele P, et al. A pharmaco-metabolomics approach in a clinical trial of ALS: Identification of predictive markers of progression. PLoS One. 2018;13(6):e0198116.
159. Bede P, Murad A, Lope J, Li Hi Shing S, Finegan E, Chipika RH, et al. Phenotypic categorisation of individual subjects with motor neuron disease based on radiological disease burden patterns: A machine-learning approach. Journal of the neurological sciences. 2021;432:120079.
160. Rohrer JD, Geser F, Zhou J, Gennatas ED, Sidhu M, Trojanowski JQ, et al. TDP-43 subtypes are associated with distinct atrophy patterns in frontotemporal dementia. Neurology. 2010;75(24):2204-11.
161. Whitwell JL, Jack CR, Jr., Parisi JE, Senjem ML, Knopman DS, Boeve BF, et al. Does TDP-43 type confer a distinct pattern of atrophy in frontotemporal lobar degeneration? Neurology. 2010;75(24):2212-20.
162. Perry DC, Brown JA, Possin KL, Datta S, Trujillo A, Radke A, et al. Clinicopathological correlations in behavioural variant frontotemporal dementia. Brain : a journal of neurology. 2017;140(12):3329-45.
163. Bocchetta M, Gordon E, Cardoso MJ, Modat M, Ourselin S, Warren JD, et al. Thalamic atrophy in frontotemporal dementia - Not just a C9orf72 problem. Neuroimage Clin. 2018;18:675-81.

164. Bocchetta M, Iglesias JE, Neason M, Cash DM, Warren JD, Rohrer JD. Thalamic nuclei in frontotemporal dementia: Mediodorsal nucleus involvement is universal but pulvinar atrophy is unique to C9orf72. Human brain mapping. 2020;41(4):1006-16.
165. Hutchinson AD, Mathias JL. Neuropsychological deficits in frontotemporal dementia and Alzheimer's disease: a meta-analytic review. Journal of Neurology, Neurosurgery & Psychiatry. 2007;78(9):917.
166. Graham A, Davies R, Xuereb J, Halliday G, Kril J, Creasey H, et al. Pathologically proven frontotemporal dementia presenting with severe amnesia. Brain. 2005;128(3):597-605.
167. Knopman DS, Boeve BF, Parisi JE, Dickson DW, Smith GE, Ivnik RJ, et al. Antemortem diagnosis of frontotemporal lobar degeneration. Annals of Neurology. 2005;57(4):480-8.
168. Boutoleau-Bretonnière C, Lebouvier T, Delaroche O, Lamy E, Evrard C, Charriau T, et al. Value of neuropsychological testing, imaging, and CSF biomarkers for the differential diagnosis and prognosis of clinically ambiguous dementia. J Alzheimers Dis. 2012;28(2):323-36.
169. Swift IJ, Sogorb-Esteve A, Heller C, Synofzik M, Otto M, Graff C, et al. Fluid biomarkers in frontotemporal dementia: past, present and future. Journal of Neurology, Neurosurgery & Psychiatry. 2021;92(2):204-15.
170. Chouliaras L, Thomas A, Malpetti M, Donaghy P, Kane J, Mak E, et al. Differential levels of plasma biomarkers of neurodegeneration in Lewy body dementia, Alzheimer's disease, frontotemporal dementia and progressive supranuclear palsy. J Neurol Neurosurg Psychiatry. 2022.
171. Pemberton HG, Goodkin O, Prados F, Das RK, Vos SB, Moggridge J, et al. Automated quantitative MRI volumetry reports support diagnostic interpretation in dementia: a multi-rater, clinical accuracy study. Eur Radiol. 2021;31(7):5312-23.
172. Chipika RH, Finegan E, Li Hi Shing S, Hardiman O, Bede P. Tracking a Fast-Moving Disease: Longitudinal Markers, Monitoring, and Clinical Trial Endpoints in ALS. Front Neurol. 2019;10:229.
173. Stonnington CM, Tan G, Kloppel S, Chu C, Draganski B, Jack CR, Jr., et al. Interpreting scan data acquired from multiple scanners: a study with Alzheimer's disease. Neuroimage. 2008;39(3):1180-5.
174. Rosen H, Boeve B, Boxer A. Tracking disease progression in familial and sporadic frontotemporal lobar degeneration: Recent findings from ARTFL and LEFFTDS. Alzheimer's & dementia : the journal of the Alzheimer's Association. 2020;16:71-8.
175. Greaves CV, Rohrer JD. An update on genetic frontotemporal dementia. Journal of neurology. 2019;266(8):2075-86.
176. Panman JL, Venkatraghavan V, van der Ende EL, Steketee RME, Jiskoot LC, Poos JM, et al. Modelling the cascade of biomarker changes in GRN-related frontotemporal dementia. J Neurol Neurosurg Psychiatry. 2021;92(5):494-501.
177. Lulé DE, Müller HP, Finsel J, Weydt P, Knehr A, Winroth I, et al. Deficits in verbal fluency in presymptomatic C9orf72 mutation gene carriers-a developmental disorder. J Neurol Neurosurg Psychiatry. 2020;91(11):1195-200.
178. Fumagalli GG, Basilico P, Arighi A, Bocchetta M, Dick KM, Cash DM, et al. Distinct patterns of brain atrophy in Genetic Frontotemporal Dementia Initiative (GENFI) cohort revealed by visual rating scales. Alzheimer's research & therapy. 2018;10(1):46-.
179. Popuri K, Dowds E, Beg MF, Balachandar R, Bhalla M, Jacova C, et al. Gray matter changes in asymptomatic C9orf72 and GRN mutation carriers. NeuroImage: Clinical. 2018;18:591-8.
180. Le Blanc G, Jetté Pomerleau V, McCarthy J, Borroni B, van Swieten J, Galimberti D, et al. Faster Cortical Thinning and Surface Area Loss in Presymptomatic and Symptomatic C9orf72 Repeat Expansion Adult Carriers. Ann Neurol. 2020;88(1):113-22.
181. Panman JL, Jiskoot LC, Bouts MJRJ, Meeter LHH, van der Ende EL, Poos JM, et al. Gray and white matter changes in presymptomatic genetic frontotemporal dementia: a longitudinal MRI study. Neurobiology of Aging. 2019;76:115-24.
182. Walhout R, Schmidt R, Westeneng H-J, Verstraete E, Seelen M, van Rheenen W, et al. Brain morphologic changes in asymptomatic C9orf72 repeat expansion carriers. Neurology. 2015;85(20):1780.
183. Bocchetta M, Todd EG, Peakman G, Cash DM, Convery RS, Russell LL, et al. Differential early subcortical involvement in genetic FTD within the GENFI cohort. NeuroImage: Clinical. 2021;30:102646.
184. Bertrand A, Wen J, Rinaldi D, Houot M, Sayah S, Camuzat A, et al. Early Cognitive, Structural, and Microstructural Changes in Presymptomatic C9orf72 Carriers Younger Than 40 Years. JAMA Neurology. 2018;75(2):236-45.
185. Lee SE, Sias AC, Mandelli ML, Brown JA, Brown AB, Khazenzon AM, et al. Network degeneration and dysfunction in presymptomatic C9ORF72 expansion carriers. Neuroimage Clin. 2016;14:286-97.
186. Olney NT, Ong E, Goh SM, Bajorek L, Dever R, Staffaroni AM, et al. Clinical and volumetric changes with increasing functional impairment in familial frontotemporal lobar degeneration. Alzheimer's & dementia : the journal of the Alzheimer's Association. 2020;16(1):49-59.
187. Russell LL, Greaves CV, Bocchetta M, Nicholas J, Convery RS, Moore K, et al. Social cognition impairment in genetic frontotemporal dementia within the GENFI cohort. Cortex; a journal devoted to the study of the nervous system and behavior. 2020;133:384-98.

188. Papma JM, Jiskoot LC, Panman JL, Dopper EG, den Heijer T, Donker Kaat L, et al. Cognition and gray and white matter characteristics of presymptomatic C9orf72 repeat expansion. Neurology. 2017;89(12):1256.
189. McKenna MC, Chipika RH, Li Hi Shing S, Christidi F, Lope J, Doherty MA, et al. Infratentorial pathology in frontotemporal dementia: cerebellar grey and white matter alterations in FTD phenotypes. Journal of neurology. 2021;268(12):4687-97.
190. Tavares TP, Mitchell DGV, Coleman K, Shoesmith C, Bartha R, Cash DM, et al. Ventricular volume expansion in presymptomatic genetic frontotemporal dementia. Neurology. 2019;93(18):e1699-e706.
191. . !!! INVALID CITATION !!! 179, 182-185, 188.
192. Cury C, Durrleman S, Cash DM, Lorenzi M, Nicholas JM, Bocchetta M, et al. Spatiotemporal analysis for detection of pre-symptomatic shape changes in neurodegenerative diseases: Initial application to the GENFI cohort. NeuroImage. 2019;188:282-90.
193. McKenna MC, Li Hi Shing S, Murad A, Lope J, Hardiman O, Hutchinson S, et al. Focal thalamus pathology in frontotemporal dementia: Phenotype-associated thalamic profiles. Journal of the neurological sciences. 2022;436:120221.
194. Chipika RH, Christidi F, Finegan E, Li Hi Shing S, McKenna MC, Chang KM, et al. Amygdala pathology in amyotrophic lateral sclerosis and primary lateral sclerosis. Journal of the neurological sciences. 2020;417:117039.
195. Waugh RE, Danielian LE, Shoukry RFS, Floeter MK. Longitudinal changes in network homogeneity in presymptomatic C9orf72 mutation carriers. Neurobiol Aging. 2021;99:1-10.
196. Gazzina S, Grassi M, Premi E, Cosseddu M, Alberici A, Archetti S, et al. Education modulates brain maintenance in presymptomatic frontotemporal dementia. J Neurol Neurosurg Psychiatry. 2019;90(10):1124-30.
197. Premi E, Grassi M, van Swieten J, Galimberti D, Graff C, Masellis M, et al. Cognitive reserve and TMEM106B genotype modulate brain damage in presymptomatic frontotemporal dementia: a GENFI study. Brain. 2017;140(6):1784-91.
198. Malpetti M, Jones PS, Tsvetanov KA, Rittman T, van Swieten JC, Borroni B, et al. Apathy in presymptomatic genetic frontotemporal dementia predicts cognitive decline and is driven by structural brain changes. Alzheimer's & Dementia. 2021;17(6):969-83.
199. Caverzasi E, Battistella G, Chu SA, Rosen H, Zanto TP, Karydas A, et al. Gyrification abnormalities in presymptomatic c9orf72 expansion carriers. Journal of Neurology, Neurosurgery & Psychiatry. 2019;90(9):1005.
200. Wen J, Zhang H, Alexander DC, Durrleman S, Routier A, Rinaldi D, et al. Neurite density is reduced in the presymptomatic phase of C9orf72 disease. J Neurol Neurosurg Psychiatry. 2019;90(4):387-94.
201. Floeter MK, Bageac D, Danielian LE, Braun LE, Traynor BJ, Kwan JY. Longitudinal imaging in C9orf72 mutation carriers: Relationship to phenotype. Neuroimage Clin. 2016;12:1035-43.
202. Popuri K, Beg MF, Lee H, Balachandar R, Wang L, Sossi V, et al. FDG-PET in presymptomatic C9orf72 mutation carriers. NeuroImage: Clinical. 2021;31:102687.
203. Convery RS, Bocchetta M, Greaves CV, Moore KM, Cash DM, Van Swieten J, et al. Abnormal pain perception is associated with thalamo-cortico-striatal atrophy in C9orf72 expansion carriers in the GENFI cohort. Journal of Neurology, Neurosurgery & Psychiatry. 2020;91(12):1325.
204. Lulé DE, Müller H-P, Finsel J, Weydt P, Knehr A, Winroth I, et al. Deficits in verbal fluency in presymptomatic C9orf72 mutation gene carriers—a developmental disorder. Journal of Neurology, Neurosurgery & Psychiatry. 2020;91(11):1195-200.
205. Querin G, Bede P, El Mendili MM, Li M, Pélégrini-Issac M, Rinaldi D, et al. Presymptomatic spinal cord pathology in c9orf72 mutation carriers: A longitudinal neuroimaging study. Annals of Neurology. 2019;86(2):158-67.
206. Sudre CH, Bocchetta M, Cash D, Thomas DL, Woollacott I, Dick KM, et al. White matter hyperintensities are seen only in GRN mutation carriers in the GENFI cohort. Neuroimage Clin. 2017;15:171-80.
207. Premi E, Calhoun VD, Diano M, Gazzina S, Cosseddu M, Alberici A, et al. The inner fluctuations of the brain in presymptomatic Frontotemporal Dementia: The chronnectome fingerprint. NeuroImage. 2019;189:645-54.
208. Rittman T, Borchert R, Jones S, van Swieten J, Borroni B, Galimberti D, et al. Functional network resilience to pathology in presymptomatic genetic frontotemporal dementia. Neurobiol Aging. 2019;77:169-77.
209. De Vocht J, Blommaert J, Devrome M, Radwan A, Van Weehaeghe D, De Schaepdryver M, et al. Use of Multimodal Imaging and Clinical Biomarkers in Presymptomatic Carriers of C9orf72 Repeat Expansion. JAMA Neurology. 2020;77(8):1008-17.
210. Malpetti M, Holland N, Jones PS, Ye R, Cope TE, Fryer TD, et al. Synaptic density in carriers of C9orf72 mutations: a [(11) C]UCB-J PET study. Ann Clin Transl Neurol. 2021;8(7):1515-23.
211. Mutsaerts HJMM, Mirza SS, Petr J, Thomas DL, Cash DM, Bocchetta M, et al. Cerebral perfusion changes in presymptomatic genetic frontotemporal dementia: a GENFI study. Brain. 2019;142(4):1108-20.

212. Shoukry RS, Waugh R, Bartlett D, Raitcheva D, Floeter MK. Longitudinal changes in resting state networks in early presymptomatic carriers of C9orf72 expansions. NeuroImage: Clinical. 2020;28:102354.
213. Tsvetanov KA, Gazzina S, Jones PS, van Swieten J, Borroni B, Sanchez-Valle R, et al. Brain functional network integrity sustains cognitive function despite atrophy in presymptomatic genetic frontotemporal dementia. Alzheimer's & dementia : the journal of the Alzheimer's Association. 2021;17(3):500-14.
214. Borroni B, Alberici A, Cercignani M, Premi E, Serra L, Cerini C, et al. Granulin mutation drives brain damage and reorganization from preclinical to symptomatic FTLD. Neurobiol Aging. 2012;33(10):2506-20.
215. Borrego-Écija S, Sala-Llonch R, van Swieten J, Borroni B, Moreno F, Masellis M, et al. Disease-related cortical thinning in presymptomatic granulin mutation carriers. NeuroImage: Clinical. 2021;29:102540.
216. Premi E, Cauda F, Costa T, Diano M, Gazzina S, Gualeni V, et al. Looking for Neuroimaging Markers in Frontotemporal Lobar Degeneration Clinical Trials: A Multi-Voxel Pattern Analysis Study in Granulin Disease. J Alzheimers Dis. 2016;51(1):249-62.
217. Lee SE, Sias AC, Kosik EL, Flagan TM, Deng J, Chu SA, et al. Thalamo-cortical network hyperconnectivity in preclinical progranulin mutation carriers. Neuroimage Clin. 2019;22:101751.
218. Caroppo P, Habert MO, Durrleman S, Funkiewiez A, Perlbarg V, Hahn V, et al. Lateral Temporal Lobe: An Early Imaging Marker of the Presymptomatic GRN Disease? J Alzheimers Dis. 2015;47(3):751-9.
219. Gazzina S, Benussi A, Premi E, Paternicò D, Cristillo V, Dell'Era V, et al. Neuroanatomical Correlates of Transcranial Magnetic Stimulation in Presymptomatic Granulin Mutation Carriers. Brain Topogr. 2018;31(3):488-97.
220. Olm CA, McMillan CT, Irwin DJ, Van Deerlin VM, Cook PA, Gee JC, et al. Longitudinal structural gray matter and white matter MRI changes in presymptomatic progranulin mutation carriers. Neuroimage Clin. 2018;19:497-506.
221. Chen Q, Boeve BF, Senjem M, Tosakulwong N, Lesnick T, Brushaber D, et al. Trajectory of lobar atrophy in asymptomatic and symptomatic GRN mutation carriers: a longitudinal MRI study. Neurobiol Aging. 2020;88:42-50.
222. Milanesi E, Bonvicini C, Alberici A, Pilotto A, Cattane N, Premi E, et al. Molecular signature of disease onset in granulin mutation carriers: a gene expression analysis study. Neurobiol Aging. 2013;34(7):1837-45.
223. Sudre CH, Bocchetta M, Heller C, Convery R, Neason M, Moore KM, et al. White matter hyperintensities in progranulin-associated frontotemporal dementia: A longitudinal GENFI study. Neuroimage Clin. 2019;24:102077-.
224. McKenna MC, Murad A, Huynh W, Lope J, Bede P. The changing landscape of neuroimaging in frontotemporal lobar degeneration: from group-level observations to single-subject data interpretation. Expert review of neurotherapeutics. 2022;22(3):179-207.
225. Jacova C, Hsiung GY, Tawankanjanachot I, Dinelle K, McCormick S, Gonzalez M, et al. Anterior brain glucose hypometabolism predates dementia in progranulin mutation carriers. Neurology. 2013;81(15):1322-31.
226. Dopper EGP, Chalos V, Ghariq E, den Heijer T, Hafkemeijer A, Jiskoot LC, et al. Cerebral blood flow in presymptomatic MAPT and GRN mutation carriers: A longitudinal arterial spin labeling study. Neuroimage Clin. 2016;12:460-5.
227. Premi E, Cauda F, Gasparotti R, Diano M, Archetti S, Padovani A, et al. Multimodal FMRI resting-state functional connectivity in granulin mutations: the case of fronto-parietal dementia. PLoS One. 2014;9(9):e106500-e.
228. Premi E, Gazzina S, Bozzali M, Archetti S, Alberici A, Cercignani M, et al. Cognitive reserve in granulin-related frontotemporal dementia: from preclinical to clinical stages. PLoS One. 2013;8(9):e74762-e.
229. Costello E, Rooney J, Pinto-Grau M, Burke T, Elamin M, Bede P, et al. Cognitive reserve in amyotrophic lateral sclerosis (ALS): a population-based longitudinal study. J Neurol Neurosurg Psychiatry. 2021.
230. Premi E, Giunta M, Iraji A, Rachakonda S, Calhoun VD, Gazzina S, et al. Dissemination in time and space in presymptomatic granulin mutation carriers: a GENFI spatial chronnectome study. Neurobiol Aging. 2021;108:155-67.
231. Proudfoot M, Bede P, Turner MR. Imaging Cerebral Activity in Amyotrophic Lateral Sclerosis. Front Neurol. 2018;9:1148.
232. Bede P, Bogdahn U, Lope J, Chang KM, Xirou S, Christidi F. Degenerative and regenerative processes in amyotrophic lateral sclerosis: motor reserve, adaptation and putative compensatory changes. Neural regeneration research. 2021;16(6):1208-9.
233. Paternicò D, Premi E, Gazzina S, Cosseddu M, Alberici A, Archetti S, et al. White matter hyperintensities characterize monogenic frontotemporal dementia with granulin mutations. Neurobiol Aging. 2016;38:176-80.
234. Chen Q, Boeve BF, Tosakulwong N, Lesnick T, Brushaber D, Dheel C, et al. Brain MR Spectroscopy Changes Precede Frontotemporal Lobar Degeneration Phenoconversion in Mapt Mutation Carriers. J Neuroimaging. 2019;29(5):624-9.

235. Clarke MTM, St-Onge F, Beauregard JM, Bocchetta M, Todd E, Cash DM, et al. Early anterior cingulate involvement is seen in presymptomatic MAPT P301L mutation carriers. Alzheimers Res Ther. 2021;13(1):42.
236. Domínguez-Vivero C, Wu L, Lee S, Manoochehri M, Cines S, Brickman AM, et al. Structural Brain Changes in Pre-Clinical FTD MAPT Mutation Carriers. J Alzheimers Dis. 2020;75(2):595-606.
237. Miyoshi M, Shinotoh H, Wszolek ZK, Strongosky AJ, Shimada H, Arakawa R, et al. In vivo detection of neuropathologic changes in presymptomatic MAPT mutation carriers: A PET and MRI study. Parkinsonism & Related Disorders. 2010;16(6):404-8.
238. Kantarci K, Boeve BF, Wszolek ZK, Rademakers R, Whitwell JL, Baker MC, et al. MRS in presymptomatic MAPT mutation carriers: a potential biomarker for tau-mediated pathology. Neurology. 2010;75(9):771-8.
239. Chen Q, Boeve BF, Schwarz CG, Reid R, Tosakulwong N, Lesnick TG, et al. Tracking white matter degeneration in asymptomatic and symptomatic MAPT mutation carriers. Neurobiol Aging. 2019;83:54-62.
240. Christidi F, Karavasilis E, Argyropoulos GD, Velonakis G, Zouvelou V, Murad A, et al. Neurometabolic Alterations in Motor Neuron Disease: Insights from Magnetic Resonance Spectroscopy. Journal of integrative neuroscience. 2022;21(3):87.
241. Chen Q, Boeve BF, Tosakulwong N, Lesnick T, Brushaber D, Dheel C, et al. Frontal lobe (1)H MR spectroscopy in asymptomatic and symptomatic MAPT mutation carriers. Neurology. 2019;93(8):e758-e65.
242. Wolters EE, Papma JM, Verfaillie SCJ, Visser D, Weltings E, Groot C, et al. [(18)F]Flortaucipir PET Across Various MAPT Mutations in Presymptomatic and Symptomatic Carriers. Neurology. 2021;97(10):e1017-e30.
243. Bede P, Siah WF, McKenna MC, Li Hi Shing S. Consideration of C9orf72-associated ALS-FTD as a neurodevelopmental disorder: insights from neuroimaging. J Neurol Neurosurg Psychiatry. 2020.
244. Brettschneider J, Del Tredici K, Irwin DJ, Grossman M, Robinson JL, Toledo JB, et al. Sequential distribution of pTDP-43 pathology in behavioral variant frontotemporal dementia (bvFTD). Acta Neuropathologica. 2014;127(3):423-39.
245. Yeh T-H, Liu H-F, Li Y-W, Lu C-S, Shih H-Y, Chiu C-C, et al. C9orf72 is essential for neurodevelopment and motility mediated by Cyclin G1. Experimental Neurology. 2018;304:114-24.
246. Xu W, Xu J. C9orf72 Dipeptide Repeats Cause Selective Neurodegeneration and Cell-Autonomous Excitotoxicity in Drosophila Glutamatergic Neurons. J Neurosci. 2018;38(35):7741-52.
247. Chipika RH, Finegan E, Li Hi Shing S, McKenna MC, Christidi F, Chang KM, et al. "Switchboard" malfunction in motor neuron diseases: Selective pathology of thalamic nuclei in amyotrophic lateral sclerosis and primary lateral sclerosis. Neuroimage Clin. 2020;27:102300.
248. Chipika RH, Siah WF, McKenna MC, Li Hi Shing S, Hardiman O, Bede P. The presymptomatic phase of amyotrophic lateral sclerosis: are we merely scratching the surface? Journal of neurology. 2021;268(12):4607-29.
249. El Mendili MM, Querin G, Bede P, Pradat PF. Spinal Cord Imaging in Amyotrophic Lateral Sclerosis: Historical Concepts-Novel Techniques. Front Neurol. 2019;10:350.
250. Bede P, Bokde AL, Byrne S, Elamin M, Fagan AJ, Hardiman O. Spinal cord markers in ALS: diagnostic and biomarker considerations. Amyotrophic lateral sclerosis : official publication of the World Federation of Neurology Research Group on Motor Neuron Diseases. 2012;13(5):407-15.
251. Tran H, Moazami MP, Yang H, McKenna-Yasek D, Douthwright CL, Pinto C, et al. Suppression of mutant C9orf72 expression by a potent mixed backbone antisense oligonucleotide. Nature Medicine. 2022;28(1):117-24.
252. Tabrizi SJ, Reilmann R, Roos RA, Durr A, Leavitt B, Owen G, et al. Potential endpoints for clinical trials in premanifest and early Huntington's disease in the TRACK-HD study: analysis of 24 month observational data. Lancet Neurol. 2012;11(1):42-53.
253. Tahedl M, Murad A, Lope J, Hardiman O, Bede P. Evaluation and categorisation of individual patients based on white matter profiles: Single-patient diffusion data interpretation in neurodegeneration. Journal of the neurological sciences. 2021;428:117584.
254. Burke T, Elamin M, Bede P, Pinto-Grau M, Lonergan K, Hardiman O, et al. Discordant performance on the 'Reading the Mind in the Eyes' Test, based on disease onset in amyotrophic lateral sclerosis. Amyotrophic lateral sclerosis & frontotemporal degeneration. 2016;17(7-8):467-72.
255. Pradat PF, Bernard E, Corcia P, Couratier P, Jublanc C, Querin G, et al. The French national protocol for Kennedy's disease (SBMA): consensus diagnostic and management recommendations. Orphanet journal of rare diseases. 2020;15(1):90.
256. Querin G, El Mendili MM, Lenglet T, Behin A, Stojkovic T, Salachas F, et al. The spinal and cerebral profile of adult spinal-muscular atrophy: A multimodal imaging study. Neuroimage Clin. 2019;21:101618.
257. Benatar M, Turner MR, Wuu J. Defining pre-symptomatic amyotrophic lateral sclerosis. Amyotrophic lateral sclerosis & frontotemporal degeneration. 2019;20(5-6):303-9.
258. Querin G, El Mendili M-M, Lenglet T, Behin A, Stojkovic T, Salachas F, et al. The spinal and cerebral profile of adult spinal-muscular atrophy: A multimodal imaging study. NeuroImage: Clinical. 2019;21:101618.

259. de Borba FC, Querin G, França MC, Pradat P-F. Cerebellar degeneration in adult spinal muscular atrophy patients. Journal of neurology. 2020;267(9):2625-31.
260. Finegan E, Shing SLH, Chipika RH, Chang KM, McKenna MC, Doherty MA, et al. Extra-motor cerebral changes and manifestations in primary lateral sclerosis. Brain imaging and behavior. 2021.
261. Montuschi A, Iazzolino B, Calvo A, Moglia C, Lopiano L, Restagno G, et al. Cognitive correlates in amyotrophic lateral sclerosis: a population-based study in Italy. J Neurol Neurosurg Psychiatry. 2015;86(2):168-73.
262. Phukan J, Elamin M, Bede P, Jordan N, Gallagher L, Byrne S, et al. The syndrome of cognitive impairment in amyotrophic lateral sclerosis: a population-based study. J Neurol Neurosurg Psychiatry. 2012;83(1):102-8.
263. de Vries BS, Spreij LA, Rustemeijer LMM, Bakker LA, Veldink JH, van den Berg LH, et al. A neuropsychological and behavioral study of PLS. Amyotrophic lateral sclerosis & frontotemporal degeneration. 2019;20(5-6):376-84.
264. de Vries BS, Rustemeijer LMM, Bakker LA, Schröder CD, Veldink JH, van den Berg LH, et al. Cognitive and behavioural changes in PLS and PMA:challenging the concept of restricted phenotypes. J Neurol Neurosurg Psychiatry. 2019;90(2):141-7.
265. Traynor BJ, Codd MB, Corr B, Forde C, Frost E, Hardiman O. Amyotrophic lateral sclerosis mimic syndromes: a population-based study. Arch Neurol. 2000;57(1):109-13.
266. Denora PS, Smets K, Zolfanelli F, Ceuterick-de Groote C, Casali C, Deconinck T, et al. Motor neuron degeneration in spastic paraplegia 11 mimics amyotrophic lateral sclerosis lesions. Brain. 2016;139(6):1723-34.
267. Romagnolo A, Masera S, Mattioda A, Superti G, Santorelli FM, Mongini T, et al. Atypical hereditary spastic paraplegia mimicking multiple sclerosis associated with a novel SPG11 mutation. European Journal of Neurology. 2014;21(2):e14-e5.
268. Visser J, van den Berg-Vos RM, Franssen H, van den Berg LH, Vogels OJ, Wokke JHJ, et al. Mimic syndromes in sporadic cases of progressive spinal muscular atrophy. Neurology. 2002;58(11):1593.
269. Rasmussen H, Hellzen O, Stordal E, Enmarker I. Family caregivers experiences of the pre-diagnostic stage in frontotemporal dementia. Geriatric Nursing. 2019;40(3):246-51.
270. Diehl-Schmid J, Schmidt E-M, Nunnemann S, Riedl L, Kurz A, Förstl H, et al. Caregiver Burden and Needs in Frontotemporal Dementia. Journal of Geriatric Psychiatry and Neurology. 2013;26(4):221-9.
271. Le Forestier N, Maisonobe T, Piquard A, Rivaud S, Crevier-Buchman L, Salachas F, et al. Does primary lateral sclerosis exist? A study of 20 patients and a review of the literature. Brain. 2001;124(Pt 10):1989-99.
272. Finegan E, Chipika RH, Li Hi Shing S, Doherty MA, Hengeveld JC, Vajda A, et al. The clinical and radiological profile of primary lateral sclerosis: a population-based study. Journal of neurology. 2019;266(11):2718-33.
273. de Vries BS, Rustemeijer LMM, van der Kooi AJ, Raaphorst J, Schröder CD, Nijboer TCW, et al. A case series of PLS patients with frontotemporal dementia and overview of the literature. Amyotrophic Lateral Sclerosis and Frontotemporal Degeneration. 2017;18(7-8):534-48.
274. Canu E, Agosta F, Galantucci S, Chio A, Riva N, Silani V, et al. Extramotor damage is associated with cognition in primary lateral sclerosis patients. PLoS ONE [Electronic Resource]. 2013;8(12):e82017.
275. Meoded A, Kwan JY, Peters TL, Huey ED, Danielian LE, Wiggs E, et al. Imaging Findings Associated with Cognitive Performance in Primary Lateral Sclerosis and Amyotrophic Lateral Sclerosis. Dementia and geriatric cognitive disorders extra. 2013;3(1):233-50.
276. Van Der Graaff MM, Sage CA, Caan MWA, Akkerman EM, Lavini C, Majoie CB, et al. Upper and extra-motoneuron involvement in early motoneuron disease: A diffusion tensor imaging study. Brain. 2011;134(4):1211-28.
277. Tartaglia MC, Laluz V, Rowe A, Findlater K, Lee DH, Kennedy K, et al. Brain atrophy in primary lateral sclerosis. Neurology. 2009;72(14):1236-41.
278. Agosta F, Canu E, Inuggi A, Chio A, Riva N, Silani V, et al. Resting state functional connectivity alterations in primary lateral sclerosis. Neurobiol Aging. 2014;35(4):916-25.
279. Clark MG, Smallwood Shoukry R, Huang CJ, Danielian LE, Bageac D, Floeter MK. Loss of functional connectivity is an early imaging marker in primary lateral sclerosis. Amyotrophic Lateral Sclerosis and Frontotemporal Degeneration. 2018:1-8.
280. Mitsumoto H, Ulug AM, Pullman SL, Gooch CL, Chan S, Tang MX, et al. Quantitative objective markers for upper and lower motor neuron dysfunction in ALS. Neurology. 2007;68(17):1402-10.
281. Menke RA, Abraham I, Thiel CS, Filippini N, Knight S, Talbot K, et al. Fractional anisotropy in the posterior limb of the internal capsule and prognosis in amyotrophic lateral sclerosis. Archives of Neurology. 2012;69(11):1493-9.
282. Fabes J, Matthews L, Filippini N, Talbot K, Jenkinson M, Turner MR. Quantitative FLAIR MRI in Amyotrophic Lateral Sclerosis. Academic Radiology. 2017;24(10):1187-94.
283. Kolind S, Sharma R, Knight S, Johansen-Berg H, Talbot K, Turner MR. Myelin imaging in amyotrophic and primary lateral sclerosis. Amyotrophic Lateral Sclerosis and Frontotemporal Degeneration. 2013;14(7-8):562-73.

284. Kwan JY, Meoded A, Danielian LE, Wu T, Floeter MK. Structural imaging differences and longitudinal changes in primary lateral sclerosis and amyotrophic lateral sclerosis. NeuroImage: Clinical. 2013;2(1):151-60.
285. Smith CD. Serial MRI findings in a case of primary lateral sclerosis. Neurology. 2002;58(4):647-9.
286. Turner MR, Hammers A, Al-Chalabi A, Shaw CE, Andersen PM, Brooks DJ, et al. Cortical involvement in four cases of primary lateral sclerosis using [11C]-flumazenil PET. Journal of neurology. 2007;254(8):1033-6.
287. Van Weehaeghe D, Ceccarini J, Delva A, Robberecht W, Van Damme P, Van Laere K. Prospective validation of 18F-FDG brain PET discriminant analysis methods in the diagnosis of amyotrophic lateral sclerosis. Journal of Nuclear Medicine. 2016;57(8):1238-43.
288. Van Laere K, Vanhee A, Verschueren J, De Coster L, Driesen A, Dupont P, et al. Value of 18fluorodeoxyglucose-positron-emission tomography in amyotrophic lateral sclerosis: a prospective study. JAMA Neurol. 2014;71(5):553-61.
289. Paganoni S, Alshikho MJ, Zürcher NR, Cernasov P, Babu S, Loggia ML, et al. Imaging of glia activation in people with primary lateral sclerosis. NeuroImage: Clinical. 2018;17:347-53.
290. Turner MR, Gerhard A, Al-Chalabi A, Shaw CE, Hughes RAC, Banati RB, et al. Mills' and other isolated upper motor neurone syndromes: in vivo study with 11C-(R)-PK11195 PET. J Neurol Neurosurg Psychiatry. 2005;76(6):871-4.
291. Alshikho MJ, Zurcher NR, Loggia ML, Cernasov P, Reynolds B, Pijanowski O, et al. Integrated magnetic resonance imaging and [(11) C]-PBR28 positron emission tomographic imaging in amyotrophic lateral sclerosis. Ann Neurol. 2018;83(6):1186-97.
292. Charil A, Corbo M, Filippi M, Kesavadas C, Agosta F, Munerati E, et al. Structural and metabolic changes in the brain of patients with upper motor neuron disorders: A multiparametric MRI study. Amyotrophic Lateral Sclerosis. 2009;10(5-6):269-79.
293. van der Graaff MM, Lavini C, Akkerman EM, Majoie Ch B, Nederveen AJ, Zwinderman AH, et al. MR spectroscopy findings in early stages of motor neuron disease. AJNR Am J Neuroradiol. 2010;31(10):1799-806.
294. Zhai P, Pagan F, Statland J, Butman JA, Floeter MK. Primary lateral sclerosis. Neurology. 2003;60(8):1258.
295. Chan S, Shungu DC, Douglas-Akinwande A, Lange DJ, Rowland LP. Motor Neuron Diseases: Comparison of Single-Voxel Proton MR Spectroscopy of the Motor Cortex with MR Imaging of the Brain. Radiology. 1999;212(3):763-9.
296. Meoded A, Morrissette AE, Katipally R, Schanz O, Gotts SJ, Floeter MK. Cerebro-cerebellar connectivity is increased in primary lateral sclerosis. NeuroImage Clinical. 2015;7:288-96.
297. Basaia S, Agosta F, Cividini C, Trojsi F, Riva N, Spinelli EG, et al. Structural and functional brain connectome in motor neuron diseases. A multicenter MRI study. 2020;95(18):e2552-e64.
298. Gazulla J, Ferrer I, Izquierdo-Alvarez S, Alvarez S, Sánchez-Alcudia R, Bestué-Cardiel M, et al. Hereditary primary lateral sclerosis and progressive nonfluent aphasia. Journal of neurology. 2019;266(5):1079-90.
299. Kobayashi Z, Tsuchiya K, Arai T, Yokota O, Yoshida M, Shimomura Y, et al. Clinicopathological characteristics of FTLD-TDP showing corticospinal tract degeneration but lacking lower motor neuron loss. Journal of the neurological sciences. 2010;298(1-2):70-7.
300. Konagaya M, Sakai M, Matsuoka Y, Konagaya Y, Hashizume Y. Upper motor neuron predominant degeneration with frontal and temporal lobe atrophy. Acta Neuropathologica. 1998;96(5):532-6.
301. Mochizuki A, Komatsuzaki Y, Iwamoto H, Shoji S. Frontotemporal dementia with ubiquitinated neuronal inclusions presenting with primary lateral sclerosis and parkinsonism: clinicopathological report of an autopsy case. Acta Neuropathol. 2004;107(4):377-80.
302. Tan CF, Kakita A, Piao YS, Kikugawa K, Endo K, Tanaka M, et al. Primary lateral sclerosis: a rare upper-motor-predominant form of amyotrophic lateral sclerosis often accompanied by frontotemporal lobar degeneration with ubiquitinated neuronal inclusions? Report of an autopsy case and a review of the literature. Acta Neuropathologica. 2003;105(6):615-20.
303. Kosaka T, Fu YJ, Shiga A, Ishidaira H, Tan CF, Tani T, et al. Primary lateral sclerosis: upper-motor-predominant amyotrophic lateral sclerosis with frontotemporal lobar degeneration--immunohistochemical and biochemical analyses of TDP-43. Neuropathology : official journal of the Japanese Society of Neuropathology. 2012;32(4):373-84.
304. Hirsch-Reinshagen V, Alfaify OA, Hsiung GR, Pottier C, Baker M, Perkerson RB, 3rd, et al. Clinicopathologic correlations in a family with a TBK1 mutation presenting as primary progressive aphasia and primary lateral sclerosis. Amyotrophic lateral sclerosis & frontotemporal degeneration. 2019;20(7-8):568-75.
305. Mackenzie IRA, Briemberg H. TDP-43 pathology in primary lateral sclerosis. Amyotrophic lateral sclerosis & frontotemporal degeneration. 2020:1-7.
306. Liewluck T, Saperstein DS. Progressive Muscular Atrophy. Neurol Clin. 2015;33(4):761-73.
307. Nishihira Y, Tan C-F, Hoshi Y, Iwanaga K, Yamada M, Kawachi I, et al. Sporadic amyotrophic lateral sclerosis of long duration is associated with relatively mild TDP-43 pathology. Acta Neuropathologica. 2008;117(1):45.

308. Geser F, Stein B, Partain M, Elman LB, McCluskey LF, Xie SX, et al. Motor neuron disease clinically limited to the lower motor neuron is a diffuse TDP-43 proteinopathy. Acta Neuropathologica. 2011;121(4):509-17.
309. Kim WK, Liu X, Sandner J, Pasmantier M, Andrews J, Rowland LP, et al. Study of 962 patients indicates progressive muscular atrophy is a form of ALS. Neurology. 2009;73(20):1686-92.
310. Ince PG, Evans J, Knopp M, Forster G, Hamdalla HHM, Wharton SB, et al. Corticospinal tract degeneration in the progressive muscular atrophy variant of ALS. Neurology. 2003;60(8):1252-8.
311. Raaphorst J, de Visser M, van Tol M-J, Linssen WHJP, van der Kooi AJ, de Haan RJ, et al. Cognitive dysfunction in lower motor neuron disease: executive and memory deficits in progressive muscular atrophy. Journal of Neurology, Neurosurgery & Psychiatry. 2011;82(2):170-5.
312. Agosta F, Ferraro PM, Riva N, Spinelli EG, Chiò A, Canu E, et al. Structural brain correlates of cognitive and behavioral impairment in MND. Human brain mapping. 2016;37(4):1614-26.
313. Raaphorst J, van Tol MJ, Groot PF, Altena E, van der Werf YD, Majoie CB, et al. Prefrontal involvement related to cognitive impairment in progressive muscular atrophy. Neurology. 2014;83(9):818-25.
314. Kew JJ, Brooks DJ, Passingham RE, Rothwell JC, Frackowiak RS, Leigh PN. Cortical function in progressive lower motor neuron disorders and amyotrophic lateral sclerosis: a comparative PET study. Neurology. 1994;44(6):1101-10.
315. Quinn C, Elman L, McCluskey L, Hoskins K, Karam C, Woo JH, et al. Frontal lobe abnormalities on MRS correlate with poor letter fluency in ALS. Neurology. 2012;79(6):583-8.
316. Wicks P, Abrahams S, Leigh PN, Williams T, Goldstein LH. Absence of cognitive, behavioral, or emotional dysfunction in progressive muscular atrophy. Neurology. 2006;67(9):1718-9.
317. Riku Y, Atsuta N, Yoshida M, Tatsumi S, Iwasaki Y, Mimuro M, et al. Differential motor neuron involvement in progressive muscular atrophy: a comparative study with amyotrophic lateral sclerosis. BMJ Open. 2014;4(5):e005213.
318. D'Amico A, Mercuri E, Tiziano FD, Bertini E. Spinal muscular atrophy. Orphanet journal of rare diseases. 2011;6(1):71.
319. Losito L, Gennaro L, Lucarelli E, Trabacca A. Brain MRI abnormalities in a child with spinal muscular atrophy type II. Acta Neurologica Belgica. 2020.
320. Maeda K, Chong PF, Yamashita F, Akamine S, Kawakami S, Saito K, et al. Global Central Nervous System Atrophy in Spinal Muscular Atrophy Type 0. Ann Neurol. 2019;86(5):801-2.
321. Ito Y, Kumada S, Uchiyama A, Saito K, Osawa M, Yagishita A, et al. Thalamic lesions in a long-surviving child with spinal muscular atrophy type I: MRI and EEG findings. Brain and Development. 2004;26(1):53-6.
322. Mendonça RH, Rocha AJ, Lozano-Arango A, Diaz AB, Castiglioni C, Silva AMS, et al. Severe brain involvement in 5q spinal muscular atrophy type 0. Annals of Neurology. 2019;86(3):458-62.
323. Mix L, Schreiber-Katz O, Wurster CD, Uzelac Z, Platen S, Gipperich C, et al. Executive function is inversely correlated with physical function: the cognitive profile of adult Spinal Muscular Atrophy (SMA). Orphanet journal of rare diseases. 2021;16(1):10.
324. Billard C, Gillet P, Signoret JL, Uicaut E, Bertrand P, Fardeau M, et al. Cognitive functions in duchenne muscular dystrophy: A reappraisal and comparison with spinal muscular atrophy. Neuromuscular Disorders. 1992;2(5):371-8.
325. Billard C, Gillet P, Barthez M-A, Hommet C, Bertrand P. Reading ability and processing in Duchenne muscular dystrophy and spinal muscular atrophy. Developmental Medicine & Child Neurology. 1998;40(1):12-20.
326. Oudgenoeg-Paz O, Rivière J. Self-locomotion and spatial language and spatial cognition: insights from typical and atypical development. Front Psychol. 2014;5:521.
327. Polido GJ, de Miranda MMV, Carvas N, Mendonça RdH, Caromano FA, Reed UC, et al. Cognitive performance of children with spinal muscular atrophy: A systematic review. Dement Neuropsychol. 2019;13(4):436-43.
328. Bénony C, Bénony H. Precocity of the acquisition of language and type II spinal muscular atrophy in 3-4-year-old children: a study of 12 cases. Eur J Paediatr Neurol. 2005;9(2):71-6.
329. Rivière J, Lécuyer R. Spatial cognition in young children with spinal muscular atrophy. Dev Neuropsychol. 2002;21(3):273-83.
330. Riviere J, Lecuyer R. The C-not-B error: a comparative study. Cognitive Development. 2003;18(3):285-97.
331. Leaffer E, Hinton V, Salazar R, Montes J, Dunaway Young S, Holuba LaMarca N, et al. Pediatrics-1Spinal Muscular Atrophy Type I: Cases of Normal Cognitive Function Despite having Limited Motor Function and Physical-Environmental Interaction. Archives of Clinical Neuropsychology. 2015;30(6):481-.
332. von Gontard A, Zerres K, Backes M, Laufersweiler-Plass C, Wendland C, Melchers P, et al. Intelligence and cognitive function in children and adolescents with spinal muscular atrophy. Neuromuscular Disorders. 2002;12(2):130-6.
333. Polido GJ, Barbosa AF, Morimoto CH, Caromano FA, Favero FM, Zanoteli E, et al. Matching pairs difficulty in children with spinal muscular atrophy type I. Neuromuscul Disord. 2017;27(5):419-27.
334. Thirunavukkarasu B, Gupta K, Bansal A, Dhanasekaran N, Baranwal A. Spinal Muscular Atrophy: Autopsy Based Neuropathological Demonstration. Neurol India. 2020;68(4):882-5.

335. Kuru S, Sakai M, Konagaya M, Yoshida M, Hashizume Y, Saito K. An autopsy case of spinal muscular atrophy type III (Kugelberg-Welander disease). Neuropathology : official journal of the Japanese Society of Neuropathology. 2009;29(1):63-7.
336. Harding BN, Kariya S, Monani UR, Chung WK, Benton M, Yum SW, et al. Spectrum of Neuropathophysiology in Spinal Muscular Atrophy Type I. Journal of Neuropathology & Experimental Neurology. 2015;74(1):15-24.
337. Araki S, Hayashi M, Tamagawa K, Saito M, Kato S, Komori T, et al. Neuropathological analysis in spinal muscular atrophy type II. Acta Neuropathol. 2003;106(5):441-8.
338. Finsterer J, Scorza FA. Central nervous system abnormalities in spinal and bulbar muscular atrophy (Kennedy's disease). Clinical Neurology and Neurosurgery. 2019;184:105426.
339. Manzano R, Sorarú G, Grunseich C, Fratta P, Zuccaro E, Pennuto M, et al. Beyond motor neurons: expanding the clinical spectrum in Kennedy's disease. Journal of Neurology, Neurosurgery & Psychiatry. 2018;89(8):808-12.
340. Kennedy WR, Alter M, Sung JH. Progressive proximal spinal and bulbar muscular atrophy of late onset. A sex-linked recessive trait. 1998;50(3):583-.
341. Soukup GR, Sperfeld A-D, Uttner I, Karitzky J, Ludolph AC, Kassubek J, et al. Frontotemporal cognitive function in X-linked spinal and bulbar muscular atrophy (SBMA): a controlled neuropsychological study of 20 patients. Journal of neurology. 2009;256(11):1869-75.
342. Di Rosa E, Sorarù G, Kleinbub JR, Calvo V, Vallesi A, Querin G, et al. Theory of mind, empathy and neuropsychological functioning in X-linked Spinal and Bulbar Muscular Atrophy: a controlled study of 20 patients. Journal of neurology. 2015;262(2):394-401.
343. Kasper E, Wegrzyn M, Marx I, Korp C, Kress W, Benecke R, et al. Minor cognitive disturbances in X-linked spinal and bulbar muscular atrophy, Kennedy's disease. Amyotrophic Lateral Sclerosis and Frontotemporal Degeneration. 2014;15(1-2):15-20.
344. Pieper CC, Konrad C, Sommer J, Teismann I, Schiffbauer H. Structural changes of central white matter tracts in Kennedy's disease – a diffusion tensor imaging and voxel-based morphometry study. Acta Neurologica Scandinavica. 2013;127(5):323-8.
345. Kassubek J, Juengling FD, Sperfeld A-D. Widespread white matter changes in Kennedy disease: a voxel based morphometry study. Journal of Neurology, Neurosurgery & Psychiatry. 2007;78(11):1209-12.
346. Lai T-H, Liu R-S, Yang B-H, Wang P-S, Lin K-P, Lee Y-C, et al. Cerebral involvement in spinal and bulbar muscular atrophy (Kennedy's disease): A pilot study of PET. Journal of the neurological sciences. 2013;335(1):139-44.
347. Unrath A, Müller H-P, Riecker A, Ludolph AC, Sperfeld A-D, Kassubek J. Whole brain-based analysis of regional white matter tract alterations in rare motor neuron diseases by diffusion tensor imaging. Human brain mapping. 2010;31(11):1727-40.
348. Garaci F, Toschi N, Lanzafame S, Marfia GA, Marziali S, Meschini A, et al. Brain MR diffusion tensor imaging in Kennedy's disease. Neuroradiol J. 2015;28(2):126-32.
349. Karitzky J, Block W, Mellies JK, Träber F, Sperfeld A, Schild HH, et al. Proton Magnetic Resonance Spectroscopy in Kennedy Syndrome. Archives of Neurology. 1999;56(12):1465-71.
350. Mader I, Karitzky J, Klose U, Seeger U, Sperfeld A, Naegele T, et al. Proton MRS in Kennedy disease: Absolute metabolite and macromolecular concentrations. Journal of Magnetic Resonance Imaging. 2002;16(2):160-7.
351. Cianfoni A, Law M, Re TJ, Dubowitz DJ, Rumboldt Z, Imbesi SG. Clinical pitfalls related to short and long echo times in cerebral MR spectroscopy. Journal of Neuroradiology. 2011;38(2):69-75.
352. Kessler H, Prudlo J, Kraft S, Supprian T. Dementia of frontal lobe type in Kennedy's disease. Amyotrophic Lateral Sclerosis. 2005;6(4):250-3.
353. Shaw PJ, Thagesen H, Tomkins J, Slade JY, Usher P, Jackson A, et al. Kennedy's disease: unusual molecular pathologic and clinical features. Neurology. 1998;51(1):252-5.
354. Sobue GEN, Hashizume Y, Mukai E, Hirayama M, Mitsuma T, Takahashi A. X-LINKED RECESSIVE BULBOSPINAL NEURONOPATHY: A CLINICOPATHOLOGICAL STUDY. Brain. 1989;112(1):209-32.
355. Adachi H, Katsuno M, Minamiyama M, Waza M, Sang C, Nakagomi Y, et al. Widespread nuclear and cytoplasmic accumulation of mutant androgen receptor in SBMA patients. Brain. 2005;128(3):659-70.
356. Trojan DA, Narayanan S, Francis SJ, Caramanos Z, Robinson A, Cardoso M, et al. Brain volume and fatigue in patients with postpoliomyelitis syndrome. Pm r. 2014;6(3):215-20.
357. Bruno RL, Cohen JM, Galski T, Frick NM. The neuroanatomy of post-polio fatigue. Arch Phys Med Rehabil. 1994;75(5):498-504.
358. Bruno RL, Zimmerman JR. Word finding difficulty as a post-polio sequelae. Am J Phys Med Rehabil. 2000;79(4):343-8.
359. Ostlund G, Borg K, Wahlin A. Cognitive functioning in post-polio patients with and without general fatigue. J Rehabil Med. 2005;37(3):147-51.
360. Hazendonk KM, Crowe SF. A neuropsychological study of the postpolio syndrome: support for depression without neuropsychological impairment. Neuropsychiatry Neuropsychol Behav Neurol. 2000;13(2):112-8.
361. Li Hi Shing S, Lope J, Chipika RH, Hardiman O, Bede P. Extra-motor manifestations in post-polio syndrome (PPS): fatigue, cognitive symptoms and radiological features. Neurological Sciences. 2021.

362. Li Hi Shing S, Lope J, McKenna MC, Chipika RH, Hardiman O, Bede P. Increased cerebral integrity metrics in poliomyelitis survivors: putative adaptation to longstanding lower motor neuron degeneration. Journal of the neurological sciences. 2021:117361.
363. Demir CF, Berilgen MS, Mungen B, Bulut S. Do polio survivors have a higher risk of epilepsy? Epilepsy Res. 2012;98(1):72-5.
364. França MC, Schmutzler KMR, Garibaldi SG, Zanardi VA, Nucci A. Bilateral substantia nigra involvement in vaccine-associated poliomyelitis. Neurology. 2006;66(10):1597-8.
365. MATZKE HA, BAKER AB. POLIOMYELITIS: IV. A Study of the Midbrain. AMA Archives of Neurology & Psychiatry. 1951;65(1):1-15.
366. Miller DC. Post-polio syndrome spinal cord pathology. Case report with immunopathology. Ann N Y Acad Sci. 1995;753:186-93.
367. Shimada A, Lange DJ, Hays AP. Amyotrophic lateral sclerosis in an adult following acute paralytic poliomyelitis in early childhood. Acta Neuropathol. 1999;97(3):317-21.
368. Casula M, Steentjes K, Aronica E, van Geel BM, Troost D. Concomitant CNS pathology in a patient with amyotropic lateral sclerosis following poliomyelitis in childhood. Clin Neuropathol. 2011;30(3):111-7.
369. Agosta F, Scarlato M, Spinelli EG, Canu E, Benedetti S, Bassi MT, et al. Hereditary Spastic Paraplegia: Beyond Clinical Phenotypes toward a Unified Pattern of Central Nervous System Damage. Radiology. 2015;276(1):207-18.
370. da Graça FF, de Rezende TJR, Vasconcellos LFR, Pedroso JL, Barsottini OGP, França MC, Jr. Neuroimaging in Hereditary Spastic Paraplegias: Current Use and Future Perspectives. Frontiers in neurology. 2019;9:1117-.
371. Kassubek J, Sperfeld AD, Baumgartner A, Huppertz HJ, Riecker A, Juengling FD. Brain atrophy in pure and complicated hereditary spastic paraparesis: a quantitative 3D MRI study. European Journal of Neurology. 2006;13(8):880-6.
372. Montanaro D, Vavla M, Frijia F, Aghakhanyan G, Baratto A, Coi A, et al. Multimodal MRI Longitudinal Assessment of White and Gray Matter in Different SPG Types of Hereditary Spastic Paraparesis. Frontiers in neuroscience. 2020;14:325-.
373. Oğuz KK, Sanverdi E, Has A, Temuçin Ç, Türk S, Doerschner K. Tract-based spatial statistics of diffusion tensor imaging in hereditary spastic paraplegia with thin corpus callosum reveals widespread white matter changes. Diagn Interv Radiol. 2013;19(3):181-6.
374. Duning T, Warnecke T, Schirmacher A, Schiffbauer H, Lohmann H, Mohammadi S, et al. Specific pattern of early white-matter changes in pure hereditary spastic paraplegia. Movement Disorders. 2010;25(12):1986-92.
375. Aghakhanyan G, Martinuzzi A, Frijia F, Vavla M, Hlavata H, Baratto A, et al. Brain White Matter Involvement in Hereditary Spastic Paraplegias: Analysis with Multiple Diffusion Tensor Indices. American Journal of Neuroradiology. 2014;35(8):1533-8.
376. França MC, Yasuda CL, Pereira FRS, D'Abreu A, Lopes-Ramos CM, Rosa MV, et al. White and grey matter abnormalities in patients with SPG11 mutations. Journal of Neurology, Neurosurgery & Psychiatry. 2012;83(8):828-33.
377. Faber I, Martinez ARM, de Rezende TJR, Martins CR, Jr., Martins MP, Lourenço CM, et al. SPG11 mutations cause widespread white matter and basal ganglia abnormalities, but restricted cortical damage. Neuroimage Clin. 2018;19:848-57.
378. Stromillo ML, Malandrini A, Dotti MT, Battaglini M, Borgogni F, Tessa A, et al. Structural and metabolic damage in brains of patients with SPG11-related spastic paraplegia as detected by quantitative MRI. Journal of neurology. 2011;258(12):2240-7.
379. Pizzini F, Fatemi AS, Barker PB, Nagae-Poetscher LM, Horská A, Zimmerman AW, et al. Proton MR spectroscopic imaging in Pelizaeus-Merzbacher disease. AJNR Am J Neuroradiol. 2003;24(8):1683-9.
380. Fraidakis MJ, Brunetti M, Blackstone C, Filippi M, Chiò A. Novel Compound Heterozygous Spatacsin Mutations in a Greek Kindred with Hereditary Spastic Paraplegia SPG11 and Dementia. Neurodegener Dis. 2016;16(5-6):373-81.
381. Roos P, Svenstrup K, Danielsen ER, Thomsen C, Nielsen JE. CYP7B1: novel mutations and magnetic resonance spectroscopy abnormalities in hereditary spastic paraplegia type 5A. Acta Neurol Scand. 2014;129(5):330-4.
382. Dreha-Kulaczewski S, Dechent P, Helms G, Frahm J, Gärtner J, Brockmann K. Cerebral metabolic and structural alterations in hereditary spastic paraplegia with thin corpus callosum assessed by MRS and DTI. Neuroradiology. 2006;48(12):893-8.
383. Erichsen AK, Server A, Landrø NI, Sandvik L, Tallaksen CM. Proton magnetic resonance spectroscopy and cognition in patients with spastin mutations. Journal of the neurological sciences. 2009;277(1-2):124-9.
384. Svenstrup K, Giraud G, Boespflug-Tanguy O, Danielsen ER, Thomsen C, Rasmussen K, et al. Hereditary spastic paraplegia caused by the PLP1 'rumpshaker mutation'. J Neurol Neurosurg Psychiatry. 2010;81(6):666-72.
385. Orlén H, Melberg A, Raininko R, Kumlien E, Entesarian M, Söderberg P, et al. SPG11 mutations cause Kjellin syndrome, a hereditary spastic paraplegia with thin corpus callosum and central retinal degeneration. Am J Med Genet B Neuropsychiatr Genet. 2009;150b(7):984-92.

386. Hehr U, Bauer P, Winner B, Schule R, Olmez A, Koehler W, et al. Long-term course and mutational spectrum of spatacsin-linked spastic paraplegia. Ann Neurol. 2007;62(6):656-65.
387. Ma J, Xiong L, Chang Y, Jing X, Huang W, Hu B, et al. Novel mutations c.[5121_5122insAG]+[6859C>T] of the SPG11 gene associated with cerebellum hypometabolism in a Chinese case of hereditary spastic paraplegia with thin corpus callosum. Parkinsonism Relat Disord. 2014;20(2):256-9.
388. Nielsen JE, Johnsen B, Koefoed P, Scheuer KH, Grønbech-Jensen M, Law I, et al. Hereditary spastic paraplegia with cerebellar ataxia: a complex phenotype associated with a new SPG4 gene mutation. Eur J Neurol. 2004;11(12):817-24.
389. Samaranch L, Riverol M, Masdeu JC, Lorenzo E, Vidal-Taboada JM, Irigoyen J, et al. SPG11 compound mutations in spastic paraparesis with thin corpus callosum. Neurology. 2008;71(5):332-6.
390. Scheuer KH, Nielsen JE, Krabbe K, Simonsen C, Koefoed P, Sørensen SA, et al. Reduced regional cerebral blood flow in SPG4-linked hereditary spastic paraplegia. Journal of the neurological sciences. 2005;235(1-2):23-32.
391. Terada T, Kono S, Ouchi Y, Yoshida K, Hamaya Y, Kanaoka S, et al. SPG3A-linked hereditary spastic paraplegia associated with cerebral glucose hypometabolism. Ann Nucl Med. 2013;27(3):303-8.
392. Liao X, Huang M, Xing W, Wu X, Liao W, Wang X, et al. Resting state fMRI studies in SPG4-linked hereditary spastic paraplegia. Journal of the neurological sciences. 2018;384:1-6.
393. Tomberg T, Braschinsky M, Rannikmäe K, Kepler J, Kepler K, Kõrv J, et al. Functional MRI of the cortical sensorimotor system in patients with hereditary spastic paraplegia. Spinal Cord. 2012;50(12):885-90.
394. Koritnik B, Azam S, Knific J, Zidar J. Functional changes of the cortical motor system in hereditary spastic paraparesis. Acta Neurol Scand. 2009;120(3):182-90.
395. Lindig T, Bender B, Hauser T-K, Mang S, Schweikardt D, Klose U, et al. Gray and white matter alterations in hereditary spastic paraplegia type SPG4 and clinical correlations. Journal of neurology. 2015;262(8):1961-71.
396. Rezende TJR, de Albuquerque M, Lamas GM, Martinez ARM, Campos BM, Casseb RF, et al. Multimodal MRI-Based Study in Patients with SPG4 Mutations. PLoS One. 2015;10(2):e0117666.
397. Tallaksen CME, Guichart-Gomez E, Verpillat P, Hahn-Barma V, Ruberg M, Fontaine B, et al. Subtle Cognitive Impairment but No Dementia in Patients With Spastin Mutations. Archives of Neurology. 2003;60(8):1113-8.
398. Byrne PC, Mc Monagle P, Webb S, Fitzgerald B, Parfrey NA, Hutchinson M. Age-related cognitive decline in hereditary spastic paraparesis linked to chromosome 2p. Neurology. 2000;54(7):1510-7.
399. Murphy S, Gorman G, Beetz C, Byrne P, Dytko M, McMonagle P, et al. Dementia in SPG4 hereditary spastic paraplegia. Clinical, genetic, and neuropathologic evidence. 2009;73(5):378-84.
400. McMonagle P, Byrne P, Hutchinson M. Further evidence of dementia in SPG4-linked autosomal dominant hereditary spastic paraplegia. Neurology. 2004;62(3):407-10.
401. Goizet C, Boukhris A, Maltete D, Guyant-Maréchal L, Truchetto J, Mundwiller E, et al. SPG15 is the second most common cause of hereditary spastic paraplegia with thin corpus callosum. Neurology. 2009;73(14):1111-9.
402. Chen Q, Lui S, Wang J-G, Ou-Yang L, Zhou D, Burgunder J-M, et al. Diffusion tensor imaging of two unrelated Chinese men with hereditary spastic paraplegia associated with thin corpus callosum. Neuroscience Letters. 2008;441(1):21-4.
403. Pan M-K, Huang S-C, Lo Y-C, Yang C-C, Cheng T-W, Yang C-C, et al. Microstructural Integrity of Cerebral Fiber Tracts in Hereditary Spastic Paraparesis with SPG11 Mutation. American Journal of Neuroradiology. 2013;34(5):990-6.
404. Schneider-Gold C, Dekomien G, Regensburger M, Schneider R, Trampe N, Krogias C, et al. Monozygotic twins with a new compound heterozygous SPG11 mutation and different disease expression. Journal of the neurological sciences. 2017;381:265-8.
405. Warnecke T, Duning T, Schwan A, Lohmann H, Epplen JT, Young P. A novel form of autosomal recessive hereditary spastic paraplegia caused by a new SPG7 mutation. Neurology. 2007;69(4):368.
406. Warnecke T, Duning T, Schirmacher A, Mohammadi S, Schwindt W, Lohmann H, et al. A novel splice site mutation in the SPG7 gene causing widespread fiber damage in homozygous and heterozygous subjects. Movement Disorders. 2010;25(4):413-20.
407. Kuru S, Sakai M, Konagaya M, Yoshida M, Hashizume Y. Autopsy case of hereditary spastic paraplegia with thin corpus callosum showing severe gliosis in the cerebral white matter. Neuropathology : official journal of the Japanese Society of Neuropathology. 2005;25(4):346-52.
408. Nomura H, Koike F, Tsuruta Y, Iwaki A, Iwaki T. Autopsy case of autosomal recessive hereditary spastic paraplegia with reference to the muscular pathology. Neuropathology : official journal of the Japanese Society of Neuropathology. 2001;21(3):212-7.
409. Ferrer I, Olive M, Rivera R, Pou A, Narberhaust B, Ugartet A. Hereditary spastic paraparesis with dementia, amyotrophy and peripheral neuropathy. A neuropathological study. Neuropathology and Applied Neurobiology. 1995;21(3):255-61.
410. Kiernan MC, Vucic S, Cheah BC, Turner MR, Eisen A, Hardiman O, et al. Amyotrophic lateral sclerosis. Lancet. 2011;377(9769):942-55.

411. Strong MJ, Abrahams S, Goldstein LH, Woolley S, McLaughlin P, Snowden J, et al. Amyotrophic lateral sclerosis - frontotemporal spectrum disorder (ALS-FTSD): Revised diagnostic criteria. Amyotrophic lateral sclerosis & frontotemporal degeneration. 2017;18(3-4):153-74.
412. Ciccarelli O, Behrens TE, Johansen-Berg H, Talbot K, Orrell RW, Howard RS, et al. Investigation of white matter pathology in ALS and PLS using tract-based spatial statistics. Human brain mapping. 2009;30(2):615-24.
413. Rosskopf J, Muller HP, Dreyhaupt J, Gorges M, Ludolph AC, Kassubek J. Ex post facto assessment of diffusion tensor imaging metrics from different MRI protocols: preparing for multicentre studies in ALS. Amyotrophic lateral sclerosis & frontotemporal degeneration. 2015;16(1-2):92-101.
414. Sato K, Aoki S, Iwata NK, Masutani Y, Watadani T, Nakata Y, et al. Diffusion tensor tract-specific analysis of the uncinate fasciculus in patients with amyotrophic lateral sclerosis. Neuroradiology. 2010;52(8):729-33.
415. Prell T, Peschel T, Hartung V, Kaufmann J, Klauschies R, Bodammer N, et al. Diffusion tensor imaging patterns differ in bulbar and limb onset amyotrophic lateral sclerosis. Clin Neurol Neurosurg. 2013;115(8):1281-7.
416. Abe O, Yamada H, Masutani Y, Aoki S, Kunimatsu A, Yamasue H, et al. Amyotrophic lateral sclerosis: diffusion tensor tractography and voxel-based analysis. NMR in biomedicine. 2004;17(6):411-6.
417. Agosta F, Pagani E, Rocca MA, Caputo D, Perini M, Salvi F, et al. Voxel-based morphometry study of brain volumetry and diffusivity in amyotrophic lateral sclerosis patients with mild disability. Human brain mapping. 2007;28(12):1430-8.
418. Filippini N, Douaud G, Mackay CE, Knight S, Talbot K, Turner MR. Corpus callosum involvement is a consistent feature of amyotrophic lateral sclerosis. Neurology. 2010;75(18):1645-52.
419. Keil C, Prell T, Peschel T, Hartung V, Dengler R, Grosskreutz J. Longitudinal diffusion tensor imaging in amyotrophic lateral sclerosis. BMC neuroscience. 2012;13:141.
420. Sach M, Winkler G, Glauche V, Liepert J, Heimbach B, Koch MA, et al. Diffusion tensor MRI of early upper motor neuron involvement in amyotrophic lateral sclerosis. Brain. 2004;127(Pt 2):340-50.
421. Sage CA, Peeters RR, Gorner A, Robberecht W, Sunaert S. Quantitative diffusion tensor imaging in amyotrophic lateral sclerosis. Neuroimage. 2007;34(2):486-99.
422. Sage CA, Van Hecke W, Peeters R, Sijbers J, Robberecht W, Parizel P, et al. Quantitative diffusion tensor imaging in amyotrophic lateral sclerosis: revisited. Human brain mapping. 2009;30(11):3657-75.
423. Thivard L, Pradat PF, Lehericy S, Lacomblez L, Dormont D, Chiras J, et al. Diffusion tensor imaging and voxel based morphometry study in amyotrophic lateral sclerosis: relationships with motor disability. J Neurol Neurosurg Psychiatry. 2007;78(8):889-92.
424. Sarro L, Agosta F, Canu E, Riva N, Prelle A, Copetti M, et al. Cognitive functions and white matter tract damage in amyotrophic lateral sclerosis: a diffusion tensor tractography study. AJNR Am J Neuroradiol. 2011;32(10):1866-72.
425. Consonni M, Contarino VE, Catricalà E, Dalla Bella E, Pensato V, Gellera C, et al. Cortical markers of cognitive syndromes in amyotrophic lateral sclerosis. Neuroimage Clin. 2018;19:675-82.
426. Illán-Gala I, Montal V, Pegueroles J, Vilaplana E, Alcolea D, Dols-Icardo O, et al. Cortical microstructure in the amyotrophic lateral sclerosis–frontotemporal dementia continuum. Neurology. 2020;95(18):e2565.
427. Schuster C, Kasper E, Dyrba M, Machts J, Bittner D, Kaufmann J, et al. Cortical thinning and its relation to cognition in amyotrophic lateral sclerosis. Neurobiol Aging. 2014;35(1):240-6.
428. Shen D, Cui L, Fang J, Cui B, Li D, Tai H. Voxel-Wise Meta-Analysis of Gray Matter Changes in Amyotrophic Lateral Sclerosis. Front Aging Neurosci. 2016;8:64-.
429. Bede P, Bokde A, Elamin M, Byrne S, McLaughlin RL, Jordan N, et al. Grey matter correlates of clinical variables in amyotrophic lateral sclerosis (ALS): a neuroimaging study of ALS motor phenotype heterogeneity and cortical focality. J Neurol Neurosurg Psychiatry. 2013;84(7):766-73.
430. Chang JL, Lomen-Hoerth C, Murphy J, Henry RG, Kramer JH, Miller BL, et al. A voxel-based morphometry study of patterns of brain atrophy in ALS and ALS/FTLD. Neurology. 2005;65(1):75-80.
431. Christidi F, Karavasilis E, Riederer F, Zalonis I, Ferentinos P, Velonakis G, et al. Gray matter and white matter changes in non-demented amyotrophic lateral sclerosis patients with or without cognitive impairment: A combined voxel-based morphometry and tract-based spatial statistics whole-brain analysis. Brain imaging and behavior. 2018;12(2):547-63.
432. Bede P, Hardiman O. Longitudinal structural changes in ALS: a three time-point imaging study of white and gray matter degeneration. Amyotrophic lateral sclerosis & frontotemporal degeneration. 2018;19(3-4):232-41.
433. Bede P, Iyer PM, Schuster C, Elamin M, McLaughlin RL, Kenna K, et al. The selective anatomical vulnerability of ALS: 'disease-defining' and 'disease-defying' brain regions. Amyotrophic lateral sclerosis & frontotemporal degeneration. 2016;17(7-8):561-70.
434. Christidi F, Karavasilis E, Zalonis I, Ferentinos P, Giavri Z, Wilde EA, et al. Memory-related white matter tract integrity in amyotrophic lateral sclerosis: an advanced neuroimaging and neuropsychological study. Neurobiol Aging. 2017;49:69-78.

435. Bede P, Elamin M, Byrne S, McLaughlin RL, Kenna K, Vajda A, et al. Patterns of cerebral and cerebellar white matter degeneration in ALS. Journal of Neurology, Neurosurgery & Psychiatry. 2015;86(4):468.
436. Alruwaili AR, Pannek K, Coulthard A, Henderson R, Kurniawan ND, McCombe P. A combined tract-based spatial statistics and voxel-based morphometry study of the first MRI scan after diagnosis of amyotrophic lateral sclerosis with subgroup analysis. J Neuroradiol. 2018;45(1):41-8.
437. Murphy JM, Henry RG, Langmore S, Kramer JH, Miller BL, Lomen-Hoerth C. Continuum of frontal lobe impairment in amyotrophic lateral sclerosis. Arch Neurol. 2007;64(4):530-4.
438. Tsujimoto M, Senda J, Ishihara T, Niimi Y, Kawai Y, Atsuta N, et al. Behavioral changes in early ALS correlate with voxel-based morphometry and diffusion tensor imaging. Journal of the neurological sciences. 2011;307(1-2):34-40.
439. Woolley SC, Zhang Y, Schuff N, Weiner MW, Katz JS. Neuroanatomical correlates of apathy in ALS using 4 Tesla diffusion tensor MRI. Amyotrophic lateral sclerosis : official publication of the World Federation of Neurology Research Group on Motor Neuron Diseases. 2011;12(1):52-8.
440. Femiano C, Trojsi F, Caiazzo G, Siciliano M, Passaniti C, Russo A, et al. Apathy Is Correlated with Widespread Diffusion Tensor Imaging (DTI) Impairment in Amyotrophic Lateral Sclerosis. Behav Neurol. 2018;2018:2635202.
441. Christidi F, Karavasilis E, Rentzos M, Velonakis G, Zouvelou V, Xirou S, et al. Hippocampal pathology in amyotrophic lateral sclerosis: selective vulnerability of subfields and their associated projections. Neurobiol Aging. 2019;84:178-88.
442. Bede P, Bokde AL, Byrne S, Elamin M, McLaughlin RL, Kenna K, et al. Multiparametric MRI study of ALS stratified for the C9orf72 genotype. Neurology. 2013;81(4):361-9.
443. Masuda M, Senda J, Watanabe H, Epifanio B, Tanaka Y, Imai K, et al. Involvement of the caudate nucleus head and its networks in sporadic amyotrophic lateral sclerosis-frontotemporal dementia continuum. Amyotrophic lateral sclerosis & frontotemporal degeneration. 2016;17(7-8):571-9.
444. Westeneng HJ, Walhout R, Straathof M, Schmidt R, Hendrikse J, Veldink JH, et al. Widespread structural brain involvement in ALS is not limited to the C9orf72 repeat expansion. J Neurol Neurosurg Psychiatry. 2016;87(12):1354-60.
445. Bede P, Elamin M, Byrne S, McLaughlin RL, Kenna K, Vajda A, et al. Basal ganglia involvement in amyotrophic lateral sclerosis. Neurology. 2013;81(24):2107-15.
446. Westeneng HJ, Verstraete E, Walhout R, Schmidt R, Hendrikse J, Veldink JH, et al. Subcortical structures in amyotrophic lateral sclerosis. Neurobiol Aging. 2015;36(2):1075-82.
447. Pinkhardt EH, van Elst LT, Ludolph AC, Kassubek J. Amygdala size in amyotrophic lateral sclerosis without dementia: an in vivo study using MRI volumetry. BMC neurology. 2006;6:48.
448. Machts J, Loewe K, Kaufmann J, Jakubiczka S, Abdulla S, Petri S, et al. Basal ganglia pathology in ALS is associated with neuropsychological deficits. Neurology. 2015;85(15):1301-9.
449. Bede P, Chipika RH, Finegan E, Li Hi Shing S, Doherty MA, Hengeveld JC, et al. Brainstem pathology in amyotrophic lateral sclerosis and primary lateral sclerosis: A longitudinal neuroimaging study. Neuroimage Clin. 2019;24:102054.
450. Bede P, Chipika RH, Finegan E, Li Hi Shing S, Chang KM, Doherty MA, et al. Progressive brainstem pathology in motor neuron diseases: Imaging data from amyotrophic lateral sclerosis and primary lateral sclerosis. Data in brief. 2020;29:105229.
451. Pagani M, Chio A, Valentini MC, Oberg J, Nobili F, Calvo A, et al. Functional pattern of brain FDG-PET in amyotrophic lateral sclerosis. Neurology. 2014;83(12):1067-74.
452. Renard D, Collombier L, Castelnovo G, Fourcade G, Kotzki PO, LaBauge P. Brain FDG-PET changes in ALS and ALS-FTD. Acta Neurol Belg. 2011;111(4):306-9.
453. Cistaro A, Valentini MC, Chio A, Nobili F, Calvo A, Moglia C, et al. Brain hypermetabolism in amyotrophic lateral sclerosis: a FDG PET study in ALS of spinal and bulbar onset. European journal of nuclear medicine and molecular imaging. 2012;39(2):251-9.
454. Ludolph AC, Langen KJ, Regard M, Herzog H, Kemper B, Kuwert T, et al. Frontal lobe function in amyotrophic lateral sclerosis: a neuropsychologic and positron emission tomography study. Acta Neurol Scand. 1992;85(2):81-9.
455. Abrahams S, Leigh PN, Kew JJ, Goldstein LH, Lloyd CM, Brooks DJ. A positron emission tomography study of frontal lobe function (verbal fluency) in amyotrophic lateral sclerosis. Journal of the neurological sciences. 1995;129 Suppl:44-6.
456. Rajagopalan V, Pioro EP. Comparing brain structural MRI and metabolic FDG-PET changes in patients with ALS-FTD: 'the chicken or the egg?' question. J Neurol Neurosurg Psychiatry. 2015;86(9):952-8.
457. Cistaro A, Cuccurullo V, Quartuccio N, Pagani M, Valentini MC, Mansi L. Role of PET and SPECT in the study of amyotrophic lateral sclerosis. BioMed research international. 2014;2014:237437.
458. Turner MR, Cagnin A, Turkheimer FE, Miller CC, Shaw CE, Brooks DJ, et al. Evidence of widespread cerebral microglial activation in amyotrophic lateral sclerosis: an [11C](R)-PK11195 positron emission tomography study. Neurobiology of disease. 2004;15(3):601-9.
459. Corcia P, Tauber C, Vercoullie J, Arlicot N, Prunier C, Praline J, et al. Molecular imaging of microglial activation in amyotrophic lateral sclerosis. PLoS One. 2012;7(12):e52941.

460. Zurcher NR, Loggia ML, Lawson R, Chonde DB, Izquierdo-Garcia D, Yasek JE, et al. Increased in vivo glial activation in patients with amyotrophic lateral sclerosis: assessed with [(11)C]-PBR28. Neuroimage Clin. 2015;7:409-14.
461. Johansson A, Engler H, Blomquist G, Scott B, Wall A, Aquilonius SM, et al. Evidence for astrocytosis in ALS demonstrated by [11C](L)-deprenyl-D2 PET. Journal of the neurological sciences. 2007;255(1-2):17-22.
462. Usman U, Choi C, Camicioli R, Seres P, Lynch M, Sekhon R, et al. Mesial prefrontal cortex degeneration in amyotrophic lateral sclerosis: a high-field proton MR spectroscopy study. AJNR Am J Neuroradiol. 2011;32(9):1677-80.
463. Sudharshan N, Hanstock C, Hui B, Pyra T, Johnston W, Kalra S. Degeneration of the Mid-Cingulate Cortex in Amyotrophic Lateral Sclerosis Detected In Vivo with MR Spectroscopy. American Journal of Neuroradiology. 2011;32(2):403.
464. Abe K, Takanashi M, Watanabe Y, Tanaka H, Fujita N, Hirabuki N, et al. Decrease in N-acetylaspartate/creatine ratio in the motor area and the frontal lobe in amyotrophic lateral sclerosis. Neuroradiology. 2001;43(7):537-41.
465. Verma G, Woo JH, Chawla S, Wang S, Sheriff S, Elman LB, et al. Whole-brain analysis of amyotrophic lateral sclerosis by using echo-planar spectroscopic imaging. Radiology. 2013;267(3):851-7.
466. Strong MJ, Grace GM, Orange JB, Leeper HA, Menon RS, Aere C. A prospective study of cognitive impairment in ALS. Neurology. 1999;53(8):1665-70.
467. Srivastava O, Hanstock C, Chenji S, Mah D, Eurich D, Ta D, et al. Cerebral degeneration in amyotrophic lateral sclerosis: A prospective multicenter magnetic resonance spectroscopy study. Neurol Clin Pract. 2019;9(5):400-7.
468. Mohammadi B, Kollewe K, Samii A, Krampfl K, Dengler R, Munte TF. Changes of resting state brain networks in amyotrophic lateral sclerosis. Exp Neurol. 2009;217(1):147-53.
469. Fekete T, Zach N, Mujica-Parodi LR, Turner MR. Multiple kernel learning captures a systems-level functional connectivity biomarker signature in amyotrophic lateral sclerosis. PLoS One. 2013;8(12):e85190.
470. Agosta F, Canu E, Valsasina P, Riva N, Prelle A, Comi G, et al. Divergent brain network connectivity in amyotrophic lateral sclerosis. Neurobiol Aging. 2013;34(2):419-27.
471. Luo C, Chen Q, Huang R, Chen X, Chen K, Huang X, et al. Patterns of spontaneous brain activity in amyotrophic lateral sclerosis: a resting-state FMRI study. PLoS One. 2012;7(9):e45470.
472. Trojsi F, Esposito F, de Stefano M, Buonanno D, Conforti FL, Corbo D, et al. Functional overlap and divergence between ALS and bvFTD. Neurobiol Aging. 2015;36(1):413-23.
473. Tietz F HV, Prell T, Penzlin S, Ilse B, Bokemeyer M, et al. The resting state default mode network (DMN) is pathologically hyperactive in amyotrophic lateral sclerosis. Amyotrophic lateral sclerosis & frontotemporal degeneration. 2012;13:171.
474. Tedeschi G, Trojsi F, Tessitore A, Corbo D, Sagnelli A, Paccone A, et al. Interaction between aging and neurodegeneration in amyotrophic lateral sclerosis. Neurobiol Aging. 2012;33(5):886-98.
475. Goldstein LH, Newsom-Davis IC, Bryant V, Brammer M, Leigh PN, Simmons A. Altered patterns of cortical activation in ALS patients during attention and cognitive response inhibition tasks. Journal of neurology. 2011;258(12):2186-98.
476. Keller J, Böhm S, Aho-Özhan HEA, Loose M, Gorges M, Kassubek J, et al. Functional reorganization during cognitive function tasks in patients with amyotrophic lateral sclerosis. Brain imaging and behavior. 2018;12(3):771-84.
477. Witiuk K, Fernandez-Ruiz J, McKee R, Alahyane N, Coe BC, Melanson M, et al. Cognitive deterioration and functional compensation in ALS measured with fMRI using an inhibitory task. J Neurosci. 2014;34(43):14260-71.
478. Jelsone-Swain L, Persad C, Burkard D, Welsh RC. Action processing and mirror neuron function in patients with amyotrophic lateral sclerosis: an fMRI study. PLoS One. 2015;10(4):e0119862-e.
479. Palmieri A, Naccarato M, Abrahams S, Bonato M, D'Ascenzo C, Balestreri S, et al. Right hemisphere dysfunction and emotional processing in ALS: an fMRI study. Journal of neurology. 2010;257(12):1970-8.
480. Passamonti L, Fera F, Tessitore A, Russo A, Cerasa A, Gioia CM, et al. Dysfunctions within limbic-motor networks in amyotrophic lateral sclerosis. Neurobiol Aging. 2013;34(11):2499-509.
481. Aho-Özhan HE, Keller J, Heimrath J, Uttner I, Kassubek J, Birbaumer N, et al. Perception of Emotional Facial Expressions in Amyotrophic Lateral Sclerosis (ALS) at Behavioural and Brain Metabolic Level. PLoS One. 2016;11(10):e0164655.
482. Lule D, Diekmann V, Anders S, Kassubek J, Kubler A, Ludolph AC, et al. Brain responses to emotional stimuli in patients with amyotrophic lateral sclerosis (ALS). Journal of neurology. 2007;254(4):519-27.
483. Stoppel CM, Vielhaber S, Eckart C, Machts J, Kaufmann J, Heinze H-J, et al. Structural and functional hallmarks of amyotrophic lateral sclerosis progression in motor- and memory-related brain regions. Neuroimage Clin. 2014;5:277-90.
484. Vellage A-K, Veit M, Kobeleva X, Petri S, Vielhaber S, Müller NG. Working Memory Network Changes in ALS: An fMRI Study. Frontiers in neuroscience. 2016;10(158).

485. Abrahams S, Goldstein LH, Simmons A, Brammer M, Williams SC, Giampietro V, et al. Word retrieval in amyotrophic lateral sclerosis: a functional magnetic resonance imaging study. Brain. 2004;127(Pt 7):1507-17.
486. Turner MR, Kiernan MC. Does interneuronal dysfunction contribute to neurodegeneration in amyotrophic lateral sclerosis? Amyotrophic lateral sclerosis : official publication of the World Federation of Neurology Research Group on Motor Neuron Diseases. 2012;13(3):245-50.
487. Douaud G, Filippini N, Knight S, Talbot K, Turner MR. Integration of structural and functional magnetic resonance imaging in amyotrophic lateral sclerosis. Brain. 2011;134(Pt 12):3470-9.
488. Abidi M, de Marco G, Couillandre A, Feron M, Mseddi E, Termoz N, et al. Adaptive functional reorganization in amyotrophic lateral sclerosis: coexisting degenerative and compensatory changes. Eur J Neurol. 2020;27(1):121-8.
489. Feron M, Couillandre A, Mseddi E, Termoz N, Abidi M, Bardinet E, et al. Extrapyramidal deficits in ALS: a combined biomechanical and neuroimaging study. Journal of neurology. 2018;265(9):2125-36.
490. Proudfoot M, Rohenkohl G, Quinn A, Colclough GL, Wuu J, Talbot K, et al. Altered cortical beta-band oscillations reflect motor system degeneration in amyotrophic lateral sclerosis. Human brain mapping. 2017;38(1):237-54.
491. Dukic S, McMackin R, Buxo T, Fasano A, Chipika R, Pinto-Grau M, et al. Patterned functional network disruption in amyotrophic lateral sclerosis. Human brain mapping. 2019;40(16):4827-42.
492. McMackin R, Dukic S, Broderick M, Iyer PM, Pinto-Grau M, Mohr K, et al. Dysfunction of attention switching networks in amyotrophic lateral sclerosis. Neuroimage Clin. 2019;22:101707.
493. Nasseroleslami B, Dukic S, Broderick M, Mohr K, Schuster C, Gavin B, et al. Characteristic Increases in EEG Connectivity Correlate With Changes of Structural MRI in Amyotrophic Lateral Sclerosis. Cereb Cortex. 2019;29(1):27-41.
494. McMackin R, Dukic S, Costello E, Pinto-Grau M, McManus L, Broderick M, et al. Cognitive network hyperactivation and motor cortex decline correlate with ALS prognosis. Neurobiol Aging. 2021;104:57-70.
495. Pettit LD, Bastin ME, Smith C, Bak TH, Gillingwater TH, Abrahams S. Executive deficits, not processing speed relates to abnormalities in distinct prefrontal tracts in amyotrophic lateral sclerosis. Brain. 2013;136(Pt 11):3290-304.
496. Burke T, Pinto-Grau M, Lonergan K, Elamin M, Bede P, Costello E, et al. Measurement of Social Cognition in Amyotrophic Lateral Sclerosis: A Population Based Study. PLoS One. 2016;11(8):e0160850.
497. Burke T, Pinto-Grau M, Lonergan K, Bede P, O'Sullivan M, Heverin M, et al. A Cross-sectional population-based investigation into behavioral change in amyotrophic lateral sclerosis: subphenotypes, staging, cognitive predictors, and survival. Ann Clin Transl Neurol. 2017;4(5):305-17.
498. Crockford C, Newton J, Lonergan K, Chiwera T, Booth T, Chandran S, et al. ALS-specific cognitive and behavior changes associated with advancing disease stage in ALS. Neurology. 2018.
499. Radakovic R, Gray D, Dudley K, Mioshi E, Dick D, Melchiorre G, et al. Reliability and validity of the brief dimensional apathy scale. Archives of Clinical Neuropsychology. 2020;35(5):539-44.
500. Burke T, Elamin M, Bede P, Pinto-Grau M, Lonergan K, Hardiman O, et al. Discordant performance on the 'Reading the Mind in the Eyes' Test, based on disease onset in amyotrophic lateral sclerosis. Amyotrophic lateral sclerosis & frontotemporal degeneration. 2016:1-6.
501. Christidi F, Karavasilis E, Velonakis G, Ferentinos P, Rentzos M, Kelekis N, et al. The Clinical and Radiological Spectrum of Hippocampal Pathology in Amyotrophic Lateral Sclerosis. Front Neurol. 2018;9:523.
502. De Vocht J, Blommaert J, Devrome M, Radwan A, Van Weehaeghe D, De Schaepdryver M, et al. Use of Multimodal Imaging and Clinical Biomarkers in Presymptomatic Carriers of C9orf72 Repeat Expansion. JAMA neurology. 2020;77(8):1-10.
503. Devos D, Moreau C, Kyheng M, Garcon G, Rolland AS, Blasco H, et al. A ferroptosis-based panel of prognostic biomarkers for Amyotrophic Lateral Sclerosis. Sci Rep. 2019;9(1):2918.
504. Gregory JM, McDade K, Bak TH, Pal S, Chandran S, Smith C, et al. Executive, language and fluency dysfunction are markers of localised TDP-43 cerebral pathology in non-demented ALS. J Neurol Neurosurg Psychiatry. 2020;91(2):149-57.
505. Geser F, Martinez-Lage M, Robinson J, Uryu K, Neumann M, Brandmeir NJ, et al. Clinical and pathological continuum of multisystem TDP-43 proteinopathies. Arch Neurol. 2009;66(2):180-9.
506. Brettschneider J, Del Tredici K, Toledo JB, Robinson JL, Irwin DJ, Grossman M, et al. Stages of pTDP-43 pathology in amyotrophic lateral sclerosis. Ann Neurol. 2013;74(1):20-38.
507. Prudlo J, König J, Schuster C, Kasper E, Büttner A, Teipel S, et al. TDP-43 pathology and cognition in ALS: A prospective clinicopathologic correlation study. Neurology. 2016;87(10):1019-23.
508. Mollink J, Hiemstra M, Miller KL, Huszar IN, Jenkinson M, Raaphorst J, et al. White matter changes in the perforant path area in patients with amyotrophic lateral sclerosis. Neuropathol Appl Neurobiol. 2019;45(6):570-85.
509. Shefner JM, Al-Chalabi A, Baker MR, Cui LY, de Carvalho M, Eisen A, et al. A proposal for new diagnostic criteria for ALS. Clinical neurophysiology : official journal of the International Federation of Clinical Neurophysiology. 2020;131(8):1975-8.
510. Elamin M, Bede P, Byrne S, Jordan N, Gallagher L, Wynne B, et al. Cognitive changes predict functional decline in ALS: a population-based longitudinal study. Neurology. 2013;80(17):1590-7.

511. Roche JC, Rojas-Garcia R, Scott KM, Scotton W, Ellis CE, Burman R, et al. A proposed staging system for amyotrophic lateral sclerosis. Brain : a journal of neurology. 2012;135(Pt 3):847-52.
512. Chiò A, Hammond ER, Mora G, Bonito V, Filippini G. Development and evaluation of a clinical staging system for amyotrophic lateral sclerosis. Journal of Neurology, Neurosurgery & Psychiatry. 2015;86(1):38.
513. Turner MR, Barohn RJ, Corcia P, Fink JK, Harms MB, Kiernan MC, et al. Primary lateral sclerosis: consensus diagnostic criteria. Journal of Neurology, Neurosurgery & Psychiatry. 2020;91(4):373.
514. Almeida V, de Carvalho M, Scotto M, Pinto S, Pinto A, Ohana B, et al. Primary lateral sclerosis: predicting functional outcome. Amyotrophic lateral sclerosis & frontotemporal degeneration. 2013;14(2):141-5.
515. Abrahams S, Newton J, Niven E, Foley J, Bak TH. Screening for cognition and behaviour changes in ALS. Amyotrophic lateral sclerosis & frontotemporal degeneration. 2014;15(1-2):9-14.
516. Radakovic R, Stephenson L, Colville S, Swingler R, Chandran S, Abrahams S. Multidimensional apathy in ALS: validation of the Dimensional Apathy Scale. J Neurol Neurosurg Psychiatry. 2016;87(6):663-9.
517. Burrell JR, Kiernan MC, Vucic S, Hodges JR. Motor Neuron dysfunction in frontotemporal dementia. Brain. 2011;134(9):2582-94.
518. Kortte KB, Rogalski EJ. Behavioural interventions for enhancing life participation in behavioural variant frontotemporal dementia and primary progressive aphasia. International Review of Psychiatry. 2013;25(2):237-45.
519. Henry ML, Meese MV, Truong S, Babiak MC, Miller BL, Gorno-Tempini ML. Treatment for apraxia of speech in nonfluent variant primary progressive aphasia. Behav Neurol. 2013;26(1-2):77-88.
520. Jokel R, Anderson ND. Quest for the best: effects of errorless and active encoding on word re-learning in semantic dementia. Neuropsychol Rehabil. 2012;22(2):187-214.
521. Filippi M, Basaia S, Canu E, Imperiale F, Meani A, Caso F, et al. Brain network connectivity differs in early-onset neurodegenerative dementia. Neurology. 2017;89(17):1764.
522. Ravanfar P, Loi SM, Syeda WT, Van Rheenen TE, Bush AI, Desmond P, et al. Systematic Review: Quantitative Susceptibility Mapping (QSM) of Brain Iron Profile in Neurodegenerative Diseases. Frontiers in neuroscience. 2021;15:618435-.
523. Cheng J-X, Zhang H-Y, Peng Z-K, Xu Y, Tang H, Wu J-T, et al. Divergent topological networks in Alzheimer's disease: a diffusion kurtosis imaging analysis. Translational Neurodegeneration. 2018;7(1):10.
524. Broad RJ, Gabel MC, Dowell NG, Schwartzman DJ, Seth AK, Zhang H, et al. Neurite orientation and dispersion density imaging (NODDI) detects cortical and corticospinal tract degeneration in ALS. J Neurol Neurosurg Psychiatry. 2019;90(4):404-11.
525. Mitsumoto H, Brooks BR, Silani V. Clinical trials in amyotrophic lateral sclerosis: why so many negative trials and how can trials be improved? Lancet Neurol. 2014;13(11):1127-38.
526. Miller T, Cudkowicz M, Shaw PJ, Andersen PM, Atassi N, Bucelli RC, et al. Phase 1–2 Trial of Antisense Oligonucleotide Tofersen for SOD1 ALS. New England Journal of Medicine. 2020;383(2):109-19.
527. Baranello G, Darras BT, Day JW, Deconinck N, Klein A, Masson R, et al. Risdiplam in Type 1 Spinal Muscular Atrophy. New England Journal of Medicine. 2021;384(10):915-23.
528. Mercuri E, Darras BT, Chiriboga CA, Day JW, Campbell C, Connolly AM, et al. Nusinersen versus Sham Control in Later-Onset Spinal Muscular Atrophy. New England Journal of Medicine. 2018;378(7):625-35.
529. Musarò A, Dobrowolny G, Cambieri C, Onesti E, Ceccanti M, Frasca V, et al. Neuromuscular magnetic stimulation counteracts muscle decline in ALS patients: results of a randomized, double-blind, controlled study. Sci Rep. 2019;9(1):2837.
530. Fang J, Zhou M, Yang M, Zhu C, He L. Repetitive transcranial magnetic stimulation for the treatment of amyotrophic lateral sclerosis or motor neuron disease. Cochrane Database Syst Rev. 2013;2013(5):Cd008554.
531. Crespi C, Dodich A, Iannaccone S, Marcone A, Falini A, Cappa SF, et al. Diffusion tensor imaging evidence of corticospinal pathway involvement in frontotemporal lobar degeneration. Cortex; a journal devoted to the study of the nervous system and behavior. 2020;125:1-11.
532. Häkkinen S, Chu SA, Lee SE. Neuroimaging in genetic frontotemporal dementia and amyotrophic lateral sclerosis. Neurobiology of disease. 2020;145:105063.
533. Meng X, D'Arcy C. Education and Dementia in the Context of the Cognitive Reserve Hypothesis: A Systematic Review with Meta-Analyses and Qualitative Analyses. PLoS One. 2012;7(6):e38268.
534. Beyer L, Meyer-Wilmes J, Schönecker S, Schnabel J, Sauerbeck J, Scheifele M, et al. Cognitive reserve hypothesis in frontotemporal dementia: A FDG-PET study. NeuroImage: Clinical. 2021;29:102535.
535. Temp AGM, Prudlo J, Vielhaber S, Machts J, Hermann A, Teipel SJ, et al. "Cognitive Reserve and Regional Brain Volume in Amyotrophic Lateral Sclerosis". Cortex; a journal devoted to the study of the nervous system and behavior. 2021.

536. Canosa A, Palumbo F, Iazzolino B, Peotta L, Di Pede F, Manera U, et al. The interplay among education, brain metabolism, and cognitive impairment suggests a role of cognitive reserve in Amyotrophic Lateral Sclerosis. Neurobiology of Aging. 2021;98:205-13.
537. Bak TH, Chandran S. What wires together dies together: Verbs, actions and neurodegeneration in motor neuron disease. Cortex; a journal devoted to the study of the nervous system and behavior. 2012;48(7):936-44.
538. Papeo L, Cecchetto C, Mazzon G, Granello G, Cattaruzza T, Verriello L, et al. The processing of actions and action-words in amyotrophic lateral sclerosis patients. Cortex; a journal devoted to the study of the nervous system and behavior. 2015;64:136-47.
539. Hauk O, Johnsrude I, Pulvermüller F. Somatotopic Representation of Action Words in Human Motor and Premotor Cortex. Neuron. 2004;41(2):301-7.
540. Lule D, Diekmann V, Kassubek J, Kurt A, Birbaumer N, Ludolph AC, et al. Cortical plasticity in amyotrophic lateral sclerosis: motor imagery and function. Neurorehabil Neural Repair. 2007;21(6):518-26.
541. O'Callaghan C, Bertoux M, Hornberger M. Beyond and below the cortex: the contribution of striatal dysfunction to cognition and behaviour in neurodegeneration. J Neurol Neurosurg Psychiatry. 2013.
542. Seeley WW, Crawford RK, Zhou J, Miller BL, Greicius MD. Neurodegenerative diseases target large-scale human brain networks. Neuron. 2009;62(1):42-52.
543. Finegan E, Li Hi Shing S, Siah WF, Chipika RH, Chang KM, McKenna MC, et al. Evolving diagnostic criteria in primary lateral sclerosis: The clinical and radiological basis of “probable PLS”. Journal of the neurological sciences. 2020;417:117052.
544. Leoni TB, Rezende TJR, Peluzzo TM, Martins MP, Neto ARC, Gonzalez-Salazar C, et al. Structural brain and spinal cord damage in symptomatic and pre-symptomatic VAPB-related ALS. Journal of the neurological sciences. 2022;434:120126.
545. Olney NT, Bischof A, Rosen H, Caverzasi E, Stern WA, Lomen-Hoerth C, et al. Measurement of spinal cord atrophy using phase sensitive inversion recovery (PSIR) imaging in motor neuron disease. PLoS One. 2018;13(11):e0208255.
546. Paquin M, El Mendili MM, Gros C, Dupont SM, Cohen-Adad J, Pradat PF. Spinal Cord Gray Matter Atrophy in Amyotrophic Lateral Sclerosis. AJNR Am J Neuroradiol. 2018;39(1):184-92.
547. van der Burgh HK, Westeneng HJ, Meier JM, van Es MA, Veldink JH, Hendrikse J, et al. Cross-sectional and longitudinal assessment of the upper cervical spinal cord in motor neuron disease. Neuroimage Clin. 2019;24:101984.
548. Wimmer T, Schreiber F, Hensiek N, Garz C, Kaufmann J, Machts J, et al. The upper cervical spinal cord in ALS assessed by cross-sectional and longitudinal 3T MRI. Sci Rep. 2020;10(1):1783.
549. Nigri A, Dalla Bella E, Ferraro S, Medina Carrion JP, Demichelis G, Bersano E, et al. Cervical spinal cord atrophy in amyotrophic lateral sclerosis across disease stages. Ann Clin Transl Neurol. 2023;10(2):213-24.
550. Toh C, Keslake A, Payne T, Onwuegbuzie A, Harding J, Baster K, et al. Analysis of brain and spinal MRI measures in a common domain to investigate directional neurodegeneration in motor neuron disease. Journal of neurology. 2023;270(3):1682-90.
551. Barry RL, Torrado-Carvajal A, Kirsch JE, Arabasz GE, Albrecht DS, Alshelh Z, et al. Selective atrophy of the cervical enlargement in whole spinal cord MRI of amyotrophic lateral sclerosis. Neuroimage Clin. 2022;36:103199.
552. Branco LM, De Albuquerque M, De Andrade HM, Bergo FP, Nucci A, França MC, Jr. Spinal cord atrophy correlates with disease duration and severity in amyotrophic lateral sclerosis. Amyotrophic lateral sclerosis & frontotemporal degeneration. 2014;15(1-2):93-7.
553. de Albuquerque M, Branco LM, Rezende TJ, de Andrade HM, Nucci A, França MC, Jr. Longitudinal evaluation of cerebral and spinal cord damage in Amyotrophic Lateral Sclerosis. Neuroimage Clin. 2017;14:269-76.
554. Pisharady PK, Eberly LE, Cheong I, Manousakis G, Guliani G, Clark HB, et al. Tract-specific analysis improves sensitivity of spinal cord diffusion MRI to cross-sectional and longitudinal changes in amyotrophic lateral sclerosis. Commun Biol. 2020;3(1):370.
555. Cohen-Adad J, El Mendili MM, Morizot-Koutlidis R, Lehéricy S, Meininger V, Blancho S, et al. Involvement of spinal sensory pathway in ALS and specificity of cord atrophy to lower motor neuron degeneration. Amyotrophic lateral sclerosis & frontotemporal degeneration. 2013;14(1):30-8.
556. El Mendili MM, Cohen-Adad J, Pelegrini-Issac M, Rossignol S, Morizot-Koutlidis R, Marchand-Pauvert V, et al. Multi-parametric spinal cord MRI as potential progression marker in amyotrophic lateral sclerosis. PLoS One. 2014;9(4):e95516.
557. Querin G, El Mendili MM, Lenglet T, Delphine S, Marchand-Pauvert V, Benali H, et al. Spinal cord multi-parametric magnetic resonance imaging for survival prediction in amyotrophic lateral sclerosis. Eur J Neurol. 2017;24(8):1040-6.
558. Rasoanandrianina H, Grapperon AM, Taso M, Girard OM, Duhamel G, Guye M, et al. Region-specific impairment of the cervical spinal cord (SC) in amyotrophic lateral sclerosis: A preliminary study using SC templates and quantitative MRI (diffusion tensor imaging/inhomogeneous magnetization transfer). NMR in biomedicine. 2017;30(12).

559. Agosta F, Rocca MA, Valsasina P, Sala S, Caputo D, Perini M, et al. A longitudinal diffusion tensor MRI study of the cervical cord and brain in amyotrophic lateral sclerosis patients. Journal of Neurology, Neurosurgery & Psychiatry. 2009;80(1):53.
560. Valsasina P, Agosta F, Benedetti B, Caputo D, Perini M, Salvi F, et al. Diffusion anisotropy of the cervical cord is strictly associated with disability in amyotrophic lateral sclerosis. J Neurol Neurosurg Psychiatry. 2007;78(5):480-4.
561. Agosta F, Spinelli EG, Marjanovic IV, Stevic Z, Pagani E, Valsasina P, et al. Unraveling ALS due to SOD1 mutation through the combination of brain and cervical cord MRI. Neurology. 2018;90(8):e707-e16.
562. Grolez G, Kyheng M, Lopes R, Moreau C, Timmerman K, Auger F, et al. MRI of the cervical spinal cord predicts respiratory dysfunction in ALS. Sci Rep. 2018;8(1):1828.
563. Wang Y, Liu L, Ma L, Huang X, Lou X, Wang Y, et al. Preliminary study on cervical spinal cord in patients with amyotrophic lateral sclerosis using MR diffusion tensor imaging. Acad Radiol. 2014;21(5):590-6.
564. Patzig M, Bochmann K, Lutz J, Stahl R, Küpper C, Liebig T, et al. Measurement of structural integrity of the spinal cord in patients with amyotrophic lateral sclerosis using diffusion tensor magnetic resonance imaging. PLoS One. 2019;14(10):e0224078.
565. Nair G, Carew JD, Usher S, Lu D, Hu XP, Benatar M. Diffusion tensor imaging reveals regional differences in the cervical spinal cord in amyotrophic lateral sclerosis. Neuroimage. 2010;53(2):576-83.
566. Iglesias C, Sangari S, El Mendili MM, Benali H, Marchand-Pauvert V, Pradat PF. Electrophysiological and spinal imaging evidences for sensory dysfunction in amyotrophic lateral sclerosis. BMJ Open. 2015;5(2):e007659.
567. Fukui Y, Hishikawa N, Sato K, Nakano Y, Morihara R, Shang J, et al. Detecting spinal pyramidal tract of amyotrophic lateral sclerosis patients with diffusion tensor tractography. Neuroscience Research. 2018;133:58-63.
568. Budrewicz S, Szewczyk P, Bladowska J, Podemski R, Koziorowska-Gawron E, Ejma M, et al. The possible meaning of fractional anisotropy measurement of the cervical spinal cord in correct diagnosis of amyotrophic lateral sclerosis. Neurol Sci. 2016;37(3):417-21.
569. Sperfeld AD, Bretschneider V, Flaith L, Unrath A, Hanemann CO, Ludolph AC, et al. MR-Pathologic Comparison of the Upper Spinal Cord in Different Motor Neuron Diseases. European Neurology. 2005;53(2):74-7.
570. Cohen-Adad J, Zhao W, Keil B, Ratai EM, Triantafyllou C, Lawson R, et al. 7-T MRI of the spinal cord can detect lateral corticospinal tract abnormality in amyotrophic lateral sclerosis. Muscle Nerve. 2013;47(5):760-2.
571. Ikeda K, Murata K, Kawase Y, Kawabe K, Kano O, Yoshii Y, et al. Relationship between cervical cord 1H-magnetic resonance spectroscopy and clinoco-electromyographic profile in amyotrophic lateral sclerosis. Muscle Nerve. 2013;47(1):61-7.
572. Carew JD, Nair G, Andersen PM, Wuu J, Gronka S, Hu X, et al. Presymptomatic spinal cord neurometabolic findings in SOD1-positive people at risk for familial ALS. Neurology. 2011;77(14):1370-5.
573. Carew JD, Nair G, Pineda-Alonso N, Usher S, Hu X, Benatar M. Magnetic resonance spectroscopy of the cervical cord in amyotrophic lateral sclerosis. Amyotrophic lateral sclerosis : official publication of the World Federation of Neurology Research Group on Motor Neuron Diseases. 2011;12(3):185-91.
574. Dvorak AV, Ljungberg E, Vavasour IM, Liu H, Johnson P, Rauscher A, et al. Rapid myelin water imaging for the assessment of cervical spinal cord myelin damage. NeuroImage: Clinical. 2019;23:101896.
575. Wendebourg MJ, Weigel M, Richter L, Gocheva V, Hafner P, Orsini AL, et al. Spinal cord gray matter atrophy is associated with functional decline in post-polio syndrome. Eur J Neurol. 2022;29(5):1435-45.
576. El Mendili MM, Lenglet T, Stojkovic T, Behin A, Guimarães-Costa R, Salachas F, et al. Cervical Spinal Cord Atrophy Profile in Adult SMN1-Linked SMA. PLoS One. 2016;11(4):e0152439.
577. Querin G, El Mendili MM, Lenglet T, Behin A, Stojkovic T, Salachas F, et al. The spinal and cerebral profile of adult spinal-muscular atrophy: A multimodal imaging study. Neuroimage Clin. 2019;21:101618.
578. Stam M, Haakma W, Kuster L, Froeling M, Philippens MEP, Bos C, et al. Magnetic resonance imaging of the cervical spinal cord in spinal muscular atrophy. Neuroimage Clin. 2019;24:102002.
579. Querin G, Lenglet T, Debs R, Stojkovic T, Behin A, Salachas F, et al. Development of new outcome measures for adult SMA type III and IV: a multimodal longitudinal study. Journal of neurology. 2021;268(5):1792-802.
580. Piccinin CC, Rezende TJR, de Paiva JLR, Moysés PC, Martinez ARM, Cendes F, et al. A 5-Year Longitudinal Clinical and Magnetic Resonance Imaging Study in Spinocerebellar Ataxia Type 3. Mov Disord. 2020;35(9):1679-84.
581. Higgins JJ, Harvey-White JD, Nee LE, Colli MJ, Grossi TA, Kopin IJ. Brain MRI, lumbar CSF monoamine concentrations, and clinical descriptors of patients with spinocerebellar ataxia mutations. J Neurol Neurosurg Psychiatry. 1996;61(6):591-5.
582. Fahl CN, Branco LM, Bergo FP, D'Abreu A, Lopes-Cendes I, França MC, Jr. Spinal cord damage in Machado-Joseph disease. Cerebellum. 2015;14(2):128-32.

583. Rezende TJR, de Paiva JLR, Martinez ARM, Lopes-Cendes I, Pedroso JL, Barsottini OGP, et al. Structural signature of SCA3: From presymptomatic to late disease stages. Ann Neurol. 2018;84(3):401-8.
584. Martins CR, Jr., Martinez ARM, de Rezende TJR, Branco LMT, Pedroso JL, Barsottini OGP, et al. Spinal Cord Damage in Spinocerebellar Ataxia Type 1. Cerebellum. 2017;16(4):792-6.
585. Lukas C, Hahn HK, Bellenberg B, Hellwig K, Globas C, Schimrigk SK, et al. Spinal cord atrophy in spinocerebellar ataxia type 3 and 6 : impact on clinical disability. Journal of neurology. 2008;255(8):1244-9.
586. Hernandez-Castillo CR, Diaz R, Rezende TJR, Adanyeguh I, Harding IH, Mochel F, et al. Cervical Spinal Cord Degeneration in Spinocerebellar Ataxia Type 7. AJNR Am J Neuroradiol. 2021;42(9):1735-9.
587. Faber J, Schaprian T, Berkan K, Reetz K, França MC, Jr., de Rezende TJR, et al. Regional Brain and Spinal Cord Volume Loss in Spinocerebellar Ataxia Type 3. Mov Disord. 2021;36(10):2273-81.
588. Chevis CF, da Silva CB, D'Abreu A, Lopes-Cendes I, Cendes F, Bergo FP, et al. Spinal cord atrophy correlates with disability in Friedreich's ataxia. Cerebellum. 2013;12(1):43-7.
589. Dogan I, Romanzetti S, Didszun C, Mirzazade S, Timmann D, Saft C, et al. Structural characteristics of the central nervous system in Friedreich ataxia: an in vivo spinal cord and brain MRI study. Journal of Neurology, Neurosurgery & Psychiatry. 2019;90(5):615.
590. Hernandez A, Rezende TJR, Martinez ARM, de Brito MR, França MC, Jr. Tract-Specific Spinal Cord Diffusion Tensor Imaging in Friedreich's Ataxia. Mov Disord. 2022;37(2):354-64.
591. Rezende TJR, Martinez ARM, Faber I, Girotto Takazaki KA, Martins MP, de Lima FD, et al. Developmental and neurodegenerative damage in Friedreich's ataxia. European Journal of Neurology. 2019;26(3):483-9.
592. Rezende TJR, Adanyeguh IM, Arrigoni F, Bender B, Cendes F, Corben LA, et al. Progressive Spinal Cord Degeneration in Friedreich's Ataxia: Results from ENIGMA-Ataxia. Mov Disord. 2023;38(1):45-56.
593. Joers JM, Adanyeguh IM, Deelchand DK, Hutter DH, Eberly LE, Iltis I, et al. Spinal cord magnetic resonance imaging and spectroscopy detect early-stage alterations and disease progression in Friedreich ataxia. Brain Commun. 2022;4(5):fcac246.
594. Georgiou-Karistianis N, Corben LA, Reetz K, Adanyeguh IM, Corti M, Deelchand DK, et al. A natural history study to track brain and spinal cord changes in individuals with Friedreich's ataxia: TRACK-FA study protocol. PLoS One. 2022;17(11):e0269649.
595. Gama MTD, Piccinin CC, Rezende TJR, Dion PA, Rouleau GA, França Junior MC, et al. Multimodal neuroimaging analysis in patients with SYNE1 Ataxia. Journal of the neurological sciences. 2018;390:227-30.
596. Hedera P, Eldevik OP, Maly P, Rainier S, Fink JK. Spinal cord magnetic resonance imaging in autosomal dominant hereditary spastic paraplegia. Neuroradiology. 2005;47(10):730-4.
597. Hocquel A, Ravel JM, Lambert L, Bonnet C, Banneau G, Kol B, et al. Reduced penetrance of an eastern French mutation in ATL1 autosomal-dominant inheritance (SPG3A): extended phenotypic spectrum coupled with brain (18)F-FDG PET. Neurogenetics. 2022;23(4):241-55.
598. Lin Q, Liu Y, Ye Z, Hu J, Cai W, Weng Q, et al. Potential markers for sample size estimations in hereditary spastic paraplegia type 5. Orphanet journal of rare diseases. 2021;16(1):391.
599. Liu Y, Ye Z, Hu J, Xiao Z, Zhang F, Yang X, et al. White Matter Alterations in Spastic Paraplegia Type 5: A Multiparametric Structural MRI Study and Correlations with Biochemical Measurements. AJNR Am J Neuroradiol. 2022;43(1):56-62.
600. Navas-Sánchez FJ, Marcos-Vidal L, de Blas DM, Fernández-Pena A, Alemán-Gómez Y, Guzmán-de-Villoria JA, et al. Tract-specific damage at spinal cord level in pure hereditary spastic paraplegia type 4: a diffusion tensor imaging study. Journal of neurology. 2022;269(6):3189-203.
601. Servelhere KR, Casseb RF, de Lima FD, Rezende TJR, Ramalho LP, França MC, Jr. Spinal Cord Gray and White Matter Damage in Different Hereditary Spastic Paraplegia Subtypes. AJNR Am J Neuroradiol. 2021;42(3):610-5.
602. Sperfeld AD, Baumgartner A, Kassubek J. Magnetic resonance investigation of the upper spinal cord in pure and complicated hereditary spastic paraparesis. Eur Neurol. 2005;54(4):181-5.
603. Lindig T, Ruff C, Rattay TW, König S, Schöls L, Schüle R, et al. Detection of spinal long fiber tract degeneration in HSP: Improved diffusion tensor imaging. Neuroimage Clin. 2022;36:103213.
604. Krabbe K, Nielsen JE, Fallentin E, Fenger K, Herning M. MRI of autosomal dominant pure spastic paraplegia. Neuroradiology. 1997;39(10):724-7.
605. Mühlau M, Engl C, Boucard CC, Schmidt P, Biberacher V, Görsch I, et al. Spinal cord atrophy in early Huntington's disease. Ann Clin Transl Neurol. 2014;1(4):302-6.
606. Wilhelms W, Bellenberg B, Köster O, Weiler F, Hoffmann R, Gold R, et al. Progressive spinal cord atrophy in manifest and premanifest Huntington's disease. J Neurol Neurosurg Psychiatry. 2017;88(7):614-6.
607. Castellano A, Papinutto N, Cadioli M, Brugnara G, Iadanza A, Scigliuolo G, et al. Quantitative MRI of the spinal cord and brain in adrenomyeloneuropathy: in vivo assessment of structural changes. Brain. 2016;139(Pt 6):1735-46.
608. Politi LS, Castellano A, Papinutto N, Mauro E, Pareyson D, Henry RG, et al. Longitudinal quantitative magnetic resonance imaging in adrenomyeloneuropathy. Eur J Neurol. 2019;26(10):1341-4.

609. van de Stadt SIW, van Ballegoij WJC, Labounek R, Huffnagel IC, Kemp S, Nestrasil I, et al. Spinal cord atrophy as a measure of severity of myelopathy in adrenoleukodystrophy. J Inherit Metab Dis. 2020;43(4):852-60.
610. Casseb RF, de Paiva JL, Branco LM, Martinez AR, Reis F, de Lima-Junior JC, et al. Spinal cord diffusion tensor imaging in patients with sensory neuronopathy. Neuroradiology. 2016;58(11):1103-8.
611. Bao Y-F, Tang W-J, Zhu D-Q, Li Y-X, Zee C-S, Chen X-J, et al. Sensory neuronopathy involves the spinal cord and brachial plexus: a quantitative study employing multiple-echo data image combination (MEDIC) and turbo inversion recovery magnitude (TIRM). Neuroradiology. 2013;55(1):41-8.
612. Evangelou IE, Massoud R, Jacobson S. HTLV-I-associated myelopathy/tropical spastic paraparesis: semiautomatic quantification of spinal cord atrophy from 3-dimensional MR images. J Neuroimaging. 2014;24(1):74-8.
613. Liu W, Nair G, Vuolo L, Bakshi A, Massoud R, Reich DS, et al. In vivo imaging of spinal cord atrophy in neuroinflammatory diseases. Ann Neurol. 2014;76(3):370-8.
614. Taniguchi A, Mochizuki H, Yamashita A, Shiomi K, Asada Y, Nakazato M. Spinal cord anteroposterior atrophy in HAM/TSP: Magnetic resonance imaging and neuropathological analyses. Journal of the neurological sciences. 2017;381:135-40.
615. Vilchez C, Gonzalez-Reinoso M, Cubbison C, Perez-Then E, Roa P, Martínez A, et al. Atrophy, focal spinal cord lesions and alterations of diffusion tensor imaging (DTI) parameters in asymptomatic virus carriers and patients suffering from human T-lymphotrophic virus type 1 (HTLV-1)-associated myelopathy/tropical spastic paraparesis (HAM/TSP). J Neurovirol. 2014;20(6):583-90.
616. Théaudin M, Saliou G, Denier C, Adams D, Ducreux D. A correlation between fractional anisotropy variations and clinical recovery in spinal cord infarctions. J Neuroimaging. 2013;23(2):256-8.
617. Malm J, Kristensen B, Karlsson T, Carlberg B, Fagerlund M, Olsson T. Cognitive impairment in young adults with infratentorial infarcts. Neurology. 1998;51(2):433-40.
618. Stoodley CJ, MacMore JP, Makris N, Sherman JC, Schmahmann JD. Location of lesion determines motor vs. cognitive consequences in patients with cerebellar stroke. NeuroImage: Clinical. 2016;12:765-75.
619. E KH, Chen SH, Ho MH, Desmond JE. A meta-analysis of cerebellar contributions to higher cognition from PET and fMRI studies. Human brain mapping. 2014;35(2):593-615.
620. Stoodley CJ, Schmahmann JD. Functional topography in the human cerebellum: a meta-analysis of neuroimaging studies. Neuroimage. 2009;44(2):489-501.
621. Argyropoulos GPD, van Dun K, Adamaszek M, Leggio M, Manto M, Masciullo M, et al. The Cerebellar Cognitive Affective/Schmahmann Syndrome: a Task Force Paper. Cerebellum (London, England). 2020;19(1):102-25.
622. Tedesco AM, Chiricozzi FR, Clausi S, Lupo M, Molinari M, Leggio MG. The cerebellar cognitive profile. Brain. 2011;134(12):3672-86.
623. Van Overwalle F, D'Aes T, Marien P. Social cognition and the cerebellum: A meta-analytic connectivity analysis. Human brain mapping. 2015;36(12):5137-54.
624. Runnqvist E, Bonnard M, Gauvin HS, Attarian S, Trébuchon A, Hartsuiker RJ, et al. Internal modeling of upcoming speech: A causal role of the right posterior cerebellum in non-motor aspects of language production. Cortex; a journal devoted to the study of the nervous system and behavior. 2016;81:203-14.
625. Finegan E, Chipika RH, Li Hi Shing S, Hardiman O, Bede P. Pathological Crying and Laughing in Motor Neuron Disease: Pathobiology, Screening, Intervention. Front Neurol. 2019;10:260.
626. Bede P, Finegan E. Revisiting the pathoanatomy of pseudobulbar affect: mechanisms beyond corticobulbar dysfunction. Amyotrophic lateral sclerosis & frontotemporal degeneration. 2018;19(1-2):4-6.
627. Levisohn L, Cronin-Golomb A, Schmahmann JD. Neuropsychological consequences of cerebellar tumour resection in children: Cerebellar cognitive affective syndrome in a paediatric population. Brain. 2000;123(5):1041-50.
628. Tan R, Devenney E, Kiernan M, Halliday G, Hodges J, Hornberger M. Terra incognita—cerebellar contributions to neuropsychiatric and cognitive dysfunction in behavioral variant frontotemporal dementia. Front Aging Neurosci. 2015;7(121).
629. Bocchetta M, Cardoso MJ, Cash DM, Ourselin S, Warren JD, Rohrer JD. Patterns of regional cerebellar atrophy in genetic frontotemporal dementia. Neuroimage Clin. 2016;11:287-90.
630. Chen Y, Kumfor F, Landin-Romero R, Irish M, Hodges JR, Piguet O. Cerebellar atrophy and its contribution to cognition in frontotemporal dementias. Ann Neurol. 2018;84(1):98-109.
631. Snowden JS, Rollinson S, Thompson JC, Harris JM, Stopford CL, Richardson AM, et al. Distinct clinical and pathological characteristics of frontotemporal dementia associated with C9ORF72 mutations. Brain. 2012;135(Pt 3):693-708.
632. Chen Y, Kumfor F, Landin-Romero R, Irish M, Piguet O. The Cerebellum in Frontotemporal Dementia: a Meta-Analysis of Neuroimaging Studies. Neuropsychol Rev. 2019;29(4):450-64.
633. Chen Y, Landin-Romero R, Kumfor F, Irish M, Hodges JR, Piguet O. Cerebellar structural connectivity and contributions to cognition in frontotemporal dementias. Cortex; a journal devoted to the study of the nervous system and behavior. 2020;129:57-67.

634. Gellersen HM, Guo CC, O'Callaghan C, Tan RH, Sami S, Hornberger M. Cerebellar atrophy in neurodegeneration—a meta-analysis. Journal of Neurology, Neurosurgery & Psychiatry. 2017;88(9):780-8.
635. Tan RH, Devenney E, Dobson-Stone C, Kwok JB, Hodges JR, Kiernan MC, et al. Cerebellar Integrity in the Amyotrophic Lateral Sclerosis - Frontotemporal Dementia Continuum. PLoS One. 2014;9(8):e105632.
636. Guo CC, Tan R, Hodges JR, Hu X, Sami S, Hornberger M. Network-selective vulnerability of the human cerebellum to Alzheimer's disease and frontotemporal dementia. Brain : a journal of neurology. 2016;139(Pt 5):1527-38.
637. Hardiman O, Doherty CP, Elamin M, Bede P. Neurodegenerative Disorders: A Clinical Guide. 2016 ed. Springer Cham Heidelberg New York Dordrecht London© Springer International Publishing Switzerland 2016: Springer International Publishing; 2016. 1-336 p.
638. Schmahmann JD. Dysmetria of thought: clinical consequences of cerebellar dysfunction on cognition and affect. Trends in Cognitive Sciences. 1998;2(9):362-71.
639. Ishii K, Sakamoto S, Sasaki M, Kitagaki H, Yamaji S, Hashimoto M, et al. Cerebral glucose metabolism in patients with frontotemporal dementia. J Nucl Med. 1998;39(11):1875-8.
640. Devenney E, Hornberger M, Irish M, Mioshi E, Burrell J, Tan R, et al. Frontotemporal Dementia Associated With the C9ORF72 Mutation: A Unique Clinical Profile. JAMA Neurology. 2014;71(3):331-9.
641. Simón-Sánchez J, Dopper EG, Cohn-Hokke PE, Hukema RK, Nicolaou N, Seelaar H, et al. The clinical and pathological phenotype of C9ORF72 hexanucleotide repeat expansions. Brain. 2012;135(Pt 3):723-35.
642. Mahoney CJ, Beck J, Rohrer JD, Lashley T, Mok K, Shakespeare T, et al. Frontotemporal dementia with the C9ORF72 hexanucleotide repeat expansion: clinical, neuroanatomical and neuropathological features. Brain : a journal of neurology. 2012;135(Pt 3):736-50.
643. Whitwell JL, Weigand SD, Boeve BF, Senjem ML, Gunter JL, DeJesus-Hernandez M, et al. Neuroimaging signatures of frontotemporal dementia genetics: C9ORF72, tau, progranulin and sporadics. Brain. 2012;135(Pt 3):794-806.
644. Ferrer I, Legati A, García-Monco JC, Gomez-Beldarrain M, Carmona M, Blanco R, et al. Familial behavioral variant frontotemporal dementia associated with astrocyte-predominant tauopathy. J Neuropathol Exp Neurol. 2015;74(4):370-9.
645. Rascovsky K, Hodges JR, Knopman D, Mendez MF, Kramer JH, Neuhaus J, et al. Sensitivity of revised diagnostic criteria for the behavioural variant of frontotemporal dementia. Brain. 2011;134:2456-77.
646. Bede P, Elamin M, Byrne S, Hardiman O. Sexual dimorphism in ALS: exploring gender-specific neuroimaging signatures. Amyotrophic lateral sclerosis & frontotemporal degeneration. 2014;15(3-4):235-43.
647. Diedrichsen J, Balsters JH, Flavell J, Cussans E, Ramnani N. A probabilistic MR atlas of the human cerebellum. Neuroimage. 2009;46(1):39-46.
648. Manjon JV, Coupe P. volBrain: An Online MRI Brain Volumetry System. Frontiers in neuroinformatics. 2016;10:30.
649. Romero JE, Coupe P, Giraud R, Ta VT, Fonov V, Park MTM, et al. CERES: A new cerebellum lobule segmentation method. Neuroimage. 2017;147:916-24.
650. Argyropoulos GD, Christidi F, Karavasilis E, Velonakis G, Antoniou A, Bede P, et al. Cerebro-cerebellar white matter connectivity in bipolar disorder and associated polarity subphenotypes. Progress in neuro-psychopharmacology & biological psychiatry. 2021;104:110034.
651. Grodd W, Hülsmann E, Lotze M, Wildgruber D, Erb M. Sensorimotor mapping of the human cerebellum: fMRI evidence of somatotopic organization. Human brain mapping. 2001;13(2):55-73.
652. Bushara KO, Wheat JM, Khan A, Mock BJ, Turski PA, Sorenson J, et al. Multiple tactile maps in the human cerebellum. Neuroreport. 2001;12(11):2483-6.
653. Tavano A, Grasso R, Gagliardi C, Triulzi F, Bresolin N, Fabbro F, et al. Disorders of cognitive and affective development in cerebellar malformations. Brain. 2007;130(Pt 10):2646-60.
654. Lupo M, Olivito G, Siciliano L, Masciullo M, Bozzali M, Molinari M, et al. Development of a Psychiatric Disorder Linked to Cerebellar Lesions. Cerebellum. 2018;17(4):438-46.
655. Turkel SB, Brumm VL, Mitchell WG, Tavare CJ. Mood and behavioral dysfunction with opsoclonus-myoclonus ataxia. J Neuropsychiatry Clin Neurosci. 2006;18(2):239-41.
656. Strakowski SM, Delbello MP, Adler CM. The functional neuroanatomy of bipolar disorder: a review of neuroimaging findings. Mol Psychiatry. 2005;10(1):105-16.
657. Bernard JA, Mittal VA. Cerebellar-motor dysfunction in schizophrenia and psychosis-risk: the importance of regional cerebellar analysis approaches. Front Psychiatry. 2014;5:160.
658. Brissenden JA, Levin EJ, Osher DE, Halko MA, Somers DC. Functional Evidence for a Cerebellar Node of the Dorsal Attention Network. The Journal of neuroscience : the official journal of the Society for Neuroscience. 2016;36(22):6083-96.
659. Buckner RL, Krienen FM, Castellanos A, Diaz JC, Yeo BTT. The organization of the human cerebellum estimated by intrinsic functional connectivity. J Neurophysiol. 2011;106(5):2322-45.
660. Palesi F, De Rinaldis A, Castellazzi G, Calamante F, Muhlert N, Chard D, et al. Contralateral cortico-ponto-cerebellar pathways reconstruction in humans in vivo: implications for reciprocal cerebro-cerebellar structural connectivity in motor and non-motor areas. Sci Rep. 2017;7(1):12841.

661. Takahashi E, Song JW, Folkerth RD, Grant PE, Schmahmann JD. Detection of postmortem human cerebellar cortex and white matter pathways using high angular resolution diffusion tractography: a feasibility study. NeuroImage. 2013;68:105-11.
662. Steele CJ, Anwander A, Bazin PL, Trampel R, Schaefer A, Turner R, et al. Human Cerebellar Sub-millimeter Diffusion Imaging Reveals the Motor and Non-motor Topography of the Dentate Nucleus. Cerebral Cortex. 2017;27(9):4537-48.
663. Bede P, Omer T, Finegan E, Chipika RH, Iyer PM, Doherty MA, et al. Connectivity-based characterisation of subcortical grey matter pathology in frontotemporal dementia and ALS: a multimodal neuroimaging study. Brain imaging and behavior. 2018;12(6):1696-707.
664. Rohrer JD, Nicholas JM, Cash DM, van Swieten J, Dopper E, Jiskoot L, et al. Presymptomatic cognitive and neuroanatomical changes in genetic frontotemporal dementia in the Genetic Frontotemporal dementia Initiative (GENFI) study: a cross-sectional analysis. Lancet neurology. 2015;14(3):253-62.
665. Querin G, Bede P, El Mendili MM, Li M, Pelegrini-Issac M, Rinaldi D, et al. Presymptomatic spinal cord pathology in c9orf72 mutation carriers: A longitudinal neuroimaging study. Ann Neurol. 2019;86(2):158-67.
666. Finegan E, Shing SLH, Chipika RH, Chang KM, McKenna MC, Doherty MA, et al. Extra-motor cerebral changes and manifestations in primary lateral sclerosis. Brain imaging and behavior. 2021.
667. Finegan E, Chipika RH, Shing SLH, Hardiman O, Bede P. Primary lateral sclerosis: a distinct entity or part of the ALS spectrum? Amyotrophic lateral sclerosis & frontotemporal degeneration. 2019;20(3-4):133-45.
668. Yunusova Y, Plowman EK, Green JR, Barnett C, Bede P. Clinical Measures of Bulbar Dysfunction in ALS. Front Neurol. 2019;10:106.
669. Christidi F, Karavasilis E, Rentzos M, Kelekis N, Evdokimidis I, Bede P. Clinical and Radiological Markers of Extra-Motor Deficits in Amyotrophic Lateral Sclerosis. Front Neurol. 2018;9:1005.
670. Verstraete E, Turner MR, Grosskreutz J, Filippi M, Benatar M. Mind the gap: the mismatch between clinical and imaging metrics in ALS. Amyotrophic lateral sclerosis & frontotemporal degeneration. 2015;16(7-8):524-9.
671. Abidi M, de Marco G, Grami F, Termoz N, Couillandre A, Querin G, et al. Neural Correlates of Motor Imagery of Gait in Amyotrophic Lateral Sclerosis. Journal of magnetic resonance imaging : JMRI. 2020.
672. Rolfs A, Koeppen AH, Bauer I, Bauer P, Buhlmann S, Topka H, et al. Clinical features and neuropathology of autosomal dominant spinocerebellar ataxia (SCA17). Ann Neurol. 2003;54(3):367-75.
673. Tahedl M, Chipika RH, Lope J, Li Hi Shing S, Hardiman O, Bede P. Cortical progression patterns in individual ALS patients across multiple timepoints: a mosaic-based approach for clinical use. Journal of neurology. 2021.
674. Panza F, Lozupone M, Seripa D, Daniele A, Watling M, Giannelli G, et al. Development of disease-modifying drugs for frontotemporal dementia spectrum disorders. Nature reviews Neurology. 2020;16(4):213-28.
675. Bonelli RM, Cummings JL. Frontal-subcortical circuitry and behavior. Dialogues Clin Neurosci. 2007;9(2):141-51.
676. Krauth A, Blanc R, Poveda A, Jeanmonod D, Morel A, Székely G. A mean three-dimensional atlas of the human thalamus: Generation from multiple histological data. NeuroImage. 2010;49(3):2053-62.
677. Schmahmann JD. Vascular Syndromes of the Thalamus. Stroke. 2003;34(9):2264-78.
678. Vertes RP, Linley SB, Hoover WB. Limbic circuitry of the midline thalamus. Neurosci Biobehav Rev. 2015;54:89-107.
679. Tan RH, Wong S, Kril JJ, Piguet O, Hornberger M, Hodges JR, et al. Beyond the temporal pole: limbic memory circuit in the semantic variant of primary progressive aphasia. Brain. 2014;137(7):2065-76.
680. Hornberger M, Wong S, Tan R, Irish M, Piguet O, Kril J, et al. In vivo and post-mortem memory circuit integrity in frontotemporal dementia and Alzheimer's disease. Brain. 2012;135(10):3015-25.
681. Kumar VJ, van Oort E, Scheffler K, Beckmann CF, Grodd W. Functional anatomy of the human thalamus at rest. Neuroimage. 2017;147:678-91.
682. Behrens TEJ, Johansen-Berg H, Woolrich MW, Smith SM, Wheeler-Kingshott CAM, Boulby PA, et al. Non-invasive mapping of connections between human thalamus and cortex using diffusion imaging. Nature Neuroscience. 2003;6(7):750-7.
683. Zhang Y, Zhang J, Oishi K, Faria AV, Jiang H, Li X, et al. Atlas-guided tract reconstruction for automated and comprehensive examination of the white matter anatomy. NeuroImage. 2010;52(4):1289-301.
684. Zhang D, Snyder AZ, Fox MD, Sansbury MW, Shimony JS, Raichle ME. Intrinsic functional relations between human cerebral cortex and thalamus. J Neurophysiol. 2008;100(4):1740-8.
685. Zhang D, Snyder AZ, Shimony JS, Fox MD, Raichle ME. Noninvasive Functional and Structural Connectivity Mapping of the Human Thalamocortical System. Cerebral Cortex. 2010;20(5):1187-94.
686. Alfano V, Federico G, Mele G, Garramone F, Esposito M, Aiello M, et al. Brain Networks Involved in Depression in Patients with Frontotemporal Dementia and Parkinson's Disease: An

Exploratory Resting-State Functional Connectivity MRI Study. Diagnostics (Basel, Switzerland). 2022;12(4).
687. Brown EC, Clark DL, Hassel S, MacQueen G, Ramasubbu R. Thalamocortical connectivity in major depressive disorder. Journal of affective disorders. 2017;217:125-31.
688. Bocchetta M, Iglesias JE, Neason M, Cash DM, Warren JD, Rohrer JD. Thalamic nuclei in frontotemporal dementia: Mediodorsal nucleus involvement is universal but pulvinar atrophy is unique to C9orf72. Hum Brain Mapp. 2020;41(4):1006-16.
689. Kawles A, Nishihira Y, Feldman A, Gill N, Minogue G, Keszycki R, et al. Cortical and subcortical pathological burden and neuronal loss in an autopsy series of FTLD-TDP-type C. Brain. 2022;145(3):1069-78.
690. Yang Y, Halliday GM, Hodges JR, Tan RH. von Economo Neuron Density and Thalamus Volumes in Behavioral Deficits in Frontotemporal Dementia Cases with and without a C9ORF72 Repeat Expansion. J Alzheimers Dis. 2017;58(3):701-9.
691. Ahmed RM, Irish M, Henning E, Dermody N, Bartley L, Kiernan MC, et al. Assessment of Eating Behavior Disturbance and Associated Neural Networks in Frontotemporal Dementia. JAMA Neurol. 2016;73(3):282-90.
692. Ahmed RM, Landin-Romero R, Liang CT, Keogh JM, Henning E, Strikwerda-Brown C, et al. Neural networks associated with body composition in frontotemporal dementia. Ann Clin Transl Neurol. 2019;6(9):1707-17.
693. Ahmed RM, Bocchetta M, Todd EG, Tse NY, Devenney EM, Tu S, et al. Tackling clinical heterogeneity across the amyotrophic lateral sclerosis-frontotemporal dementia spectrum using a transdiagnostic approach. Brain Commun. 2021;3(4):fcab257.
694. Bocchetta M, Gordon E, Cardoso MJ, Modat M, Ourselin S, Warren JD, et al. Thalamic atrophy in frontotemporal dementia - Not just a C9orf72 problem. Neuroimage Clin. 2018;18:675-81.
695. Bocchetta M, Iglesias JE, Russell LL, Greaves CV, Marshall CR, Scelsi MA, et al. Segmentation of medial temporal subregions reveals early right-sided involvement in semantic variant PPA. Alzheimers Res Ther. 2019;11(1):41.
696. Bocchetta M, Iglesias Espinosa MDM, Lashley T, Warren JD, Rohrer JD. In vivo staging of frontotemporal lobar degeneration TDP-43 type C pathology. Alzheimer's research & therapy. 2020;12(1):34-.
697. Branco LMT, de Rezende TJR, Roversi CdO, Zanao T, Casseb RF, de Campos BM, et al. Brain signature of mild stages of cognitive and behavioral impairment in amyotrophic lateral sclerosis. Psychiatry Research: Neuroimaging. 2018;272:58-64.
698. Cajanus A, Katisko K, Kontkanen A, Jääskeläinen O, Hartikainen P, Haapasalo A, et al. Serum neurofilament light chain in FTLD: association with C9orf72, clinical phenotype, and prognosis. Annals of clinical and translational neurology. 2020;7(6):903-10.
699. Cardenas VA, Boxer AL, Chao LL, Gorno-Tempini ML, Miller BL, Weiner MW, et al. Deformation-based morphometry reveals brain atrophy in frontotemporal dementia. Archives of neurology. 2007;64(6):873-7.
700. De Reuck JL, Deramecourt V, Auger F, Durieux N, Cordonnier C, Devos D, et al. Iron deposits in post-mortem brains of patients with neurodegenerative and cerebrovascular diseases: a semi-quantitative 7.0 T magnetic resonance imaging study. Eur J Neurol. 2014;21(7):1026-31.
701. De Reuck J, Devos D, Moreau C, Auger F, Durieux N, Deramecourt V, et al. Topographic distribution of brain iron deposition and small cerebrovascular lesions in amyotrophic lateral sclerosis and in frontotemporal lobar degeneration: a post-mortem 7.0-tesla magnetic resonance imaging study with neuropathological correlates. Acta Neurol Belg. 2017;117(4):873-8.
702. Devenney EM, Landin-Romero R, Irish M, Hornberger M, Mioshi E, Halliday GM, et al. The neural correlates and clinical characteristics of psychosis in the frontotemporal dementia continuum and the C9orf72 expansion. NeuroImage: Clinical. 2017;13:439-45.
703. Devenney EM, Tu S, Caga J, Ahmed RM, Ramsey E, Zoing M, et al. Neural mechanisms of psychosis vulnerability and perceptual abnormalities in the ALS-FTD spectrum. Ann Clin Transl Neurol. 2021;8(8):1576-91.
704. Fletcher PD, Downey LE, Golden HL, Clark CN, Slattery CF, Paterson RW, et al. Pain and temperature processing in dementia: a clinical and neuroanatomical analysis. Brain. 2015;138(Pt 11):3360-72.
705. Garibotto V, Borroni B, Agosti C, Premi E, Alberici A, Eickhoff SB, et al. Subcortical and deep cortical atrophy in Frontotemporal Lobar Degeneration. Neurobiol Aging. 2011;32(5):875-84.
706. Harper L, Bouwman F, Burton EJ, Barkhof F, Scheltens P, O'Brien JT, et al. Patterns of atrophy in pathologically confirmed dementias: a voxelwise analysis. J Neurol Neurosurg Psychiatry. 2017;88(11):908-16.
707. Irwin DJ, McMillan CT, Brettschneider J, Libon DJ, Powers J, Rascovsky K, et al. Cognitive decline and reduced survival in C9orf72 expansion frontotemporal degeneration and amyotrophic lateral sclerosis. J Neurol Neurosurg Psychiatry. 2013;84(2):163-9.
708. Irwin DJ, Brettschneider J, McMillan CT, Cooper F, Olm C, Arnold SE, et al. Deep clinical and neuropathological phenotyping of Pick disease. Ann Neurol. 2016;79(2):272-87.
709. Kumfor F, Hutchings R, Irish M, Hodges JR, Rhodes G, Palermo R, et al. Do I know you? Examining face and object memory in frontotemporal dementia. Neuropsychologia. 2015;71:101-11.

710. Landin-Romero R, Kumfor F, Leyton CE, Irish M, Hodges JR, Piguet O. Disease-specific patterns of cortical and subcortical degeneration in a longitudinal study of Alzheimer's disease and behavioural-variant frontotemporal dementia. Neuroimage. 2017;151:72-80.
711. Links KA, Chow TW, Binns M, Freedman M, Stuss DT, Scott CJ, et al. Apathy is not associated with basal ganglia atrophy in frontotemporal dementia. Am J Geriatr Psychiatry. 2009;17(9):819-21.
712. Mahoney CJ, Rohrer JD, Goll JC, Fox NC, Rossor MN, Warren JD. Structural neuroanatomy of tinnitus and hyperacusis in semantic dementia. J Neurol Neurosurg Psychiatry. 2011;82(11):1274-8.
713. Manera AL, Dadar M, Collins DL, Ducharme S. Deformation based morphometry study of longitudinal MRI changes in behavioral variant frontotemporal dementia. Neuroimage Clin. 2019;24:102079.
714. Mann DM, South PW. The topographic distribution of brain atrophy in frontal lobe dementia. Acta Neuropathol. 1993;85(3):334-40.
715. McMillan CT, Russ J, Wood EM, Irwin DJ, Grossman M, McCluskey L, et al. C9orf72 promoter hypermethylation is neuroprotective. Neurology. 2015;84(16):1622.
716. Meysami S, Raji CA, Mendez MF. Quantified Brain Magnetic Resonance Imaging Volumes Differentiate Behavioral Variant Frontotemporal Dementia from Early-Onset Alzheimer's Disease. J Alzheimers Dis. 2022;87(1):453-61.
717. Mioshi E, Hodges JR, Hornberger M. Neural correlates of activities of daily living in frontotemporal dementia. J Geriatr Psychiatry Neurol. 2013;26(1):51-7.
718. Möller C, Dieleman N, van der Flier WM, Versteeg A, Pijnenburg Y, Scheltens P, et al. More atrophy of deep gray matter structures in frontotemporal dementia compared to Alzheimer's disease. J Alzheimers Dis. 2015;44(2):635-47.
719. Pasquini L, Nana AL, Toller G, Brown JA, Deng J, Staffaroni A, et al. Salience Network Atrophy Links Neuron Type-Specific Pathobiology to Loss of Empathy in Frontotemporal Dementia. Cereb Cortex. 2020;30(10):5387-99.
720. Possin KL, Chester SK, Laluz V, Bostrom A, Rosen HJ, Miller BL, et al. The frontal-anatomic specificity of design fluency repetitions and their diagnostic relevance for behavioral variant frontotemporal dementia. J Int Neuropsychol Soc. 2012;18(5):834-44.
721. San Lee J, Yoo S, Park S, Kim HJ, Park K-C, Seong J-K, et al. Differences in neuroimaging features of early- versus late-onset nonfluent/agrammatic primary progressive aphasia. Neurobiology of Aging. 2020;86:92-101.
722. Sellami L, Bocchetta M, Masellis M, Cash DM, Dick KM, van Swieten J, et al. Distinct Neuroanatomical Correlates of Neuropsychiatric Symptoms in the Three Main Forms of Genetic Frontotemporal Dementia in the GENFI Cohort. J Alzheimers Dis. 2018;65(1):147-63.
723. Sha SJ, Takada LT, Rankin KP, Yokoyama JS, Rutherford NJ, Fong JC, et al. Frontotemporal dementia due to C9ORF72 mutations: clinical and imaging features. Neurology. 2012;79(10):1002-11.
724. Spinelli EG, Ghirelli A, Basaia S, Cividini C, Riva N, Canu E, et al. Structural MRI Signatures in Genetic Presentations of the Frontotemporal Dementia/Motor Neuron Disease Spectrum. Neurology. 2021;97(16):e1594-e607.
725. Sturm VE, Perry DC, Wood K, Hua AY, Alcantar O, Datta S, et al. Prosocial deficits in behavioral variant frontotemporal dementia relate to reward network atrophy. Brain and behavior. 2017;7(10):e00807.
726. Sturm VE, Sible IJ, Datta S, Hua AY, Perry DC, Kramer JH, et al. Resting parasympathetic dysfunction predicts prosocial helping deficits in behavioral variant frontotemporal dementia. Cortex; a journal devoted to the study of the nervous system and behavior. 2018;109:141-55.
727. Toller G, Ranasinghe K, Cobigo Y, Staffaroni A, Appleby B, Brushaber D, et al. Revised Self-Monitoring Scale: A potential endpoint for frontotemporal dementia clinical trials. Neurology. 2020;94(22):e2384-e95.
728. van der Burgh HK, Westeneng HJ, Walhout R, van Veenhuijzen K, Tan HHG, Meier JM, et al. Multimodal longitudinal study of structural brain involvement in amyotrophic lateral sclerosis. Neurology. 2020;94(24):e2592-e604.
729. Downey LE, Mahoney CJ, Buckley AH, Golden HL, Henley SM, Schmitz N, et al. White matter tract signatures of impaired social cognition in frontotemporal lobar degeneration. Neuroimage Clin. 2015;8:640-51.
730. Spotorno N, Lindberg O, Nilsson C, Landqvist Waldö M, van Westen D, Nilsson K, et al. Plasma neurofilament light protein correlates with diffusion tensor imaging metrics in frontotemporal dementia. PLoS One. 2020;15(10):e0236384.
731. Agosta F, Ferraro PM, Riva N, Spinelli EG, Domi T, Carrera P, et al. Structural and functional brain signatures of C9orf72 in motor neuron disease. Neurobiology of Aging. 2017;57:206-19.
732. Farb NA, Grady CL, Strother S, Tang-Wai DF, Masellis M, Black S, et al. Abnormal network connectivity in frontotemporal dementia: evidence for prefrontal isolation. Cortex; a journal devoted to the study of the nervous system and behavior. 2013;49(7):1856-73.
733. Lee SE, Khazenzon AM, Trujillo AJ, Guo CC, Yokoyama JS, Sha SJ, et al. Altered network connectivity in frontotemporal dementia with C9orf72 hexanucleotide repeat expansion. Brain : a journal of neurology. 2014;137(Pt 11):3047-60.

734. Ng ASL, Wang J, Ng KK, Chong JSX, Qian X, Lim JKW, et al. Distinct network topology in Alzheimer's disease and behavioral variant frontotemporal dementia. Alzheimer's research & therapy. 2021;13(1):13-.
735. Rijpma MG, Yang WFZ, Toller G, Battistella G, Sokolov AA, Sturm VE, et al. Influence of periaqueductal gray on other salience network nodes predicts social sensitivity. Human brain mapping. 2022;43(5):1694-709.
736. Rombouts SA, van Swieten JC, Pijnenburg YA, Goekoop R, Barkhof F, Scheltens P. Loss of frontal fMRI activation in early frontotemporal dementia compared to early AD. Neurology. 2003;60(12):1904-8.
737. Toller G, Brown J, Sollberger M, Shdo SM, Bouvet L, Sukhanov P, et al. Individual differences in socioemotional sensitivity are an index of salience network function. Cortex; a journal devoted to the study of the nervous system and behavior. 2018;103:211-23.
738. Cistaro A, Pagani M, Montuschi A, Calvo A, Moglia C, Canosa A, et al. The metabolic signature of C9ORF72-related ALS: FDG PET comparison with nonmutated patients. European journal of nuclear medicine and molecular imaging. 2014;41(5):844-52.
739. Diehl-Schmid J, Grimmer T, Drzezga A, Bornschein S, Riemenschneider M, Förstl H, et al. Decline of cerebral glucose metabolism in frontotemporal dementia: a longitudinal 18F-FDG-PET-study. Neurobiol Aging. 2007;28(1):42-50.
740. Diehl-Schmid J, Licata A, Goldhardt O, Förstl H, Yakushew I, Otto M, et al. FDG-PET underscores the key role of the thalamus in frontotemporal lobar degeneration caused by C9ORF72 mutations. Translational Psychiatry. 2019;9(1):54.
741. Frisch S, Dukart J, Vogt B, Horstmann A, Becker G, Villringer A, et al. Dissociating memory networks in early Alzheimer's disease and frontotemporal lobar degeneration - a combined study of hypometabolism and atrophy. PLoS One. 2013;8(2):e55251.
742. Grimmer T, Diehl J, Drzezga A, Förstl H, Kurz A. Region-specific decline of cerebral glucose metabolism in patients with frontotemporal dementia: a prospective 18F-FDG-PET study. Dementia and geriatric cognitive disorders. 2004;18(1):32-6.
743. Jang YK, Lyoo CH, Park S, Oh SJ, Cho H, Oh M, et al. Head to head comparison of [(18)F] AV-1451 and [(18)F] THK5351 for tau imaging in Alzheimer's disease and frontotemporal dementia. European journal of nuclear medicine and molecular imaging. 2018;45(3):432-42.
744. Jeong Y, Cho SS, Park JM, Kang SJ, Lee JS, Kang E, et al. 18F-FDG PET findings in frontotemporal dementia: an SPM analysis of 29 patients. J Nucl Med. 2005;46(2):233-9.
745. Leuzy A, Zimmer ER, Dubois J, Pruessner J, Cooperman C, Soucy JP, et al. In vivo characterization of metabotropic glutamate receptor type 5 abnormalities in behavioral variant FTD. Brain Struct Funct. 2016;221(3):1387-402.
746. Matias-Guiu JA, Cabrera-Martín MN, Fernádez-Matarrubia M, Moreno-Ramos T, Valles-Salgado M, Porta-Etessam J, et al. Topography of primitive reflexes in dementia: an F-18 fluorodeoxyglucose positron emission tomography study. Eur J Neurol. 2015;22(8):1201-7.
747. Poljansky S, Ibach B, Hirschberger B, Männer P, Klünemann H, Hajak G, et al. A visual [18F]FDG-PET rating scale for the differential diagnosis of frontotemporal lobar degeneration. Eur Arch Psychiatry Clin Neurosci. 2011;261(6):433-46.
748. Schaeverbeke J, Gabel S, Meersmans K, Bruffaerts R, Liuzzi AG, Evenepoel C, et al. Single-word comprehension deficits in the nonfluent variant of primary progressive aphasia. Alzheimers Res Ther. 2018;10(1):68.
749. Soleimani-Meigooni DN, Iaccarino L, La Joie R, Baker S, Bourakova V, Boxer AL, et al. 18F-flortaucipir PET to autopsy comparisons in Alzheimer's disease and other neurodegenerative diseases. Brain. 2020;143(11):3477-94.
750. Moller C, Dieleman N, van der Flier WM, Versteeg A, Pijnenburg Y, Scheltens P, et al. More atrophy of deep gray matter structures in frontotemporal dementia compared to Alzheimer's disease. Journal of Alzheimer's disease : JAD. 2015;44(2):635-47.
751. McKenna MC, Corcia P, Couratier P, Siah WF, Pradat PF, Bede P. Frontotemporal Pathology in Motor Neuron Disease Phenotypes: Insights From Neuroimaging. Front Neurol. 2021;12:723450.
752. Broe M, Hodges JR, Schofield E, Shepherd CE, Kril JJ, Halliday GM. Staging disease severity in pathologically confirmed cases of frontotemporal dementia. Neurology. 2003;60(6):1005-11.
753. Cykowski MD, Takei H, Van Eldik LJ, Schmitt FA, Jicha GA, Powell SZ, et al. Hippocampal Sclerosis but Not Normal Aging or Alzheimer Disease Is Associated With TDP-43 Pathology in the Basal Forebrain of Aged Persons. Journal of neuropathology and experimental neurology. 2016;75(5):397-407.
754. Diehl-Schmid J, Grimmer T, Drzezga A, Bornschein S, Riemenschneider M, Forstl H, et al. Decline of cerebral glucose metabolism in frontotemporal dementia: a longitudinal 18F-FDG-PET-study. Neurobiol Aging. 2007;28(1):42-50.
755. Vatsavayai SC, Yoon SJ, Gardner RC, Gendron TF, Vargas JN, Trujillo A, et al. Timing and significance of pathological features in C9orf72 expansion-associated frontotemporal dementia. Brain. 2016;139(Pt 12):3202-16.
756. Davidson Y, Robinson AC, Liu X, Wu D, Troakes C, Rollinson S, et al. Neurodegeneration in frontotemporal lobar degeneration and motor neurone disease associated with expansions in C9orf72 is linked to TDP-43 pathology and not associated with aggregated forms of dipeptide repeat proteins. Neuropathology and Applied Neurobiology. 2016;42(3):242-54.

757. Troakes C, Maekawa S, Wijesekera L, Rogelj B, Siklos L, Bell C, et al. An MND/ALS phenotype associated with C9orf72 repeat expansion: abundant p62-positive, TDP-43-negative inclusions in cerebral cortex, hippocampus and cerebellum but without associated cognitive decline. Neuropathology : official journal of the Japanese Society of Neuropathology. 2012;32(5):505-14.
758. Chipika RH, Siah WF, Shing SLH, Finegan E, McKenna MC, Christidi F, et al. MRI data confirm the selective involvement of thalamic and amygdalar nuclei in amyotrophic lateral sclerosis and primary lateral sclerosis. Data in brief. 2020:106246.
759. Schönecker S, Neuhofer C, Otto M, Ludolph A, Kassubek J, Landwehrmeyer B, et al. Atrophy in the Thalamus But Not Cerebellum Is Specific for C9orf72 FTD and ALS Patients – An Atlas-Based Volumetric MRI Study. Front Aging Neurosci. 2018;10.
760. Mahoney CJ, Downey LE, Ridgway GR, Beck J, Clegg S, Blair M, et al. Longitudinal neuroimaging and neuropsychological profiles of frontotemporal dementia with C9ORF72 expansions. Alzheimer's Research & Therapy. 2012;4(5):41.
761. Chow TW, Izenberg A, Binns MA, Freedman M, Stuss DT, Scott CJ, et al. Magnetic resonance imaging in frontotemporal dementia shows subcortical atrophy. Dementia and geriatric cognitive disorders. 2008;26(1):79-88.
762. Bak TH, Chandran S. What wires together dies together: verbs, actions and neurodegeneration in motor neuron disease. Cortex. 2012;48(7):936-44.
763. Feiler MS, Strobel B, Freischmidt A, Helferich AM, Kappel J, Brewer BM, et al. TDP-43 is intercellularly transmitted across axon terminals. The Journal of cell biology. 2015;211(4):897-911.
764. Nonaka T, Masuda-Suzukake M, Arai T, Hasegawa Y, Akatsu H, Obi T, et al. Prion-like properties of pathological TDP-43 aggregates from diseased brains. Cell reports. 2013;4(1):124-34.
765. Smethurst P, Newcombe J, Troakes C, Simone R, Chen YR, Patani R, et al. In vitro prion-like behaviour of TDP-43 in ALS. Neurobiology of disease. 2016;96:236-47.
766. Grossman M, Anderson C, Khan A, Avants B, Elman L, McCluskey L. Impaired action knowledge in amyotrophic lateral sclerosis. Neurology. 2008;71(18):1396-401.
767. McKenna MC, Lope J, Tan EL, Bede P. Pre-symptomatic radiological changes in frontotemporal dementia: propagation characteristics, predictive value and implications for clinical trials. Brain imaging and behavior. 2022.
768. Tan HHG, Westeneng HJ, Nitert AD, van Veenhuijzen K, Meier JM, van der Burgh HK, et al. MRI clustering reveals three ALS subtypes with unique neurodegeneration patterns. Ann Neurol. 2022.
769. Bede P, Murad A, Lope J, Hardiman O, Chang KM. Clusters of anatomical disease-burden patterns in ALS: a data-driven approach confirms radiological subtypes. Journal of neurology. 2022.
770. Dukic S, McMackin R, Costello E, Metzger M, Buxo T, Fasano A, et al. Resting-state EEG reveals four subphenotypes of amyotrophic lateral sclerosis. Brain. 2022;145(2):621-31.
771. Long Z, Irish M, Foxe D, Hodges JR, Piguet O, Burrell JR. Heterogeneity of behavioural and language deficits in FTD–MND. Journal of neurology. 2021;268(8):2876-89.
772. Bede P, Chang KM, Tan EL. Machine-learning in motor neuron diseases: Prospects and pitfalls. Eur J Neurol. 2022.
773. Querin G, Biferi MG, Pradat PF. Biomarkers for C9orf7-ALS in Symptomatic and Pre-symptomatic Patients: State-of-the-art in the New Era of Clinical Trials. Journal of neuromuscular diseases. 2022;9(1):25-37.
774. Finegan E, Li Hi Shing S, Chipika RH, Doherty MA, Hengeveld JC, Vajda A, et al. Widespread subcortical grey matter degeneration in primary lateral sclerosis: a multimodal imaging study with genetic profiling. Neuroimage Clin. 2019;24:102089.
775. Finegan E, Siah WF, Shing SLH, Chipika RH, Chang KM, McKenna MC, et al. Imaging and clinical data indicate considerable disease burden in 'probable' PLS: patients with UMN symptoms for 2-4 years. Data in brief. 2020:106247.
776. Finegan E, Shing SLH, Chipika RH, Chang KM, McKenna MC, Doherty MA, et al. Extra-motor cerebral changes and manifestations in primary lateral sclerosis. Brain imaging and behavior. 2021;15(5):2283-96.
777. Bede P, Pradat PF, Lope J, Vourc'h P, Blasco H, Corcia P. Primary Lateral Sclerosis: Clinical, radiological and molecular features. Rev Neurol (Paris). 2021.
778. Mulkerrin G, França MC, Jr., Lope J, Tan EL, Bede P. Neuroimaging in hereditary spastic paraplegias: from qualitative cues to precision biomarkers. Expert review of molecular diagnostics. 2022;22(7):745-60.
779. Querin G, Bede P, Marchand-Pauvert V, Pradat PF. Biomarkers of Spinal and Bulbar Muscle Atrophy (SBMA): A Comprehensive Review. Front Neurol. 2018;9:844.
780. Clark AL, Sorg SF, Holiday K, Bigler ED, Bangen KJ, Evangelista ND, et al. Fatigue Is Associated With Global and Regional Thalamic Morphometry in Veterans With a History of Mild Traumatic Brain Injury. The Journal of head trauma rehabilitation. 2018;33(6):382-92.
781. Li Hi Shing S, Chipika RH, Finegan E, Murray D, Hardiman O, Bede P. Post-polio Syndrome: More Than Just a Lower Motor Neuron Disease. Front Neurol. 2019;10:773.
782. Seok JM, Cho W, Son DH, Shin JH, Cho EB, Kim ST, et al. Association of subcortical structural shapes with fatigue in neuromyelitis optica spectrum disorder. Sci Rep. 2022;12(1):1579.
783. Li Hi Shing S, Lope J, Chipika RH, Hardiman O, Bede P. Extra-motor manifestations in post-polio syndrome (PPS): fatigue, cognitive symptoms and radiological features. Neurol Sci. 2021;42(11):4569-81.

784. Ferguson BR, Gao WJ. Thalamic Control of Cognition and Social Behavior Via Regulation of Gamma-Aminobutyric Acidergic Signaling and Excitation/Inhibition Balance in the Medial Prefrontal Cortex. Biological psychiatry. 2018;83(8):657-69.
785. Wolff M, Vann SD. The Cognitive Thalamus as a Gateway to Mental Representations. J Neurosci. 2019;39(1):3-14.
786. King RR, Reiss JP. The epidemiology and pathophysiology of pseudobulbar affect and its association with neurodegeneration. Degenerative neurological and neuromuscular disease. 2013;3:23-31.
787. Chipika RH, Mulkerrin G, Murad A, Lope J, Hardiman O, Bede P. Alterations in somatosensory, visual and auditory pathways in amyotrophic lateral sclerosis: an under-recognised facet of ALS. Journal of integrative neuroscience. 2022;21(3):88.
788. Iglesias JE, Insausti R, Lerma-Usabiaga G, Bocchetta M, Van Leemput K, Greve DN, et al. A probabilistic atlas of the human thalamic nuclei combining ex vivo MRI and histology. Neuroimage. 2018;183:314-26.
789. Patenaude B, Smith SM, Kennedy DN, Jenkinson M. A Bayesian model of shape and appearance for subcortical brain segmentation. Neuroimage. 2011;56(3):907-22.
790. Sharma KR, Saigal G, Maudsley AA, Govind V. 1H MRS of basal ganglia and thalamus in amyotrophic lateral sclerosis. NMR in biomedicine. 2011;24(10):1270-6.
791. Zarkali A, McColgan P, Leyland LA, Lees AJ, Weil RS. Longitudinal thalamic white and grey matter changes associated with visual hallucinations in Parkinson's disease. J Neurol Neurosurg Psychiatry. 2022;93(2):169-79.
792. Behrens TE, Johansen-Berg H, Woolrich MW, Smith SM, Wheeler-Kingshott CA, Boulby PA, et al. Non-invasive mapping of connections between human thalamus and cortex using diffusion imaging. Nat Neurosci. 2003;6(7):750-7.
793. Bosch-Bouju C, Hyland BI, Parr-Brownlie LC. Motor thalamus integration of cortical, cerebellar and basal ganglia information: implications for normal and parkinsonian conditions. Frontiers in computational neuroscience. 2013;7:163.
794. Blackshaw S, Scholpp S, Placzek M, Ingraham H, Simerly R, Shimogori T. Molecular pathways controlling development of thalamus and hypothalamus: from neural specification to circuit formation. J Neurosci. 2010;30(45):14925-30.
795. Cistaro A, Pagani M, Montuschi A, Calvo A, Moglia C, Canosa A, et al. The metabolic signature of C9ORF72-related ALS: FDG PET comparison with nonmutated patients. European journal of nuclear medicine and molecular imaging. 2014.
796. Johansen-Berg H, Behrens TE, Sillery E, Ciccarelli O, Thompson AJ, Smith SM, et al. Functional-anatomical validation and individual variation of diffusion tractography-based segmentation of the human thalamus. Cereb Cortex. 2005;15(1):31-9.
797. Tu S, Menke RAL, Talbot K, Kiernan MC, Turner MR. Regional thalamic MRI as a marker of widespread cortical pathology and progressive frontotemporal involvement in amyotrophic lateral sclerosis. J Neurol Neurosurg Psychiatry. 2018;89(12):1250-8.
798. Zhang JQ, Ji B, Zhou CY, Li LC, Li ZH, Hu XP, et al. Differential Impairment of Thalamocortical Structural Connectivity in Amyotrophic Lateral Sclerosis. CNS neuroscience & therapeutics. 2017;23(2):155-61.
799. Bede P. Deciphering neurodegeneration: A paradigm shift from focality to connectivity. Neurology. 2017.
800. Radanovic M, Rosemberg S, Adas R, Miranda SC, Caramelli P, Caixeta L, et al. Frontotemporal dementia with severe thalamic involvement: a clinical and neuropathological study. Arq Neuropsiquiatr. 2003;61(4):930-5.
801. Chipika RH, Christidi F, Finegan E, Li Hi Shing S, McKenna MC, Chang KM, et al. Amygdala pathology in amyotrophic lateral sclerosis and primary lateral sclerosis. J Neurol Sci. 2020:117039.
802. Winkler AM, Ridgway GR, Webster MA, Smith SM, Nichols TE. Permutation inference for the general linear model. Neuroimage. 2014;92:381-97.
803. Desikan RS, Segonne F, Fischl B, Quinn BT, Dickerson BC, Blacker D, et al. An automated labeling system for subdividing the human cerebral cortex on MRI scans into gyral based regions of interest. Neuroimage. 2006;31(3):968-80.
804. Grodd W, Kumar VJ, Schüz A, Lindig T, Scheffler K. The anterior and medial thalamic nuclei and the human limbic system: tracing the structural connectivity using diffusion-weighted imaging. Sci Rep. 2020;10(1):10957.
805. Llano D. The Thalamus and Language. 2016. p. 95-114.
806. Llano DA. Functional imaging of the thalamus in language. Brain and Language. 2013;126(1):62-72.
807. Tiedt HO, Ehlen F, Wyrobnik M, Klostermann F. Thalamic but Not Subthalamic Neuromodulation Simplifies Word Use in Spontaneous Language. Front Hum Neurosci. 2021;15.
808. Ehlen F, Schoenecker T, Kühn AA, Klostermann F. Differential effects of deep brain stimulation on verbal fluency. Brain Lang. 2014;134:23-33.
809. Johnson MD, Ojemann GA. The role of the human thalamus in language and memory: evidence from electrophysiological studies. Brain Cogn. 2000;42(2):218-30.

810. Südmeyer M, Pieperhoff P, Ferrea S, Krause H, Groiss SJ, Elben S, et al. Longitudinal Deformation-Based Morphometry Reveals Spatio-Temporal Dynamics of Brain Volume Changes in Patients with Corticobasal Syndrome. PLoS One. 2012;7(7):e41873.
811. Hess CP, Christine CW, Apple AC, Dillon WP, Aminoff MJ. Changes in the Thalamus in Atypical Parkinsonism Detected Using Shape Analysis and Diffusion Tensor Imaging. American Journal of Neuroradiology. 2014;35(5):897.
812. van de Mortel LA, Thomas RM, van Wingen GA, Alzheimer's Disease Neuroimaging I. Grey Matter Loss at Different Stages of Cognitive Decline: A Role for the Thalamus in Developing Alzheimer's Disease. J Alzheimers Dis. 2021;83(2):705-20.
813. Braak H, Braak E. Alzheimer's disease affects limbic nuclei of the thalamus. Acta Neuropathol. 1991;81(3):261-8.
814. Reyes P, Ortega-Merchan MP, Rueda A, Uriza F, Santamaria-García H, Rojas-Serrano N, et al. Functional Connectivity Changes in Behavioral, Semantic, and Nonfluent Variants of Frontotemporal Dementia. Behavioural neurology. 2018;2018:9684129-.
815. Kim EJ, Hwang JL, Gaus SE, Nana AL, Deng J, Brown JA, et al. Evidence of corticofugal tau spreading in patients with frontotemporal dementia. Acta Neuropathol. 2020;139(1):27-43.
816. Omer T, Finegan E, Hutchinson S, Doherty M, Vajda A, McLaughlin RL, et al. Neuroimaging patterns along the ALS-FTD spectrum: a multiparametric imaging study. Amyotrophic Lateral Sclerosis and Frontotemporal Degeneration. 2017;18(7-8):611-23.
817. Whitwell JL, Jack CR, Parisi JE, Knopman DS, Boeve BF, Petersen RC, et al. Imaging Signatures of Molecular Pathology in Behavioral Variant Frontotemporal Dementia. Journal of Molecular Neuroscience. 2011;45(3):372.
818. Rohrer JD, Lashley T, Schott JM, Warren JE, Mead S, Isaacs AM, et al. Clinical and neuroanatomical signatures of tissue pathology in frontotemporal lobar degeneration. Brain. 2011;134(9):2565-81.
819. Nishio Y, Nakano Y, Matsumoto K, Hashimoto M, Kazui H, Hirono N, et al. Striatal infarcts mimicking frontotemporal dementia: a case report. European Journal of Neurology. 2003;10(4):457-60.
820. Campanella F, Shallice T, Ius T, Fabbro F, Skrap M. Impact of brain tumour location on emotion and personality: a voxel-based lesion–symptom mapping study on mentalization processes. Brain. 2014;137(9):2532-45.
821. Baez S, Couto B, Torralva T, Sposato LA, Huepe D, Montañes P, et al. Comparing Moral Judgments of Patients With Frontotemporal Dementia and Frontal Stroke. JAMA Neurology. 2014;71(9):1172-6.
822. Kito Y, Kazui H, Kubo Y, Yoshida T, Takaya M, Wada T, et al. Neuropsychiatric symptoms in patients with idiopathic normal pressure hydrocephalus. Behavioural Neurology. 2009;21:165-74.
823. Younes K, Lepow LA, Estrada C, Schulz PE. Auto-antibodies against P/Q- and N-type voltage-dependent calcium channels mimicking frontotemporal dementia. SAGE Open Medical Case Reports. 2018;6:2050313X17750928.
824. Kotagal V, Lorincz MT, Bohnen NI. A Frontotemporal Dementia-like Syndrome Mimicking Postpartum Depression Detected by 18F Fluorodeoxyglucose Positron Emission Tomography. Clinical Nuclear Medicine. 2012;37(9).
825. De Maindreville A, Bedos L, Bakchine S. Systemic Sarcoidosis Mimicking a Behavioural Variant of Frontotemporal Dementia. Case Reports in Neurological Medicine. 2015;2015:409126.
826. McKeon A, Marnane M, O'Connell M, Stack JP, Kelly PJ, Lynch T. Potassium Channel Antibody–Associated Encephalopathy Presenting With a Frontotemporal Dementia–like Syndrome. Archives of Neurology. 2007;64(10):1528-30.
827. Di Fede G, Catania M, Atzori C, Moda F, Pasquali C, Indaco A, et al. Clinical and neuropathological phenotype associated with the novel V189I mutation in the prion protein gene. Acta Neuropathologica Communications. 2019;7(1):1.
828. Aizpurua M, Selvackadunco S, Yull H, Kipps CM, Ironside JW, Bodi I. Variably protease-sensitive prionopathy mimicking frontotemporal dementia. Neuropathology : official journal of the Japanese Society of Neuropathology. 2019;39(2):135-40.
829. Adachi M, Kawanami T, Ohshima H, Sugai Y, Hosoya T. Morning Glory Sign: A Particular MR Finding in Progressive Supranuclear Palsy. Magnetic Resonance in Medical Sciences. 2004;3(3):125-32.
830. Way C, Pettersson D, Hiller A. The 'Hot Cross Bun' Sign Is Not Always Multiple System Atrophy: Etiologies of 11 Cases. J Mov Disord. 2019;12(1):27-30.
831. MUQIT MMK, MORT D, MISZKIEL KA, SHAKIR RA. "Hot cross bun" sign in a patient with parkinsonism secondary to presumed vasculitis. Journal of Neurology, Neurosurgery & Psychiatry. 2001;71(4):565-6.
832. Mueller C, Hussl A, Krismer F, Heim B, Mahlknecht P, Nocker M, et al. The diagnostic accuracy of the hummingbird and morning glory sign in patients with neurodegenerative parkinsonism. Parkinsonism & Related Disorders. 2018;54:90-4.
833. Harper L, Barkhof F, Scheltens P, Schott JM, Fox NC. An algorithmic approach to structural imaging in dementia. Journal of Neurology, Neurosurgery & Psychiatry. 2014;85(6):692-8.
834. Bede P, Querin G, Pradat PF. The changing landscape of motor neuron disease imaging: the transition from descriptive studies to precision clinical tools. Current opinion in neurology. 2018;31(4):431-8.

835. McMahon P, Araki S, Sandberg E, Neumann P, Gazelle G. Cost-Effectiveness of PET in the Diagnosis of Alzheimer Disease1. Radiology. 2003;228:515-22.
836. Shivamurthy VKN, Tahari AK, Marcus C, Subramaniam RM. Brain FDG PET and the Diagnosis of Dementia. American Journal of Roentgenology. 2014;204(1):W76-W85.
837. Rajagopalan V, Pioro EP. Comparing brain structural MRI and metabolic FDG-PET changes in patients with ALS-FTD: 'the chicken or the egg?' question. Journal of Neurology, Neurosurgery & Psychiatry. 2015;86(9):952-8.
838. Hodges JR, Mitchell J, Dawson K, Spillantini MG, Xuereb JH, McMonagle P, et al. Semantic dementia: demography, familial factors and survival in a consecutive series of 100 cases. Brain. 2010;133(Pt 1):300-6.
839. Snowden J, Neary D, Mann D. Frontotemporal lobar degeneration: clinical and pathological relationships. Acta Neuropathol. 2007;114(1):31-8.
840. Ahmed RM, Paterson RW, Warren JD, Zetterberg H, O'Brien JT, Fox NC, et al. Biomarkers in dementia: clinical utility and new directions. Journal of Neurology, Neurosurgery & Psychiatry. 2014;85(12):1426-34.
841. Paterson RW, Slattery CF, Poole T, Nicholas JM, Magdalinou NK, Toombs J, et al. Cerebrospinal fluid in the differential diagnosis of Alzheimer's disease: clinical utility of an extended panel of biomarkers in a specialist cognitive clinic. Alzheimer's Research & Therapy. 2018;10(1):32.
842. Steinacker P, Semler E, Anderl-Straub S, Diehl-Schmid J, Schroeter ML, Uttner I, et al. Neurofilament as a blood marker for diagnosis and monitoring of primary progressive aphasias. Neurology. 2017;88(10):961-9.
843. Meeter LHH, Steketee RME, Salkovic D, Vos ME, Grossman M, McMillan CT, et al. Clinical value of cerebrospinal fluid neurofilament light chain in semantic dementia. Journal of Neurology, Neurosurgery & Psychiatry. 2019;90(9):997-1004.
844. Harris JM, Gall C, Thompson JC, Richardson AMT, Neary D, du Plessis D, et al. Sensitivity and specificity of FTDC criteria for behavioral variant frontotemporal dementia. Neurology. 2013;80(20):1881.
845. Piguet O, Hornberger M, Shelley BP, Kipps CM, Hodges JR. Sensitivity of current criteria for the diagnosis of behavioral variant frontotemporal dementia. Neurology. 2009;72(8):732-7.
846. Besser LM, Galvin JE. Diagnostic experience reported by caregivers of patients with frontotemporal degeneration. Neurology: Clinical Practice. 2020;10(4):298-306.
847. Elamin M, Pinto-Grau M, Burke T, Bede P, Rooney J, O'Sullivan M, et al. Identifying behavioural changes in ALS: Validation of the Beaumont Behavioural Inventory (BBI). Amyotrophic lateral sclerosis & frontotemporal degeneration. 2017;18(1-2):68-73.
848. Spreadbury JH, Kipps C. Measuring younger onset dementia: What the qualitative literature reveals about the 'lived experience' for patients and caregivers. Dementia. 2017;18(2):579-98.
849. Fried-Oken M, Mooney A, Peters B. Supporting communication for patients with neurodegenerative disease. NeuroRehabilitation. 2015;37(1):69-87.
850. Harrison Dening K, Sampson EL, De Vries K. Advance care planning in dementia: recommendations for healthcare professionals. Palliat Care. 2019;12:1178224219826579-.
851. Byrne S, Elamin M, Bede P, Shatunov A, Walsh C, Corr B, et al. Cognitive and clinical characteristics of patients with amyotrophic lateral sclerosis carrying a C9orf72 repeat expansion: a population-based cohort study. Lancet Neurol. 2012;11(3):232-40.
852. Shafto MA, Tyler LK, Dixon M, Taylor JR, Rowe JB, Cusack R, et al. The Cambridge Centre for Ageing and Neuroscience (Cam-CAN) study protocol: a cross-sectional, lifespan, multidisciplinary examination of healthy cognitive ageing. BMC neurology. 2014;14:204.
853. Marcus DS, Harwell J, Olsen T, Hodge M, Glasser MF, Prior F, et al. Informatics and data mining tools and strategies for the human connectome project. Frontiers in neuroinformatics. 2011;5:4.
854. Van Essen DC, Ugurbil K, Auerbach E, Barch D, Behrens TE, Bucholz R, et al. The Human Connectome Project: a data acquisition perspective. Neuroimage. 2012;62(4):2222-31.
855. Dickie EW, Anticevic A, Smith DE, Coalson TS, Manogaran M, Calarco N, et al. Ciftify: A framework for surface-based analysis of legacy MR acquisitions. Neuroimage. 2019;197:818-26.
856. Schaefer A, Kong R, Gordon EM, Laumann TO, Zuo X-N, Holmes AJ, et al. Local-Global Parcellation of the Human Cerebral Cortex from Intrinsic Functional Connectivity MRI. Cerebral Cortex. 2018;28(9):3095-114.
857. Yeo BT, Krienen FM, Sepulcre J, Sabuncu MR, Lashkari D, Hollinshead M, et al. The organization of the human cerebral cortex estimated by intrinsic functional connectivity. J Neurophysiol. 2011;106(3):1125-65.
858. McFarquhar M, McKie S, Emsley R, Suckling J, Elliott R, Williams S. Multivariate and repeated measures (MRM): A new toolbox for dependent and multimodal group-level neuroimaging data. Neuroimage. 2016;132:373-89.
859. Fukutomi H, Glasser MF, Zhang H, Autio JA, Coalson TS, Okada T, et al. Neurite imaging reveals microstructural variations in human cerebral cortical gray matter. Neuroimage. 2018;182:488-99.
860. Trojsi F, D'Alvano G, Bonavita S, Tedeschi G. Genetics and Sex in the Pathogenesis of Amyotrophic Lateral Sclerosis (ALS): Is There a Link? International journal of molecular sciences. 2020;21(10).

861. Seo SW, Ahn J, Yoon U, Im K, Lee J-M, Tae Kim S, et al. Cortical Thinning in Vascular Mild Cognitive Impairment and Vascular Dementia of Subcortical Type. Journal of Neuroimaging. 2010;20(1):37-45.
862. Burke T, Lonergan K, Pinto-Grau M, Elamin M, Bede P, Madden C, et al. Visual encoding, consolidation, and retrieval in amyotrophic lateral sclerosis: executive function as a mediator, and predictor of performance. Amyotrophic lateral sclerosis & frontotemporal degeneration. 2017;18(3-4):193-201.
863. Qin Q, Tang Y, Dou X, Qu Y, Xing Y, Yang J, et al. Default mode network integrity changes contribute to cognitive deficits in subcortical vascular cognitive impairment, no dementia. Brain imaging and behavior. 2021;15(1):255-65.
864. Schuster C, Elamin M, Hardiman O, Bede P. The segmental diffusivity profile of amyotrophic lateral sclerosis associated white matter degeneration. Eur J Neurol. 2016;23(8):1361-71.
865. Grollemund V, Le Chat G, Secchi-Buhour MS, Delbot F, Pradat-Peyre JF, Bede P, et al. Manifold learning for amyotrophic lateral sclerosis functional loss assessment : Development and validation of a prognosis model. Journal of neurology. 2020.
866. Bejanin A, Tammewar G, Marx G, Cobigo Y, Iaccarino L, Kornak J, et al. Longitudinal structural and metabolic changes in frontotemporal dementia. Neurology. 2020;95(2):e140-e54.
867. Lam BYK, Halliday GM, Irish M, Hodges JR, Piguet O. Longitudinal white matter changes in frontotemporal dementia subtypes. Human brain mapping. 2014;35(7):3547-57.
868. Schwindt GC, Graham NL, Rochon E, Tang-Wai DF, Lobaugh NJ, Chow TW, et al. Whole-brain white matter disruption in semantic and nonfluent variants of primary progressive aphasia. Human brain mapping. 2013;34(4):973-84.
869. Feis RA, Bouts M, Panman JL, Jiskoot LC, Dopper EGP, Schouten TM, et al. Single-subject classification of presymptomatic frontotemporal dementia mutation carriers using multimodal MRI. Neuroimage Clin. 2018;20:188-96.
870. Lule D, Diekmann V, Muller HP, Kassubek J, Ludolph AC, Birbaumer N. Neuroimaging of multimodal sensory stimulation in amyotrophic lateral sclerosis. J Neurol Neurosurg Psychiatry. 2010;81(8):899-906.
871. Aho-Ozhan HE, Keller J, Heimrath J, Uttner I, Kassubek J, Birbaumer N, et al. Perception of Emotional Facial Expressions in Amyotrophic Lateral Sclerosis (ALS) at Behavioural and Brain Metabolic Level. PLoS One. 2016;11(10):e0164655.
872. Trojsi F, Siciliano M, Femiano C, Santangelo G, Lunetta C, Calvo A, et al. Comparative Analysis of C9orf72 and Sporadic Disease in a Large Multicenter ALS Population: The Effect of Male Sex on Survival of C9orf72 Positive Patients. Frontiers in neuroscience. 2019;13:485.
873. Trojsi F, Di Nardo F, Siciliano M, Caiazzo G, Femiano C, Passaniti C, et al. Frontotemporal degeneration in amyotrophic lateral sclerosis (ALS): a longitudinal MRI one-year study. CNS spectrums. 2020:1-10.
874. Pioro EP, Turner MR, Bede P. Neuroimaging in primary lateral sclerosis. Amyotrophic lateral sclerosis & frontotemporal degeneration. 2020;21(sup1):18-27.
875. Li Hi Shing S, Lope J, Chipika RH, Hardiman O, Bede P. Extra-motor manifestations in post-polio syndrome (PPS): fatigue, cognitive symptoms and radiological features. Neurol Sci. 2021.
876. Li Hi Shing S, Lope J, McKenna MC, Chipika RH, Hardiman O, Bede P. Increased cerebral integrity metrics in poliomyelitis survivors: putative adaptation to longstanding lower motor neuron degeneration. J Neurol Sci. 2021;424:117361.
877. Brooks BR. El Escorial World Federation of Neurology criteria for the diagnosis of amyotrophic lateral sclerosis. Subcommittee on Motor Neuron Diseases/Amyotrophic Lateral Sclerosis of the World Federation of Neurology Research Group on Neuromuscular Diseases and the El Escorial "Clinical limits of amyotrophic lateral sclerosis" workshop contributors. Journal of the neurological sciences. 1994;124 Suppl:96-107.
878. Kenna KP, McLaughlin RL, Byrne S, Elamin M, Heverin M, Kenny EM, et al. Delineating the genetic heterogeneity of ALS using targeted high-throughput sequencing. Journal of medical genetics. 2013;50(11):776-83.
879. Raffelt DA, Tournier JD, Smith RE, Vaughan DN, Jackson G, Ridgway GR, et al. Investigating white matter fibre density and morphology using fixel-based analysis. Neuroimage. 2017;144(Pt A):58-73.
880. Tahedl M, Li Hi Shing S, Finegan E, Chipika RH, Lope J, Hardiman O, et al. Propagation patterns in motor neuron diseases: Individual and phenotype-associated disease-burden trajectories across the UMN-LMN spectrum of MNDs. Neurobiol Aging. 2021;109:78-87.
881. Abidi M, de Marco G, Grami F, Termoz N, Couillandre A, Querin G, et al. Neural Correlates of Motor Imagery of Gait in Amyotrophic Lateral Sclerosis. Journal of magnetic resonance imaging : JMRI. 2021;53(1):223-33.
882. Lebouteux MV, Franques J, Guillevin R, Delmont E, Lenglet T, Bede P, et al. Revisiting the spectrum of lower motor neuron diseases with snake eyes appearance on magnetic resonance imaging. Eur J Neurol. 2014;21(9):1233-41.
883. Trojsi F, Di Nardo F, Caiazzo G, Siciliano M, D'Alvano G, Ferrantino T, et al. Hippocampal connectivity in Amyotrophic Lateral Sclerosis (ALS): more than Papez circuit impairment. Brain imaging and behavior. 2020.

884. Bede P, Chipika RH, Christidi F, Hengeveld JC, Karavasilis E, Argyropoulos GD, et al. Genotype-associated cerebellar profiles in ALS: focal cerebellar pathology and cerebro-cerebellar connectivity alterations. J Neurol Neurosurg Psychiatry. 2021.
885. Josephs KA, Hodges JR, Snowden JS, Mackenzie IR, Neumann M, Mann DM, et al. Neuropathological background of phenotypical variability in frontotemporal dementia. Acta Neuropathol. 2011;122(2):137-53.
886. Chare L, Hodges JR, Leyton CE, McGinley C, Tan RH, Kril JJ, et al. New criteria for frontotemporal dementia syndromes: clinical and pathological diagnostic implications. J Neurol Neurosurg Psychiatry. 2014;85(8):865-70.
887. Geser F, Prvulovic D, O'Dwyer L, Hardiman O, Bede P, Bokde AL, et al. On the development of markers for pathological TDP-43 in amyotrophic lateral sclerosis with and without dementia. Progress in neurobiology. 2011;95(4):649-62.
888. Bocchetta M, Iglesias Espinosa MDM, Lashley T, Warren JD, Rohrer JD. In vivo staging of frontotemporal lobar degeneration TDP-43 type C pathology. Alzheimer's research & therapy. 2020;12(1):34.
889. Spinelli EG, Mandelli ML, Miller ZA, Santos-Santos MA, Wilson SM, Agosta F, et al. Typical and atypical pathology in primary progressive aphasia variants. Ann Neurol. 2017;81(3):430-43.
890. Gorno-Tempini ML, Hillis AE, Weintraub S, Kertesz A, Mendez M, Cappa SF, et al. Classification of primary progressive aphasia and its variants. Neurology. 2011;76(11):1006.
891. Belder CRS, Chokesuwattanaskul A, Marshall CR, Hardy CJD, Rohrer JD, Warren JD. The problematic syndrome of right temporal lobe atrophy: Unweaving the phenotypic rainbow. Front Neurol. 2022;13:1082828.
892. Ulugut Erkoyun H, Groot C, Heilbron R, Nelissen A, van Rossum J, Jutten R, et al. A clinical-radiological framework of the right temporal variant of frontotemporal dementia. Brain. 2020;143(9):2831-43.
893. Younes K, Borghesani V, Montembeault M, Spina S, Mandelli ML, Welch AE, et al. Right temporal degeneration and socioemotional semantics: semantic behavioural variant frontotemporal dementia. Brain. 2022;145(11):4080-96.
894. Kumfor F, Landin-Romero R, Devenney E, Hutchings R, Grasso R, Hodges JR, et al. On the right side? A longitudinal study of left- versus right-lateralized semantic dementia. Brain. 2016;139(Pt 3):986-98.
895. Seeley WW, Bauer AM, Miller BL, Gorno-Tempini ML, Kramer JH, Weiner M, et al. The natural history of temporal variant frontotemporal dementia. Neurology. 2005;64(8):1384-90.
896. Edwards-Lee T, Miller BL, Benson DF, Cummings JL, Russell GL, Boone K, et al. The temporal variant of frontotemporal dementia. Brain. 1997;120 (Pt 6):1027-40.
897. Chan D, Anderson V, Pijnenburg Y, Whitwell J, Barnes J, Scahill R, et al. The clinical profile of right temporal lobe atrophy. Brain. 2009;132(Pt 5):1287-98.
898. Kamminga J, Kumfor F, Burrell JR, Piguet O, Hodges JR, Irish M. Differentiating between right-lateralised semantic dementia and behavioural-variant frontotemporal dementia: an examination of clinical characteristics and emotion processing. J Neurol Neurosurg Psychiatry. 2015;86(10):1082-8.
899. Szaflarski JP, Binder JR, Possing ET, McKiernan KA, Ward BD, Hammeke TA. Language lateralization in left-handed and ambidextrous people. Neurology. 2002;59(2):238.
900. Brambati SM, Rankin KP, Narvid J, Seeley WW, Dean D, Rosen HJ, et al. Atrophy progression in semantic dementia with asymmetric temporal involvement: A tensor-based morphometry study. Neurobiology of Aging. 2009;30(1):103-11.
901. Rosen HJ, Perry RJ, Murphy J, Kramer JH, Mychack P, Schuff N, et al. Emotion comprehension in the temporal variant of frontotemporal dementia. Brain. 2002;125(Pt 10):2286-95.
902. Gainotti G. Different patterns of famous people recognition disorders in patients with right and left anterior temporal lesions: a systematic review. Neuropsychologia. 2007;45(8):1591-607.
903. Irish M, Kumfor F, Hodges JR, Piguet O. A tale of two hemispheres: contrasting socioemotional dysfunction in right- versus left-lateralised semantic dementia. Dement Neuropsychol. 2013;7(1):88-95.
904. Rankin KP, Gorno-Tempini ML, Allison SC, Stanley CM, Glenn S, Weiner MW, et al. Structural anatomy of empathy in neurodegenerative disease. Brain. 2006;129(Pt 11):2945-56.
905. Irish M, Hodges JR, Piguet O. Right anterior temporal lobe dysfunction underlies theory of mind impairments in semantic dementia. Brain. 2014;137(Pt 4):1241-53.
906. Rankin KP, Salazar A, Gorno-Tempini ML, Sollberger M, Wilson SM, Pavlic D, et al. Detecting sarcasm from paralinguistic cues: anatomic and cognitive correlates in neurodegenerative disease. Neuroimage. 2009;47(4):2005-15.
907. Mendez MF, McMurtray A, Chen AK, Shapira JS, Mishkin F, Miller BL. Functional neuroimaging and presenting psychiatric features in frontotemporal dementia. J Neurol Neurosurg Psychiatry. 2006;77(1):4-7.
908. Ulugut H, Dijkstra AA, Scarioni M, Barkhof F, Scheltens P, Rozemuller AJM, et al. Right temporal variant frontotemporal dementia is pathologically heterogeneous: a case-series and a systematic review. Acta Neuropathol Commun. 2021;9(1):131.
909. Josephs KA, Whitwell JL, Knopman DS, Boeve BF, Vemuri P, Senjem ML, et al. Two distinct subtypes of right temporal variant frontotemporal dementia. Neurology. 2009;73(18):1443-50.